## Optoelectronic Properties of Tin Chalcogenide Thin Films Prepared by Spray Pyrolysis Technique Applicable for Solar Cells



#### Thesis submitted to

## Bharathidasan University, Tiruchirappalli

In partial fulfilment of the requirements for the award of the degree of

#### DOCTOR OF PHILOSOPHY IN PHYSICS

Submitted by

#### A. ANITHA EZHIL MANGAIYAR KARASI

Ref: 34830/Ph.D.K2/Physics/Part-Time/Oct. 2014

Under the guidance of

Dr. R. SAMBASIVAM, M.Sc., M.Phil., M.C.A., Ph.D.,



## DEPARTMENT OF PHYSICS URUMU DHANALAKSHMI COLLEGE

Affiliated to Bharathidasan University
TIRUCHIRAPPALLI - 620 019

**MARCH 2022** 

Dr. R. SAMBASIVAM, M.Sc., M.Phil., M.C.A., Ph.D.,

Associate Professor and Head,

**Department of physics** 

Urumu Dhanalakshmi College,

Tiruchirappalli - 620019.

email:sambasivam63@gmail.com

Mobile: +91 9443410088

CERTIFICATE

Certified that the thesis entitled "Optoelectronic Properties of Tin

Chalcogenide Thin Films Prepared by Spray Pyrolysis Technique Applicable for

Solar Cells" submitted by A. Anitha Ezhil Mangaiyar Karasi, is a record of

research work carried out by her for the Degree of Doctor of Philosophy in Physics

under my guidance. This thesis is the original work of the candidate and to the best of

my knowledge the work has not been submitted, in part or in full, for any Diploma,

Degree, Associateship, Fellowship or other similar title in this or any other

University. No portion of the thesis is a reproduction from any other source, published

or unpublished, without acknowledgement.

Place: Tiruchirapalli

Dr. R. SAMBASIVAM

Date:

Research Supervisor

## A. Anitha Ezhil Mangaiyar Karasi

Ph.D. Part-time Research scholar, Department of Physics, Urumu Dhanalakshmi College, Kattur, Trichy - 620 019.

#### **DECLARATION**

I hereby declare that the thesis entitled "Optoelectronic Properties of Tin Chalcogenide Thin Films Prepared by Spray Pyrolysis Technique Applicable for Solar Cells" submitted to Bharathidasan University, Tiruchirappalli under the supervision & guidance of Dr. R. SAMBASIVAM, Associate Professor and Head, Department of physics Urmu Dhanalakshmi College, Kattur, Trichirappalli – 620019, has not been submitted for the award of any Degree / Diploma / Associateship / Fellowship or similar title to any candidate of any University or Institute.

(A. ANITHA EZHIL MANGAIYAR KARASI)



#### **Document Information**

Analyzed document A. Anitha Ezhil Mangaiyar Karasi - Physics - Intro & Review.pdf (D130661741)

**Submitted** 2022-03-17T13:12:00.0000000

**Submitted by** Dr.S.Vanitha

Submitter email vanitha@bdu.ac.in

Similarity 6%

Analysis address navitha.bdu@analysis.urkund.com

## Sources included in the report

Jour	ces included in the report		
SA	Electronics Tahira Mir PhD Thesis.pdf Document Electronics Tahira Mir PhD Thesis.pdf (D111409971)		1
SA	<b>Vu Thien Trang thesis 240621.docx</b> Document Vu Thien Trang thesis 240621.docx (D109642292)		2
W	URL: https://www.european-mrs.com/thin-film-chalcogenide-photovoltaic-materials-emrs Fetched: 2019-10-18T07:18:15.9400000		3
SA	<b>Thesis Arun Physics.pdf</b> Document Thesis Arun Physics.pdf (D38854903)		4
W	URL: https://www.researchgate.net/publication/248269035_The_structure_and_properties_of_SnS _thin_films_prepared_by_pulse_electro-deposition Fetched: 2021-01-29T19:44:58.1000000		6
W	URL: https://www.researchgate.net/publication/251496582_Electrodeposited_tin_selenide_thin_fil ms_for_photovoltaic_applications Fetched: 2019-10-31T06:30:14.1300000		6
SA	<b>Kavitha Thesis.doc</b> Document Kavitha Thesis.doc (D40707923)		1
SA	meena synopsis.docx Document meena synopsis.docx (D33664035)	88	3
W	URL: https://core.ac.uk/download/pdf/4146242.pdf Fetched: 2021-09-23T09:06:42.8900000	88	1
W	URL: https://www.sciencedirect.com/science/article/pii/S0749603619310389 Fetched: 2022-03-17T13:14:31.7370000		1
W	URL: https://pubmed.ncbi.nlm.nih.gov/22250530/ Fetched: 2022-03-17T13:14:34.7670000	88	1
W	URL: https://core.ac.uk/download/pdf/286716173.pdf Fetched: 2021-06-11T08:13:43.0530000		3



#### **Document Information**

Analyzed document A. Anitha Ezhil Mangaiyar Karasi - Physics - Remaining Chapters.pdf (D130661742)

**Submitted** 2022-03-17T13:12:00.0000000

**Submitted by** Dr.S.Vanitha

Submitter email vanitha@bdu.ac.in

Similarity 6%

Analysis address navitha.bdu@analysis.urkund.com

## Sources included in the report

Jour	ces included in the report	
SA	S. REX ROSARIO PhD Thesis Physics.pdf Document S. REX ROSARIO PhD Thesis Physics.pdf (D58343070)	<u> </u>
SA	<b>Thesis Arun Physics.pdf</b> Document Thesis Arun Physics.pdf (D38854903)	<b>::</b> 1
SA	<b>full thesis.docx</b> Document full thesis.docx (D42275542)	<del>  </del>
W	URL: https://docplayer.net/102745270-Metal-semiconductor-interface-for-schottky-barrier-devices-and-ohmic-contacts-physics-narinder-kumar-supervised-by-prof.html Fetched: 2021-07-30T06:04:29.5800000	<b>12</b>
SA	Chapters.pdf Document Chapters.pdf (D29982202)	<del>  </del>
SA	<b>R_Murugesan_Physics.pdf</b> Document R_Murugesan_Physics.pdf (D38140418)	6
W	URL: https://core.ac.uk/download/pdf/286716173.pdf Fetched: 2021-06-11T08:13:43.0530000	₩ 2
SA	Physics Ibrahim Mohammed Saleh Mohammed Thesis.pdf Document Physics Ibrahim Mohammed Saleh Mohammed Thesis.pdf (D113238620)	<b>2</b>
SA	Studies on the effect of transition metal doped CdO thin film.docx  Document Studies on the effect of transition metal doped CdO thin film.docx (D45751233)	10
SA	thesis zeba. EDITED1.pdf Document thesis zeba. EDITED1.pdf (D128096962)	<b>::</b> 1
SA	5. Thesis Body.pdf Document 5. Thesis Body.pdf (D38456461)	<b>#</b> 1
SA	Paresh Saha_Chemistry.pdf  Document Paresh Saha_Chemistry.pdf (D21161417)	<b>## 1</b>

#### ACKNOWLEDGEMENT

I am thankful to **Lord Almighty** for showering his benevolent blessings upon me in my life.

Completion of this doctoral dissertation was possible with the support of several people. I would like to express my sincere gratitude to all of them.

I thank sincerely the Management and **Dr. E. R. Ravichandran**, Ph.D., Principal, Urumu Dhanalakshmi College, Tiruchirappalli for the academic support and the facilities provided to carry out the research work at the institute.

I express my loving thanks and gratitude to my research advisor **Dr. R. Sambasivam**, M.Sc., M.Phil., M.C.A., Ph.D., Associate Professor and Head, Department of Physics, Urumu Dhanalakshmi College, Tiruchirappalli. He has taught me, both consciously and unconsciously, how good experimental Physics is done. I appreciate all his contributions of time and ideas to make my Ph.D. experience productive and stimulating. The joy and enthusiasm he has for research was contagious and motivational for me, even during tough times in the Ph.D. pursuit. I am also thankful for the excellent example he has provided as a successful physicist and professor.

I wish to express my deepest sense of gratitude to **Dr. L. Amalraj**, M.Sc., Ph.D., Associate Professor and Head (Retd.), PG and Research, Department of Physics, V.H.N.S.N. College (Autonomous), Virudhunagar, the man who consistently extended his research expertise and research facilities throughout my work. I am deeply indebted to him for his gentle and inspiring thoughts, constant encouragement and support.

I take immense pleasure in thanking to the members of the doctoral committee, **Dr. C. Hariharan**, Assistant Professor, Jamal Mohamed College (Autonomous), Tiruchirappalli and **Dr. S. Muruganantham**, Assistant Professor, National College, Tiruchirappalli, without whose knowledge and assistance this study would not have been successful.

I sincerely thank **Dr. C. Sanjeeviraja** (Retd.), CSIR-Emeritus Scientist, Department of Physics, Alagappa Chettiar College of Engineering & Technology, Karaikudi, **Dr. N. Gopalakrishnan**, Associate Professor & Head, National Institute of Technology, Tiruchirappalli, **Dr. K. Jeyadheepan**, Assistant Professor (Research), School of Electrical and Electronics Engineering, SASTRA University, Vallam and **Dr. K. Ravichandran**, Associate Professor and Head, AVVM Sri Poondi Pushpam College, Thanjavur, for providing me all the necessary laboratory facilities in the initial stage of my research work.

I thank sincerely the **Management**, Secretary **Dr. K. Meena**, Former Vice-Chancellor, Bharathidasan University, Tiruchirappalli and **Dr. S. Vidyalakshmi**, Principal, Shrimati Indira Gandhi College, Tiruchichirappalli, for their constant support and encouragement to pursue the research work.

I gratefully acknowledge the help and inspiration from **all the faculty members** of the Department of Physics, Urumu Dhanalakshmi College, Tiruchirappalli for their encouragement and support.

I should thank from the bottom of my heart **The HOD and all the Faculty Members**, Department of Physics, Shrimati Indira Gandhi College, Tiruchirappalli, whose support helped me in pursuing my research work in a successful manner.

I thank my beloved **parents**, **husband** and my kids for their love, care, constant encouragement and untiring support towards the completion of this research work.

Lastly, I offer my regards to everyone, who helped me at various stages of the work and without their help this would not be possible.

A. Anitha Ezhil Mangaiyar Karasi

## CONTENTS

		Page No
Chap	oter I	
INTE	RODUCTION	1 - 29
1.1	Introduction	1
1.2	Silicon Solar Cells	3
	1.2.1 Crystalline Si solar cells	4
	1.2.2 Polycrystalline wafer Si solar cells	4
	1.2.3 Amorphous silicon (a-Si) solar cells	5
	1.2.4 a-Si solar cell configurations	7
	1.2.5 Multiple-junction or tandem solar cells	9
	1.2.6 Hybrid solar cells	9
	1.2.7 Monolithic modules	9
	1.2.8 Flexible a-Si solar cells	10
1.3	Copper Indium Gallium Selenide (CIGS) Solar Ce Configuration	ell 11
	1.3.1 Electrical back-contact	11
	1.3.2 CIGS absorber layer	11
	1.3.3 Buffer layer	12
	1.3.4 Front electrical contact	13
	1.3.5 Sodium incorporation in CIGS	14
1.4	Flexible CIGS Solar Cells	14
1.5	III-V Single and Multi-Junction Solar Cells	14
1.6	Nano Photovoltaics	15
	1.6.1 Quantum well solar cells	15
	1.6.2 Quantum dot solar cells	16
1.7	Recent Thin Film Market	17
1.8	Thin-Film Metal Chalcogenide Solar Cells	18
	1.8.1 IV–VI Semiconductor solar cells	19
19	Role of SnS/SnSe in Thin Film Solar Cells	20

1.10	Role o	f SnSSe in Photo Electro Chemical (PEC) Solar Cells	22
1.11	Motiv	ation for the Present Work	24
Refere	ences		25
Chap	ter II		
LITE	RATUI	RE REVIEW OF SnS AND SnSe THIN FILMS	30 - 72
2.1	Introd	uction	30
2.2	Structi	ure of SnS	31
2.3	Structi	ure of SnSe	33
2.4	Literat	ture Survey on Tin Sulfide (SnS)	35
2.5	Literat	ture Survey on Tin Selenide (SnSe)	53
Refere	ences		66
Chap	ter III		
EXPE TOO		NTAL TECHNIQUES AND CHARACTERIZATION	73 - 116
			<b>73 - 116</b>
TOO	LS		
TOO	LS Introd	uction	73
TOO	Introde	uction  Basic aspects of thin films	73 73
TOO	Introde 3.1.1 3.1.2 3.1.3	Basic aspects of thin films Thin film growth process	73 73 75
<b>TOO</b> 1 3.1	Introde 3.1.1 3.1.2 3.1.3 Differen	Basic aspects of thin films Thin film growth process Thin film growth modes	73 73 75 78
3.1 3.2	Introde 3.1.1 3.1.2 3.1.3 Differen	Basic aspects of thin films Thin film growth process Thin film growth modes ent Thin Film Deposition Methods	73 73 75 78 81
3.1 3.2	Introde 3.1.1 3.1.2 3.1.3 Difference Chemic	Basic aspects of thin films Thin film growth process Thin film growth modes ent Thin Film Deposition Methods ical Vapour Deposition	73 73 75 78 81 82
3.1 3.2	Introde 3.1.1 3.1.2 3.1.3 Differe Chemi 3.3.1	Basic aspects of thin films Thin film growth process Thin film growth modes ent Thin Film Deposition Methods ical Vapour Deposition Plasma enhanced chemical vapor deposition	73 73 75 78 81 82 83
3.1 3.2	Introde 3.1.1 3.1.2 3.1.3 Differe Chemi 3.3.1 3.3.2 3.3.3	Basic aspects of thin films Thin film growth process Thin film growth modes ent Thin Film Deposition Methods ical Vapour Deposition Plasma enhanced chemical vapor deposition Metal-organic chemical vapour deposition	73 73 75 78 81 82 83
3.1 3.2 3.3	Introde 3.1.1 3.1.2 3.1.3 Differe Chemi 3.3.1 3.3.2 3.3.3 Solution	Basic aspects of thin films Thin film growth process Thin film growth modes ent Thin Film Deposition Methods ical Vapour Deposition Plasma enhanced chemical vapor deposition Metal-organic chemical vapour deposition Low-pressure chemical vapour deposition	73 73 75 78 81 82 83 84

	3.5.2	Spray pyrolysis technique	92
	3.5.3	Principle and thin film formation mechanism	92
3.6	Nebul	ized Spray Pyrolysis (NSP) Technique	93
	3.6.1	Mechanism of a nebulizer	93
	3.6.2	Venturi effect	95
	3.6.3	Working principle of nebulized spray pyrolysis technique	95
	3.6.4	Advantages of NSP technique	96
3.7	Chara	cterization Techniques	97
	3.7.1	Thickness measurement of Stylus profilometer	98
	3.7.2	X-ray diffraction technique	99
	3.7.3	Scanning electron microscopy (SEM)	102
	3.7.4	Electrical conductivity characterization	104
	3.7.5	Energy Dispersive X-Ray Analysis (EDAX)	108
	3.7.6	Optical and absorption studies	110
	3.7.7	Photoluminescence (PL) studies	112
Refer	rences		115
Chap	ter IV		
CHE		TION OF SUBSTRATE TEMPERATURE IN SPRAY PYROLYSIS TECHNIQUE TO GET P-TYPE S SnS THIN FILMS	117 - 137
4.1	Introd	uction	117
4.2.	Exper	imental Details	119
4.3.	Result	s and Discussions	120
	4.3.1	Morphological Properties	127
	4.3.2	Optical Properties	130
	4.3.3	Electrical Properties	133

	4.3.4.	Optimization of precursor at different temperature for p-type SnS absorber layer.	134
4.4.	Concl	usion	135
Refer	rences		136
Chap	oter V		
	SICAL	OF TIN PRECURSOR CONCENTRATION ON PROPERTIES OF SPRAY DEPOSITED TIN HIN FILMS	138 - 157
5.1	Introd	uction	138
5.2.	Exper	imental Details	138
5.3.	Result	ts and Discussions	139
	5.3.1	Structural Studies	140
	5.3.2	Surface Morphology	144
	5.3.3	Optical Properties	147
	5.3.4	Electrical Properties	151
5.4.	Concl	usion	152
Refer	rences		154
Chap	oter VI		
	PERTII	E OF SUBSTRATE TEMPERATURE ON PHYSICAL ES OF NEBULIZED SPRAY DEPOSITED SnSe THIN	158 - 182
6.1	Introd	uction	158
6.2.	Exper	imental Technique	159
	6.2.1	Materials and methods	159
	6.2.2	Characterization technique	160
6.3	Result	ts and Discussion	160
	6.3.1	Structural properties on SnSe thin films	161
	6.3.2	Analysis of surface morphology of SnSe thin films	166
	6.3.3	Compositional analysis of SnSe thin films	168
	6.3.4	A report on optical absorption analysis of SnSe thin films	169

	6.3.5	Photoluminescence studies on SnSe thin films	172
	6.3.6	Electrical conductivity studies on SnSe thin films	174
6.4	Concl	usion	177
Refer	rences		179
Chap	ter VII		
	PERTII	F PRECURSOR CONCENTRATION ON PHYSICAL ES OF NEBULIZED SPRAY DEPOSITED SnSe THIN	183 - 208
7.1	Introd	uction	184
7.2.	Exper	imental Technique	185
	7.2.1	Materials and methods	185
7.3	Result	s and Discussion	186
	7.3.1	X-ray diffraction studies of SnSe thin films for different Precursor concentration	188
	7.3.2	Surface morphological studies of SnSe thin films for different precursor concentration using SEM	193
	7.3.3	Compositional analysis of SnSe thin films by EDAX	194
	7.3.4	Optical absorption analysis of SnSe thin films	197
	7.3.5.	Photoluminescence studies on SnSe thin films	200
	7.3.6.	Electrical conductivity studies on SnSe thin films	202
7.4	Concl	usion	205
Refer	rences		207
Chap	oter VII	[	
		AL, OPTICAL AND PHOTOSENSING PROPERTIES PYROLYZED SnSSe THIN FILMS	209 - 220
8.1	Introd	uction	209
8.2.	Exper	imental Materials and Methods	210
8.3	Result	s and Discussion	211
	8.3.1	Structural properties	211
	8.3.2	Optical Properties of SnSSe films	213

SUMMARY AND CONCLUSIONS			221 - 224
Chapt	ter IX		
Refere	ences		219
8.4	Concl	usion	218
0.4		Photo Sensing Performance	215
	021	Photo Consina Doutoumonas	215
	8.3.3	Electrical Properties	215

## LIST OF FIGURES

Figure No.	Title	Page No.
1.1.	(a) Single-junction a-Si solar cell in superstructure configuration (b) Energy band diagram of p—i—n solar cell structure	6
1.2.	(a) a-Si solar cell in "superstrate" (p-i-n) configuration, and (b) "substrate" (n-i-p) configuration	8
1.3.	Multi-junction cell architecture	10
1.4.	(a) CIGS solar cell in "substrate" configuration (b) Qualitative energy band diagram of CIGS solar cell	12
1.5.	SnS based solar cell	20
1.6	Earth-abundance of elements for absorber materials such as $SnS(Se)$ CZTS(Se), CIGS(Se), $Sb_2S_3(Se_3)$ and CdTe based solar cell	22
2.1	Schematic diagram of double-layered structured SnS	32
2.2	Crystal structure of (a) $\alpha$ -SnS and (b) $\beta$ -SnS (Strong Sn-S bonds are indicated by lines)	32
2.3	Crystal structures of SnSe	34
3.1	Three modes of thin film growth processes	77
3.2	Schematic cross sections of substrate-film, in three successive growth stages, of the four extended growth modes for epitaxial thin film: (a) Columnar-Growth, (b) Step-Flow, (c) Step-Bunching and (d) Screw-Island modes	80
3.3	Different physical and chemical thin film deposition processes	81
3.4	Schematic of aerosol transport	90
3.5	Description of the deposition processes initiated with increasing substrate temperature	90
3.6	A typical spray pyrolysis system	92
3.7	Schematic diagram of a simple nebulizer	94
3.8	Experimental setup of nebulized spray pyrolysis technique	96
3.9	Schematic diagram and image of MITOTOYO SJ-300 stylus profilometer	98
3.10	Photograph of X-Pert Pro X-ray diffractometer	100
3.11	X-ray diffraction	100

3.12	Diagram for (a) image formation of a typical SEM (b) instrumental set up	103
3.13	Schematic diagram of four probe set-up	106
3.14	Photograph of Hall Effect instrument	107
3.15	(a) Emission of X-ray (b) Example of EDAX spectra of CdS thin film	109
3.16	Schematic of electron transitions responsible for the production of (a) $K_{\alpha}$ and $K_{\beta}$ (b) $L_{\alpha}$ and $L_{\beta}$ X-rays	109
3.17	(a) Schematic diagram (b) sample graph of absorption of light	111
3.18	Photograph of varian cary eclipse photoluminescence spectrophotometer	113
4.1	Variation of film thickness of SnS thin films at different substrate temperatures	121
4.2	X-ray diffraction pattern of SnS thin films at different substrate temperatures (a) $T_S$ =250°C (b) $T_S$ =275°C (c) $T_S$ = 300°C (d) $T_S$ =350°C and (e) $T_S$ = 375°C.	123
4.3	Variation of crystallite size versus SnS thin films at different substrate temperatures	124
4.4	Texture coefficient of the SnS thin films at different substrate temperatures	126
4.5	Strain versus different substrate temperatures	127
4.6	Scanning electron microscope (SEM) images of SnS thin films for different substrate temperatures from 250 $^{\circ}C-375$ $^{\circ}C$	128
4.7	Energy dispersive X-ray (EDX) spectra of SnS thin films for different substrate temperatures from 250 $^{\circ}C-375$ $^{\circ}C$	129
4.8	Absorbance spectra of SnS thin films at different substrate temperatures	131
4.9	Transmittance spectra of SnS thin films at different substrate temperatures	131
4.10	Energy band gap of SnS thin films at different substrate temperatures	132
4.11	Variation of Sn/S ratio with different substrate temperatures	132
4.12	Variation of Band gap of the films with different substrate temperatures	133
5.1	XRD of SnS thin films with different precursor concentrations	141

5.2	The variation of structural parameters with different tin concentration of SnS thin films	143
5.3	SEM images of SnS thin films with different precursor concentrations	145
5.4	EDAX images of SnS thin films with different precursor concentrations	146
5.5	A plot of transmittance spectra of SnS thin films with different precursor concentrations	147
5.6	A plot of absorption co-efficient with wavelength of SnS thin films with different precursor concentrations of tin species	148
5.7	The $(\alpha h \nu)^2$ versus $h \nu$ curves for the optical band gap determination of SnS thin films at different concentration of tin species	150
5.8	PL spectra of SnS thin films with different precursor concentrations of tin species	150
6.1	X-ray diffraction pattern of SnSe thin films deposited for different substrate temperature	163
6.2	Variation of average crystallite size as a function of temperatures	165
6.3	SEM photographs of the SnSe films deposited at different substrate temperature	167
6.4	EDAX spectra of SnSe films prepared at different substrate temperature	169
6.5	Transmittance spectra of nebulized spray deposited SnSe thin films at different substrate temperature	171
6.6	Absorption coefficient spectra of nebulized spray deposited SnSe thin films at different substrate temperature	171
6.7	Plot of $(\alpha hv)^2$ versus photon energy for nebulized spray deposited SnSe thin films at substrate temperatures a) 250 °C b) 275 °C c) 300 °C d) 325 °C	172
6.8	Photoluminescence (PL) spectra of SnSe thin films deposited under different substrate temperatures	173
6.9	Variation of resistivity, carrier concentration and mobility of SnSe thin films of different substrate temperature	176
6.10	Arrhenius plot of SnSe thin films of different substrate temperature	177
7.1	Variation of thickness of SnSe thin films at different precursor concentrations	187

7.2	X-ray diffraction pattern of SnSe thin films prepared at different precursor concentration	189
7.3	The variation average crystallite size with different precursor concentration of SnSe thin films	191
7.4	Scanning electron microscope (SEM) images of SnSe thin films for different precursor concentration	195
7.5	Energy dispersive X-ray (EDX) pictures of SnSe thin films for different precursor concentration	196
7.6	Transmittance spectra of SnSe thin films at different precursor concentration	198
7.7	Absorption coefficient (α) spectra for SnSe thin films prepared for different precursor concentration	198
7.8	The $(\alpha h \nu)^2$ versus $h \nu$ curves for the optical band gap determination of SnSe thin films of different precursor concentration	200
7.9	Photoluminescence (PL) spectra of SnSe thin films under different precursor concentration	201
7.10	Variation of resistivity and mobility of SnSe thin films at different precursor concentration	203
7.11	Arrhenius plot for SnSe thin films at different precursor concentration	204
8.1	XRD pattern of SnSSe thin film deposited at 325 $^{\circ}$ C	212
8.2	Absorbance spectra of SnSSe thin films deposited at 325 °C	214
8.3	Transmittance spectra on SnSSe thin films deposited at 325 °C	214
8.4	Band gap of SnSSe thin films deposited at 325 °C	214
8.5	Experimental setup of measurement of photosensitivity.	216
8.6	Photoluminescence of SnSSe thin films deposited at 325 °C	217

## LIST OF TABLE

Table No.	Title	Page No.
4.1	Electrical resistivity, Carrier concentration and Mobility for SnS thin films deposited at different substrate temperatures	134
5.1	Variation of structural and elemental properties of SnS thin films with different precursor concentration	143
5.2	The optical and electrical parameters of SnS thin films with different precursor concentrations of tin	152
6.1	Structural parameters of SnSe thin films at different substrate temperature	164
6.2	Value of texture coefficient, dislocation density and number of crystallites for different temperatures from 250 °C to 325 °C	166
6.3	Variation of elemental analysis of SnSe thin films at differentsubstrate temperature	168
6.4	Variation of optical and electrical properties of SnSe thin films at different substrate temperature	176
7.1	Structural parameters of SnSe thin films deposited at different precursor concentration $(m_c)$	190
7.2	Value of texture coefficient, dislocation density, number of crystallites and stacking fault for different precursor concentration $(m_c)$	192
7.3	The quantitative analysis of the weight percentage of the compositional elements presents in the SnSe thin films at different precursor concentration	197
7.4	Variation of optical and electrical properties of SnSe thin films at different precursor concentration	205

## CHAPTER - I

### INTRODUCTION

#### 1.1 INTRODUCTION

Presently, the world energy consumption is 10 terawatts (TW) per year and by 2050, it is projected to be about 30 TW. The world will need about 20 TW of non-CO<sub>2</sub> energy to stabilize CO<sub>2</sub> in the atmosphere by mid-century. The simplest scenario to stabilize CO<sub>2</sub> by mid-century is one in which photovoltaic (PV) and other renewables are used for electricity (10 TW), hydrogen for transportation (10 TW) and fossil fuels for residential and industrial heating (10 TW) [1]. Thus, PV will play a significant role in meeting the world future energy demand.

The PV effect was discovered in 1839 by Becquerel while studying the effect of light on electrolytic cells. A long period was required to reach sufficiently high efficiency. Solar cells were developed rapidly in 1950s owing to space programs and used on satellites. The energy crisis of the 1970s greatly stimulated research and development (R&D) for PV solar cells based on compound semiconductors (III–V and II–VI) that were first investigated in the 1960s. At the same time, polycrystalline Si (pc-Si) and thin-film solar cell technologies were developed to provide high production capacity at reduced material consumption and energy input in the fabrication process and integration in the structure of modules by the deposition process and consequently cost reduction for large-scale terrestrial applications.

According to Shockley and Queisser [2], the thermodynamic efficiency for an ideal single homo junction cell is 31%. The efficiency of a single-junction device is limited by transmission losses of photons with energies below the band gap and thermal relaxation of

carriers created by photons with energies above the band gap. Several methods have been offered to increase the power conversion efficiency of solar cells, including tandem cells, impurity-band and intermediate-band devices, hot-electron extraction and carrier multiplication, the so-called "third generation" PV cells.

Carrier multiplication which was first observed in bulk semiconductors in the 1950s would provide increased power conversion efficiency in the form of increased solar cell photocurrent. The process of inverse Auger recombination or impact ionization, as it is more commonly known, has also been considered as a mechanism to use some of the excess energy of photo-generated carriers to create additional electron-hole pairs in PV devices. When carrier multiplication is active, the effective photon-to-pair generation quantum yield may be greater than 1 for photon energies greater than twice the band gap. The predicted limiting efficiencies are 44.7% and 85.9% for devices with maximum multiplication under unconcentrated and fully concentrated (blackbody) sunlight, respectively [3].

The purpose of a multi-junction device is to capture a larger fraction of the solar spectrum while minimizing thermalization losses. By stacking cells in the order of their band gaps, with the cell with the largest band gap at the top, light is automatically filtered as it passes through the stack, ensuring that it is absorbed in the cell that can convert it most efficiently. If band gaps are appropriately selected, all the cells in the stack will generate close to the same current, so the cells can be interconnected in series. The highest efficiency solar cells known are multi-junction cells based on GaAs and related group III–V materials. These cells are expensive for large-scale applications, but are commonly used at the focus of mirrors or lenses that concentrate the solar light by a factor of 50-1000. A multi-junction cell with a large number of cells in the stack can theoretically approach 68.5% efficiency. Continuously increasing demand for PV modules and the need for low-cost PV options have stretched these advantages to the limit and have exposed some inherent disadvantages of

c-Si technology, such as the scarcity of feedstock material, costly processing of materials and complex device fabrication steps, as well as the inability of monolithic interconnections.

These, in turn, restrict the potential of Si wafer technology and it appears difficult to achieve PV module production costs below \$1/W, which is considered essential for cost-competitive generation of solar electricity. It is generally agreed that c-Si wafer technology would not be able to meet the low-cost targets, whereas thin-film technologies have the potential to provide a viable alternative in the near future.

#### 1.2 SILICON SOLAR CELLS

Hundreds of solar cells (also called photovoltaic cells) make up a solar photovoltaic (PV) array. Solar cells are the components of solar arrays that convert radiant light from the sun into electricity that is then used to power electrical devices to heat and cool homes and businesses. Solar cells contain materials with semiconducting properties in which the electrons become excited and turned into an electrical current when struck by sunlight. While there are dozens of variations of solar cells, the two most common types are those made of crystalline silicon (both monocrystalline and polycrystalline) and those made with what is called thin film technology. The majority of solar cells on the market today are made up of some type of silicon by some estimates, 90% of all solar cells are made up of silicon. However, silicon can take many different forms. Variations are mostly distinguished by the purity of the silicon purity in this sense is the way in which the silicon modules are aligned. The greater the purity of the silicon molecules, the more efficient the solar cell is at converting sunlight into electricity. The majority of silicon based solar cells on the market about 95% are comprised of crystalline silicon, making this the most common type of solar cell. But there are two types of crystalline - monocrystalline and polycrystalline.

#### 1.2.1 Crystalline Si solar cells

Most commercial Si solar cells have used boron-doped single-crystal wafers grown by the Czochralski (CZ) process. CZ Si is free from lattice defects, however, it contains residual impurities such as oxygen, carbon and transition-metal ions. Oxygen introduced from a quartz crucible is beneficial for microelectronics, because the oxygen strengthens the wafers and can also be used for guttering defects from wafer surfaces. Oxygen reacts with the boron to form an electronically active defect that limits the quality of the material after illumination [4]. Magnetic confinement is used to reduce the amount of oxygen by transferring material from the crucible within the melt. Si grown by the float zone process is preferable for solar cells of highest efficiencies because it has the lowest recombination losses.

Si cell efficiency can be divided into four stages, with each stage corresponding to new solutions in technology or cell structure. In the beginning of the "semiconductor era", the rapid progress of silicon technology allowed production of Si solar cells with 15% efficiency. In the second stage (1970s), 17% efficiency Si solar cells were fabricated due to achievements in microelectronics (e.g. photolithography). The most significant results have been obtained in the third (1980s) and fourth (2000+) stages, where Si cell efficiencies close to 25% have been achieved. These efficiencies were due to improved contact and surface passivation of the cell, along the front and rear surfaces, as well as an improved understanding of the significant role of light-trapping in Si devices. For Si cells of 80 μm thick have the maximum efficiency of 28.8%.

#### 1.2.2 Polycrystalline wafer Si solar cells

The poly-Si wafers can be fabricated over large areas. Plasma processing of lower-cost pc-Si is used to form a highly transmissive surface and to increase the light absorption known as reactive-ion etching, this process allows about a 40% relative increase in

absorption. Bulk hydrogenation and nitride passivation of the cell surface have produced good results. Despite a number of advantages of pc-Si, there is no significant difference between the costs of c-Si and pc-Si solar cells. Commercial pc-Si cells have efficiencies of 12–15%.

#### 1.2.3 Amorphous silicon (a-Si) solar cells

The basic structure of an a-Si solar cell configuration is a "p-i-n" junction, shown in Fig. 1.1a which illustrates qualitatively the thickness of different layers in the device in the "superstrate" configuration with applied texturing (roughness) of the transparent conducting electrodes for enhanced light-trapping in the a-Si layer. The p-i-n type configuration for the a-Si solar cell [5], where an intrinsic layer of a-Si:H is sandwiched between the n- and p-type doped layers of a-Si:H or its alloys is shown in Fig. 1.1b. Because of very short lifetime (or high recombination) of the carriers, the doped layers do not contribute to the photocurrent generation (the photons absorbed in these layers contribute to optical losses) but these p- and n-layers build up the electric field across the i-layer.

This electric field drives the electrons and holes, photo-generated in the i-layer in opposite directions, so that the i-layer essentially acts as the absorber layer in a-Si:H solar cells. The electrical field depends on the doping concentration of p- and n-layers, as well as the thickness of the i-layer. Because of the p- and n-doped layers do not contribute to photocurrents and can cause further recombination of the generated carriers before sweeping across the layer, it is essential to minimize their thickness, which is typically ~10-30 nm. There is an upper limit to the thickness of the i-layer (~0.5  $\mu$ m), because charge defects reduce the effective field and thus, if the width of the i-layer exceeds the space-charge width, then the extra width would act as a "dead" layer without actually contributing to photocurrent.

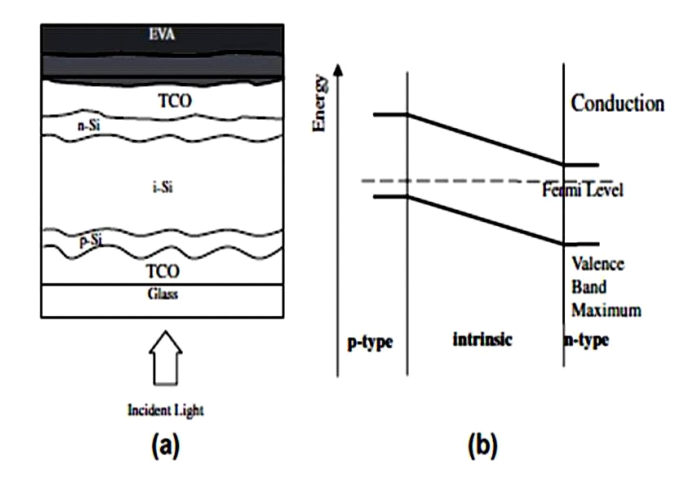


Fig. 1.1 (a) Single-junction a-Si solar cell in superstructure configuration (b) Energy band diagram of p—i—n solar cell structure

The initial results of a-Si cells in the 1970s, indicated very promising potential for attaining efficiencies well above 10%. However, it was observed that a-Si solar cells suffer from an inherent problem of light dependent degradation on their performance under continuous light exposure [6]. It was observed that in a timescale of a few months, the performance of the cells dropped about 30–40%, then stabilized at efficiency lower than the initial value.

An explanation for the light-induced degradation is that with light exposure, the Si–H bonds break and further increase the density of the dangling bonds. Thus, the system is driven into an excited or higher energy state, with active defect centers leading to higher recombination of the free carriers and hence leading to reduction in efficiency. The efficiency drop depends on the illumination level and operating temperature of the solar cell. It has been observed that efficiencies may be partially recovered by heating the cells.

The first problem of the technology is that SWE (Society of women engineers) cannot be eliminated, but can be reduced by engineering of the device's structure (e.g., by employing a thinner i-layer at the expense of absorption loss). The second problem is that the doping of the a-Si leads to an increase of trap density therefore, limiting the thickness of

the doped layers to 10–30 nm for minimized recombination effects. The limits on i layer and n- and p-doped layer thicknesses together have a direct bearing on the overall device structure and performance stability.

#### 1.2.4 a-Si solar cell configurations

An advantage of a-Si is that the solar cells can be grown in both "superstrate" and "substrate" configurations, as shown in Fig.1.2. In the "superstrate" configuration, the cell is grown in the p-i-n sequence (starting with the p-layer, followed by i- and n-layers) onto a substrate that must be transparent (such as glass) hence, this configuration is not suitable for metal or highly opaque polymeric substrates. In contrast, the "substrate" configuration can be grown on any type of substrates, which could be rigid glass or flexible metal or polymer foil. It bears an n-i-p configuration (cell growth starting with n-layer followed by i- and p-layers) and the light enters through the last grown p-layer.

Generally, a-Si solar cells on glass are available in the superstrate configuration starting with a Transparent Conducting Oxide (TCO) window, then having p-i-n layers grown on it, followed by another TCO layer and a metallic back-reflector layer. The layers can be grown in n-i-p or p-i-n sequence. But irrespective of the substrate or superstrate configuration, incident light is allowed through the p-side, because it has a higher band gap than the i- or n-layers. Also, because the mobility of holes is smaller than compared to electrons, a thin front p-layer supports hole collection in the device [7].

The choice of TCO material, as well as its electrical and optical properties, is important for electrical contacts also for efficient light-trapping through the device. Light trapping is essential for efficient performance of a-Si solar cells, where device thickness is limited by several inimical factors, e.g., thinner i-layer is desired for minimizing light-induced performance degradation.

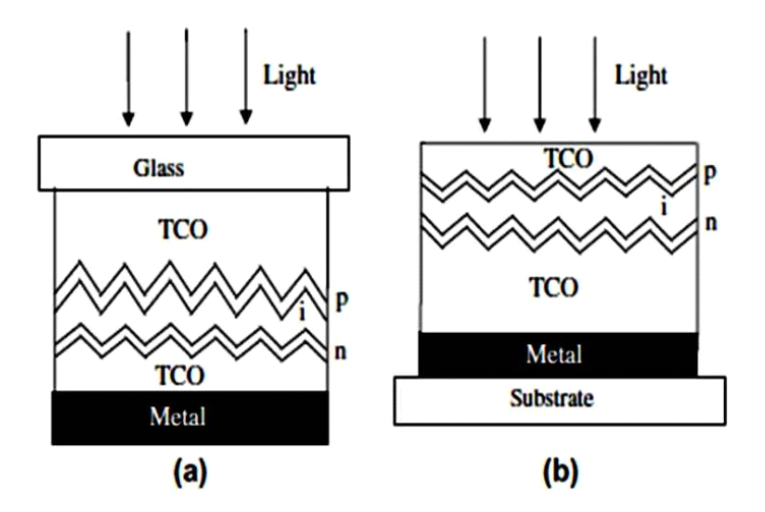


Fig. 1.2 (a) a-Si solar cell in "superstrate" (p-i-n) configuration and (b) "substrate" (n-i-p) configuration

TCOs such as SnO<sub>x</sub>:F, indium tin oxide (ITO) and ZnO:Al have been extensively used in a-Si solar cells. Some requirements for good a-Si:H solar cells are the following:

- Glass and front TCO should have a high (>80%) transparency over the whole spectral range.
- TCO with a sheet resistance of at most 10–15 Ohm/square (high conductivity) obtained by enhancing carrier mobility rather than the carrier concentration to minimize free-carrier absorption over the near-infrared region.
- TCO layers and doped silicon layers, which do not contribute to photo-generation
  and collection, should be kept as thin as possible and have very low absorption
  coefficients.
- TCO layer should not degrade by chemical reduction during a-S: H deposition.
- Use of back reflectors with as little absorption as possible.

#### 1.2.5 Multiple-junction or tandem solar cells.

Light induced degradation has become the biggest bottleneck of the a-Si technology and it has serious implications. The general effects of high density of trap and recombination centers have restricted the thickness of the device layers, which consequently limits the absorption of the incoming light. The p—i—n configuration thought to have great promise for high efficiency at lower cost was also hindered by this instability issue. Tandem cells using double and triple junctions have been thoroughly pursued worldwide to work within the limits of an -layer thickness of ~300 nm and using different light-trapping arrangements.

Multi junction solar cells are used for better use of the solar spectrum and to improve stability. The stabilized efficiency (small area) for single-junction cells is 9.3%, whereas it is 12.4% for double-junction and 13.0% for triple-junction cells using a-Si:H and its alloys [8]. Fig. 1.3 presents schematics of different multi-junction structures.

#### 1.2.6 Hybrid solar cells

Amorphous silicon cells have been combined with nano crystalline silicon-junction cells and cells of other materials such as Copper Indium Gallium Selenide (CIGS). Another significant design in development is the formation of a thick/thin type of interface structure (hetero structure) between the a-Si:H layer and the c-Si wafer. Their efficiency is close to 21% over a cell area of 10 cm<sup>2</sup>. This technology uses an n-type CZ-silicon wafer as the base (light absorber) and low-temperature processes with a device structure of a- Si(p+)/a-Si(i)/c-Si(n)/a-Si(i)/a-Si(n-). The intrinsic a-Si layer is important because it contacts c-Si at both ends and it provides passivation and extra stability to the system.

#### 1.2.7 Monolithic modules

All solar modules require a number of solar cells to be electrically connected in series to provide power, depending on size and cell efficiency. Additional processing steps

such as attachment of leads and encapsulation for protection against external influences are done to finalize the module structure. The "superstrate" configuration has an advantage for monolithic electrical interconnection of solar cells to form solar modules because the substrate (e.g., glass, polymer) is insulating. In contrast, in the "substrate" configuration, individual large-area solar cells are mechanically connected cell to cell, as done in c-Si technology.

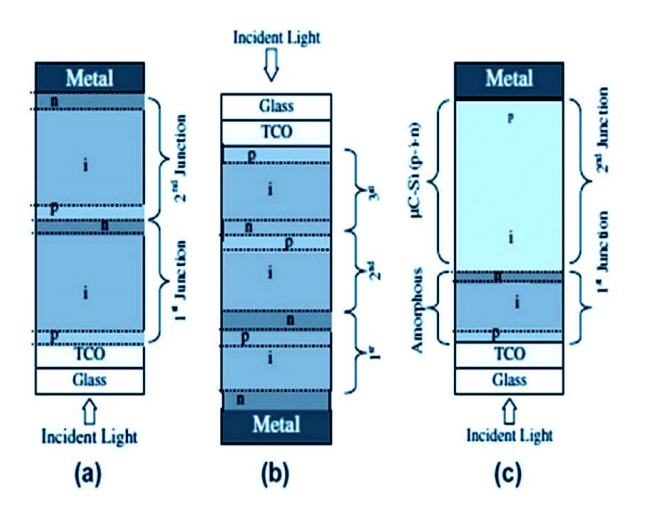


Fig.1.3 Multi-junction cell architecture
(a) double-junction "superstrate" configuration
(b) triple-junction in "substrate" configuration
(c) "micromorph" junction in "superstrate" configuration

#### 1.2.8 Flexible a-Si solar cells

Another important perspective of thin-film PV technology is flexible modules with strategic space and military use, integration in roofs and building facades and use in portable power sources, automobiles and consumer electronics. Since they can be made in different shades (even semi-transparent), shapes and sizes, these flexible a-Si solar cells are likely to be very popular and in demand for applications in the low to medium range of power.

# 1.3 COPPER INDIUM GALLIUM SELENIDE (CIGS) SOLAR CELL CONFIGURATION

Copper Indium Gallium Selenide (CIGS) solar cells can be grown in both "substrate" and "superstrate" configuration, but the substrate configuration gives the highest efficiency due to favorable process conditions (Fig. 1.4). However, it requires an additional encapsulation layer and glass to protect the cell surface, which is not required in the superstrate configuration.

#### 1.3.1 Electrical back-contact

CIGS solar cells in substrate configuration can be grown on glass, as well as on metal and polymer foils. Molybdenum (Mo) is the most commonly used electrical back-contact material for CIGS solar cells. Growth of the solar cell starts with the deposition of Mo on the substrate, which forms an electrically conducting back-electrode with CIGS. When CIGS is grown on Mo, an interface layer of MoSe<sub>2</sub> is automatically formed that helps in ohmic transportation between CIGS and Mo.

#### 1.3.2 CIGS absorber layer

High-efficiency cells have p-type Cu(In,Ga)Se<sub>2</sub> in bulk, whereas a defect-chalcopyrite Cu(In,Ga)<sub>3</sub>Se<sub>5</sub> phase, in the form of a thin layer that segregates at the top surface, is n-type especially when doped by cation atoms diffusing from the buffer layer [9]. It is believed that this inverted surface, leading to a p—n homo junction in the CIGS absorber, is crucial for high-efficiency cells.

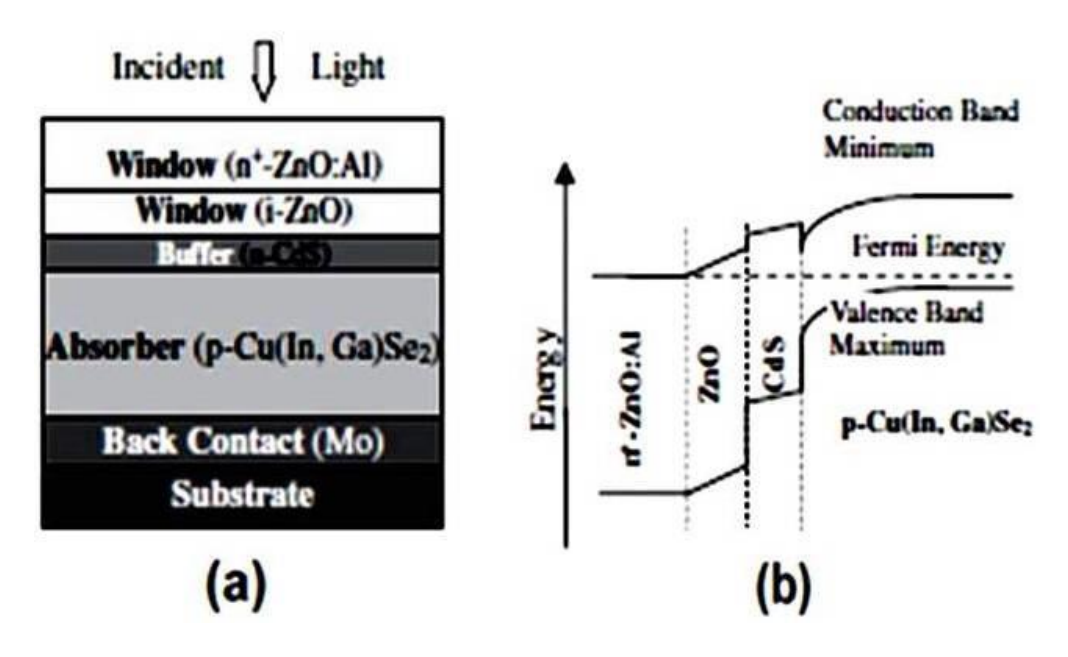


Fig. 1.4 (a) CIGS solar cell in "substrate" configuration (b) Qualitative energy band diagram of CIGS solar cell

#### 1.3.3 Buffer layer

The primary function of a buffer layer in a hetero junction is to form a junction with the absorber layer while admitting a maximum amount of light to the junction region and absorber layer [10]. In addition, this layer should have minimal absorption losses and should be capable of driving out the photo generated carries with minimum recombination losses and transporting the photo generated carriers to the outer circuit with minimal electrical resistance. For high optical throughput with minimal resistive loss the band gap of the window layer should be as high as possible and the layer should be as thin as possible to maintain low series resistance. It is also important that any potential 'spike' in the conduction band at the hetero junction be minimized for optimal minority carrier transport. Lattice mismatch (and consequent effects) at the junction is important for consideration for epitaxial or highly oriented layers. In the case of microcrystalline layers, mismatch varies spatially and thus the complicated effect, if any, averages out.

Efficiency gain of the thin film solar cells greatly depends upon the quality and thickness of the buffer layer. The standard Copper Indium Selenide (CIS) solar cell needs optimized thickness of buffer layer between the absorber layer and the transparent front contact layer to improve efficiency. It drives out the photo generated carriers with minimal losses while coupling light to the junction with minimum absorption losses, yielding a highly efficient solar cell. Thin film hetero junction solar cells provide more light towards the junction as it has wide band gap buffer layer in contrast with optimal low band gap absorber layer. This provides the most reliable way of increasing the efficiency of the cell. The beneficial effects of the buffer layer ranges from modifying the absorber surface chemistry to protecting the sensitive interface during the subsequent window deposition [11]. Favorable properties of the interface are suggested to be related to the match between lattice parameters.

Several semiconductor compounds with n-type conductivity and band gap between 2.0 and 3.4 eV have been applied as a buffer to form a hetero-junction in CIGS solar cells. However, SnS remains one of the most widely investigated buffer layer, because it has continuously yielded high-efficiency cells. According to the Shockley–Queisser criteria, the spectroscopic limits, maximum efficiency up to 33% could be achieved for the material having  $E_g$  of 1.3 eV [12]. However, a maximum efficiency of 2.04% in pulsed Chemical Vapor Deposition (CVD) method [13] and 1.3% in sprayed [14] and sputtered [15] has been recorded so far.

#### 1.3.4 Front electrical contact

TCOs with band gap above 3.0 eV are the most appropriate material and have become the ultimate choice for front electrical contacts due to their excellent optical transparency (>85%) and good electrical conductivity [16]. CIGS solar cells use either Indium Tin Oxide (ITO) or Al-doped ZnO. A combination of an intrinsic and a doped ZnO

layer is commonly used. However investigations show boron to be a feasible alternative because it yields a high mobility of charge carriers and a higher transmission in the long-wavelength spectral region, giving rise to higher currents.

#### 1.3.5 Sodium incorporation in CIGS

One of the breakthroughs in CIGS PV technology occurred when the alumina or borosilicate glass substrate was replaced by soda-lime glass to match the thermal expansion coefficients, resulting in substantial's improved efficiency. Subsequently, sodium was realized to play an important role in high-efficiency CIGS solar cells because it affects the microstructure (grain size) and passivates the grain boundaries, leading to changes in electronic conductivity by up to two orders of magnitude [17].

#### 1.4 FLEXIBLE CIGS SOLAR CELLS

The ultimate advantage of thin-film technology is roll-to-roll manufacturing to produce monolithically interconnected solar modules leading to low time for energy payback because of high-throughput processing and to low cost of the overall system. A large number of activities on highly efficient, stable and flexible thin-film modules based on CIGS has recently drawn much interest for flexible solar cells on metal and plastic foils. Apart from the expected high efficiency and long-term stability for terrestrial applications, flexible CIGS has excellent potential for space application because of their tolerance to space radiation, being 2–4 times superior to conventional Si and GaAs cells. Lightweight and rollable solar array structures will reduce the overall cost of space-deployable solar modules, but can also substantially save on the cost of launching satellites.

#### 1.5 III-V SINGLE AND MULTI-JUNCTION SOLAR CELLS

The theoretical efficiency of a single-junction cell is around 31%. Better efficiencies could be obtained with more-efficient use of the solar spectrum. Combining two or more

cells of different bandgaps into a multi-junction arrangement increases the amount of work done per photon. To increase the efficiency, tandem cells having a larger number of materials with different band gaps are constructed. In case of space power applications, the Si cell efficiency is low and susceptible to radiation damage. In the late 1980s, GaAs cells were used to fabricate flat-plate arrays due to high efficiencies and lower radiation-induced degradation than Si cells. Enhanced efficiencies may be realized by stacking GaAs on booster cells of lower-band gap materials such as Si, Ge, CIS, GaSb, or InGaAs. However, in this case, GaAs films contain dislocations and impurity diffusion from highly doped tunnel junctions during overgrowth of the top cell, increases the resistivity of the tunnel junction. The InGaP/InGaAs/Ge triple-junction concentrator solar cell has demonstrated ~37.0% efficiency. High conversion efficiency of more than 36% is measured under concentrated light with a concentration ratio ranging from 30 suns to 200 suns of AM1.5G. At a concentration ratio of 200 suns of AM1.5G, the conversion efficiency was measured at 37.4% [18].

## 1.6 NANO PHOTOVOLTAICS

The superior optical, electric and chemical properties of nano materials offer the chance for solar cells to get higher efficiencies. At present, three competing types of nanotechnology are being applied to solar cell development, each classified by material: crystalline semiconductor, polymeric materials and carbon-based nanostructures. Each has different potential applications and different ways of attempting to overcome the cost and efficiency trade-off.

#### 1.6.1 Quantum well solar cells

Competitive costs and performance can be achieved by using quantum wells and quantum dots in crystalline solar cells. The Quantum Well Solar Cell (QWSC) is a novel device with the potential to achieve high efficiency in an alternative approach to tandem or

cascade solar cells [19]. In the simple QWSC, quantum wells of a lower-band gap material are grown within the space-charge region of p–n or p–i–n-structures. Incorporating CdTe quantum wells into Cd<sub>x</sub>Mn<sub>1-x</sub>Te of p–i–n structures has been shown to successfully extend the photo response to longer wavelengths [20]. An AlGaAs/GaAs QWSC also enhances efficiency over comparable AlGaAs cells because of reducing recombination losses [19, 21].

#### 1.6.2 Quantum dot solar cells

Quantum dots (QDs) are nanometer-sized crystallite semiconductors. The advantage of QDs is the ability to tune the absorption threshold simply by choosing the dot diameter. A QD is a granule of a semiconductor material on the nanometer scale and these nanocrystallites behave essentially as a three-dimensional potential well for electrons. By introducing a nano-sized dot into an ordered array within the intrinsic region of a p-i-n solar cell [22], a theoretical efficiency of 63% was calculated.

Quantum dots are commonly known as "artificial atoms" because they provide the opportunity to control the energy of carrier states by adjusting the confinements in all three spatial dimensions. With QDs closely packed, the confined levels overlap to form minibands in QD superlattices. This extends the range of electronic and optical properties that can be provided by semiconductor materials. With the control of miniband energy level and bandwidth, QD superlattices have interesting possible applications in "third-generation" PV, especially for tandem solar cells. QDs have already been used successfully to improve the performance of devices such as lasers, light-emitting diodes and photo detectors.

The basic principle behind the efficiency increase offered by QD intermediate-band solar cells is that the discrete states that result from the inclusion of the dots allow for absorption of sub-band gap energies. The reason that this approach can exceed the efficiency

of an ordinary dual-junction cell is that when the current is extracted, it is limited by the host band gap and not the individual photon energies. In a dual-junction solar cell, the current must be "matched" between the two junctions. This means the same amount of current must be passed through both junctions. Therefore, the overall device efficiency is limited by the current-generating ability of the weaker of the two junctions.

In addition, if a dual-junction or other multijunction device is grown monolithically, with the junctions connected in series, then there must be tunnel junctions grown between the various active regions. Problems with lattice mismatch and the increased number of interfaces (and consequently, interfacial defects) are impediments to this approach. Although tremendous achievements have been made in developing multi-junction solar cells, this problem will be compounded with increasing the number of junctions. These problems with lattice mismatch and interfacial defects have plagued the development of multiple quantum well structures.

#### 1.7 RECENT THIN FILM MARKET

Currently, as thin film solar cell technology reaches large industrial-scale production, it is crucial for further growth to adopt processing measures, that are low-cost, contaminant-free and industrially applicable. In 2013, the solar market share for all thin film solar cells technology was 11% with n-CdS/p-CdTe hetero junction solar cells leading the annual production by 2 GWp (Gigawatt peak). The solar PV share for thin film solar cells is expected to grow at an annual rate of 24%, reaching 22 GW by the end of 2020 [23]. In the past, chemical bath deposited (CBD)-CdS regularly featured as a buffer material in CIGS- and CdTe-based solar cells, yielding maximum energy conversion efficiencies up to 21.7% [24] and 21.5% [25] respectively. However, from an environmental/health/economic standpoint, scientists are seeking a buffer material (for example, SnS/SnSe), which can serve as an alternative to hazardous CdS, in order to reduce or eliminate its environmental impact

[26,27] consequently, avoiding climate change and human health-risks, which potentially poses risk to the economy. In addition, because of the prohibition of toxic cadmium (Cd) and increase in stringent legislation relating to its use and disposal, several countries are holding restrictions upon solar PV market share for Cd-containing solar cells [28]. This opens the gates for In<sub>2</sub>S<sub>3</sub> to enter the thin film solar cells technology market. Although some reservations have surfaced regarding the availability and high price of indium (In), the primary annual reported production of In in 2011 was 550–650 MT (Metric Tons) [29]. According to Indium Corporation, Indium (In) is quite abundant in the crust of the earth and there is enough available to meet the present and future needs. In is more abundant than silver (Ag), which has annual production of about 20,000 MT, nearly 40 times more than that of In. The currently-observed price fluctuations are primarily due to a time lag between emerging demand and available supply [30].

#### 1.8 THIN-FILM METAL CHALCOGENIDE SOLAR CELLS

Chalcogenide-based thin-film solar cells provide a critical pathway to replace the Sibased solar cells. A typical metal chalcogenide polycrystalline thin film was comprised of a thin layer on top as "window" layer and an absorbing layer. The window layer lets most of the light through the interface to the absorbing layer and the absorbing layer has a high absorption to be effective in the generation of current and a suitable band gap to provide good voltage. The double-layer structure makes it more efficient to create an electric field at an interface between two different metal chalcogenide semiconductor materials, known as a heterojunction. Lots of metal chalcogenides-based thin-film solar cells have been proposed [31–37], but until now, only CdTe and Cu(In,Ga)(S,Se)<sub>2</sub>(CIGS) technologies have reached commercial module production with stable power conversion efficiencies of over 9% [38,39]. Cu(In<sub>1-x</sub>Ga<sub>x</sub>)(S,Se)<sub>2</sub>(CIGSSe) and CdTe solar cells are already in production with record cell efficiencies of 20.3% and 17.3% [39,40], respectively, while

their commercial modules correspondingly reach efficiencies as high as 15.7% and 13.5% respectively [41]. Photovoltaic conversion efficiency of 4% reported in 2014 for thin film solar cell of tin sulfide (SnS) deposited by Atomic Layer Deposition testifies to the prospect of SnS as a promising absorber material [42]. It may be improved by fabrication methods.

#### 1.8.1 IV-VI Semiconductor solar cells

Recent efforts were made on IV-VI semiconductors (SnS, SnSe, SnTe, GeS, GeSe, PbS and PbSe) for their applications towards photovoltaic devices. Lead chalcogenide (PbS and PbSe) semiconductors were the first of the IV-VI class of semiconductor to receive experimental interest as practical PV materials and it have been explored as potential earth abundant active layers in PV devices. The importance of exploring alternative semiconductor materials that are less toxic, but have been otherwise similar properties to the lead chalcogenides, tin and germanium metal chalcogenides are less toxic than the lead chalcogenides and also they are alternative targets as the photo absorbant material in photovoltaic [43].

In recent years, a great deal of attention is paid to tin based thin films because of their applications in solar cells and optoelectronic devices. SnS thin films have suitable electro-optical properties for photovoltaic applications [44, 45]. It exhibits p-type electrical conduction [46] and orthorhombic crystal structure with high absorption coefficient (>10<sup>4</sup> cm<sup>-1</sup>) [47,48]. These properties make it as a suitable 'absorber' layer material in the fabrication of thin-film heterojunction solar cells. In addition, the elemental constituents of this material are cheap, non-toxic and abundant in nature.

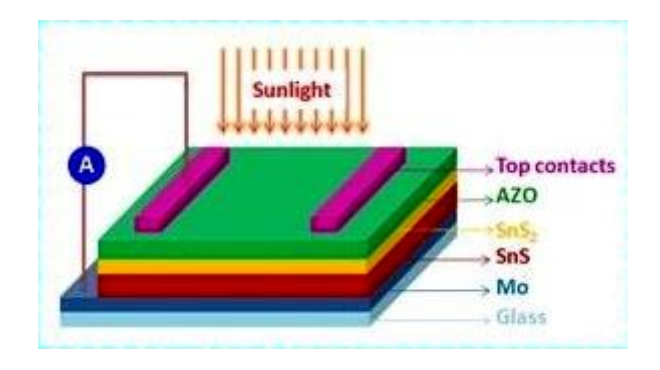


Fig. 1.5 SnS based solar cell

Fig. 1.5 shows SnS-based thin film solar cell, fabricated with a glass/Mo/p-SnS/n-SnS<sub>2</sub>/Aluminum doped Zinc Oxide (AZO)/Ag structure using optimized chemical bath deposited SnS and SnS<sub>2</sub> as absorber and buffer layer respectively.

SnSe is a narrow band gap binary IV–VI semiconductor exhibiting anisotropic character. Tin selenide exists as a layered compound with an orthorhombic crystal structure. Motivated by the potential applications of tin chalcogenides, investigations of these compounds are becoming particularly active in the field of materials chemistry.

Among IV–VI ternary compounds, Tin sulfo selenide (SnSSe) compound has recently attracted much interest in solar energy conversion because of the bandgap tailoring effect by the incorporation of sulfur (S) in tin selenide (SnSe) [49–51].

### 1.9 ROLE OF SnS/SnSe IN THIN FILM SOLAR CELLS

In this scenario, tin-based binary semiconductors, such as SnS and SnSe are expected to play a crucial role in solar cell technologies in the near future owing to their relatively earth-abundance, non-toxic nature and easy controllability of stoichiometry Fig. 1.6. On the other hand, tin-based nanomaterials have also been used in various fields such as photoelectrochemical [52], heat transfer fluids [53], hydrogen generation [54], hydrogen sensing [55] and Li-ion battery electrodes [56]. Moreover, the annual production of tin, sulfur and

selenium is large (at lower price) compared to other absorber elements [57]. In addition, the binary SnS and SnSe materials possess the required band gaps (close to optimum spectral region) for the efficient collection of solar radiation. These materials exhibit favourable properties, such as high chemical stability, suitable band gap (1.0 eV-1.5 eV) and high absorption coefficient (~10<sup>5</sup> cm<sup>-1</sup>) with p-type conductivity [58-61] and they show a maximum theoretical efficiency of 33% [2].

Therefore, these materials have great potential to replace the toxic CdTe and scarce elements based (CIGS) absorbers in photovoltaic devices. On the other hand, the solar cells fabricated from these materials (SnS and SnSe) currently exhibited lower efficiencies (≤1% by non-vacuum methods and <5% by vacuum methods) than CIGS and CZTS solar cells. The lower efficiency has been attributed to the lack of precise control over the pure phase formation and fine-tuning of the band gap by the adopted technology. In thermal methods, owing to high volatility of sulfur, it is very difficult to maintain the 1:1 ratio of Sn:S. The sulfur deficiency can lead to the tin migration to grain boundaries, surfaces, interfaces, interstitial sites, or sulfur anti-sites. In addition, the problem of a good heterojunction partner has not been fully rectified. All the aforesaid issues can strongly influence the recombination losses at the device level [62].

In addition, the added advantages of solution-based approaches are the low energy consumption, relatively high throughput, high material utilization and easy industrialization. The recent world record efficiency of 12.6% in CZTSSe by a hydrazine pure-solution approach is proof of the competence of solution growth techniques [63]. Therefore, the synthesis of tin- based binary SnS and SnSe nanoparticles form the solution- phase along with their solar cell fabrication is an important and timely issue. Therefore, the nanoparticle based approaches of SnSe and SnS absorbers are expected to lead in the PVs market with a considerable decrease in the weight, cost and other architectural issues.

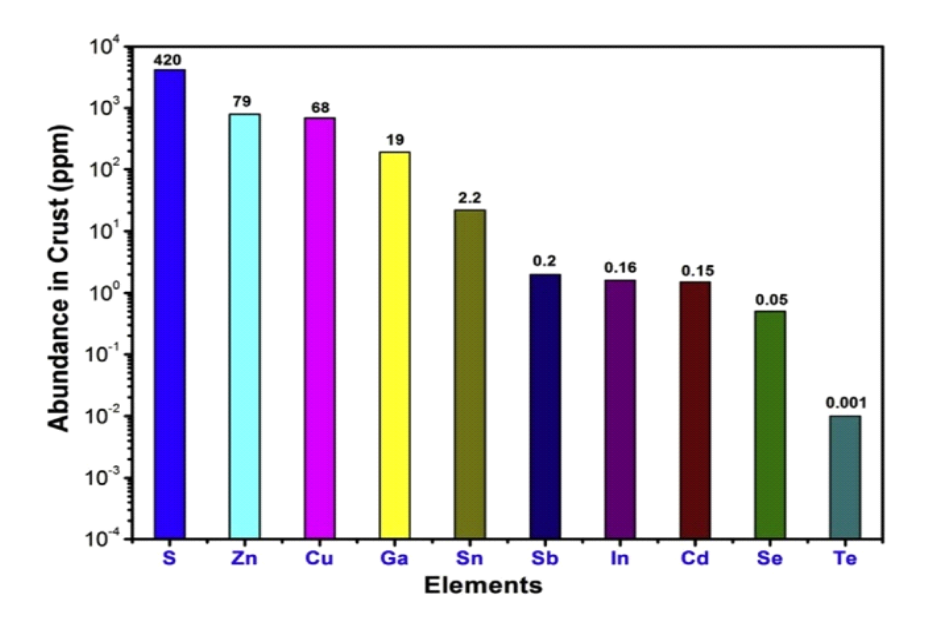


Fig. 1.6 Earth-abundance of elements for absorber materials such as SnS(Se) CZTS(Se), CIGS(Se), Sb<sub>2</sub>S<sub>3</sub>(Se<sub>3</sub>) and CdTe based solar cell[64]

# 1.10 ROLE OF SnSSe IN PHOTO ELECTRO CHEMICAL (PEC) SOLAR CELLS

In the last few years much attention has been given for investigating potential materials for device fabrication in solar to electrical energy conversion systems. A high degree of sophistication has already been achieved in the fabrication of p—n junction solar cells, but in 1970s, an alternative way was suggested in which a solid—liquid junction was used. Semiconductor liquid junction solar cells have been attracting a great deal of attention during last few years due to growing interest in solar energy conversion. Comparing solid—solid junction of conventional solar cells, a semiconductor electrode dipped in a suitable liquid electrolyte provides the necessary charge transfer, a redox ionic species being used to obtain photo voltage / photo current, which has in-built storage capability after a little modification. Semiconductor electrolyte interface may be used for photoelectrolysis, photocatalysis and photoelectrochemical (PEC) power conversion [65-69]. The ternary chalcogenide materials have been studied for the development of photoelectrochemical solar cells for the sustained and efficient capture of solar energy conversion. SnSSe ternary

compound has recently attracted much interest in solar energy conversion because of the band gap tailoring effected by the incorporation of sulfur (S) in tin selenide (SnSe). Structural properties of the material play a dominant role in the performance of the devices and knowledge of the influence of various deposition parameters on the structural properties of thin films is essential before the application of this material in devices [70–72]. Cathodic deposition of SnSSe thin films on tin oxide coated conducting glass substrates have been carried out potentiostatically under various deposition potentials. The direct bandgap energy is estimated to be 1.08 eV and the films are found to be very good application in opto-electronic devices. The value of refractive index and extinction coefficient are found to be 2.65 and 0.037, respectively, for optimized condition. Complex dielectric constants and optical conductivity of the SnSSe thin films are calculated. The surface is observed to be smooth, uniform and pellet shaped grains for films obtained at deposition potential of -900 mV versus saturated calomel electrode(SCE). Semiconductors with a bandgap of 1.08 eV have appropriate optical characteristics suitable for use in diversified applications [73]. SnSSe thin films were electrosyntheized from an aqueous solution by potentio-static method. A direct bandgap in SnSSe thin films are found to be in the range of 1.08–1.25 eV. The blue emission luminescence peak was observed at 460 nm for SnSSe film [74]. Thin films of tin sulfoselenide have been electrodeposited from an aqueous solution on tin oxide coated glass substrates by potentiostatic technique. The photoelectrochemical behavior of the film was studied in the electrolyte method. Optical studies revealed the indirect transistion nature of the films. It could be a promising candidate for photoelectrochemical solar cell if the efficiency is improved [75].

### 1.11 MOTIVATION FOR THE PRESENT WORK

Among the several p-type semi conductor materials, it has been observed that SnS is the most promising hetero junction partner for the well known polycrystalline photovoltaic materials. SnS layer is used as an absorber material. As the world of thin film solar cells started to look forward indium sulfide as the future buffer layer and potential competent to SnS, reservations have surfaced on the availability and the inflated price of indium.

For large area, thin film device fabrication becomes complex and requires proper control over the entire process sequence. Proper understanding of thin film deposition processes can help in achieving high efficiency (more than 20 %) devices. Owing to that, a new deposition technique such as Nebulized Chemical Spray Pyrolysis (NSP) technique have been initiated to prepare SnS and SnSe thin films. Such cheap and moderately efficient thin film solar cells are expected to receive a due commercial place under the sun.

In the present study, Tin sulfide (SnS) and Tin Selenide (SnSe) thin films were prepared by this simple NSP technique which is benefited by low production cost. The structural, morphological, elemental, optical and electrical conductivity properties of the asdeposited films were investigated and analyzed. This deep analysis of SnS and SnSe thin films using NSP technique may be used to improve the efficiency of solar cell.

### **REFERENCES**

[1] K. Zweibel, J. Poortmans, V. Archipov (Eds.), Thin Film Solar Cells: Fabrication, Characterization and Application. John Wiley, (2005) pp. 18.

- [2] W. Shockley, H.J. Queisser, J. Appl. Phys. 32 (1961) 510.
- [3] A. De Vos, B. Desoete, Sol. Energy Mater. Sol. Cells 51 (1998) 413.
- [4] M.A. Green, J. Zhao, A. Wang, S.R. Wenhan, Sol. Energy Mater. Sol. Cells 65 (2001) 9.
- [5] D. Carlson, C. Wronski, Appl. Phys. Lett. 28 (1976) 671.
- [6] D.L. Staebler, C.R. Wronski, Appl. Phys. Lett. 31 (1977) 292.
- [7] B. Rech, H. Wagner, Appl. Phys. A 69 (1999) 155.
- [8] S. Guha, Sol. Energy 77 (2004) 887.
- [9] D. Yogi Goswami, Frank Kreith, Energy conversion, second edition, CRC Press, 2017.
- [10] B.E. McCandless, S.S Hegedus, Proc. of the 22th IEEE Photovoltaic Specialists Conference, (1991) 967.
- [11] J. Sterner, Comprehensive Summaries of Uppsala Dissertations from the Faculty of Science and Technology 942 (2004) 14.
- [12] L. Yu, A. Zunger, Phys. Rev. Lett. 108 (2012) 068701.
- [13] P. Sinsermsuksakul, K. Hartman, S. Bok Kim, J. Heo, L. Sun, H. Hejin Park, R. Chakraborty, T. Buonassisi, R.G. Gordon, Appl. Phys. Lett. 102 (2013) 053901.
- [14] K. Ramakrishna Reddy, N. Koteswara Reddy, R. Miles, Sol. Energy Mater. Sol. Cells 90 (2006) 3041.
- [15] K. Hartman, J. Johnson, M.I. Bertoni, D. Recht, M.J. Aziz, M.A. Scarpulla, T. Buonassisi, Thin Solid Films 519 (2011) 7421.
- [16] Z.A. Wang, H.B. Zhu, D.W. Zhang, J.H. Shi, X.D. Li, W.J. Cheng, Z. Sun, S.M. Huang, In: Conference Record of the IEEE Photovoltaic Specialists Conference, Art. No. 5411587 (2009) pp. 000676.
- [17] J. Hedstrom, H. Ohlsen, M. Bodegard, A. Kylner, L. Stolt, D. Hariskos, M. Ruckh, H.W. Schock, The Proceedings of the 23<sup>rd</sup> IEEE Photovoltaic Specialists Conference, New York, (1993) pp. 364.

[18] M. Yamaguchi, T. Takamoto, K. Arak, N. Ekins-Daukes, Sol. Energy 79 (1) (2005) 78.

- [19] K.W.J. Barnham, P. Abbott, I. Ballard, D.B. Bushnell, J.P. Connolly, N.J. Ekins-Daukes, M. Mazzer, J. Nelson, C. Rohr, T.N. Tibbits, R. Airey, G. Hill, J.S. Roberts, Proc. of the 3rd World Conference on Photovoltaic Energy Conversion, VA, (2003) pp. 606.
- [20] D.E. Ashenford, A.W. Dweydare, D. Sands, C.G. Scott, M. Yousaf, E. Aperathitis,Z. Hatzopoulos, P. Panagotatos, J.Cryst. Growth 159 (1995) 920.
- [21] N. Ekins-Daukes, D. Bushnell, J. Zhang, K. Barnham, M. Mazzer, Proc.28th IEEE PV Specialists Conference, USA, (2000)pp. 1273.
- [22] A. Luque, A. Marti, Phys. Review Lett. 78 (14) (1997) 5014.
- [23] L. Wood, Research and markets: Thin-film photovoltaic (PV) cells market analysis to 2020-CIGS (Copper indium gallium diselenide) to emerge as the major technology by 2020, Global business intelligence.
- [24] P. Jackson, D. Hariskos, R. Wuerz, O. Kiowski, A. Bauer, T.M. Friedlmeier, M. Powalla, Phys. Status Solidi RRL 9 (2015) 28.
- [25] First Solar Inc, 2015. First solar achieves 21.5% efficiency, durability milestones. Available at http://investor.firstsolar.com/releasedetail. cfm? Release ID = 895118
- [26] D. Dimova-Malinovska, J. Phys: Conf. Ser. 253 (2010) 1.
- [27] Y. Hamakawa, 2004. Thin-Film Solar Cells: Next Generation Photovoltaics and Its Applications, 2004 ed. Springer Series in Photonics, Berlin, New York.
- [28] Nordic Council of Ministers, 2003. Cadmium review, vol. 4. Availableat http://www.who.int/ifcs/documents/forums/forum5/nmr\_cadmium.pdf
- [29] M. Woodhouse, A. Goodrich, R. Margolis, T.L. James, M. Lokanc., R. Eggert, IEEE J. Photovolt. 3 (2012) 833.
- [30] Gowans, C., 2010. Indium 101—earth abundant material or rare? The Indium Corporation. Available at http://blogs.indium.com/blog/- carol-gowans/indium 101-earth-abundant-material-or-rare
- [31] G. Zoppi, I. Forbes, R. W. Miles, P. J. Dale, J. J. Scragg, L. M. Peter, Prog. Photovolt.: Res. Appl. 17 (2009) 315.
- [32] K. Govender, D. S. Boyle, P. O'Brien, J. Mater. Chem. 13 (2003) 2242.

[33] K. Djessas, S. Yapi, G. Masse, M. Ibannain, J. L. Gauffier, J. Appl. Phys. 95 (2004) 4111.

- [34] J. F. Sa'nchez-Royo, A. Segura, O. Lang, E. Schaar, C. Pettenkofer, W. Jaegermann, L. Roa, A. Chevy, J. Appl. Phys. 90 (2001) 2818.
- [35] V. M. Nikale, C.H. Bhosale, Sol. Energy Mater. Sol. Cells. 82 (2004) 3.
- [36] X.J. Xiong, Y. Xie, G.A. Du, X. B. Tian, J. Mater. Chem. 12 (2002) 98.
- [37] S.L. Castro, S.G. Bailey, R.P. Raffaelle, K.K. Banger, A.F. Hepp, J. Phys. Chem. B. 108 (2004) 12429.
- [38] M.A. Green, K. Emery, Y. Hishikawa, W. Warta, Prog. Photovolt.: Res. Appl.17 (2009) 85.
- [39] D. Butler, Nature. 454 (2008) 558.
- [40] P. Jackson, D. Hariskos, E. Lotter, S. Paetel, R. Wuerz, R. Menner, W. Wischmann, M. Powalla, Prog. Photovoltaics. 19 (2011) 894.
- [41] http://investor.firstsolar.com/releasedetail.cfm?ReleaseID=593994,accessed January 3, 2012.
- [42] Prasert Sinsermsuksakul, Leizhi Sun, Sang Woon Lee, Helen Hejin Park, Sang Bok Kim, Chuanxi Yang, Roy G. Gordon, Adv. Energy Mater. 1400496 (2014) 1.
- [43] Priscilla D. Antunez, Jannise J. Buckley and Richard L. Brutchey, Nanoscale 3 (2011) 2399.
- [44] R.D. Engelken, H.E. Mc Cloud, C. Lee, M. Slayton, H. Ghoreishi, J. Electrochem. Soc. 134 (1987) 2696.
- [45] H. Noguchi, A. Setiyadi, H. Tanamura, T. Nagatomo, O. Omoto, Solar Energy Mater., Solar Cells 35 (1994) 325.
- [46] D. Avallaneda, G. Delgado, M.T.S. Nair, P.K. Nair, Thin Solid Films 515 (2007) 5771.
- [47] N. Koteeswara Reddy, K. Ramesh, R. Ganesan, K.T. Ramakrishna Reddy, K.R. Gunasekhar, E.S.R. Gopal, Appl. Phys. A 83 (2006) 133.
- [48] M. Parenteau, C. Carlone, Phys. Rev. B Conden. Matter. 41 (1990) 5227.
- [49] D. Bhattacharya, S. Chaudhuri, A.K. Pal, S.K. Battacharya, Vacuum 42 (1991) 1113.

[50] R.D. Englken, A.K. Berry, T.P. Van Doren, J. Boone, A. Shahnazary, J. Electrochem. Soc. 133 (1985) 581.

- [51] M.F. Ladd, R.A. Palmer, Structural Determination by X-ray Crystallography, Plenum Press, New York, 1964, p. 71.
- [52] Sabli N, Talib ZA, Hilal HS, Int. J Hydrogen Energy 42 (2015) 4.
- [53] Lorenzin N, Abanades A, Int. J Hydrogen Energy 41 (2016) 6990.
- [54] Radecka M, Wnuk A, Trenczek-Zajac A, Schneider K, Zakrzewska K, Int. J Hydrogen Energy 40 (2015) 841.
- [55] Shen Y, Wang W, Fan A, Wei D, Liu W, Han C, Int. J Hydrogen Energy 40 (2015) 15773.
- [56] Kose H, Dombaycloglu S, Aydın AO, Akbulut H. Int J Hydrogen Energy 41(2016) 9924.
- [57] Peter LM. Philos Trans A Math Phys Eng Sci. 369 (2011) 1840.
- [58] Minnam Reddy VR, Gedi S, Park C, Miles RW, Ramakrishna RR. Curr Appl Phys. 15 (2015) 588.
- [59] Koteeswara Reddy N, Devika M, Gopal ESR. Crit Rev Solid State Mater Sci. 40 (2015) 359. Koteeswara Reddy N, Devika M, Gopal ESR. Crit Rev Solid State Mater Sci. 40 (2015) 359.
- [60] Dhanasekaran, Sundaram, Jung J, Mahalingam. J Mater. Sci. Mater Electron 26 (2015) 1641.
- [61] Minnam Reddy VR, Gedi S, Pejjai B, Park C. J Mater Sci Mater Electron. 27 (2016) 5491.
- [62] Banai RE, Cordell JC, Lindwall G, Tanen NJ, Shang SL, Nasr JR, et al. J Electron Mater. 45 (2016) 499.
- [63] Wang W, Winkler MT, Gunawan O, Gokmen T, Todorov TK, Zhu Y, et al. Adv Energy Mater. 4 (2014)
- [64] https://en.wikipedia.org/wiki/ Abundance of elements in Earth%27s crust
- [65] K.R. Murali, K. Thilagavathy, S. Vasantha, P. Gopalakrishnan, P.R.Oommen, Solar Energy, 84 (2010) 722.
- [66] S. Chandra, R.K. Pandey, Phys. Status Solidi (a), 72 (1982) 415.

- [67] P. Carlsson, B. Holmstro"m, Solar Energy, 36 (1986) 151.
- [68] S. Licht, Electrochem. Soc. Interface, 6 (1997) 34.
- [69] J.M. Gordon, Solar Energy, 40 (1988) 391.
- [70] D. Bhattacharya, S. Chaudhuri, A.K. Pal, S.K. Battacharya, Vacuum 42 (1991) 1113.
- [71] R.D. Englken, A.K. Berry, T.P. Van Doren, J. Boone, A. Shah- nazary, J. Electrochem. Soc. 133 (1985) 5851.
- [72] M.F. Ladd, R.A. Palmer, Structural Determination by X-ray Crystallography (Plenum Press, New York, 1964) 71.
- [73] T. Mahalingam, V. Dhanasekaran, G. Ravi, R. Chandramohan, A. Kathalingam and J. K. Rhee, ECS Transactions 35 (2011) 1.
- [74] V. Dhanasekaran, K. Sundaram, Jongwan Jung, T. Mahalingam, J Mater Sci. Mater Electron 26 (2014) 1.
- [75] B. Subramanian, C. Sanjeeviraja, M. Jayachandran, Materials Research Bulletin 38 (2003) 899.

# CHAPTER - II

# LITERATURE REVIEW OF SnS AND SnSe THIN FILMS

### 2.1 INTRODUCTION

Over the last decades, metal chalcogenide thin films have attained appreciable interest because of their potential applications in many technological fields such as: solar selective coating, photo conductors, solid state and photo electro chemical solar cells, optical imaging, hologram recording, optical mass memories, solar cell devices and photovoltaic electrics [1-4]. Among them SnS has drawn the attention of investigators as a promising candidate for solar absorber layer. It is a simple, non-toxic and low-cost alternative to other ternary and multinary compound semiconductors that are currently being explored for low-cost terrestrial photo voltaic applications. Its band gap (1.3 eV) is close to the ideal bandgap (1.5 eV) for highest photovoltaic conversion efficiency and its optical absorption coefficient is high (>10<sup>4</sup>cm<sup>-1</sup>). The predicted theoretical photovoltaic conversion efficiency was 24% [5]. SnS exhibits both p- and n-type conductivity depending on the concentration of tin [6]. Tin sulfide family (Sn-S) of metalloid glassy chalcogenide semiconductors [7] has recently shown an assuring stand in their possible application in solar cells [8], as catalysts for hydrogen production [9], on lithium micro-batteries and sensors [10-11]. Furthermore, this binary compound facilitates the control on the synthesis compared to the quaternary (Cu<sub>2</sub>ZnSnS<sub>4</sub>) Copper Zinc Tin Sulfide otherwise CZTS [12-17], another promising Cd-free absorber layer candidate.

Tin Selenide is a narrow band gap binary IV-VI semiconductor material. It is thus capable of absorbing a major portion of solar energy hence it is used in fabricating solar cells. It is also suitable for various optoelectronic applications like memory switching

devices, light emitting devices (LED), holographic recording systems among others. Optical and electrical properties of SnSe thin films are dependent on the preparation technique. Thermal evaporation is the most commonly employed method in preparation of thin films because it is very simple, economical and convenient [18]. Moreover, SnSe has higher chemical stability without passivity as compared to other semiconductors, such as Si, InP, GaAs and CdSe, which need special passivity procedures in order to avoid photocorrosion [19]. The bulk properties of SnSe have been analyzed by several researchers and concluded that SnSe belongs to the class of layered semiconductors and it has the indirect band gap of 0.95 eV [20] and direct band gap of 1.21 eV [21]. As SnSe has the energy gap of about 1.0 eV it may be utilized as an efficient material for solar energy conversion [22].

### 2.2 STRUCTURE OF SnS

In 1935, Hoffman invented the crystal structure of SnS as orthorhombic and assigned a = 0.398, b = 0.433 and c = 1.118 nm as lattice parameters of unit cell [23]. In virtual view, structure of SnS is slightly disordered NaCl-type structure since the highly electronegative S atoms draw electron pair from Sn and becomes [Ne]  $3s^2$   $3p^6$  and [Kr]  $4d^{10}$   $5S^2$   $5p^0$ . Further, the nonbonding 5s lone pair electrons of the Sn strongly distort the lattice from a rock-salt structure to distorted orthorhombic layered structure. In these disorder layered structures, each Sn atom (dark-yellow ball) is coordinated by six sulfur atoms (dark ball): three short Sn-S bonds within the layer and three long bonds in adjacent layers as shown in Fig. 2.1. It implies that these layered-structures are connected along c- axis with weak Van der Waal's forces. As a result, the layers of SnS compound can be easily cleaved perpendicular to its c-axis [24].

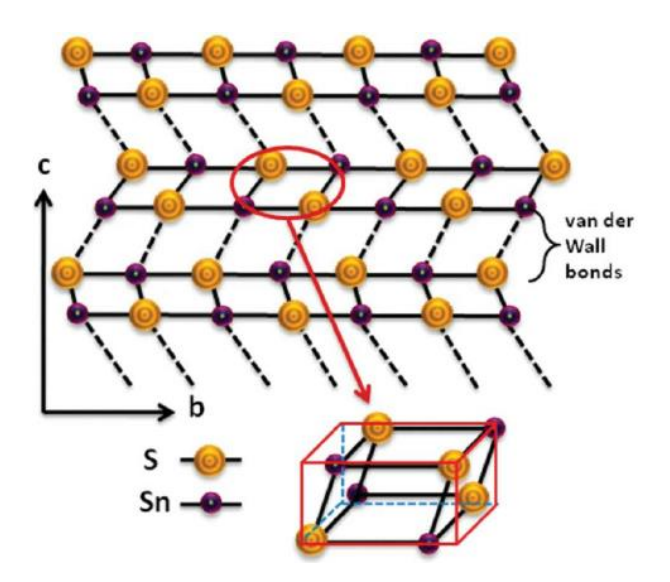


Fig. 2.1 Schematic diagram of double-layered structured SnS

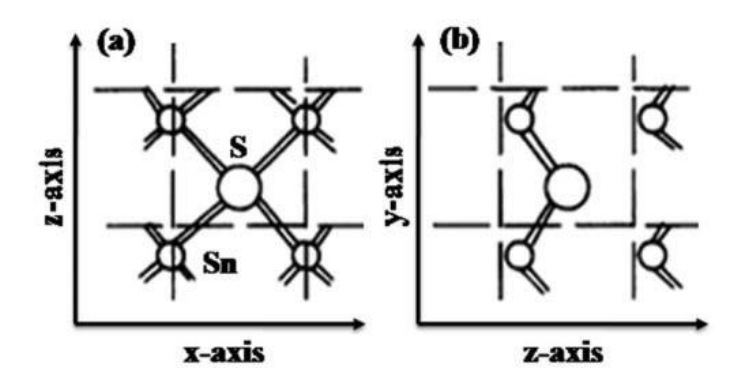


Fig. 2.2 Crystal structure of (a) α-SnS and (b) β-SnS (Strong Sn-S bonds are indicated by lines)

At NTP, the SnS exhibits a stable low-symmetric phase, i.e.,  $\alpha$ -SnS phase. Upon increasing temperature, it undergoes  $\lambda$ -type phase transition to high-symmetric phase, i.e.,  $\beta$ -SnS. In crystallographic view, orthorhombic SnS changes to tetragonal one [25]. The lattice parameters of the tetragonal phase are a=0.423 and c=1.151 nm. The low temperature phase crystallizes in germanium sulfide (GeS) type structure (B16) with the space group  $P_{bnm}$  (D<sup>16</sup><sub>2h</sub>), whereas the higher temperature phase crystallizes in thallium iodide (TII) type structure (B33) with the space group  $C_{mcm}$  (D<sup>17</sup><sub>2h</sub>). Here, the  $P_{bnm}$  (D<sup>16</sup><sub>2h</sub>) is a subgroup of  $C_{mcm}$  (D<sup>17</sup><sub>2h</sub>) of index 2 [26], i.e.,  $P_{bnm}$  retains half of symmetry elements of  $C_{mcm}$ . The phase to  $\beta$  phase transition in SnS is a second-order transition as per the usual

classification [27]. Further, upon transition of  $\alpha$ -phase to  $\beta$ -phase, two stronger bonds in  $\alpha$ -phase changes to four rather weak bonds in the  $\beta$ -phase. At the phase transition temperature (T<sub>c</sub>= 878 K), the axial ratio of lattice-parameter "a" and "c" decreases continuously from a/c > 1 to a/c < 1 [28,29].

In Fig. 2.2 (a) the structure of low-temperature phase (<878 K) consists of slabs with two atoms width. The intra-layer Sn-S bond length perpendicular to the slabs is small (<0.263 nm). However, two of the inter layer Sn-S bonds are shorter and stronger than those of intra-layer bonds and other two bonds are much weaker. Hence, the coordination number of Sn-S atoms is 3 (2+1), which results the  $\alpha$ -phase SnS obtaining a highly distorted octahedral crystal structure [30]. The crystal structures of  $\beta$ -phase SnS is shown in Fig. 2.2 (b) and it appears like NaCl-type slabs [24]. In this case, the Sn atoms are slightly pushed out of the slabs and the interlayer Sn-S bond lengths in the plane of the slabs are equal to 0.296 nm and the intra-layer Sn-S bond length perpendicular to the plane of the slabs is 0.263 nm. These structures have the coordination number of the atoms as 4+1.

#### 2.3 STRUCTURE OF SnSe

SnSe is an orthorhombic crystal with eight atoms per unit cell and lattice parameters a = 4.46, b = 4.19 and c = 11.57 Å [31]. Fig. 2.3 shows, the Sn and Se atoms forming double layers made up of two planes of zigzag Sn-Se chains perpendicular to the longest axis. Each atom has the coordination environment of a heavily distorted octahedron and the lattice can be thought of as a deformed NaCl type [32]. This structure leads to the high Grüneisen parameters, which results in the anharmonic and anisotropic bonding. The ultra low thermal conductivity of orthorhombic SnSe originates from the unique bonding nature of the crystal [33]. Large cubic structured SnSe (SnSe-CUB), which is supposed to be as stable as orthorhombic SnSe, has also been identified in nanocrystalline materials [34] and in thin films [35] recently.

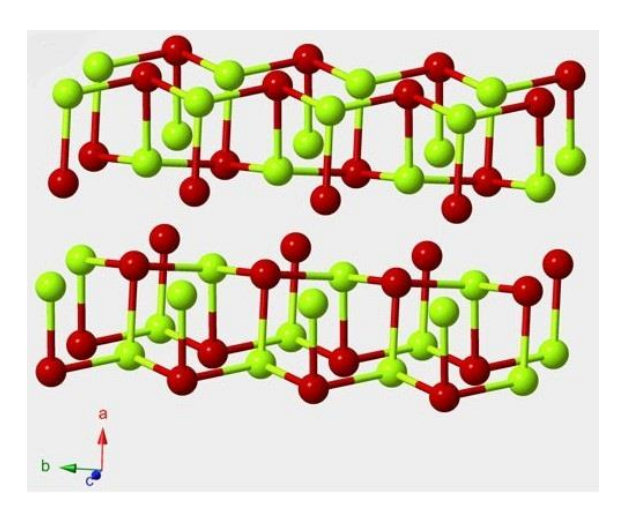


Fig. 2.3 Crystal structures of SnSe

The valence electronic configurations of tin (Sn) and selenium (Se) atoms are 4d<sup>10</sup>5s<sup>2</sup>5p<sup>2</sup> and 4s<sup>2</sup>4p<sup>4</sup>, respectively (for chalcogens it is ns<sup>2</sup>np<sup>4</sup> where n is the periodic number of the element). As the electronegativity of Se atoms is stronger than Sn atoms, Se captures two electrons from the Sn atom which leads to the change in the electronic configuration of Sn from 4d<sup>10</sup>5s<sup>2</sup>5p<sup>2</sup> to 4d<sup>10</sup>5s<sup>2</sup>5p<sup>0</sup> and that of Se to 4s<sup>2</sup>4p<sup>6</sup>[36]. The sp<sup>2</sup> hybridization results in crumpled surface and each atom forms three covalent bonds with the other three atoms [37]. As a result, Sn acquires the oxidation state of II because the two 5p electrons are engaged in bonding while the 5s<sup>2</sup> electrons occupy an inert orbital. However, the Sn(II) lone pair in the electronic structure of Sn(5s) compounds has a great influence on distorting the crystal structure. And the antibonding Sn(5s)-anion p combination, which is created by the interaction of Sn(5s) lone pair and the anion, supports the coupling of Sn(5s) and Sn(5p) leading to an active asymmetric density. From oxygen (O), sulfur (S), selenium (Se) to tellurium (Te), higher valence p states of the anion correspond to less coupling of Sn(5p) and Sn(5s), yielding less active asymmetric density, this decides the distorting level of electronic structure. Consequently, the herzenbergite structure, which does not fit the strong asymmetry on Sn in tin(II) oxide (SnO), adapts well to the Sn in tin sulfide (SnS) and SnSe [38].

## 2.4 LITERATURE SURVEY ON TIN SULFIDE (SnS)

The effects of concentration of tin salt, triethanolamine and bath temperature on the growth of tin sulphide films were systematically investigated by Jayasree et al. [39]. By optimization the bath and deposition temperature to obtain tin monosulphide films. Single phase, polycrystalline SnS films with orthorhombic structure were obtained from a bath with  $[SnCl_2] = 0.10 \text{ M}$ , [TEA] = 1.85 M and [TA] = 0.10 M at room temperature. SnS films with a terminal thickness of 270 nm could be obtained in 3 h in a single step deposition at room temperature. The deposition time is much less than those reported earlier. The Direct optical band gap of SnS films obtained under optimized conditions is found to be 1.50 eV.

Tin sulphide films were prepared by Koteeswara Reddy and Ramakrishna Reddy [40] by spray pyrolysis technique at different precursor concentrations varied in the range, 0.01–0.2 M, keeping other deposition parameters constant. The physical properties of the deposited films were systematically studied in relation to the precursor concentration. The studies indicated that the films grown in the precursor concentration range, 0.09–0.13 M were nearly stoichiometric with the Sn, S ratio of 1.06 and exhibited only SnS phase with a strong (1 1 1) preferred orientation that belongs to the orthorhombic crystal structure. These single-phase films show an average electrical resistivity of 32.9  $\Omega$ cm, Hall mobility of 139 cm<sup>2</sup> V<sup>-1</sup>s<sup>-1</sup>and carrier density of  $\sim 10^{15}$ cm<sup>-3</sup>. These films had an average optical band gap of 1.32 eV with an absorption coefficient greater than  $10^4$ cm<sup>-1</sup>. These properties demonstrated that single-phase SnS films could be used as an absorber layer in the fabrication of heterojunction solar cells.

Safonova et al. [41] studied regularities of chemical bath deposition (CBD) of tin sulphide thin films as function of tin and sulphur concentrations in the solutions. SnS thin films were deposited onto Mo-, ITO- and TO-coated glass and onto borosilicate glass substrates at room temperature for 24 hours. The concentrations of sulphur and tin (ratio

1:1) in the deposition solution were varied from 0.01 M to 0.09 M. Films were characterized by SEM and Raman spectroscopy. The structurally best tin mono-sulphide films with good adhesion to the substrate were deposited at concentration of constituents in solution 0.03 M. The films deposited at concentration of 0.01M had non-uniform and incomplete coverage of the surface on all used substrates whereas at tin and sulphur concentrations of 0.05 M and higher the films were peeling off from the substrate.

Thin films of tin sulphide (SnS) have been grown by sulphurization of sputtered tin precursor layers in a closed chamber by Vasudeva Reddy et al. [42]. The effect of sulphurization temperature (T<sub>s</sub>) that varied in the range of 150-450 °C for a fixed sulphurization time of 120 min on SnS film was studied through various characterization techniques. X-ray photoelectron spectroscopy analysis demonstrated the transformation of metallic tin layers into SnS single phase for T<sub>s</sub> between 300 °C and 350 °C. The X-ray diffraction measurements indicated that all the grown films had the (111) crystal plane as the preferred orientation and exhibited orthorhombic crystal structure. Raman analysis showed modes at 95 cm<sup>-1</sup>, 189 cm<sup>-1</sup> and 218 cm<sup>-1</sup> are related to the Ag mode of SnS. AFM images revealed a granular change in the grain growth with the increase of T<sub>s</sub>. The optical energy band gap values were estimated using the transmittance spectra and found to be varied from 1.2 eV to 1.6 eV with T<sub>s</sub>. The Hall effect measurements showed that all the films were p-type conducting nature and the layers grown at 350 °C showed a low electrical resistivity of 64 Ωcm, a net carrier concentration of 2 x 10<sup>16</sup> cm<sup>-3</sup> and mobility of 41 cm $^2V^{-1}s^{-1}$ . With the use of sprayed Zn $_{0.76}Mg_{0.24}O$  as a buffer layer and the sputtered ZnO:Al as window layer, the SnS based thin film solar cell was developed that showed a conversion efficiency of 2.02%.

Effect of antimony doping on the structural, optical and electrical properties of SnS films deposited by spray pyrolysis technique have been investigated by Santhosh Kumar et

al. **[43]**. The XRD studies indicated that the films were polycrystalline in nature with preferred grain orientation along (111) plane and exhibited an orthorhombic crystal structure. Due to antimony doping, the crystallite size increased from 97 nm to 129 nm. The film transmittance value in the visible region was found to be above 80% and the optical band gap value decreased from 1.60 eV to 1.15 eV as doping concentration was increased. The PL measurement showed a substantial red shift of the band gap, which can be interpreted in terms of band gap modulation due to Sb doping. The optical and electrical studies clearly indicated the presence of Sb into SnS. Hence the observed decreasing optical band gap and the variation in electrical resistivity could be directly attributed to the effect of Sb ion incorporation into SnS lattice. At 6% Sb doping, the film has the lowest resistivity of 2.598 x  $10^{-2}$   $\Omega$ cm while the carrier concentration was high. From the results, the properties of the SnS films can be altered by antimony doping, which may be used in optoelectronic applications.

Jacob A. Andrade-Arvizu et al. [44] reported about the synthesis and characterization of SnS thin films deposited by chemical spray pyrolysis (CSP) under different thermodynamic conditions have been investigated. The results clearly show the role of pressure and substrate temperature on the deposited films in order to get good-quality photosensitive material. Structural analysis showed that the films were polycrystalline with an orthorhombic crystal structure. The SnS layers showed a direction of preferred orientation [DPO] along the [1 1 0] direction with particle sizes in the range of 150–650 nm. An increase in the preferred orientation with an enhanced grain (and crystallite) size was noticed with increasing temperature of substrate temperature. Optical studies revealed a direct optical band gap which is in the range 1.3–1.7 eV and in a direct relationship with crystallite size and substrate temperature. In situ proper growth parameters were optimized in order to engineer the type of electrical conductivity on SnS thin films. Moreover, as the

synthesis temperature and precursor solution are the same for the synthesis of both n and p-type SnS films, it is possible to have sequential synthesis of n and p-type layers for fabrication of SnS homojunction. Finally, it is concluded that the SnS thin films are potential candidates for solar cell applications.

SnS thin films were fabricated by Shahara Banu et al. [45] using two different types of precursors: one was a solution precursor and the other was a liquid precursor. The effects of the annealing temperature and time were also investigated. In the solution precursor-derived film, binary phases such as SnS<sub>2</sub> and SnO<sub>2</sub> always coexisted with SnS in the thin films, even at high temperature (500 °C). However, by using a liquid precursor, single-phase SnS was achieved easily after annealing at 500 °C for 30 min. In particular, the morphology and the crystallinity of the films prepared by the liquid precursor were systematically investigated, focusing on the effects of temperature and time. As the temperature and time increased, the pure SnS phase was formed and secondary phases were suppressed by attaining sufficient thermal energy for the complete reaction of the precursors. In addition, simple methods were used to fabricate the SnS thin films, specifically spin-coating and a subsequent annealing treatment without preheating or additional drying; similar processing routes would be beneficial for cost-efficient solar cell production.

Santhosh Kumar et al. [46] deposited copper doped SnS thin films on microscopic glass substrates by spray pyrolysis technique at the substrate temperature of 350 °C. It was observed that the properties of SnS thin films were improved by copper doping. The PL measurement showed a substantial red-shift of the band gap, which can be interpreted in terms of band gap modulation and a minimum resistivity of 5.94  $\Omega$ cm due to copper doping, which may used in opto-electronics devices.

SnS films with the orthorhombic structure were prepared by chemical bath deposition method. Chao Gao and Honglie Shen [47] investigated the influence of the deposition parameters on the properties of the SnS films. According to our results, the compactness of the SnS films gets worse when the deposition temperature increases, while the compactness of the films gets better when the concentration ratio of Na<sub>2</sub>S<sub>2</sub>O<sub>3</sub>/SnCl<sub>2</sub> increases. The composition of the films (The molar ratio of S/Sn ranges from 46.7:53.3 to 48.9:51.1) is close to the stoichiometric ratio of SnS and the S/Sn ratio in the films increases as the deposition temperature and the Na<sub>2</sub>S<sub>2</sub>O<sub>3</sub>/SnCl<sub>2</sub> ratio increase. The dark conductivities  $(1.15\times10^{-3}~\Omega^{-1}\text{cm}^{-1}$  to  $5.56\times10^{-3}~\Omega^{-1}\text{cm}^{-1}$ ) and photo conductivities  $(5.57\times10^{-3}~\Omega^{-1}\text{cm}^{-1}$  to  $1.88\times10^{-2}~\Omega^{-1}\text{cm}^{-1}$ ) of the SnS films are all increased as the deposition temperature and the Na<sub>2</sub>S<sub>2</sub>O<sub>3</sub>/SnCl<sub>2</sub> ratio increase. The absorption edge of all the SnS films locates in the range of 950 nm to 1200 nm and the optical bandgaps of the SnS films are in the range of 1.01 eV–1.26 eV.

Jacob A. Andrade-Arvizu et al. [48] reported, the synthesis and characterization of SnS thin films deposited by close spaced vapor transport (CSVT) under different thermodynamic conditions (vacuum chamber pressure). P-type, high absorption coefficient ( $\alpha$ >10<sup>4</sup> cm<sup>-1</sup>) and near stochiometrical composition thin SnS films have been deposited by the CSVT technique. Optical studies revealed a direct optical band gap which is in the range 1.68–1.76 eV and in an indirect relationship with crystallite size and vacuum chamber pressure. The results clearly show the role of pressure on the deposited films in order to get good-quality photosensitive material. Structural analyses show that the films are polycrystalline with an orthorhombic crystal structure. The control on the direction of preferred orientation for the SnS micro-crystals as function of the pressure variation could be achieved by this technique. The pressure is determined 3.33 Pa as a transitional stage pressure between two different

DPO's. Finally, it is concluded that the SnS thin films are potential candidates for solar cell applications.

Jeong-yoon Kang et al. [49] obtained in a two-step process for a SnS photovoltaic absorber thin film by sulfurizing a metal Sn precursor with S vapor, the microstructure and crystal orientation of the grown SnS absorber layer could be controlled by inserting a thin seed SnS layer under the Sn layer. While columnar grains containing the (101) orientations were obtained without a seed layer, (040) preferentially oriented SnS equiaxed grains with a high density of grain boundaries were obtained with a 100 nm thick seed layer. This microstructure helped lower the electrical activity of the weakly bonded interlayers in the SnS unit cells, where the b-axis lattice constant was relatively large, resulting in an improved photoelectric conversion efficiency due to the improved shunt resistance.

Ogah E. Ogah et al. [50] used thermal evaporation and showed that it is possible to produce layers of SnS that are several microns thick that are pinhole free conformal to the substrate and that consist of densely packed columnar grains. The stoichiometry of the layers is strongly influenced by the source and substrate temperatures used. The layer becomes increasingly tin-rich with increasing source temperature and with decreasing substrate temperature. The X-ray diffraction data shows that the layers are predominantly SnS (orthorhombic crystal structure) although under some conditions other phases like  $Sn_2S_3$  and  $SnS_2$  are present. The optical absorption edges are consistent with a direct energy bandgap. The energy bandgap is in the range 1.3 to 1.7 eV, the lower values being obtained for film thicknesses >1  $\mu$ m.

A systematic investigation of the effect of annealing temperature on the structural and opto-electrical properties of spray deposited SnS thin films has been presented by Malkeshkumar Patel et al. [51]. SnCl<sub>2</sub>.2H<sub>2</sub>O and thiourea were used for Sn<sup>2+</sup> and S<sup>2-</sup> ion

sources, respectively in the solution without any complexing agent. Following the deposition, films were annealed in a tubular quartz furnace at different temperature in the range of 300–500 °C for 30 min and cooled down to room temperature under flowing Argon atmosphere. The surface morphology and crystallite size were modified by the annealing temperature. Structural characterization revealed nano-crystalline nature of the deposited film. The XRD spectra showed deposited films were orthorhombic-SnS with preferential (111) orientation and better phase purity, which was further improved by increasing annealing temperature to 500 °C. The effect of annealing temperature on the optical and electrical properties of SnS films was also investigated using UV–vis spectroscopy, Photoelectrochemical response and Hall Effect. The increase of annealing temperature up to 500 °C induced a substantial increase in the absorption coefficient and electrical conductivity.

Polivtseva et al. [52] reported that SnS films were grown by the chemical spray containing SnCl<sub>2</sub> and SC(NH<sub>2</sub>)<sub>2</sub> at molar ratios of 1:1 and 1:8 in air at a substrate temperature of pyrolysis method using aqueous solutions at 200 °C. As-deposited films were thermally treated at 450 °C in nitrogen and vacuum atmospheres. All samples were studied using X-ray diffractometry, Raman spectroscopy, energy-dispersive X-ray analysis and ultraviolet–visible spectroscopy. The as-grown film consisted of cubic SnS as the only crystalline phase regardless of the molar ratio of the precursors in the spray solution. Annealing of the 1:1 films in vacuum yielded metallic Sn, whereas annealing in N<sub>2</sub> produced films composed of a mixture of cubic SnS and SnO<sub>2</sub> phases, indicating the presence of oxygen-containing non-crystalline phases in the as-grown films. Thermal treatment of the 1:8 films in nitrogen yielded films composed of Sn<sub>2</sub>S<sub>3</sub>, whereas vacuum annealing produced films consisting of orthorhombic SnS with a bandgap energy of 1.4 eV.

Role of pH of the precursor solution on structural, morphological, electrical and optical properties was investigated by Sajeesh et al. [53] for SnS films prepared using chemical spray pyrolysis technique. From the study revealed that the optimum pH of the precursor solution to obtain device quality SnS thin film is 2. The resistivity of SnS films has been brought down by three orders to  $6\times10^{-2}~\Omega$ cm with considerable enhancement in the crystallinity as well as photosensitivity at this optimum pH. Band gap of the films could also be engineered by controlling the pH of the precursor solution. Arrangement of needle-like grains in the film turns out to be denser and is evident from SEM analysis.

Malkeshkumar Patel et al. [54] found that an optimization in the molar concentration ratio of S<sup>2-</sup>/Sn<sup>2+</sup>precursor used for fabrication of thin film SnS by cheap spray pyrolysis technique would lead to an improved optical, electronic and photoelectrochemical (PEC) properties. The S atomic percentage in the films was found to increase linearly with molar concentration ratio from 1.0 to 2.0. The observed photocurrent in the PEC cell was mixed cathodic and anodic type indicating it as nearly intrinsic in nature. A flat band potential of -0.57 V and a photocurrent of 0.4 mA cm<sup>-2</sup>, were obtained from photoelectrochemical cell for an optimal ratio of 1/1.3. This photocurrent could be further enhanced by the post-annealing process, ex-situ doping and selecting an appropriate electrolyte. It could be inferred that the molar concentration ratio of Sn and S precursors between 1/1.3 and 1/1.4 provides a superior quality SnS thin film on the FTO substrate for application in photoelectrochemical cells.

The tin sulphide films have been grown by spray pyrolysis technique at different substrate temperatures that vary in the range, 100–450 °C and the optical behaviour of the layer was examined by Koteswara Reddy and Ramakrishna Reddy [55] at room temperature. It has been found that the deposited films showed higher absorption coefficient, >10<sup>4</sup> cm<sup>-1</sup> and exhibited a direct allowed transition. The optical band gap of the films varied

significantly with the increase of substrate temperature, which was attributed to the presence of various phases in the layers prepared at such temperatures. The films formed in the substrate temperatures range, 300  $^{\circ}$ C<  $T_s$ < 375  $^{\circ}$ C showed only single phase with an energy band gap of ~1.32 eV. For these single phase layers some of the material parameters such as refractive index, dielectric constant, carrier effective mass, mean free path and concentration were also calculated.

SnS thin films were prepared by Sajeesh et al. [56] using automated chemical spray pyrolysis (CSP) technique. Single-phase, p-type, stoichiometric, SnS films with direct band gap of 1.33 eV and having very high absorption coefficient (>10<sup>5</sup>/cm) were deposited at substrate temperature of 375 °C. The role of substrate temperature in determining the optoelectronic and structural properties of SnS films was established and concentration ratios of anionic and cationic precursor solutions were optimized. n-type SnS samples were also prepared using CSP technique at the same substrate temperature of 375 °C, which facilitates sequential deposition of SnS homojunction. A comprehensive analysis of both types of films was done using x-ray diffraction, energy dispersive x-ray analysis, scanning electron microscopy, atomic force microscopy, optical absorption and electrical measurements. Deposition temperatures required for growth of other binary sulfide phases of tin such as SnS<sub>2</sub>, Sn<sub>2</sub>S<sub>3</sub> were also determined.

Polycrystalline thin films of tin sulphide have been synthesized using spray pyrolysis by Ramakrishna Reddy et al. [57]. The layers grown at a temperature of 350 °C had the orthorhombic crystal structure with a strong (111) preferred orientation. The films had resistivities around 30  $\Omega$ cm with an optical energy band gap (E<sub>g</sub>) of 1.32 eV. Heterojunction solar cells were fabricated using sprayed SnS as the absorber layer and indium doped cadmium sulphide as the window layer and the devices were characterised to evaluate the junction properties as well as the solar cell performance. The current transport across the

junction has been modeled as a combination of tunneling and recombination. The best devices had solar conversion efficiencies of 1.3% with a quantum efficiency of 70%.

Tin sulphide films were grown by Koteeswara Reddy and Ramakrishna Reddy [58] by spray pyrolysis technique at various precursor concentrations varied in the range, 0.01– 0.2 M at a fixed substrate temperature of 350 °C. The compositional analysis of the films indicated that the films formed in the precursor concentration range, 0.09 M \le S stoichiometric while the films grown at other concentrations showed non-stoichiometric nature. The XRD studies of the films demonstrated that the stoichiometric films contain only SnS phase and exhibited orthorhombic structure. These films showed a strong (1 1 1) preferred orientation with an average grain size of 0.35 µm. However, the nonstoichiometric films showed mixed phases with different crystal structures. The evaluated average electrical resistivity, Hall mobility and carrier density of single-phase polycrystalline films are 32.91  $\Omega$ cm, 139 cm<sup>2</sup> V<sup>-1</sup>s<sup>-1</sup> and 1.37 x10<sup>15</sup>cm<sup>-3</sup>, respectively. SnS films showed an average optical energy band gap of ~1.32 eV with a high absorption coefficient, >10<sup>4</sup> cm<sup>-1</sup>. Therefore, the single phase and nearly stoichiometric SnS layers grown at the precursor concentrations of 0.09 M  $\leq$  S<sub>C</sub> $\leq$  0.13 M might be favorable for the fabrication of photovoltaic heterojunction devices as an absorber layer due to its optical band gap and high mobility with considerable electrical resistivity.

SnS thin film was successfully deposited by Guneri et al. [59] onto glass substrates by chemical bath deposition at room temperature for 24 hour. The x-ray diffraction spectrum shows that SnS film is polycrystalline with an orthorhombic structure. According to SEM, the thin film on the substrates had good adherence and free of pinholes. From the EDX result, the film was found nearly stoichiometric. The electrical resistivity of SnS thin film was found to be  $2.53\times10^5\,\Omega$ .cm with a deep impurity level of activation energy of  $0.527\,\text{eV}$ . The direct and indirect energy band gaps of the film were determined as  $1.37\,\text{eV}$  and  $1.05\,$ 

eV, respectively. Due to the suitable direct band gap value for an absorber layer for efficient light absorption, SnS thin films can be used as absorber layer in solar cells.

Microcontroller based home built spray pyrolysis method was used by Jeyaprakash et al. [60] to prepare tin sulfide thin film on glass substrate from the precursor solution containing salts of stannous chloride and thiourea. X-ray diffraction pattern indicates the formation of single phase SnS crystalline material. SEM study shows that the film has spherical shape grains and closely packed together. Optical studies reveal that the film has direct allowed transition with bandgap of 1.35eV. It is concluded that to obtain uniform well adherent spherical grain crystalline SnS film, the substrate temperature is fixed at 300 °C.

Calixto-Rodriguez et al. **[61]** prepared tin sulfide thin films by the spray pyrolysis technique using SnCl<sub>2</sub> and N, N-dimethyl thiourea as the starting materials. Different SnS thin film compounds can be obtained by changing the substrate temperature. In the range of Ts=320–396 °C, the SnS compound with orthorhombic structure and preferential orientation along the (111) direction was obtained. The calculated  $E_g$  values for tin sulfide thin films were ~1.70 eV and it increased to 2.0 eV with the increase of Ts, which may be due to the change of phases from a mixture of SnS-SnS<sub>2</sub> to SnS-SnO<sub>2</sub>The electrical resistivity ( $\rho$ ) for the SnS thin films varied from  $8.2 \times 10^3$  to  $1.9 \times 10^4$   $\Omega$ cm. The  $\rho$  values decreased dramatically when SnS<sub>2</sub>and SnO<sub>2</sub> were the predominant phases,  $\rho$ =7.2 and 0.02  $\Omega$ -cm for films deposited at 455 and 488 °C, respectively, which may be due to the Sn excess. In order to make the SnS thin films suitable for photovoltaic applications the electrical resistivity must be lowered by adequate doping.

SnS thin films were successfully deposited by Ahmed et al. [62] onto glass substrate by spray pyrolysis method. X-ray diffraction spectrum shows that SnS films were polycrystalline with an orthorhombic structure and prefered orientation (111) plane. It is

concluded that to obtain uniform and better crystatallinity SnS film the substrate temperature should be at 350 °C. The influence of substrate temperature on optical properties were investigated and it was revealed that the increase in grain size and decrease in strain led to decrease in band gap (1.6-1.54) eV as substrate temperature increases in the range (200-350) °C. Due to suitable direct band gap value for absorber layer for efficient light absorption, SnS thin film can be used as absorber layer in solar cells.

Hankare et al. [63] deposited tin sulphide thin films by using chemical bath method on non-conducting glass substrate at room temperature. The stannous chloride and sodium thiosulphate pentahydrate are used as source materials to obtain tin sulphide films. The grown films were uniform, well adherent and brown in color. The films were characterized using X-ray diffraction, optical absorption, electrical conductivity measurements and scanning electron microscope techniques. The tin sulphide films showed an optical band gap of 1.0 eV. The films exhibited p-type conductivity with an activation energy of 0.62 eV.

Aarón Gómez et al. [64] prepared good quality SnS thin films by chemical bath deposition. Plasma treatments of these SnS thin films resulted in modification of their optical and electrical properties. Also their morphology was modified as an effect of  $O_2$  plasma treatments, there were modifications in the surface morphologies of the thin films depending on the treatment time. Optical transmittance spectra and band gap values for the plasma treated SnS thin films were evaluated. There was considerable decrease in optical transmittance due to the type of the carrier gas used for plasma treatments. The band gap value was slightly increased after plasma treatments due to the change in the grain size. The conductivity shows a marked increase with the treatment, from  $2.56 \times 10^{-6} \, (\Omega \text{cm})^{-1}$  for asdeposited film until  $0.10 \, (\Omega \text{cm})^{-1}$  for the film treated at 180 min. The results demonstrate the effective use of plasma treatment in modifications of optical and electrical properties of

SnS thin films. Further investigations are in progress to compare the effects of plasma treatments with thermal annealing effects on optoelectronic properties of SnS thin films.

SnS films have been cathodically electrodeposited by Subramanian et al. [65] on tin oxide coated glass substrates from aqueous solution containing SnCl<sub>2</sub> and thiousulphate ions. A nearly stoichiometric SnS films, as evident from XPS studies, were prepared at a deposition potential of -800 mV, keeping the bath pH at 1.5 and maintaining the bath temperature at 65 °C. The films are polycrystalline with orthorhombic structure and show p-type semiconducting nature. Annealing in vacuum at 250 °C for 30 min showed improved crystallinity and increased grain size as observed from the SEM and XRD analyses. Optical measurements revealed the indirect nature of the films. A photoelectrochemical conversion efficiency of 0.54% is obtained for the system using p-SnS as photocathode.

SnS films have been electrodeposited on ITO/glass and Ti substrates from aqueous solution containing SnCl<sub>2</sub> and thiosulphate ions at room temperature by Zulkamain Zainal et al. [66]. The deposited film at 0.7 V versus SCE appeared to be smooth and SEM images revealed that they are comprised of grains of fibrils or worm like structures. The films exhibited indirect transition bandgaps around 0.9 to 1.1 eV and showed rectifying behaviour in the polarization regime of p-type semiconduction when illuminated by light. X-ray diffraction patterns indicated that they are polycrystalline with two major peaks attributed to SnS as (101) and (111) planes of herzenbergite crystal structure. The SnS films obtained are stoichiometric as confirmed by EDAX and XPS analysis.

Naoya Sato et al. [67] deposited SnS thin films on ITO substrates from an aqueous solution containing  $SnSO_4$  and  $Na_2S_2O_3$  by electrochemical deposition (ECD) method. First, the  $V_{off}$  value of pulse voltage condition was optimized from observation of the adhesion to substrate, surface morphology and crystallinity. Au and In electrodes on SnS show ohmic

characteristics while Al electrode shows Schottky-type character. The activation energy  $E_a$  of resistivity of SnS was estimated to be about 0.05 eV in a temperature range of 190–250 K. From the result of PEC measurements, the SnS thin film exhibited photoconducting behavior under the cathodic bias, which is characteristic of p-type semiconductors.

Shuying Cheng et al. **[68]** prepared SnS films on the ITO glass substrates by constant current cathodic electro-deposition. By investigating the influence of deposition parameters on the composition of the deposited films, the deposition parameters with pH=2.7,  $\text{Sn}^{2+}/\text{S}_2\text{O}_3^{2-}=1/5$ , J=3.0 mA/cm<sup>2</sup> and t=1.5 hour. The stoichiometric SnS films with Sn/S between 0.98 and 1.02 were prepared and the experiments had good reproducibility. The films are polycrystalline with orthorhombic structure. Their direct energy gaps are between 1.21 and 1.42 eV. The films have p-type conductivity with a resistivity of 7.5~20  $\Omega$ cm. Therefore, the SnS films are suitable for absorber layers in solar cells.

The SnS:Ag thin films were deposited on glass substrates using thermal evaporation technique and post-annealing, and effect of annealing on the films was investigated byHong-Jie Jia et al. [69]. The above results indicate that appropriate annealing temperature can increase the grain size of the films, improve the uniformity and crystallization of the films, decrease the resistivities of the films and increase the absorption coefficients of the films. However, if the annealing temperature is higher than 300 °C, crystallization of the films become weaker and the films can be oxidized due to low vacuum, thereby electrical and optical properties of the films become poor. At an annealing temperature of 260 °C, the SnS: Ag films have the best properties and the direct bandgap is 1.3eV, the carrier concentration is up to  $1.132 \times 10^{17}$  cm<sup>-3</sup> and the resistivity is about  $3.1~\Omega$ cm.

To find the optimal parameters for the deposition of  $Sn_xS_y$  films three sets of experiments were carried out by Fadavieslam et al. [70]. The substrate temperature, volume and rate of spray solution were optimized for  $Sn_xS_y$  films that can be used as n or p-type light absorbed semiconductor thin film with a direct band gap suitable for solar cell applications.

SnS films were cathodically electrodeposited by Shuying Cheng et al. [71] on ITO glass substrates from an aqueous solution containing SnSO<sub>4</sub> and Na<sub>2</sub>S<sub>2</sub>O<sub>3</sub> by changing the deposition potential and the bath temperature. The deposited films were characterized with X-ray diffractograms, microstructure, composition analysis and optical measurement. When the bath temperature was kept at 30 °C, by investigating the influence of E (-0.60 to -1.1 V vs SCE) on the deposited films, it was found that the composition ratio Sn/S of the films varied with E, that is, the ratio Sn/S significantly increased and exceeded 1 at E more negative than -0.8 V vs SCE and it significantly decreased and was less than 1 at E more positive than -0.7 V vs SCE. The nearly stoichiometric SnS film was synthesized at an optimum potential value (-0.72 to -0.75 V vs SCE) and it was polycrystalline with orthorhombic structure and it had good uniformity and good adhesion to the substrate. Under the conditions of other experimental parameters keeping at optimum values, the bath temperature has little influence on the composition of the films, but the increase of the temperature improved the crystallinity of the deposit and made the scope of the wavelength of the absorbed light larger.

Mathews et al. [72] presented the results of the post-deposition annealing of SnS thin films in air. Structural studies showed that the film has reasonably good stability up to  $250\,^{\circ}$ C annealing temperature and no phase segregation was observed. However, annealing at higher temperatures resulted in the formation of SnS<sub>2</sub> as a secondary phase. Raman spectra showed characteristic modes of the SnS and evidence of trace amounts of SnS<sub>2</sub> was

observed, which is in agreement with the XRD data. Annealing at 350 °C resulted in an increase in band gap by 0.1 eV, which was interpreted as the oxidation of SnS at higher temperatures forming traces of SnS<sub>2</sub> rather than due to the morphological changes. Dark conductivity of the film increased by one order after annealing at 150 °C; however, annealing at higher temperatures resulted in decrease of photosensitivity due to the formation of secondary phases. The conductivity of the film is controlled by three shallow trap levels with activation energies 0.1, 0.05 and 0.03 eV. Our studies conclude that in order to achieve a noticeable recrystallization for SnS prepared by pulse electrodeposition, annealing temperatures higher than 350 °C are needed; however, instability of the SnS at higher temperatures is an obstacle in high temperature annealing and hence it is necessary to develop alternate technologies such as the use of a fluxing agent which can promote the recrystallization at lower temperatures.

Ichimura et al. [73] deposited SnS on In<sub>2</sub>O<sub>3</sub>-coated glass substrates using electro chemical deposition from aqueous solutions and characterized the deposit chemically, structurally and optically. The composition of the film is slightly Sn-rich and not significantly dependent on the deposition condition, unless the deposition potential is more cathodic than -1.1 V vs. SCE, under which potential the film is highly Sn-rich. XRD results indicate the deposited SnS is polycrystalline and of orthorhombic structure. The direct bandgap is estimated to be 1.3 eV from the optical transmission spectra.

SnS films were deposited on substrates at 300 and 423 K by conventional thermal evaporation technique by Abou Shama and Zeyada [74]. The films deposited at 300 K were amorphous in nature and those deposited at 423 K were partially crystalline. The radial distribution function analysis confirmed the layered structure in amorphous and thermally processed films, it also showed that the coordination number of the cation nearest neighbor to the anion is (1.3 and 3.9) atoms and located at 2.45 and 2.40 Å for amorphous and

thermally processed films, respectively. The electronic dielectric constants were measured by spectrophotometer technique in the wavelength range 250–2500 nm. The lattice dielectric constant of amorphous films increased from 8.84 to 9.68 upon thermal processing, the dispersion energy of amorphous films also increased from 6.76 to 20.28 eV upon thermal processing. The analysis of spectral behavior of dielectric function revealed an indirect forbidden and a direct allowed transitions with energy gaps 1.4 and 2.18 eV for the amorphous films and 1.38 and 2.33 eV for thermally processed films, respectively.

SILAR technique was used by Biswajit Ghosh et al. [75] to deposit SnS thin films onto corning glass substrates and ITO-coated glass substrates. X ray diffraction confirmed the presence of SnS as the dominant phase in the films. SEM images showed the nanometer sized spherical grains well- covered on the surface of the substrate. The optical direct bandgap was obtained as 1.43 eV from the UV-vis spectrophotometry which is slightly higher, for the chemically deposited SnS but close to the optimum (1.50 eV). Photoluminescence properties of SnS on ITO and glass were investigated. A near band edge emission peak at 1.50 eV was observed along with a sharp emission peak at 1.82 eV which may be ascribed due to the defect related recombination.

The p-SnS/n-ITO heterojunction was fabricated by thermal evaporation technique and studied its electrical properties at different temperatures. At all temperatures, the asgrown junction showed a weak rectifying behaviour. However, Devika et al. [76] observed strong influence of bias-voltage and temperature on the junction characteristics. At lower bias-voltages, the p-n junction exhibited a low saturation current in the order of 10<sup>-6</sup> A with a diode quality factor of ~1. However, at higher bias-voltages, we observed a high saturation current and diode quality factor due to the presence of native defect states. Based on existing theories, the current transport mechanism through the junction is distinguished by three types of mechanisms namely tunneling, recombination-tunneling and space-charge-limited

current mechanism depending on applied bias-voltage. While increasing temperature, the diffusion potential of the barrier decreased linearly and the temperature sensitivity coefficient of the junction is found to be  $\sim 1.37$  mV/ $^{\circ}$ C.

SnS films were electro-deposited onto the ITO-coated glass substrates by Shuying Cheng et al. [77]. When  $V_{off}$  is 0.1-0.3 V, the films have good uniformity, density and adhesion and the Sn/S ratio is close to 1/1. All the samples have similar XRD spectra and lattice parameters, it is indicated that  $V_{off}$  has no obvious influence on the structure of the films. The data showed that the primary composition of the deposited films is SnS, but probably there exist tiny S and other compounds. From the optical measurement, the direct band gap  $E_g$  is estimated to be between 1.23 and 1.34 eV with standard deviation within  $\pm 0.03$  eV, which is close to the theoretical value. The SnS films exhibit p-type or n-type conductivity which might be attributed to the stoichiometry of the films and their resistivity was measured to be  $16.8-43.1~\Omega cm$ .

The room temperature electrochemical growth of SnS films on ITO coated glass substrate using simplified two electrode system was done by Biswajit Ghosh et al. [78]. The electrodeposition was carried out at different pH of the bath solution using high purity graphite electrode. SnS films obtained, however, were non-stoichiometric in nature with variation from S-rich to Sn-rich compositions with increase in bath pH. XRD studies indicated that no abrupt change in the crystallographic structure occurred with the variation of Sn-to-S ratio and other impurity phase, i.e. SnS<sub>2</sub> was too little to be detected. Interestingly the bandgaps of all the SnS films would lie within a short range despite the wide variation of the non-stoichiometry, which indirectly established that there has been little or no change in band structure. Furthermore, this paper indicates that it is quite possible for the electrochemical growth of SnS on CdS coated ITO substrate to simplify the heterostructure fabrication technique. However, the photovoltaic effect obtained from this heterostructure

was too low presumably due to the presence of large number of trap states at the interface (which ultimately resulted in lowering the minority carrier diffusion length) and the high sheet resistively of vacuum evaporated CdS.

### 2.5 LITERATURE SURVEY ON TIN SELENIDE (SnSe)

Solanki et al. [79] reported the synthesis of SnSe nanoparticles by chemical precipitation method in deionized water. Chemical composition of grown powder is studied with the help of EDAX. Nanostructures of the prepared SnSe particles have been characterized through XRD, TEM, UV-VIS-NIR spectroscopy techniques. The X-ray diffraction studies indicated the formation of SnSe nanoparticles with orthorhombic phase and average particle size determined by Scherrer's formula has been found to be 9.96 nm suggesting the formation of SnSe quantum dots. The prepared nanostructures have been also analyzed by TEM. The value of the measured optical band gap has been utilized to calculate the particle size (10.13 nm). Dielectric properties of tin selenide nano particles are investigated. It showed strong frequency and temperature dependence of capacitance, dielectric loss, real and imaginary part of dielectric constant over the frequency and temperature ranges of 100 Hz-1 MHz and 300-420 K, respectively.

Multilayer structure of tin Selenide was prepared by Manonmani Parvathi et al. [80] by successive coatings of tin and selenium metals on 423 K glass substrate. The optical study reveals that the films undergone blue shift while decreasing the number of layers. The optical band gap values found to be 2.6-3.2 eV which is much larger than the bulk band gap values of SnSe. The crystalline size varied from 11 to 22 nm observed from X-ray studies. The 2 theta slightly shifted while increasing the number of layers will give the information on potential application of memory devices.

Mahalingam et al. [81] deposited tin selenide (SnSe) thin films onto indium doped tin oxide coated (ITO) glass substrates by electro deposition technique. X-ray diffraction analysis revealed that the polycrystalline nature of SnSe thin films. The deposited films are found to exhibit orthorhombic structure with preferential orientation along (311) plane. The structural parameters crystallite size, strain and dislocation density are estimated and found to depend on bath temperatures. The surface morphology of prepared films was analyzed using SEM. The average size of the grains prepared at bath temperature 80°C is found to be 0.25μm. The direct transition energy band gap was estimated as 1.1 eV.

Tin selenide multilayer thin films were prepared by Manonmani Parvathi et al. [82] by successive evaporation of tin and selenium layers. The X-ray diffraction study reveals that as deposited films (SnSe) have orthorhombic crystal structure while the annealed films (SnSe<sub>2</sub>) have hexagonal structure. The shift in absorption spectra was observed on SnSe<sub>2</sub> films from UV studies. The optical band gap values of SnSe<sub>2</sub> and SnSe are found to be 1.3 eV and 2.8 eV respectively. The emission peaks from room temperature photoluminescence spectra are related with the optical band gap of the films. The room temperature electrical resistivity of SnSe film is found to be higher than SnSe<sub>2</sub> film and the resistivity as a function of temperature has also been studied. The thermal activation energy of the prepared films is found to in the range of 0.52-0.74  $\Omega$ cm.

Makori et al. [83] deposited tin selenide (SnSe) thin films on glass substrate using thermal evaporation method. The thin films prepared had an optical transmittance of range between 0.01- 45% within the visible light region. The optical energy band gap decreased from 1.76 - 1.71 eV with increase in film thickness from 112 nm to 148 nm. The thin films were showing decrease in resistivity from 181-120  $\Omega$ cm with increase in film thickness from 112-148 nm. High absorption coefficients and low transmittance of SnSe thin films indicates that SnSe is appropriate for use as absorber layer in thin film solar cells. Of the five samples

prepared, SnSe thin film of thickness 148 nm is the most appropriate for use in thin film solar cell applications because of its high absorption coefficients and relatively low electrical resistance as compared to other samples.

Kumar et al. **[84]** deposited tin Selenide thin films by thermal evaporation method on glass substrates held at room temperature with varying the film thicknesses from 150 to 500 nm. The structural analysis suggests that the thin films were polycrystalline in nature having preferred orientation in (111) direction. The surface roughness was apparently changed with increase in film thickness. The direct energy band gap calculated from the transmission data were in the range 1.74 to 1.24 eV. The electrical data shows that the SnSe thin film indicating semiconducting behaviour with p-type conductivity. The narrow optical band gap (~1.3 eV) having p-type conductivity indicates its use in photovoltaic applications.

Tin selenide thin films were prepared by Maria sahayaraj et al. [85] by thermal evaporation technique onto room temperature glass substrates. Phase change formation from hexagonal to orthorhombic crystal structure was observed with increasing film thickness. The calculated lattice constants also agreed with the phase change upon increasing film thickness. The calculated crystalline size varied between 6 and 18 nm and the optical band gap varied between 1.9 and 2.3 eV. The room temperature photoluminescence emission centred at around 420 nm indicates the band to band transition of the prepared material. Further, the indication of the phase change even upon increasing film thickness may lead to phase change application with controlled crystallization and melting temperature.

Okoli Donald Nnanyere [86] deposited tin selenide thin films on glass substrate using chemical bath deposition technique at room temperature and at various dip-times. The technique was employed because it is cost effective, reproducible and with it large area of substrate can be coated with the film. The optical characterization performed on the films

show that the films have high absorption coefficient (0.192x10<sup>6</sup>-1.031x10<sup>6</sup>m<sup>-1</sup>), transmittance value (56-76%), optical conductivity (0.58x10<sup>13</sup>-6.47x10<sup>13</sup> S<sup>-1</sup>) and refractive index (2.05-2.55) respectively. The films were also found to exhibit band gap energy in the range of 1.2-1.70 eV and low extinction coefficient value of 0.0092-0.0262. All these desirable properties made the material to be a good candidate for photovoltaic and optoelectronic applications. For instance, the low reflectance value (0.118-0.202) property of the material disposes it for use as anti-reflection coatings for solar cells, displays and contact lenses.

Wenzhong Wang et al. [87] reported that 45 nm SnSe semiconductor was synthesized at 130°C for 5 hour by a solvothermal method. This one-step route was carried out under quite mild conditions. Ethylenediamine was used as the solvent and it mediated the formation of SnSe grain. The as-prepared SnSe was characterized by XRD and TEM. The results revealed that the SnSe grains were spherical and homogeneous; no impurities were detected. This novel method could be extended to synthesize other chalcogenides.

A.C properties of tin selenide thin films prepared by an encapsulated selenization method are investigated. The measurements obtained from Al/SnSe/Al sandwich structures showed strong indication of frequency and temperature dependence of capacitance, dielectric loss and conductance over the ranges of 5-200 kHz and 228-373 K, respectively. Dielectric behaviour was expected to be due to space charge polarization which contributed to a.c conduction. This was generally explained in terms of hopping of the charge carriers between localized states with activation energies 0.03-0.08 eV. Parameters such as trap binding energy (0.94 eV) and minimum hopping distance (1.01 nm) were also predicted by Samsudi Sakrani et al. [88].

The pulse electrodeposition technique has been employed for the first time to deposit SnSe films by Ananthi et al. [89]. SnSe films were deposited by the pulse electrodeposition technique at room temperature from a bath containing Analar grade 50 mM tin chloride (SnCl<sub>4</sub>) and 5 mM SeO<sub>2</sub>. The deposition potential was maintained as - 0.9V (SCE). Tin oxide coated glass substrates (5.0 ohms/ sq) was used as the substrate. The duty cycle was varied in the range of 6-50 %. The XRD profile of SnSe thin films deposited at different duty cycles indicate the peaks corresponding to SnSe. Atomic force microscopy studies indicated that the surface roughness increased from 0.5 nm to 1.5 nm. The transmission spectra exhibited interference fringes. The value of refractive index at 780 nm was 2.1, this value decreased to 1.95 with decrease of duty cycle. The room temperature resistivity increased from 0.1 ohm cm to 10 ohm cm with decrease of duty cycle. Photoelectrochemical cell studies were made using the films deposited at different duty cycles. For duty cycles greater than 15 % photo output was observed. For a film deposited at 50 % duty cycle, an open circuit voltage of 0.55 V and a short circuit current density of 5.0 rnA cm<sup>-2</sup> at 60 mW cm<sup>-2</sup> illumination. Capacitance voltage measurements were carried out, the value of fed back voltage  $V_{fb}$  is 0.67 V (SCE) and p type carrier density is 6.98 x  $10^{16}$  cm<sup>-3</sup>.

Brush plating technique has been adopted for the first time by Subramanian et al. [90] to coat tin selenide thin film on tin oxide coated conducting substrates at room temperature, 501 °C and 601 °C respectively. Uniform and pinhole free films were deposited at a potentials 5.0 V. XRD analysis show the polycrystalline nature of the films with orthorhombic structure. Optical studies show the indirect nature with a bandgap of 1.0 eV. SEM pictures show smooth and uniform surface morphology with a grain size of about 0.3 mm. Film roughness was characterized by atomic force microscopy. Mott–Schottky plot has been drawn to evaluate the semiconductor parameters.

Biljana PejovaandIvan Grozdanov [91] studied a chemical bath deposition method for synthesis of nanocrystalline photoconducting SnSe thin films. The method allows deposition of orthorhombic SnSe quantum dots in thin film form and offers a possibility to control their photoelectrical properties. On the basis of experimental X-ray diffraction data, the basic structural parameters of the deposited and thermally treated materials were calculated using multiple regression analysis. Debye–Scherrer approach was used to calculate the average crystal size in the case of as-deposited and annealed films. The band structure of the investigated semiconducting compound was probed by optical absorption spectroscopic measurements. It was found that the as-deposited SnSe thin films are characterized with indirect band gap energy of 1.20 eV, which decreases to 1.10 eV upon annealing due to average crystal size increase. Besides the indirect one, an additional electronic transition of a direct type was found to occur at 1.74 eV in the case of as-deposited films. The direct band gap energy exhibits a red shift to 1.65 eV upon annealing. These findings were explained in terms of three-dimensional confinement effects in SnSe quantum dots deposited in thin film form.

Preparation of nanocrystalline SnSe thin film and powder has been reported by Deep shikha et al. [92]. SEM micrographs show the uniform distribution of grain size over total coverage of the substrate with a compact and fine grained morphology. Comparison of observed d-values with the standard values confirms orthorhombic structure of SnSe with (410) as preferred orientation in these samples. The average crystallite size for these samples has been calculated as 14.92 nm (powder) and 46.94 nm (thin film). Both the samples are found to be strained which may be due to the surface tension effect. Due to large crystallite size the thin film is less strained than powder. A direct optical band gap of 1.89 eV and 2.14 eV is found for SnSe thin films and powder respectively. The narrow optical band gap of thin film as compared to powder indicates its use in photovoltaic applications. From the

above discussion, it is clear that the samples are nanocrystalline in nature and blue shift in the fundamental edge has been observed, due to the confinement effects arising from reduction in crystalline size.

Zulkarnain Zainal et al. [93] deposited Tin selenide thin films by potentiostatically from an unstirred aqueous solution containing Sn-EDTA and Na<sub>2</sub>SeO<sub>3</sub> onto indium-doped tin oxide glass substrates. The difference in the structural and compositional properties of the film before and after heat treatment in a nitrogen atmosphere were studied. The films were characterised using various techniques such as X-ray diffractometry, scanning electron microscopy and energy-dispersive X-ray analysis. Photoactivity of the samples was studied using linear sweep voltammetry. An annealing temperature of 150°C was found to be the optimum temperature.

SnSe material synthesized at a low temperature from chemical route was confirmed by Indirajith et al. [94] with powder XRD and used to deposit SnSe thin films by thermal evaporation technique at various substrate temperatures. Deposited films were annealed at 450°C under high vacuum (10<sup>-5</sup>) for 30 min. Annealing influences the intensity of XRD peaks of the as deposited samples. The grain size calculated for the annealed SnSe films shows appreciable change from that of the as deposited films. However the crystalline size calculated using (400) peak for the as deposited film at 350°C showed no change due to annealing at 450°C. The SEM image clearly gives the changes in the surface morphology due to annealing. The process of annealing changed the grain size of the crystallites of (400) peak and the band gap values effectively.

A simple thermal evaporation technique to deposit SnSe thin film at different substrate temperatures has been investigated by Kumar et al. [95]. The structural and morphological analysis of the as-deposited films suggests that the thin films were

polycrystalline in nature, having preferred orientation of grains along the (111) direction, and uniform distribution of grains at higher T<sub>s</sub>. The direct energy band gap calculated from transmission data were in the range 1.50-1.18 eV. The high optical absorption in the visible region makes the thin films suitable to be used as semi transparent layer in high-speed detectors working in the visible region and solar cell applications. Activation energy calculated from low temperature resistivity measurements were in the range 0.14 eV-0.28 eV corresponding to shallow donor level near conduction band.

Tin selenide semiconductor films have been potentiostatically deposited onto a tin substrate from an aqueous solution containing SnCl<sub>2</sub> and Na<sub>2</sub>SeO<sub>3</sub>. Deposition at various concentrations was attempted by Zulkarnain Zainal et al. [96] in order to investigate the effect of the electrolytes concentration on the film properties and to determine the optimum bath composition. The structure, morphology and photoactivity of the films were studied using X-ray diffraction, scanning electron microscopy and linear sweep photovoltammetry techniques. The semiconducting property of the deposit is strongly affected by the electrolytes concentration. The optimum bath composition was found to be 0.010 M for SnCl<sub>2</sub> and 0.015 M for Na<sub>2</sub>SeO<sub>3</sub>.

Hema Chandra et al. [97] grown Tin selenide thin films by flash evaporation method at substrate temperatures between 303–513 K at an interval of 30 K. Single phase, nearly stoichiometric and polycrystalline films with strong (4 0 0) orientation exhibiting orthorhombic structure was observed at the substrate temperature of 513 K. The optical absorption studies indicated a direct band gap of 1.26 eV with high absorption coefficient (>10<sup>4</sup> cm<sup>-1</sup>) near the fundamental absorption edge. The films were found to have an electrical resistivity 8.1 Ωcm with p-type conduction.

Resistivity, Hall effect and optical absorption coefficient measurements are performed on SnSe evaporated thin films by DangTranQuan [98]. The resistivity decreases with increasing temperature whereas the Hall mobility and carrier density increase with increasing temperature. An exponential 1/T law is observed for each of these variations. The results are explained in terms of a grain boundary potential barrier mechanism. The optical absorption coefficient is measured at 300 K over the photon energy range 0.8 to 1.3 eV. An analysis of absorption measurements indicates that the SnSe thin film absorption edge is due to allowed direct transitions across an energy gap of about 1.21 eV.

Highly oriented nano-structured SnSe thin films were deposited by R. Indirajith et al. [99] on glass substrates by thermal evaporation technique, from the tin selenide powdered source material synthesized from chemical route for the first time in the literature. XRD studies confirm that the deposited polycrystalline SnSe films belong to the orthorhombic crystal structure with orientation parallel to [100] plane. The average transmittance (1500-2500 nm) of film prepared at 150 °C and 350 °C is 39.5 and 34.4% respectively and the transmittance is well extended to the NIR region. The indirect band gap of SnSe thin films prepared at various substrate temperatures lies in the range of 1.2 - 1.4 eV and the direct band gap values lies in the range of 0.6 - 1.2 eV. SEM studies reveal that SnSe films prepared at various substrate temperatures yielded pores less smooth surface with appreciable changes in the surface morphological features with the substrate temperature. A resistivity of ~2.278 X10<sup>-2</sup> Ωcm, carrier concentration of ~4.53X  $10^{19}$ /cm<sup>3</sup> and conductivity ~43.9/Ωcm were obtained for the films prepared at 450 °C.

Tin selenide thin films were prepared by spray pyrolysis technique using tin (II) chloride and selenourea as a precursor compounds using Se:Sn atomic ratio of 1:1 in the starting solution onto glass substrates by Sharmistha Anwar et al. [100]. Deposition process was carried out in the substrate temperature range of 250-450 °C using 1ml/min flow rate.

The X-ray diffraction patterns suggest that the major phase is hexagonal-SnSe<sub>2</sub> was present when the deposition was carried out in 275-375 °C temperature range, while for the films deposited in the below and above to this range, Sn and Se precipitates into some impure and mixed phase. Raman scattering analysis allowed the assignment of peaks at 180 cm<sup>-1</sup>shows the hexagonal phase. The optical absorption study shows that the direct band gap of the film decreases with increase in substrate temperature and increasing crystallite size. The thermoelectrical measurements have shown n-type conductivity in as deposited films and the magnitude of thermo EMF for films has been found to be increasing with increasing deposition temperature, except for 350 °C sample. 350 °C deposited samples shows enhance thermoelectric value as compared to other samples. Thermoelectric study reveal that although sample deposited between 275 °C and 375 °C sample is thermoelectrically best.

Mariappan et al. [101] were successfully deposited SnSe thin films on glass substrates at temperatures 250 °C, 300 °C, 350 °C and 400 °C using an spray pyrolysis technique. X-ray diffraction analysis confirmed that the deposition SnSe films with an orthorhombic structure. Various structural parameters such as crystallite size, strain, dislocation density are calculated and are found to depend upon various temperatures. The crystallinity of the films increased with increasing temperature from 250 to 350 °C. SEM studies reveal that the SnSe films exhibited uniformly distributed grains over the entire surface of the substrate. The average sizes of the grains are found to be 478 nm. The presence of elemental constituents was confirmed from EDX analysis. Optical transmittance measurements indicate that the deposited films have a direct band gap of 1.08 eV which confirm the formation of well-crystallized SnSe films. The optimized SnSe thin film has higher crystallinity, lower resistivity.

Nano structured tin selenide based ultrathin films have been deposited by Passeri et al. [102] on fused quartz substrates by thermal evaporation. The morphological and

structural properties of the obtained polycrystalline The atomic force acoustic microscopy (AFAM) technique has been used in order to perform a preliminary characterization of the local elastic properties of a film surface. The reported results represent our first attempt to explore the capability of the AFAM technique to discriminate between different phases in such nanostructured compounds.

A simple bath deposition technique for SnSe has been described by Zainal et al. [103]. The technique is simple, economic and requires less monitoring. The SnSe films are uniform and polycrystalline in nature. The preferred orientation lies along the [201] direction. The photoresponse in the cathodic region indicate a p-type semiconductor. The band gap was found to be direct transition in nature and equal to 1.25 eV. The optical absorption in the visible region makes it possible to be used in a photoelectrochemical cell or as semitransparent layer in high speed detectors working in visible region.

Pathinettam padiyan et al. [104] reported Structural, optical, electrical and photoelectrical characteristics of SnSe thin films prepared by vacuum deposition technique have been studied. The deposition parameters are optimised to yield uniform and well adhering films. The as prepared SnSe thin film is found to be poor in crystalline nature and annealing the film at 300 °C for 2 hours improves the crystallinity. Optical studies reveal that SnSe has direct band gap energy of Eg is 1.26 eV and the indirect band gap is improbable. The conductivity measurements show that in the region 158 to 198 K, SnSe exhibits variable range hopping conduction. The steady state photoconductivity studies indicate that there is a continuous distribution of localised states. The photosensitivity increases with increasing illumination level in SnSe thin films. The photo decay process in this vacuum deposited film reveals the presence of deeper localised states and the carrier life time is found to be 1.6 second.

Polycrystalline thin films of p-type SnSe have been successfully deposited by Urmila et al. [105] onto glass substrates under optimized deposition conditions by the reactive evaporation method. The film exhibits a direct allowed transition with an optical band gap of 1.2 eV. The high absorption coefficient and good photosensitivity suggests the potential use of the reactive evaporated SnSe thin films in solar cells. The optical constants, loss factor, quality factor and optical conductivity of the film are evaluated. The variation of electrical conductivity and Seebeck coefficient with temperature reveals the non degenerate semiconducting nature of the film. The results of thermoelectric power and Hall measurements are correlated to deduce important material parameters. The high value of Seebeck coefficient  $\approx 7863~\mu\text{V/K}$ , reasonably good power factor  $7.2 \times 10^{-4}~\text{W/(mK}^2)$  and thermoelectric figure of merit 1.2 observed at 42 K indicates that the prepared SnSe thin film can also be considered as an ideal material for low temperature thermoelectric applications.

SnSe film semiconductor have been successfully electrodeposited by Zulkarnain Zainal et al. [106] on tin substrate from aqueous solution containing SnCl<sub>2</sub> and Na<sub>2</sub>SeO<sub>3</sub> in the presence of EDTA. The as-deposited film at various potentials and different electrolytes concentration ratios showed good photoactivity to the white light and exhibited p-type semiconductor behaviour. X-ray diffraction pattern confirmed that a SnSe polycrystalline with major peaks at 20=30.4°, 31.1° and 38.1° was obtained. The corresponding d-spacing of 2.92, 2.85 and 2.38 Å are indicative that an orthorhombic SnSe structure with (111), (400) and (311) planes was deposited. SEM images reaffirmed the crystallinity of the deposits whose grain size are highly effected by the deposition potential and electrolytes concentrations. Films with smaller grain size proved to have better photosensitivity, may be due to the improved crystal density of the deposit. Deposition potential of -0.85 V versus

Ag/AgCl and concentration ratio of SnCl<sub>2</sub>:Na<sub>2</sub>SeO<sub>3</sub> of 2:3 proved to offer a reasonably good SnSe film semiconductor.

Thin films of n-SnSe have been prepared by the thermal evaporation technique at low partial pressure of Ar gas. A blue shift in the fundamental edge has been observed due to the reduction in the particle size by Sharma et al. [107]. The observed blue shift in the absorption edge may be due to the outcome of confinement effects. Band gap value increases to  $(2.18 \pm 0.01)$  eV as compared to the bulk value  $(1.68 \pm 0.01)$  eV. From the band gap shift, diameter of the nanocrystallites have been calculated and found to be ~ 3 nm. Steady state photoconductivity studies indicate that there is a continuous distribution of localised states. Decay of photocurrent is slow and it is found that the deeper localised states are present in this material.

#### **REFERENCES**

- [1] R.S. Mane, C.D. Lokhande, Mater.Chem.Phys.65 (2000) 1.
- [2] P.M. Sirimanne, Y. Yasaki, N. Sonoyama, T. Sakata, Mater.Chem.Phys.78 (2002) 234.
- [3] M.A.M. Seyam, Vacuum, 63(2001) 441.
- [4] A. Datta, A. Patra, J. Phys. D: Appl. Phys. 42 (2009) 145116 (5pp)
- [5] J.J. Loferski, J. Appl. Phys. 27 (1956) 777.
- [6] K.T. Ramakrishna Reddy, N. Koteswara Reddy, R.W. Miles, Solar Energy Materials & Solar Cells 90 (2006) 3041.
- [7] O. Vigil-Galán, M. Courel, J.A. Andrade-Arvizu, Y. Sanchez, M. Espindola-Rodriguez, E.Saucedo, D. Seuret-Jimenez, M. Titsworth, J. Mater. Sci. Mater. Electron. 26 (2015) 5562.
- [8] H.H. Park, R. Heasley, L. Sun, V. Steinmann, R. Jaramillo, K.Hartman, R. Chakraborty, P.Sinsermsuksakul, D. Chua, T. Buonassisi, R.G. Gordon, Prog. Res. Appl. Photovolt. 23 (2014) 901.
- [9] S.S. Shinde, A. Sami, D.-H. Kim, J.-H. Lee, Chem. Commun., 51 (2015) 15716.
- [10] S. Sohila, M. Rajalakshmi, C. Ghosh, A.K. Arora, C. Muthamizhchelvan, J. Alloys Compd. 509(2011) 5843.
- [11] P. Sinsermsuksakul, Y.H. Jae, N. Wontae, S.H. Adam, R. G. Gordon, Adv. Energy Mater. 1(2011) 1116.
- [12] M. Courel, J.A. Andrade-Arvizu, O. Vigil-Galán, Appl. Phys. Lett. 105 (2014) 233501.
- [13] M. Courel, J.A. Andrade-Arvizu, O. Vigil-Galán, Solid-State Electron 111 (2015) 243.
- [14] V. Rajeshmon, M. Rajesh Menon, C. Sudha Kartha, K. Vijayakumar, J. Anal. Appl. Pyrolysis110 (2014) 448.
- [15] N.M. Shinde, R. Deokate, C. Lokhande, J. Anal. Appl. Pyrolysis 100 (2013) 12.
- [16] K.G. Deepa, N. Jampana, J. Anal. Appl. Pyrolysis 117 (2016) 141.
- [17] S.J. Patil, R.N. Bulakhe, C.D. Lokhande, J. Anal. Appl. Pyrolysis 117 (2016) 310.

- [18] N. Kumar, American Journal of Materials Science 2 (2012) 41.
- [19] N. E. Makori, I. A. Amatalo, P. M. Karimi, W. K. Njoroge, American Journal of Condensed Matter Physics 4 (2014) 87.
- [20] R.D. Engelken, A.K. Berry, T.P. Van Doren, J.L. Boone, A. Shahnazary, J. Electrochem. Soc. 133 (1986) 581.
- [21] K.J. John, B. Pradeep, E. Mathai, J. Mater. Sci. 29 (1994) 1581.
- [22] D.T. Quan, Thin Solid Films 149 (1987) 197.
- [23] W. Hofmann, Crystall. Mater. 92(1935) 161.
- [24] A. R. H. F. Ettema, R. A. Degroot, C. Haas and T. S. Turner, Phys. Rev. B 46 (1992) 7363.
- [25] V. I. Nasirov and K. A. Adgezalova, Inorg. Mater. 37 (2001) 1099.
- [26] Hahn, T. and Paufler, International Tables for Crystallography,vol. A,Space-group symmetry. Reidel, Dordrecht (1983), 291.
- [27] L. D. Landau and E. M. Lifshitz, Statistical Physics, PergamonPress, Oxford (1959), p. 444.
- [28] N. Koteeswara Reddy, M. Devika, M. Prashantha, K. Ramesh, and K. R. Gunasekhar, Eur. Phy. J. Appl. Phys. 60 (2012) 10102.
- [29] T. Chattopadhyay, J. Pannetier and H. G. Vonschnering, J.Phys. Chem. Solids 47(1986) 879.
- [30] H. Wiedemeier, H. G. V. Schnering, Zeitschrift Fur Kristalographie 148 (1978) 295.
- [31] Okazaki A, Ueda I, J Phys Soc Jpn 11(1956) 470.
- [32] Abriksov NKh, Bankina VF, Poretskaya LV, Shelimova LE, Skudnova EV Semiconducting II-VI, IV-VI and V-VI compounds. (1969) Plenum, New York.
- [33] L. D. Zhao, S. H. Lo, Y. Zhang, H. Sun, G. Tan, C. Uher, C. Wolverton, V. P. Dravid, M. G. Kanatzidis, Nature 508(2014) 373.
- [34] R. E. Abutbul, E. Segev, S. Samuha, L. Zeiri, V. Ezersky, G. Makov, Y. Golan, Cryst Eng Comm 18(2016) 1918.
- [35] P. K. Nair, E. Barrios-Salgado, M. T. S. Nair, Phys. Status Solidi A 213 (2016) 2229.

- [36] I. Lefebvre, M. A. Szymanski, J. Olivierfourcade, J. C. Jumas, Phys. Rev. B58 (1998) 1896.
- [37] Q. Wang, W. Yu, X. Fu, C. Qiao, C. Xia, Y. Jia, Phys. Chem. Chem. Phys. 18 (2016) 8158.
- [38] W. Aron, G. W. Watson, J. Phys. Chem. B 109 (2005) 18868.
- [39] Y. Jayasree, U. Chalapathi, P. Uday Bhaskar, V. Sundara Raja, Applied Surface Science 258 (2012) 2732.
- [40] N. Koteeswara Reddy, K.T. Ramakrishna Reddy, Materials Chemistry and Physics 102 (2007) 13.
- [41] M. Safonova, E. Mellikov, V. Mikli, K. Kerm, N. Revathi, O. Volobujeva, Advanced Materials Research 1117 (2015) 183.
- [42] M. Vasudeva Reddy, G. Sreedevi, Chinho Park, R.W. Miles and K. T. Ramakrishna Reddy, Current Applied Physics 15 (2015)588.
- [43] K. Santhosh Kumar, C. Manoharan, S. Dhanapandian, A. Gowri Manohari, Spectrochimica Acta Part A: Molecular and Biomolecular Spectroscopy 115 (2013) 840.
- [44] Jacob A. Andrade-Arvizu1, M. F. García-Sánchez, M. Courel-Piedrahita, F. Pulgarín-Agudelo, E. Santiago-Jaimes, E. Valencia-Resendiz, A. Arce-Plaza, O. Vigil-Galán, J. Anal. Appl. Pyrolysis 121 (2016) 347.
- [45] Shahara Banu, Se Jin Ahn, Young Joo Eo, Jihye Gwak, Ara Cho, Solar Energy 145 (2016) 33.
- [46] K. Santhosh Kumar, A. Gowri Manohari, Chaogang Lou, T. Mahalingam, S. Dhanapandian, Vacuum 128 (2016) 226.
- [47] Chao Gao, Honglie Shen, Thin Solid Films 520 (2012) 3523.
- [48] Jacob A. Andrade-Arvizu, M. F. García-Sánchez, M. Courel-Piedrahita, J. Santoyo-Morales, D. Jiménez-Olarte, M. Albor-Aguilera and O. Vigil-Galána, Materials & Design 110 (2016) 878.
- [49] Jeong-yoon Kang, Soo-Min Kwon, So Hyun Yang, Jung-Hwa Cha, Jin A. Bae, Chan-Wook Jeon, Journal of Alloys and Compounds 711 (2017) 294.
- [50] Ogah E. Ogah, Guillaume Zoppi, Ian Forbes, R.W. Miles, Thin Solid Films 517 (2009) 2485.

- [51] Malkeshkumar Patel, Indrajit Mukhopadhyay, Abhijit Ray, Optical Materials 35 (2013) 1693.
- [52] S. Polivtseva, A. Katerski, E. Kärber, I. Oja Acik, A. Mere, V. Mikli, M. Krunks, Thin Solid Films 633 (2017) 179.
- [53] T.H. Sajeesh, Angel Susan Cherian, C. Sudha Kartha, K.P. Vijayakumar, Energy Procedia 12 (2012) 325.
- [54] Malkeshkumar Patel, Indrajit Mukhopadhyay, Abhijit Ray, Journal of Alloys and Compounds 619 (2015) 458.
- [55] N. Koteeswara Reddy, K.T. Ramakrishna Reddy, Materials Research Bulletin 41 (2006) 414.
- [56] T.H. Sajeesh, Anita R. Warrier, C. Sudha Kartha, K.P. Vijayakumar, Thin Solid Films 518 (2010) 4370.
- [57] K.T. Ramakrishna Reddy, N. Koteswara Reddy, R.W. Miles, Solar Energy Materials & Solar Cells 90 (2006) 3041.
- [58] N. Koteeswara Reddy, K.T. Ramakrishna Reddy, Materials Chemistry and Physics 102 (2007) 13.
- [59] E. Guneri, F. Gode, C. Ulutas, F. Kirmizigul, G. Altindemir, C. Gumus, Chalcogenide Letters 7 (2010) 685.
- [60] B.G. Jeyaprakash, R. Ashok kumar, K.Kesavan, A. Amalarani, Journal of American Science 6 (2010) 22.
- [61] M. Calixto-Rodriguez, H. Martinez, A. Sanchez-Juarez, J. Campos-Alvarez, A. Tiburcio-Silver, M.E. Calixto, Thin Solid Films 517 (2009) 2497.
- [62] S.M. Ahmed, L. A. Latif, A. KH. Salim, Journal of Basrah Researches ((Sciences)) 37(2011) 1.
- [63] P.P. Hankare, A.V. Jadhav, P.A. Chate, K.C. Rathod, P.A. Chavan, S.A. Ingole, Journal of Alloys and Compounds 463 (2008) 581.
- [64] Aarón Gómez, Horacio Martínez, Manuela Calixto-Rodríguez, David Avellaneda, Pedro Guillermo Reyes, Osvaldo Flores, Journal of Materials Science and Engineering B 3 (2013) 352.
- [65] B. Subramanian, C. Sanjeeviraja, M. Jayachandran, Materials Chemistry and Physics 71 (2001) 40.

- [66] Zulkamain Zainal, Mohd Zobir Hussein, Amiza Ghazali, Solar Energy Materials and Solar Cells 40(1996)347.
- [67] Naoya Sato, Masaya Ichimura, Eisuke Arai, Yoshihisa Yamazaki, Solar Energy Materials & Solar Cells 85 (2005) 153.
- [68] Shuying Cheng, Yanqing Chen, Cichang Huang, Guonan Chen, Thin Solid Films 500 (2006) 96.
- [69] Hong-Jie Jia, Shu-Ying Cheng, Xin-Kun Wu, Yong-Li Yang, Natural Science 2(2010)197.
- [70] M. R. Fadavieslam, N. Shahtahmasebi, M. Rezaee-Roknabadi, M. M. Bagheri-Mohagheghi, Journal of Semiconductors, 32 (2011) 1.
- [71] Shuying Cheng, Guonan Chen, Yanqing Chen, Cichang Huang, Optical Materials 29 (2006) 439.
- [72] N.R. Mathews, Colin Garcia, Ildefonso Z. Torres, Materials Science in Semiconductor Processing 16 (2013) 29.
- [73] M. Ichimura, K. Takeuchi, Y. Ono, E. Arai, Thin Solid Films 361 (2000) 98.
- [74] A. Abou Shama, H.M. Zeyada, Optical Materials 24 (2003) 555.
- [75] Biswajit Ghosh, Madhumita Das, Pushan Banerjee, Subrata Das, Applied Surface Science 254 (2008) 6436.
- [76] M. Devika, N. Koteeswara Reddy, K. Ramesh, F. Patolsky, K.R. Gunasekhar, Solid-State Electronics 53 (2009) 630.
- [77] Shuying Cheng, Yanqing Chen, Yingjie He, Guonan Chen, Materials Letters 61 (2007) 1408.
- [78] Biswajit Ghosh, Rajarshi Roy, Sumit Chowdhury, Pushan Banerjee, Subrata Das, Applied Surface Science 256 (2010) 4328.
- [79] Solanki G K, Gosai N N, Patel K D, Research Journal of Chemical Sciences 5 (2015) 1.
- [80] M. Manonmani Parvathi, V. Arivazhagan, A. Mohan, S. Rajesh, AIP Conf. Proc. 1391 (2011) 108.
- [81] T. Mahalingam, V. Dhanasekaran, S. Thanikaikarasan, A. Kathalingam, Jin-Koo Rhee, AIP Conf. Proc. 1447(2012) 631.

- [82] M. Manonmani Parvathi, A. Mohan, V. Arivazhagan and S. Rajesh, AIP Conf. Proc. 1451 (2012) 206.
- [83] N. E. Makori, I. A. Amatalo, P. M. Karimi, W. K. Njoroge, American Journal of Condensed Matter Physics 4 (2014) 87.
- [84] N. Kumar, U. Parihar, R. Kumar, K. J. Patel, C. J. Panchal, N. Padha, American Journal of Materials Science 2 (2012) 41.
- [85] C. A. R. Maria sahayaraj, A. Mohan, V. Arivazhagan, S. Rajesh, Chalcogenide Letters 11 (2014) 47.
- [86] Okoli Donald Nnanyere, Journal of Natural Sciences Research 5 (2015) 124.
- [87] Wenzhong Wang, Yan Geng, Yitai Qian, Cheng Wang, Xianming Liu, Materials Research Bulletin 34 (1999) 403.
- [88] Samsudi Sakrani, Zulkafli Othaman, Karim Deraman, Yussof Wahab, J. Fiz. UTM. 3 (2008) 99.
- [89] K. Ananthi, K. Thilakavathy, S. Dhanapandian, C. Manoharan, K.R. Murali, IEEE (2011) 232.
- [90] B. Subramanian, C. Sanjeeviraja, M. Jayachandran, Journal of Crystal Growth 234 (2002) 421.
- [91] Biljana Pejova, Ivan Grozdanov, Thin Solid Films 515 (2007) 5203.
- [92] Deep shikha, R. P. Chauhan, Jeewan Sharma, Optoelectronics And Advanced Materials 6 (2012) 734.
- [93] Zulkarnain Zainal, Saravanan Nagalingam, Anuar Kassim, Mohd. Zobir Hussein, Wan Mahmood Mat Yunus, Solar Energy Materials & Solar Cells 81 (2004) 261.
- [94] R. Indirajith, M. Rajalakshmi, R. Gopalakrishnan, K. Ramamurthi, Ferroelectrics 413 (2011) 108.
- [95] N. Kumae, V. Sharma, N. Padha, N. M. Shah, M. S. Desai, C. J. Panchal, I. Yu. Protsenko, Cryst. Res. Technol. 45 (2010) 53.
- [96] Zulkarnain Zainal, Ali Jimale Ali, Anuar Kassim, Mohd Zobir Hussein, Solar Energy Materials & Solar Cells 79 (2003) 125.
- [97] G. Hema Chandra, J. Naveen Kumar, N. Madhusudhana Rao, S. Uthanna, Journal of Crystal Growth 306 (2007) 68.

- [98] Dang Tran Quan, Phys. Stat. Sol. 86 (1984) 421.
- [99] R. Indirajith, T.P. Srinivasan, K. Ramamurthi, R. Gopalakrishnan, Current Applied Physics 10 (2010) 1402.
- [100] Sharmistha Anwar, S. Gowthamaraju, B.K. Mishra, S.K. Singh, Shahid Anwar, Materials Chemistry and Physics 153(2015) 236.
- [101] R. Mariappan, M. Ragavendar, G. Gowrisankar, Chalcogenide Letters 7 (2010) 211.
- [102] D. Passeri, M. Rossi, A. Alippi, A. Bettucci, D. Manno, A. Serra, E. Filippo, M. Lucci, I. Davoli, Superlattices and Microstructures 44 (2008) 641.
- [103] Z. Zainal, N. Saravanan, K. Anuar, M.Z. Hussein, W.M.M. Yunus, Materials Science and Engineering B107 (2004) 181.
- [104] D. Pathinettam padiyan, A. Marikani, K. R. Murali, Cryst. Res. Technol. 8 (2000) 949.
- [105] K S Urmila, T A Namitha, J Rajani, R R Philip, B Pradeep, Vol., No. Journal of Semiconductors 37 (9) (2016) 093002-1.
- [106] Zulkarnain Zainal, Ali Jimale Ali, Anuar Kassim, Mohd Zobir Hussein, Malaysian Journal of Analytical Sciences7 (1) (2001) 197.
- [107] J. Sharma, G. Singh, A. Thakur, G. S. S. Saini, N. Goyal, S. K. Tripathi, Journal of Optoelectronics and Advanced Materials 7 (4) (2005) 2085.

# **CHAPTER - III**

# EXPERIMENTAL TECHNIQUES AND CHARACTERIZATION TOOLS

#### 3.1 INTRODUCTION

In this chapter, an introduction to the basic aspects of the thin films growth processes and deposition techniques is described. Afterwards, the characterization techniques like X-ray diffraction (XRD), scanning electron microscopy (SEM), thickness measurements using profilometer, energy dispersive analysis by X-rays (EDAX), Low temperature resistivity, Photoluminescence studies and optical (UV-Vis-Spectrophotometer) properties have been discussed.

# 3.1.1 Basic aspects of thin films

A thin film can be defined as a quasi-two-dimensional material created by condensing, atomic/molecular/ionic species of matter. The fabrication of thin films on a single crystal substrate is done by the deposition of individual atoms. On the other hand thick films can be defined in a different way, as a low-dimensional material created by thinning a three- dimensional material or assembling large clusters/ aggregates/grains of atomic/molecular/ionic species. For making different devices like, electronic devices such as cathode ray tube, color TVs, electroluminescent devices, radiation detectors and laser colours tele projectors [1, 2], photovoltaic devices [3-5], window layer material in tandem solar cells [6, 7], absorber layer material in solar cells [4] and photo detectors [8], thin films have been widely used for more than a half century. There are several techniques available for thin films deposition on a single crystal substrate like thermal evaporation, chemical decomposition and the evaporation of source materials by the irradiation of energetic species or photons.

In general the growth process of thin films exhibits the following features:

- Thin films of all materials created by any deposition technique starts with a random nucleation process followed by nucleation and growth stages
- ii. Nucleation and growth stages are dependent upon various deposition conditions, such as growth temperature, growth rate, the chemistry of the material and the substrate and their structure
- iii. The nucleation stage can be modified significantly by external agencies, such as electron or ion bombardment
- iv. Film microstructure, associated defect structure and film stress depend on the deposition conditions at the nucleation stage
- v. The crystal phase and the orientation of the films are governed by the deposition conditions as well as by the structure of the substrate

Film composition, crystal phase and orientation, film thickness and microstructure, are the basic properties of film and can be controlled by the deposition conditions. Some unique features like quantum size effects, impact of strain, consequence multilayer aspects that cause variety of proximity effects are observed in thin films and cannot be realized in bulk materials.

Thin films have been extensively studied in relation to their applications for making electronic devices. Thin film transistors (TFTs) composed of cadmium sulfide (CdS) semiconducting films in the early sixties and at the end of sixties the bulk Si-MOS (metal-oxide semiconductor) devices were successfully developed. In seventies, different kinds of novel thin-film devices were proposed, including thin-film surface acoustic wave (SAW) devices, integrated thin-film bulk acoustic wave (BAW) devices and thin-film integrated optics. Variety of multi-layered materials including giant magneto resistance (GMR) materials has been developed by using sputtering technology.

## 3.1.2 Thin film growth process

Three major steps constitute thin-film deposition process are, (i) production of the appropriate atomic, molecular, or ionic species, (ii) transport of these species to the substrate through a medium and (iii) condensation on the substrate, either directly or via a chemical and/or electrochemical reaction, to form a solid deposit. The step-by-step growth process is as follows:

- ❖ The unit species, on impacting the substrate, lose their velocity component normal to the substrate (provided the incident energy is not too high) and are physically adsorbed on the substrate surface.
- The adsorbed species are not in thermal equilibrium with the substrate initially and move over the substrate surface. In this process they interact among themselves, forming bigger clusters.
- The clusters or the nuclei are thermodynamically unstable and may tend to desorb in time, depending on the deposition parameters. If the deposition parameters are such that a cluster collides with other adsorbed species before getting desorbed, it starts growing in size. After reaching a certain critical size, the cluster becomes thermodynamically stable and the nucleation barrier is said to have been overcome. This step involving the formation of stable, chemisorbed, critical-sized nuclei is called the nucleation stage.
- ❖ The critical nuclei grow in number as well as in size until a saturation nucleation density is reached. The nucleation density and the average nucleus size depend on a number of parameters such as the energy of the impinging species, the rate of impingement, the activation energies of adsorption, desorption, thermal diffusion and the temperature, topography and chemical nature of the substrate. A nucleus can

grow both parallel to the substrate by surface diffusion of the adsorbed species and perpendicular to it by direct impingement of the incident species. The rate of lateral growth at this stage is much higher than the perpendicular growth. The grown nuclei are called islands.

- The next stage in the process of film formation is the coalescence stage, in which the small islands start coalescing with each other to reduce the substrate surface area. This tendency to form bigger islands is termed agglomeration and is enhanced by increasing the surface mobility of the adsorbed species by increasing the substrate temperature. In some cases, formation of new nuclei may occur on areas freshly exposed as a consequence of coalescence.
- ❖ Larger islands grow together, leaving channels and holes of uncovered substrate.

  The structure of the films at this stage changes from discontinuous island type to porous network type. Filling of the channels and holes results in the formation of a completely continuous film.

Thus statistical process of nucleation, surface-diffusion controlled growth of the three-dimensional nuclei and formation of a network structure and its subsequent filling to give a continuous film, these processes constitute the growth process. Growth stages and the initial nucleation, depends on the thermodynamic parameters of the deposit and the substrate surface, can be categorized as (a) island type, called Volmer-Weber (VW) type, (b) layer type, called Frank-Van der Merwe (FV) type and (c) mixed type, called Stranski-Krastanov (SK) type (Fig. 3.1).

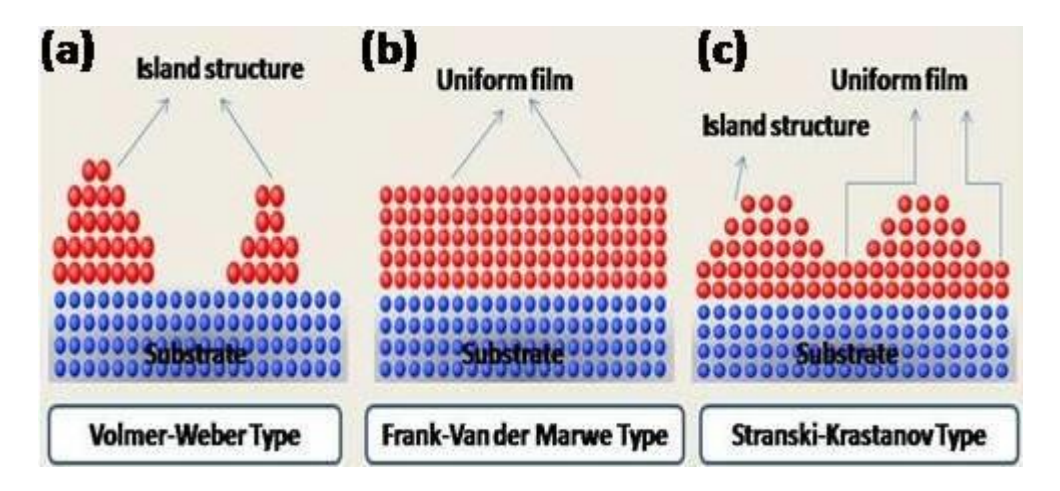


Fig. 3.1 Three modes of thin film growth processes

Island type is the most common growth process, available in almost all practical cases. Except under special conditions, the crystallographic orientations and the topographical details of different islands are randomly distributed, so that when they touch each other during growth, grain boundaries and various point and line defects are incorporated into the film due to mismatch of geometrical configurations and crystallographic orientations.

If the grains are randomly oriented, the films show a ring-type diffraction pattern and are said to be polycrystalline. Even if the orientation of different islands is the same throughout, as obtained under special deposition conditions, on suitable single crystal substrates, a single-crystal film is not obtained. Instead, the film consists of single crystal grains oriented parallel to each other and connected by low-angle grain boundaries. These films show diffraction patterns similar to those of single crystals and are called epitaxial single-crystal films.

## 3.1.3 Thin film growth modes

Thin film growth modes in materials can be characterize in three modes Volmer – Weber (VW) or island growth, Frank–Van der Merwe (FV) or layer-by-layer growth and Stranski–Krastanov (SK) or mixed type growth. These growth mechanisms are shown in Fig. 3.1 and described below one by one.

Volmer–Weber or island growth: Shown in Fig. 3.1 (a) occurs when the smallest stable clusters nucleate on the substrate and grow into three-dimensional island features. One simplistic explanation for this growth behavior is that the atoms or molecules being deposited are more strongly bonded to each other than to the substrate material. This is often the case when the film and substrate are dissimilar materials. There are a few example of such behavior in the growth of oxide films on oxide substrates, but this growth mode is typically observed when metal and semiconductor (i.e., Group IV, III–V, etc.) films are grown on oxide substrates.

Frank–Van der Merwe or layer-by-layer growth: The opposite characteristics of Volmer–Weber or island growth, however, are displayed in Frank–Van der Merwe or layer-by-layer growth (Fig. 3.1 (b)), which occurs when the extension of the smallest nucleus occurs in two dimensions resulting in the formation of planar sheets. In layer-by-layer growth the depositing atoms or molecules are more strongly bonded to the substrate than each other and each layer is progressively less strongly bonded than the previous layer. This effect extends continuously until the bulk bonding strength is reach. A typical example of this is the epitaxial growth of semiconductors and oxide materials. The field of oxide thin film growth has developed around the ability to control materials through this and other similar growth modes. Such capabilities have ushered in an era of unprecedented control of oxide materials down to the single or even half) unit cell level.

Stranski–Krastanov mode: This is the final growth mechanism shown in Fig. 3.1 (c) which is a combination of the layer-by-layer and island growth. In this growth mode, after forming one or more mono layers in a layer-by-layer fashion, continued layer-by-layer growth becomes energetically unfavorable and islands begin to form. This sort of growth is fairly common and has been observed in a number of metal-metal and metal-semiconductor systems. These different growth modes can be described in more detail with simple thermodynamic models for the nucleation and growth of film materials.

In addition to these three well-known classical epitaxial growth modes mentioned above, there are four distinct growth modes: columnar growth, step flow mode, step bunching and screw-island growth (Fig. 3.2).

**Columnar growth mode:** Starting with the Volmer-Weber (VW) growth mode, the column of Individual Island coagulates to form a continuous film. Coalescence of growth islands and columnar growth cause high density of defects (grain boundaries, dislocations, voids, anti phase boundaries, etc.).

**Step flow growth mode:** The Step flow mode is clearly distinct from layer-by layer growth in FV mode. Unidirectional step flow is induced by substrate disorientation (off cut angle). This trick is often used to avoid island formation, their coalescence and following columnar growth in epitaxy from the vapor phase.

**Step bunching growth mode:** Step bunching is observed when a high density of steps moves with large step velocities over the growth surface. By fluctuations, higher steps catch up with lower steps and then move together as double; triple and so on or in general as macro steps that can exceed thickness of thousands of mono steps. The micro steps causes different incorporation rates of impurities and dopants due to locally varying growth rate.

Screw island growth mode: Coalescence of larger number of initial growth islands may lead to screw dislocations due to the layer structure resulting in spiral-island growth mode. This has been observed in the high temperature superconductor thin films. The FV growth mode arises because the atoms of the deposit material are more strongly attracted to the substrate than they are to themselves. In the opposite case, where the deposit atoms are more strongly bound to each other than they are to the substrate, the island, or VW mode results. An intermediate case, the layer-plus-island, or SK growth mode is much more common.

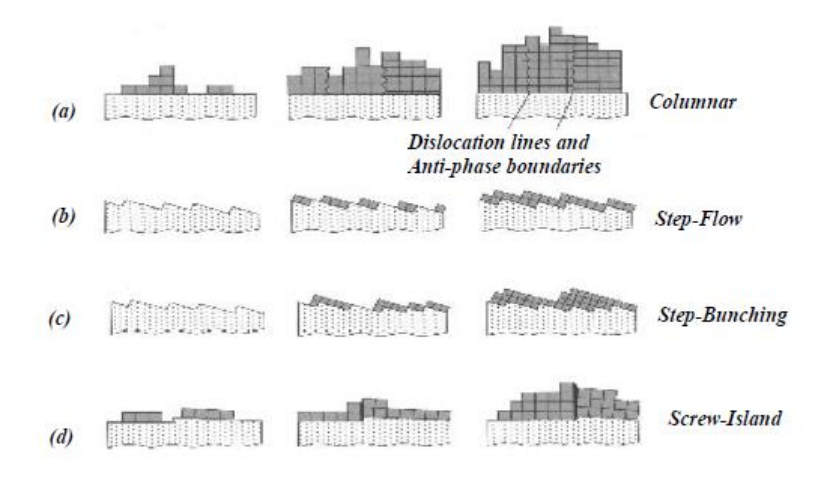


Fig. 3.2 Schematic cross sections of substrate-film, in three successive growth stages, of the four extended growth modes for epitaxial thin film: (a) Columnar-Growth, (b) Step-Flow, (c) Step-Bunching and (d) Screw-Island modes

In almost all practical cases, the growth takes place by island formation. After a continuous film is formed, anisotropic growth takes place normal to the substrate in the form of cylindrical columns. The initial nucleation density determines the lateral grain size, or crystallite size. However, if recrystallization takes place during the coalescence stage, the lateral grain size is larger than the average separation of the initial nuclei and the average number of grains per unit area of the film is less than the initial nucleation density. The grain size normal to the substrate is equal to the film thickness. For thicker films, re-nucleation

takes place at the surface of previously grown grains and each vertical column grows multigranularly with possible deviations from normal growth.

#### 3.2 DIFFERENT THIN FILM DEPOSITION METHODS

Based on the nature of deposition process the methods employed for thin oxide film deposition can be divided into two group i.e. physical and chemical methods. All possible deposition processes are shown in Fig. 3.3 the physical deposition processes include vacuum evaporation, laser ablation, molecular beam epitaxy (MBE) and sputtering. The chemical deposition processes comprise gas phase deposition methods and solution techniques. The gas phase methods are chemical vapour deposition (CVD) and atomic layer epitaxy (ALE), while spray pyrolysis, sol-gel, spin- and dip-coating methods employ precursor solutions.

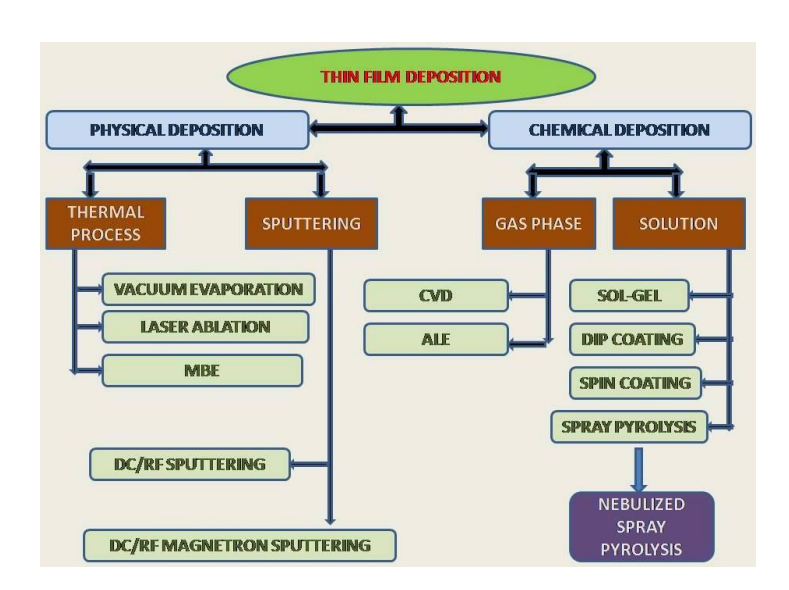


Fig. 3.3 Different physical and chemical thin film deposition processes

Vapour deposition technique describes any process in which a solid immersed in a vapour becomes larger in mass due to transference of material from the vapor onto the solid surface. The deposition is normally carried out in a vacuum chamber to enable control of the vapour composition. If the vapour is created by physical means without a chemical reaction, the process is classified as physical vapour deposition (PVD), if the material

deposited is the product of a chemical reaction; the process is classified as CVD. Many variations of these basic vapour deposition methods have been developed in efforts to balance advantages and disadvantages of various strategies based on the requirements of film purity, structural quality and the rate of growth, temperature constraints and other factors.

PVD is a technique whereby physical processes, such as evaporation, sublimation or ionic impingement on a target, facilitate the transfer of atoms from a solid or molten source onto a substrate. Evaporation and sputtering are the two most widely used PVD methods for depositing films. This section described briefly the chemical vapour deposition processes which are commonly used to grow epitaxial and polycrystalline thin films of transition metal oxides.

#### 3.3 CHEMICAL VAPOUR DEPOSITION

Chemical vapour deposition (CVD) is the process of chemically reacting volatile compound of a material to be deposited, with other gases, to produce a nonvolatile solid that deposits atomistically on a suitably placed substrate. It has emerged one of the powerful techniques of thin film growth. Among the reasons for the growing adoption of CVD methods is the ability to produce a large variety of films and coatings of metals, semiconductors and compounds in a crystalline or vitreous form, possessing high purity and desirable properties. Furthermore, the capability of controllably creating films of widely varying stoichiometry makes CVD unique among deposition techniques. Other advantages include relatively low cost of the equipment and operating expenses, suitability for both batch and semi continuous operation and compatibility with other processing steps.

Hence, many variants of CVD processing have been researched and developed in recent years, including low-pressure (LPCVD), plasma-enhanced (PECVD), metal-organic

(MOCVD) and laser-enhanced (LECVD) chemical vapour deposition. Hybrid processes combining features of both physical and chemical vapour deposition have also emerged. MOCVD has presently assumed considerable importance in the deposition of epitaxial compound semiconductor films. However, the main obstacle of MOCVD for high temperature superconductor (HTSC) and rare earth manganite oxides is the lack of thermally stable precursors. MOCVD technique has been utilized to grow different compositions of thin CMR manganite films.

## 3.3.1 Plasma enhanced chemical vapor deposition

Plasma enhanced chemical vapor deposition (PECVD) is a process by which thin films of various materials can be deposited on substrates at lower temperature than that of standard chemical vapor deposition.

In PECVD processes, deposition is achieved by introducing reactant gases between parallel electrodes - a grounded electrode and an RF-energized electrode. The capacitive coupling between the electrodes excites the reactant gases into plasma, which induces a chemical reaction and results in the reaction product being deposited on the substrate. The substrate, which is placed on the grounded electrode, is typically heated to 250°C to 350°C, depending on the specific film requirements. In comparison, CVD requires 600°C to 800°C. The lower deposition temperatures are critical in many applications where CVD temperatures could damage the devices being fabricated.

The films typically deposited using PECVD are silicon nitride  $(Si_xN_y)$ , silicon dioxide  $(SiO_2)$ , silicon oxy-nitride  $(SiO_xN_y)$ , silicon carbide (SiC) and amorphous silicon  $(\alpha$ -Si). Silane  $(SiH_4)$ , the silicon source gas, is combined with an oxygen source gas to form silicon dioxide or a nitrogen gas source to produce silicon nitride.

Silicon dioxide and silicon nitride are dielectric (insulating) materials commonly used in the fabrication of electronic devices to isolate multiple conductive layers, capacitors and for surface passivation. These films are also used for encapsulation to protect devices from corrosion by atmospheric elements such as moisture and oxygen.

# 3.3.2 Metal-organic chemical vapour deposition

Metal-organic chemical vapour deposition (MOCVD) is of great importance for large scale production of oxide thin films. It is routinely used in the electronics industry, has excellent film uniformity over large areas, is capable of conformal coating of arbitrary geometries, can be done at relatively high partial pressures of oxygen, has easy and reproducible control of film stoichiometry, has relatively high deposition rates and allows for multilayer growth, superlattices and graded compositions. MOCVD works on the principle that one can create a complex organic molecule decorated with the material desired for thin film growth. By passing an inert gas through a bubbler of a liquid precursor, these molecules are transported to the reaction chamber and passed over a substrate at high temperature. The heat helps to break the molecules and deposits the desired material on the surface. One of the biggest challenges for MOCVD growth of oxide materials is identification of the appropriate metal-organic precursors. Precursors for materials with high atomic number typically have limited vapor pressure at room temperature and thus it is essential to heat the bubblers and all the lines in the system to avoid clogging. This requires careful attention so as to avoid hot spots where premature deposition might occur as well as cool spots where condensation of the precursor can occur. In the end, very high quality thin films of oxide materials can be created using this technique.

#### 3.3.3 Low-pressure chemical vapour deposition

Low-pressure chemical vapour deposition (LPCVD) is a process used in the manufacturing of the deposition of thin films on semiconductors usually ranging from a few

nanometers to many micrometers. LPCVD is used to deposit a wide range of possible film compositions with good conformal step coverage. These films include a variety of materials including polysilicon for gate contacts, thick oxides used for isolation, doped oxides for global planarization, nitrides and other dielectrics. LPCVD is similar to other types of CVD in that it is a process where a gaseous species reacts on a solid surface or wafer and the reaction that occurs produces a solid phase material. Each and every CVD process has the same four steps that must happen. First, the reacting gaseous species must be transported to the surface. Second, the gaseous species must absorb into the surface of the wafer. Third, the heterogeneous surface reaction produces reaction products. Finally the gaseous reactants need to be removed from the surface.

LPCVD is most successfully applied in deposition of polysilicon thin films. These films are used for gate contact and short interconnect lines. This is done using compounds like SiH<sub>4</sub> in the temperature range 600-660 °C. Other thin films include undoped and doped oxides that use compounds like Dichlorosilane at 900 °C and Tetraethoxysilane at 700 °C for undoped oxides that will leave SiO<sub>2</sub> and other by-products. Doped oxides include PSG (phosphorosilicate glass) at 950-1100 °C and BPSG (Borophosphorosilicate glass) 850-950 °C which are useful for smooth interconnects.

LPCVD, while it can only be performed at high temperatures, reduces the rate of the reaction permitting greater control over film thickness and reducing thickness variations. It also improves the film's purity and internal structure. The simplicity of the process permits the processing of large wafer batch sizes.

# 3.4 SOLUTION-BASED THIN FILM DEPOSITION TECHNIQUES

There are a variety of solution-based approaches for the creation of complex oxide materials including sol-gel, chelate and metal organic decomposition solution deposition usually involves four steps:

- i. Synthesis of the precursor solution,
- ii. Deposition by spin-casting or dip-coating,
- iii. Low-temperature heat treatment for drying and/or pyrolysis of organics and formation of amorphous films (typically 300 to 400 °C),
- iv. High temperature heat treatment for densification and crystallization (anywhere from 600 to 1100 °C).

Such processes are highly scalable, cheap and very quick. Great strides have been made in utilizing such techniques to make high quality and highly oriented films for devices.

In Low-Temperature Aqueous Solution Depositions there is a set of aqueous solution-based deposition techniques that enable the creation of films at lower temperatures (25 to 100 °C). Processes such as chemical bath deposition (CBD), successive ion layer adsorption and reaction (SILAR), liquid phase deposition (LPD), electro less deposition (ED), as well as more modern variants such as photochemical deposition (PCD), deposition assisted by applied fields, ferrite plating, liquid flow deposition and more can be used to create films of oxide materials at low temperatures.

#### 3.5 SPRAY PYROLYSIS PROCESS FOR THIN FILM DEPOSITION

A wide variety of thin films has been deposited by applying the spray pyrolysis technique. Various devices such as solar cells, sensors and solid oxide fuel cells have been prepared by using these films. Preparation conditions are mainly responsible for different properties for such deposited thin films. Most critical parameter which influences the films

roughness, cracking, crystallinity, etc. is the substrate surface temperature. Atomization of the precursor solution, aerosol transport and decomposition of the precursor are the processes mainly involved in spray pyrolysis technique.

For preparing dense and porous oxide films, ceramic coatings and powders, spray pyrolysis is the most suitable processing technique [9]. Spray pyrolysis represents a very simple and relatively cost-effective method, especially regarding equipment cost. In the glass industry and in solar cell production to deposit electrically conducting electrodes spray pyrolysis has been used for several decades. Typical spray pyrolysis equipment consists of an atomizer, precursor solution, substrate heater and temperature controller. The following atomizers are usually used in spray pyrolysis technique: air blast (liquid is exposed to a stream of air), ultrasonic (ultrasonic frequencies produce the short wavelengths necessary for fine atomization) and electrostatic (liquid is exposed to a high electric field).

In literature there are various reviews concerning spray pyrolysis techniques have been published. Mooney and Radding [10] have reviewed the spray pyrolysis method, properties of the deposited films in relation to the conditions, specific films (particularly CdS) and device application. Tomar and Garcia [11] have discussed the preparation and the properties of sprayed films as well as their application in solar cells, anti-reflection coatings and gas sensors. Albin and Risbud [12] presented a review of the equipment, processing parameters and optoelectronic materials deposited by spray pyrolysis technique. Pamplin [13] has published a review of spraying solar cell materials as well as a bibliography of references on the spray pyrolysis technique. Recently thin metal oxide and chalcogenide films deposited by spray pyrolysis and different atomization techniques were reviewed by Patil [14]. Bohac and Gauckler [15] have discussed the mechanism of chemical spray deposition and presented some examples of sprayed YSZ films.

Spray pyrolysis is a versatile and effective technique to deposit metal oxide films. It is an attractive method to prepare a wide variety of powders and thin film materials for various industrial applications. Metal oxide, chalcogenide and even metal films have been deposited using this technique. Spray pyrolysis opens up the possibility to control the film morphology. The quality and properties of the films depend largely on the process parameters. The most important parameter is the substrate surface temperature. The higher the substrate temperature, the rougher and more porous are the films. If the temperatures are too low the films are cracked. In between temperatures, dense smooth films can be obtained. The deposition temperature also influences the crystallinity, texture and other physical properties of the deposited films. The precursor solution is the other important spray parameter which affects the morphology and the properties of the deposited films. In addition, the film morphology and properties can be drastically changed by using various additives in the precursor solution. It is often suggested that a modified CVD process occurs in film formation close to the surface of the substrate. However many observations contradict the involvement of a model with a CVD character. Further efforts are necessary to clarify the model for film deposition in more detail.

## 3.5.1 Main steps for film deposition by spray pyrolysis

As reported in literatures, there are too many processes that occur either sequentially or simultaneously during film formation by spray pyrolysis. These include precursor solution atomization, droplet transport and evaporation, spreading on the substrate, drying and decomposition of the precursor salt. Understanding these processes will help to improve film quality. Thin film deposition using spray pyrolysis can be divided into three main steps: atomization of the precursor solution, transportation of the resultant aerosol and decomposition of the precursor on the substrate.

## a) Atomization of precursor solution

Normally used atomizers in spray pyrolysis techniques are air blast, ultrasonic and electrostatic. Various reports were published on the mechanism of liquid atomization. Rizkalla and Lefebvre [16] examined the influence of liquid properties on air blast atomizer spray characteristics. Lampkin [17] presented results concerning the application of the air blast atomizer in a spray pyrolysis set-up. Recently a theory of ultrasonic atomization was published. Ganan-Calvo et al. [18] have studied the electrostatic atomization of liquids and derived scaling laws for droplet size from a theoretical model of charge transport. Compared with other spray techniques, the nebulized spray (air blast) deposition technique has been only recently used for deposition of manganite and multi ferroics thin films.

## b) Aerosol transport

The droplet of solution is transported and eventually evaporates in an aerosol. For making dense thin films, it is important that during transportation as many droplets as possible fly to the substrate without forming particles before reaching the surface. Sears et al. [19] investigated the mechanism of SnO<sub>2</sub> film growth. The influence of forces which determine both the trajectory of the droplets and evaporation were examined and a film growth model was proposed. Four types of forces i.e. gravitational, electric, thermophoretic and stokes forces were taken into account. The thermo phoretic force pushes the droplets away from a hot surface, because the gas molecules from the hotter side of the droplet rebound with higher kinetic energy than those from the cooler side. Thermophoretic forces keep most droplets away from the surface in non-electrostatic spray process. It was concluded that the film grows from the vapour of droplets passing very close to the hot substrate in a manner of chemical vapour deposition as shown in Fig. 3.4.

Droplets that strike the substrate form a powdery deposit. The authors suggest that forcing droplets closer to the substrate while avoiding actual contact would improve the

efficiency of film growth. Siefert [20] described the transport processes in corona spray pyrolysis. Here the droplets enter a corona discharge and are transported in an electric field to the substrate. Lenggoro et al. [21] investigated powder production by spray pyrolysis using a temperature-graded laminar flow aerosol reactor. Oh and Kim [22] have studied the behavior of an evaporating droplet in a non-isothermal field.

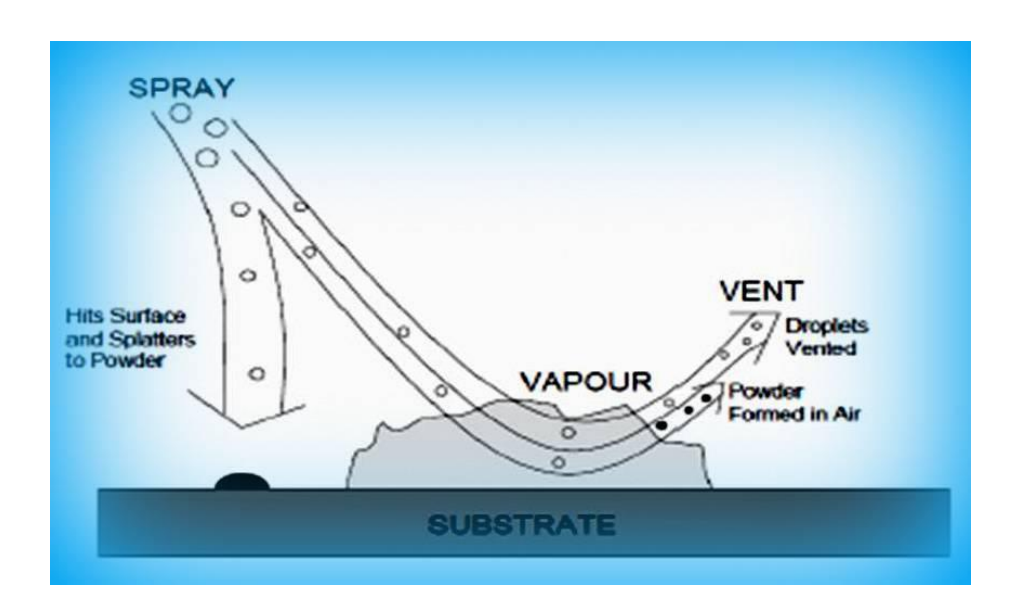


Fig. 3.4 Schematic of aerosol transport

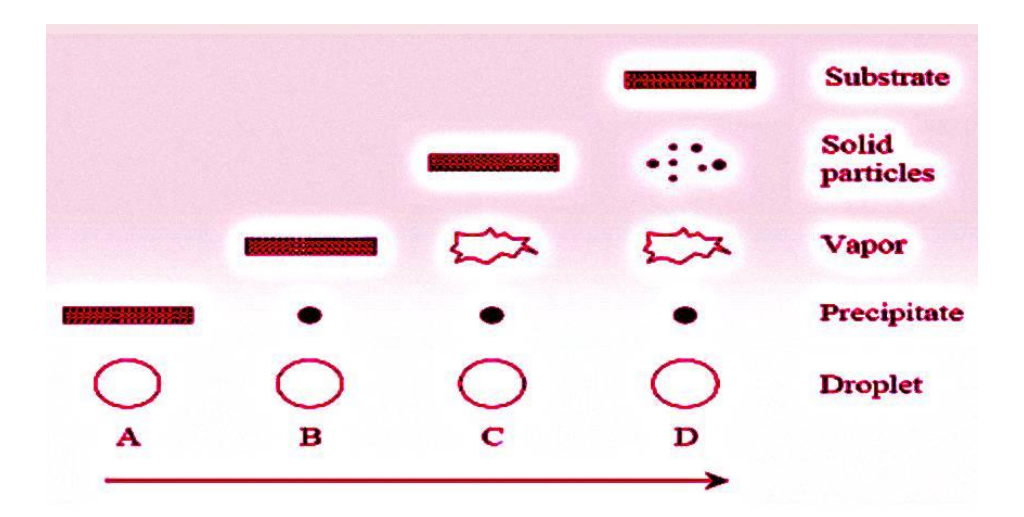


Fig. 3.5 Description of the deposition processes initiated with increasing substrate temperature

## c) Decomposition of precursor

Many processes occur simultaneously when a droplet hits the surface of the substrate: evaporation of residual solvent, spreading of the droplet and salt decomposition. Many models exist for the decomposition of a precursor. Most of the authors suggest that only a kind of CVD process gives high quality films by spray pyrolysis. Viguie and Spitz [23] proposed the following processes that occur with increasing substrate temperature. In the process A in Fig. 3.5, the lowest temperature regime the droplet splashes onto the substrate and decomposes.

At higher temperatures, in the process B the solvent evaporates completely during the flight of the droplet and dry precipitate hits the substrate, where decomposition occurs. In the process C, at even higher temperatures the solvent also evaporates before the droplet reaches the substrate. Then the solid precipitate melts and vaporizes without decomposition and the vapour diffuses to the substrate to undergo a CVD process. At the highest temperatures in process D, the precursor vaporizes before it reaches the substrate and consequently the solid particles are formed after the chemical reaction in the vapour phase. It was speculated that the processes A and D lead to rough or non-adherent films. Adherent films were obtained by CVD at low temperatures in the process C. Choy [24] proposed a deposition model for the so called electrostatic spray-assisted vapour deposition process. This technique is also known as electrostatic spray deposition. The precursor solution is atomized using an electric field. Chen et al. [25] investigated the correlations between film morphologies and deposition parameters. The films were deposited using the so-called conejet mode. The substrate temperature was indicated as the most important parameter. The concentration of the precursor solution had a minor influence on the film morphology.

## 3.5.2 Spray pyrolysis technique

Spray pyrolysis technique consists of temperature controller, spray gun, substrate heater, a thermocouple and a compressor unit. The proper pressure of compressed air was used in order to spray the solution on to the substrate which is kept on the substrate heater. The temperature of the substrate is controlled by the temperature controller via thermocouple.

The solution of the precursor is kept in a solution reservoir and the solution can be carried through a spray gun to spray on the substrate. Prior to the film deposition processes by spray pyrolysis one needs a solution of required material. The molarity (M) of solution is being optimized by making solution of different molarities followed by several characterizations. A typical spray pyrolysis system is shown in Fig. 3.6.

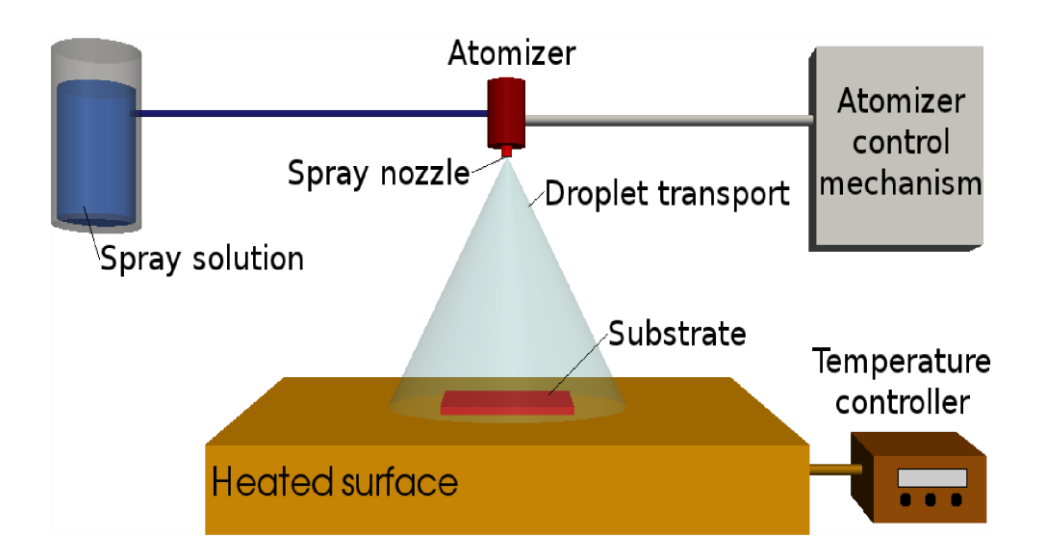


Fig. 3.6 A typical spray pyrolysis system

## 3.5.3 Principle and thin film formation mechanism

This technique involves spraying a solution containing soluble salts of the constituent atoms of the desired compound on to a hot substrate maintained at temperatures generally in the range of 300-500 °C. The hot substrate provides the necessary thermal

energy for the pyrolytic decomposition of the sprayed droplets reaching its surface of the substrate and the subsequent recombination of the constituent species to form a continuous thin film after several stages of growth. The volatile by-products and the excess solvent in the vapour phase are evacuated during the deposition process using an exhaust system.

The thin film formation is a resultant of the following processes:

- Spreading of the sprayed droplets on the surface of the hot substrate into disks
- ii. Pyrolytic reaction between the decomposed reactants
- iii. Evaporation of the solvent
- iv. Repetition of the proceeding processes with succeeding droplets.

The process parameters such as concentration of the precursor solution, type of solvent, doping material, spray nozzle geometry, flow rate of carrier gas and solution, velocities of sprayed droplets, nature and temperature of the substrate, kinetics and thermodynamics of the pyrolytic reaction mainly determine the properties of the spray deposited films.

## 3.6 NEBULIZED SPRAY PYROLYSIS (NSP) TECHNIQUE

The technique used in this work is known as the NSP technique which is one of the most widely used innovative deposition technique. It is a very easy, low cost, safe and vacuum less system of the deposition technique. The other advantage of this technique is that it can be easily adapted for production of large area uniform film coatings.

#### 3.6.1 Mechanism of a nebulizer

The nebulizer turns liquid medicine for the asthma treatment. They come in electric or battery-run versions. They also come in a larger size that's meant to sit on a table and plug into a wall and a smaller size that can be carried easily. Both are made up of a base that

holds an air compressor, a small container for liquid medicine and a tube that connects the air compressor to the medicine container. Above the medicine container is a mouthpiece or mask you use to inhale the mist.

The most commonly used nebulizers are jet nebulizers, which are also called "atomizers". Jet nebulizers are connected by tubing to a compressor, which causes compressed air or oxygen to flow at high velocity through a liquid chemical to turn it into an aerosol, which is then sprayed on the substrate through the optimized 'L' type glass tube which has small tapering at the substrate side to transmit the fine droplets. Fig. 3.7 represents the schematic diagram of the simple nebulizer [26].

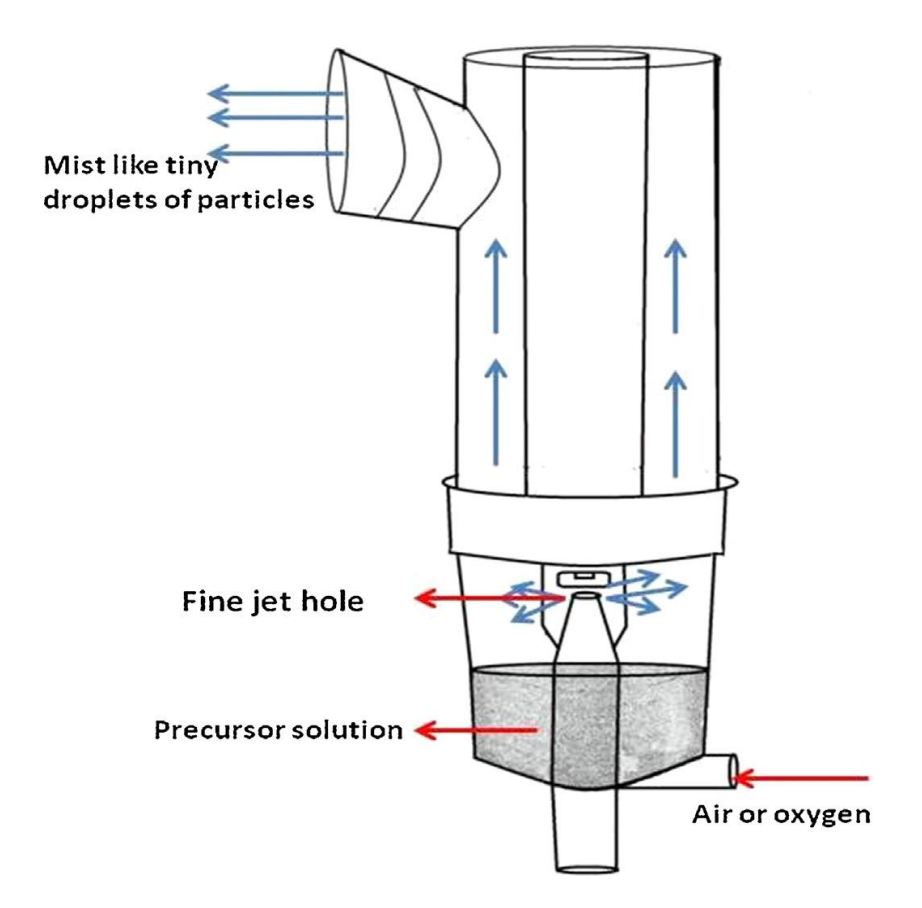


Fig. 3.7 Schematic diagram of a simple nebulizer

## 3.6.2 Venturi effect

The venture effect is the reduction in fluid pressure that results when a fluid flows through a constricted section of the tube. It is a jet effect; as with a funnel velocity of the fluid increases as the cross sectional area decreases, with the static pressure correspondingly decreasing. When a fluid flows through a tube that narrows to a smaller diameter, the partial restriction causes a higher pressure at the inlet than that at the narrow end. According to the laws governing fluid dynamics, a fluid's velocity must increase as it passes through a constriction to satisfy the principle of continuity, while its pressure must decrease to satisfy the principle of conservation of mechanical energy. Thus any gain in kinetic energy of a fluid may accrue due to its increased velocity through a constriction is negated by a drop in pressure.

## 3.6.3 Working principle of nebulized spray pyrolysis technique

Fig. 3.8 shows an experimental set-up of NSP technique. This technique consists of a nebulizer, "well" shaped furnace connected with a temperature controller and compressor unit. The precursor solution was kept inside the nebulizer unit. Nebulizers can vary greatly in size and can run, on either electricity gas pressure power. It consists of a compressor that pumps oxygen through plastic tubing into a nebulizer that holds the liquid. It has industrial applications but is most commonly known as an efficient delivery method to be confused with a pump spray, which has small nozzle, nebulizer convents a liquid into an aerosol. The purpose of a nebulizer is to create an aerosol, a mixture of gas and liquid particles. Nebulizers are attached to an electric compressor and spray unit. The compressor to pump air through the device and nebulizer turn the chemical solution into an 'L' bend tube on common size particles are sprayed as glass plate.

When the compressed air was passed through the nebulizer, fine clouds of visible air born tiny droplets of solution was generated and carried through 'L' shaped glass tube to

spray on the glass substrates. The temperature of the substrate was raised and controlled by a temperature controller. The distance between the edge of 'L' shaped tube and the glass substrate was approximately 5 cm. The flow rate of the solution was 1 ml/ min. After the deposition was over, the samples were kept on the hot plate until it reached to the room temperature and then preserved them in desiccators.

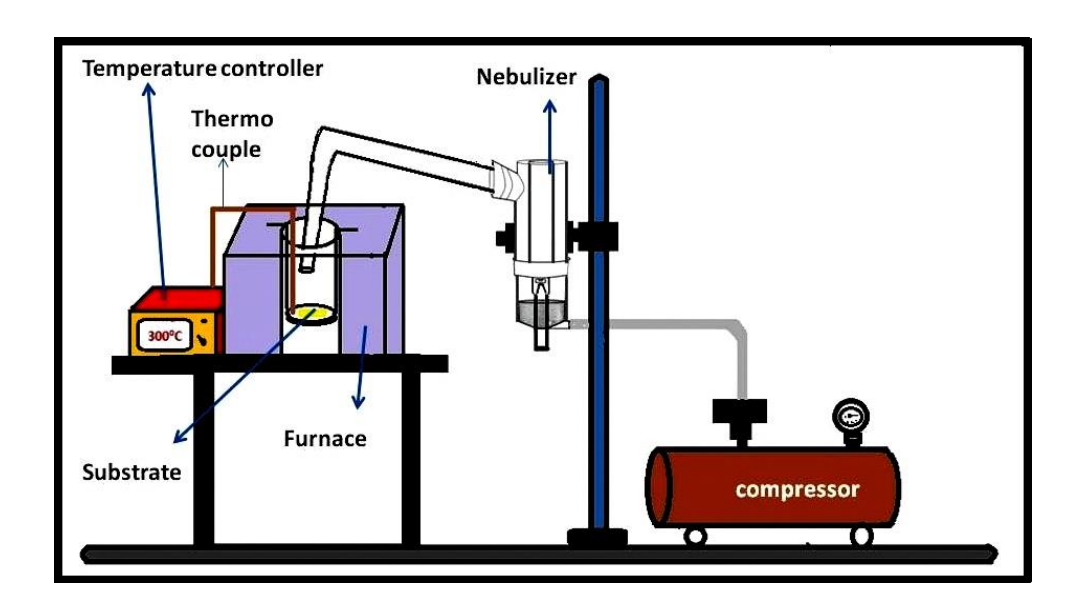


Fig. 3.8 Experimental setup of nebulized spray pyrolysis technique

## 3.6.4 Advantages of NSP technique

This technique has some advantages such as an atomization based on pressure without using any carrier gas, intermittent spraying and fine atomization.

- ◆ The advantage of chemical spray pyrolysis is manifold: nanostructure of the film (compact or porous) can be altered depending on the spray condition, repeatability, adherent of deposits and cost effective. Spraying is performed in an ambient atmosphere using air as driving gas and in most cases aqueous precursor solutions were used
- The films are having more uniform thickness and there is no pinhole

- ♦ The substrate temperature can be varied using temperature controller for each deposition in the air atmosphere
- Only the small amount was consumed in this nebulisation and 10 minutes taken for spraying 5 ml of precursor solution i.e the nebulisation rate is 0.5 ml per min
- Even though high quality and uniform films are synthesized by physical technique, they are comparably expensive and highly energy consuming. Nebulized spray pyrolysis is a versatile, simple, inexpensive, time saving and efficient way of growing thin films at room atmosphere
- This technique can be scalable to larger area deposition
- ♦ The advantages of the NSP technique over conventional pneumatic spraying is its low material consumption with better control of the spray and the soft carrier gas flow, which allows the deposition of very thin layers of uniform thickness
- The films prepared by this technique exhibit low resistivity than other techniques which can be exploited for use as electrodes in several situations.

## 3.7 CHARACTERIZATION TECHNIQUES

Thin film characterization technologies are in high demand, given the wide-spread use of coatings in all engineering and science fields. Mechanical, functional and geometrical properties of thin films can vary dramatically and this fact makes it difficult to find a general purpose characterization technique. However, confocal microscopy and interferometric optical profiling are among the few methods that can be used for this purpose. In this report it is shown how it is possible to characterize the thickness, structure, electrical conductivity, morphological and optical properties of various types of films and how this characterization technology can deliver higher quality results than those of traditional characterization methods, like indentation or scratch testing.

## 3.7.1 Thickness measurement of Stylus profilometer

Thickness is one of the most important parameter of a thin film to be characterized since it plays an important role in the film properties unlike in bulk material. Microelectronic applications generally require the maintenance of precise and reproducible film metrology (i.e., thickness as well as lateral dimensions). Various techniques are available to characterize the film thickness which are basically divided into optical and mechanical methods and are usually nondestructive. Film thickness may be measured either by in-sit monitoring of the rate of deposition or after the film deposition. Stylus profilometer is an advanced tool for thickness measurement of both thin and thick films after deposition (Fig. 3.9). It is capable of measuring steps even below 100 Å. This instrument can also be used to profile surface topography and waviness, as well as measuring surface roughness in the sub nanometer range [27].

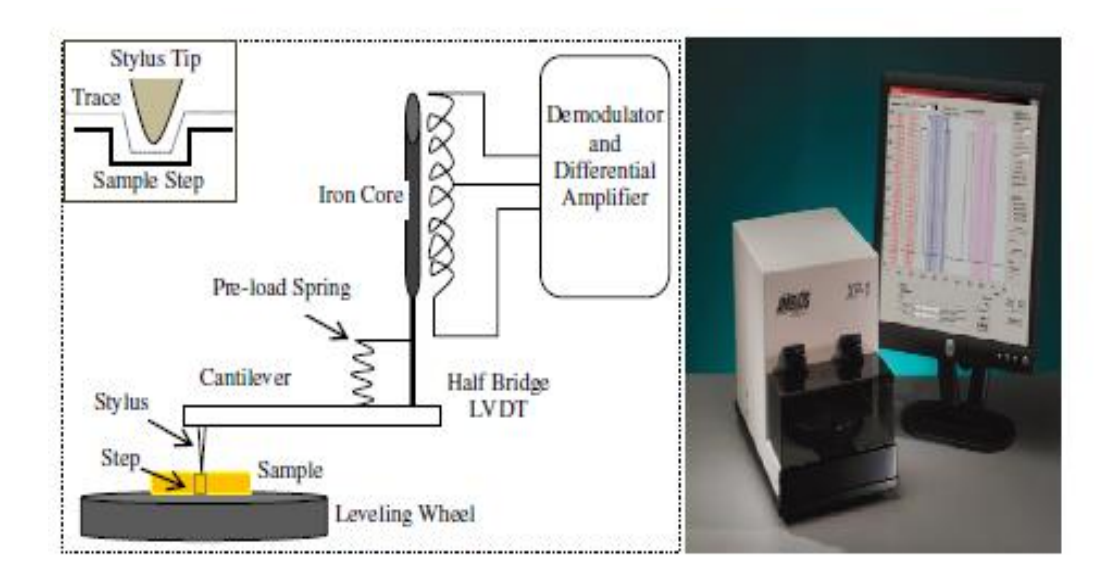


Fig. 3.9 Schematic diagram and image of MITOTOYO SJ-300 stylus profilometer

The stylus profiler takes measurements electromechanically by moving the sample beneath a diamond tipped stylus. The high precision stage moves the sample according to a user defined scan length, speed and stylus force. The stylus is mechanically coupled to the core of a linear variable differential transformer (LVDT). The stylus moves over the sample surface. Surface variations cause the stylus to be translated vertically.

Electrical signals corresponding to the stylus movement are produced as the core position of the LVDT changes. The LVDT scales an ac reference signal proportional to the position change, which in turn is conditioned and converted to a digital format through a high precision, integrating, analog-to-digital converter. The film whose thickness has to be measured is deposited with a region masked. This creates a step on the sample surface. Then the thickness of the sample can be measured accurately by measuring the vertical motion of the stylus over the step.

#### 3.7.2 X-ray diffraction technique

Fig. 3.10 shows the photograph of X-Pert Pro diffractometer. The most common technique for analyzing thin films as thin as 100 Å is to use a 'grazing incidence angle' arrangement. Samples can be analyzed using this technique in a non-destructive way. Glancing angle XRD is used when the information needed lies within a thin top layer of the material. We employed the 'Seemann-Bohlin geometry' [28, 29] for the present study. Incident x-ray is impinging on the fixed specimen at a small angle,  $\gamma$  (typically <1° to 3°) and the diffracted X-rays are detected by a detector that moves along the focusing circle. This method provides good sensitivity for thin films, due to para-focusing and the large diffracting volume, which results from  $\gamma$  being small and x-ray path length in the film being large (proportional to  $1/\sin \gamma$ ). By increasing the path length of the incident x-ray beam through the film, intensity scattered or diffracted from the film can be increased, while at the same time, the diffracted intensity from the substrate can be reduced.

Overall, there is a dramatic increase in the film signal to background ratio. During the collection of the diffracted spectrum, only the detector rotates through the angular range, keeping the incident angle, the beam path length and the irradiated area constant. XRD gives whole range of information about crystal structure, orientation, crystallite size, composition defects and stresses in thin films [30]. Experimentally determined data is compared with JCPDS file for standards.

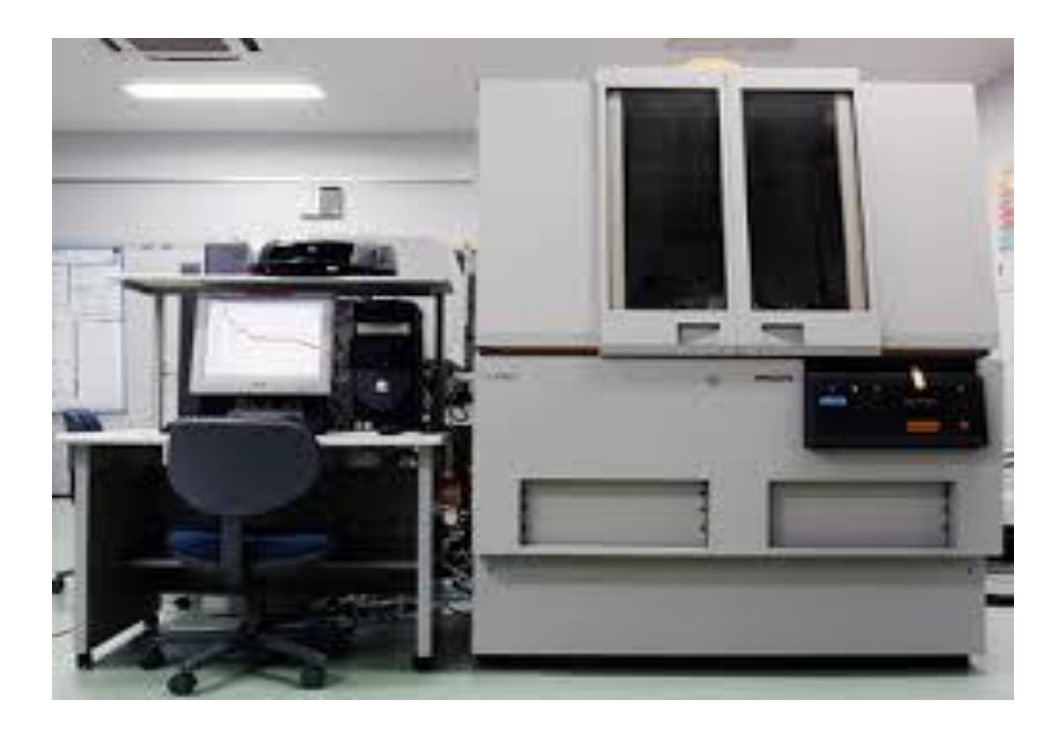


Fig. 3.10 Photograph of X-Pert Pro X-ray diffractometer

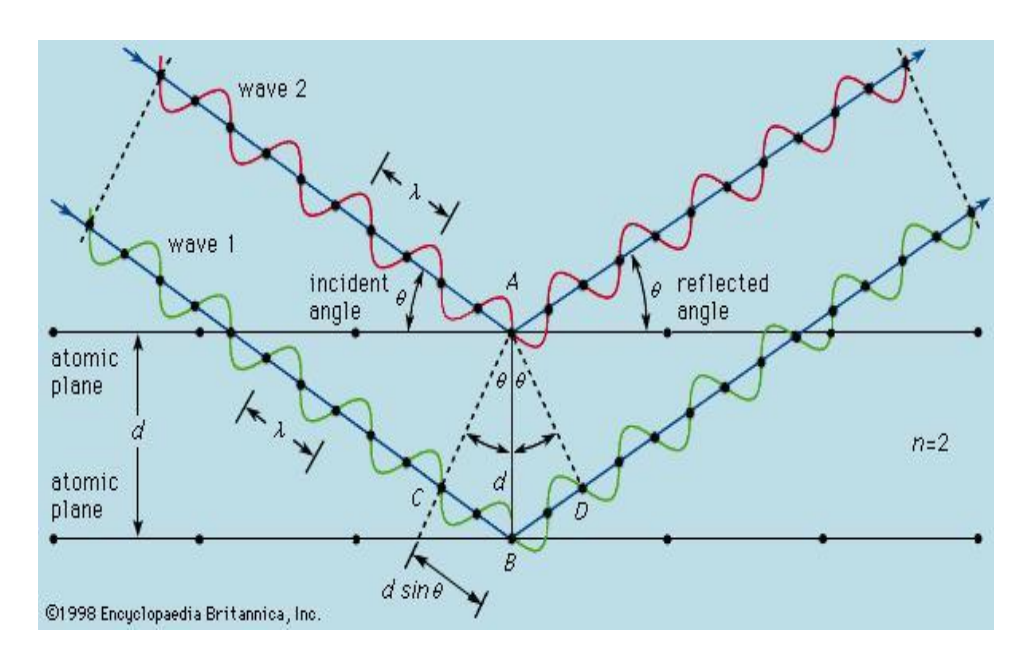


Fig. 3.12 X-ray diffraction

The inter-planar spacing (d) can be calculated from the Bragg's formula,

$$2d\sin\theta = n\lambda \qquad ...(3.1)$$

Where,  $\theta$  is the Bragg angle, n is the order of the spectrum;  $\lambda$  is the wavelength of X-rays which is equal to 1.5405 Å for Cu-K $\alpha$  radiation used for the present study. Using d values, the plane (h k l) can be identified and lattice parameters are calculated with the help of following relations for various crystallographic systems.

For the cubic system

$$\frac{1}{d^2} = \frac{h^2 + k^2 + l^2}{a^2} \qquad \dots (3.2)$$

For the tetragonal system

$$\frac{1}{d^2} = \frac{h^2 + k^2}{a^2} + \frac{l^2}{c^2} \qquad \dots (3.3)$$

For the hexagonal system

$$\frac{1}{d^2} = \frac{4}{3} \left( \frac{h^2 + hk + k^2}{a^2} \right) + \frac{l^2}{c^2} \qquad \dots (3.4)$$

For the orthorhombic systems,

$$\frac{1}{d^2} = \frac{h^2}{a^2} + \frac{k^2}{b^2} + \frac{l^2}{c^2} \qquad \dots (3.5)$$

For the rhombohedral systems,

$$\frac{1}{d^2} = \frac{\left(h^2 + k^2 + l^2\right)\sin^2\alpha + 2\left(hk + kl + hl\right)\left(\cos^2\alpha - \cos\alpha\right)}{a^2\left(1 - 3\cos^2\alpha + 2\cos^3\alpha\right)} \qquad \dots (3.6)$$

For the monoclinic systems,

$$\frac{1}{d^2} = \left(\frac{h^2}{a^2} + \frac{k^2 \sin^2 \beta}{b^2} + \frac{l^2}{c^2} - \frac{2hl \cos \beta}{ac}\right) \cos^2 \beta \qquad \dots (3.7)$$

For the triclinic systems,

$$\frac{1}{d^2} = \frac{\frac{h^2}{a^2} \sin^2 \alpha + \frac{k^2}{b^2} \sin^2 \beta + \frac{l^2}{c^2} \sin^2 \gamma}{1 - \cos^2 \alpha - \cos^2 \beta - \cos^2 \gamma + 2\cos \alpha \cos \beta \cos \gamma} \qquad \dots (3.8)$$

Where a, b and c are lattice parameters.

The crystalline size 'D' can be calculated from the Debye-Scherrer formula,

$$D = \frac{k\lambda}{\beta Cos\theta} \qquad \dots (3.9)$$

Where, k is a constant equal to 0.9 and  $\beta$  is the full width at half maximum (FWHM) measured in radians.

## 3.7.3 Scanning electron microscopy (SEM)

SEM is a powerful and most widely used technique for imaging the surfaces and provides information about the surface morphology. The high resolution of SEM makes it a convenient tool for probing nano structured materials. SEM is operated at magnifications that are easily adjustable from  $10\times$  to over  $300,000\times$  with a resolution of 50 nm -100 nm. The major components of SEM are: electron gun or cathode, electron lenses, sample stage, detectors for all signals of interest, display and data output devices.

SEM works on the principle that accelerated electrons carry significant kinetic energy. This energy is dissipated as variety of signals produced by electron–sample interactions on deceleration of incident electrons. These signals include secondary electrons (that produce SEM images), backscattered electrons, characteristic X–rays (used for elemental analysis), continuum X–rays, visible light and heat. A stream of monochromatic electrons generated by an electron gun is condensed and focused by condenser lens. A set of coils is used to scan the beam and the objective lens focuses the scanning beam on one point at a time on the desired sample area (Fig. 3.12). The electron beam hits the sample producing secondary electrons that are collected by a secondary detector, converted to a

voltage and amplified. The amplified voltage is applied to the display unit causing variation in the intensity of the light spot. The final image consists of thousands of these spots of varying intensity on the display that correspond to the morphology of the sample. In SEM analysis, sample preparation is very important depending on the nature of the sample. In order to avoid the charging of the surface, most of the samples are coated with a thin layer of conducting material, commonly carbon and gold.

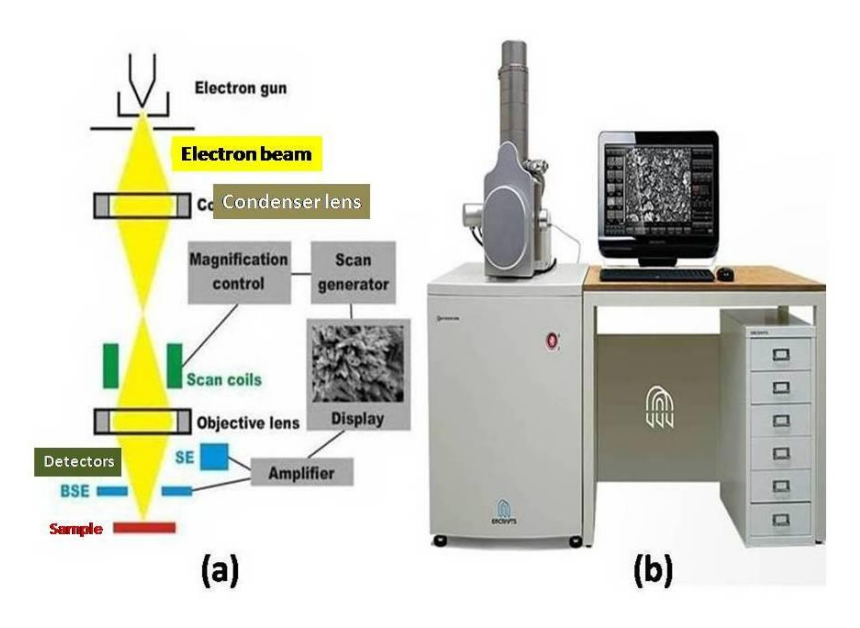


Fig. 3.12 Diagram for (a) image formation of a typical SEM (b) instrumental set up

An improved version of SEM which is capable of examining the sample without any conductive coating at low vacuum is field emission scanning electron microscopy (FESEM).

In SEM, a source of electrons is focused in vacuum into a fine probe that is rastered over surface of the specimen. The electron beam passes through scan coils and objective lens that deflects the beam horizontally and vertically so that the beam scans the surface of the sample. As electrons penetrate the surface, a number of interactions occur that can result in the emission of electrons or photons from or through the surface. A reasonable fraction of the electrons emitted can be collected by appropriate detectors and the output can be used to modulate the brightness of a cathode ray tube (CRT) whose x and y inputs are driven in

synchronism with the x-y voltage rastering the electron beam. In this way an image is produced on the CRT; every point that the beam strikes on the sample is mapped directly on to a corresponding point on the screen. Linear magnification obtained can be calculated from the simple expression [30]

$$M = L/I$$
 ... (3.10)

Where, L is the raster's length of the CRT monitor and I is the raster length on the surface of the sample.

SEM works on a voltage between 2 to 5 kV and the beam diameter that scans the specimen is in between 5 nm to 2 µm. The principle image produced in SEM is of three types: secondary electron images, backscattered electron images and elemental x-ay maps. Secondary and backscattered electrons are conventionally selected and separated according to their energies. When the energy of the emitted electron is less than about 50 eV, it is referred to as a secondary electron and backscattered electrons are considered to be the electrons that exit the specimen with energy greater than 50 eV. Detectors of each type of electrons are placed in the microscope in proper positions to collect them.

## 3.7.4 Electrical conductivity characterization

Conductivity of a semiconductor crystal is considerably affected by lattice vibrations, impurities, strain, displaced atoms in the lattice, grain boundaries etc. Conductivity can be expressed in terms of material dimensions through resistivity or resistance ( $\rho$  or R). If L and B are the length and breadth of a rectangular shaped specimen and d is the thickness [31] then

$$\rho = \frac{RBd}{L} \qquad ...(3.11)$$

Where  $\rho$  is the resistivity and its unit is  $\Omega$ .cm,

$$\sigma = \frac{1}{\rho} \qquad \dots (3.12)$$

 $\rho$  and  $\sigma$  are constants for any particular material at a fixed temperature. However, for films, since these are dependent on thickness and grain size unlike the bulk material.

$$\frac{\rho}{d} = \frac{RB}{L} = R_s \qquad \dots (3.13)$$

Where,  $R_s$  is known as the 'sheet resistance' which is expressed in ohm per square. If we assume L=B, then

$$\frac{\rho}{d} = R = R_s \qquad \dots (3.14)$$

Which means that the resistance of one square of a film is its sheet resistance  $R_S$  and it is independent of the size of the square; but this depends only on resistivity and film thickness. If the film thickness is known, then resistivity is given by,

$$\rho = d. R_s$$
 ... (3.15)

## a) Four Probe Method

This is the most common method for measuring resistivity of compound semiconducting thin films and is especially suitable for measurements in the low resistivity regime. It is an absolute measurement without recourse to calibrated standards. The idea of four point probe was first proposed by Wenner [32] in 1916 to measure the earth's resistivity and in 1954 Valdes [33] adopted this technique for the resistivity measurements of semiconductors.

Fig. 3.13 is an illustration of a collinear four probe setup. Two probes carry the current and other two probes sense the voltage. Use off our probes has an important advantage over two probes. Although the current carrying probes still have contact and spreading resistance (as given in the above section) associated with them, that is not true for

the voltage probes because the voltage is measured either with a potentiometer, which draws no current at all, or with a high impedance voltmeter, which draws little current.

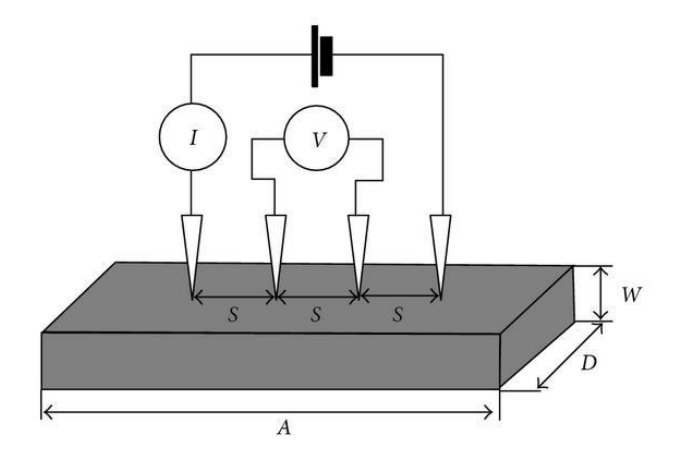


Fig. 3.13 Schematic diagram of four probe set-up

$$\rho = 2\pi s \text{ (V/I)}$$
 ... (3.16)

Where s is the distance between the probes,

## b) Hall Effect

The Hall Effect measurement technique is widely applied in the characterization of semiconductor materials as it gives resistivity, carrier density, type of carriers and mobility of carriers. When a magnetic field is applied to a material perpendicular to the current flow direction, an electric field will be developed perpendicular to the direction of magnetic field and the current. This phenomenon is known as Hall Effect and the developed voltage is called "Hall voltage". The force acting on a charge (q) moving with a velocity  $\mathbf{v}$  in the presence of an electric  $(\mathbf{E})$  and magnetic  $(\mathbf{B})$  fields is given by the vector expression,

$$\mathbf{F} = \mathbf{q} \left[ \mathbf{E} + (\mathbf{v} \times \mathbf{B}) \right] \qquad \dots (3.17)$$

For n-type and p-type samples, the electrons and holes respectively deflect to the same side of the sample for the same current direction because electrons flow in the opposite direction to holes and have opposite charge. The Hall coefficient  $R_{\rm H}$  is defined as

$$R_H = \frac{V_H d}{BI} \qquad \dots (3.18)$$

where, d is the sample thickness in the direction of magnetic field B,  $V_H$  is the Hall voltage and I is the current through the sample [27].

The carrier mobility  $(\mu)$  is determined using the relation

$$\mu = \frac{1}{en_{\nu}\rho} \qquad \dots (3.19)$$

Where  $\rho$  is resistivity,  $n_v$  is the carrier concentration of the material. The carrier concentration  $(n_v)$  is derived from the relation

$$n_{v} = \frac{1}{eR_{H}}$$
 ...(3.20)

For semiconducting films on insulating substrates, the mobility is frequently observed to decrease towards the substrate. Surface depletion forces the current to flow in the low-mobility portion of the film, giving apparent mobility lower than true mobility. Hall effect measurements are simple to interpret for uniformly doped samples. Non-uniformly doped layer measurements are more difficult to interpret. If the doping density varies with film thickness, then its resistivity and mobility also vary with thickness.



Fig. 3.14 Photograph of Hall Effect instrument

It is to be noted that Hall effect measurement gives average resistivity, carrier density and mobility. Electrical resistivity and Hall coefficients of the films described in this thesis were measured using four probe van der Pauw configuration of magnetic field at room temperature using Ecopia model No. HMS-5000 (magnetic field = 0.57 T and capable of current measurement in the range 1–25 mA) (Fig. 3.14).

#### 3.7.5 Energy Dispersive X-Ray Analysis (EDAX)

EDAX stands for energy dispersive x-ray analysis. This technique sometimes referred to also as EDS or EDX analysis, is used for identifying the elemental composition of the specimen, on an area of interest. The EDAX works as an integrated feature of a SEM and cannot be operated as its own without the latter [34]. During EDAX, the specimen is bombarded with an electron beam inside the scanning electron microscope. The bombarding electrons collide with the specimen atom's own electrons, knocking some of them off in the process. A position vacated by an ejected inner shell electron is eventually occupied by a higher-energy electron from an outer shell. To be able to do so, however, the transferring outer electron must give up some of its energy by emitting an X-ray. The amount of energy released by the transferred electron depends on which shell it is transferred from, as well as which shell it is transferring to. Furthermore, the atom of every element releases x-ray photons with unique amounts of energy during the transferring process. Thus, by measuring the energy of the x-ray photons emitted by a specimen during electron beam bombardment, the identity of the atom from which the x-ray was emitted can be established (Fig. 3.15).

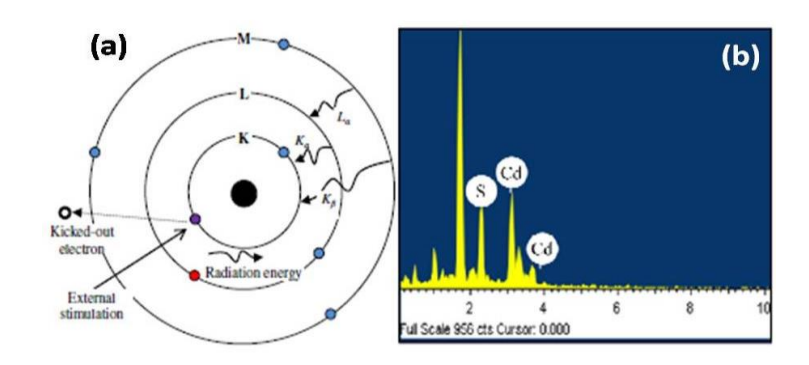


Fig. 3.15 (a) Emission of X-ray (b) Example of EDAX spectra of CdS thin film

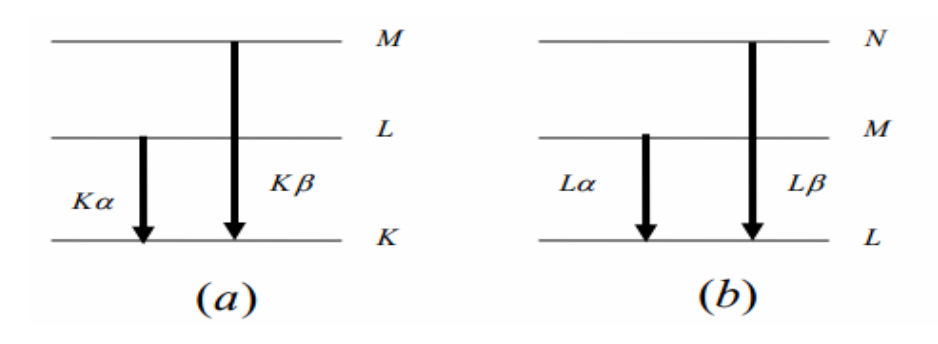


Fig. 3.16 Schematic of electron transitions responsible for the production of (a)  $K_{\alpha}$  and  $K_{\beta}$  (b)  $L_{\alpha}$  and  $L_{\beta}$  X-rays

The output of an EDAX analysis is an EDAX spectrum, which is a plot of how frequently X-ray is received for each energy level. EDAX spectrum normally displays the peaks corresponding to the energy levels for which the most X-rays had been received. Each of these peaks is unique to an atom and therefore corresponds to a single element. The higher a peak in a spectrum, the more concentrated the element is in the specimen. An EDAX spectrum not only identifies the element corresponding to each of its peaks, but the type of X-ray to which it corresponds as well. For example, a peak corresponding to the amount of energy possessed by X-rays emitted by an electron in the L-shell going down to the K-shell is identified as a  $K_{\alpha}$  peak. The peak corresponding to X-rays emitted by electrons transition from upper levels to the K-shell is identified as a  $K_{\alpha}$ ,  $K_{\beta}$ ,  $L_{\alpha}$ ,  $L_{\beta}$  respectively as shown in Fig. 3.16.

## 3.7.6 Optical and absorption studies

The measurement of absorption coefficient and optical band gap of material are essential for opto-electronic applications. The absorption coefficient for various energies provides information about the optical properties of material. UV-Vis-NIR spectroscopy is commonly used for the calculation of optical constants. UV-Vis-NIR spectrophotometer measures light intensity (absorbance (%A), reflectance (%R) and transmittance (%T)) as a function of wavelength on interaction of electromagnetic radiation with material. Typically, a double beam spectrophotometer shown in Fig. 3.17 consists of (i) a deuterium arc lamp for the UV spectral range (190 nm – 400 nm) and a tungsten lamp for the visible and near IR spectral ranges (300 nm – 1100 nm), (ii) a monochromator composed of a diffraction grating, used to select a single wavelength (iii) a sample holder, (iv) a light detector (a photo multiplier tube, a photodiode for the UV-Vis-NIR range and a PbS cell for the IR range) and (v) a computer to record UV-Vis-NIR spectrum. Most of the semiconductors absorb strongly in the visible region of the spectrum, having absorption coefficients of the order of 10<sup>4</sup> cm<sup>-1</sup>. The characteristic feature of semiconductors in the pure state is that at a certain wavelength, generally in the near or in the infra-red region, absorption coefficient drops rapidly and the material becomes fairly transparent at longer wavelengths. This marked drop in the absorption is called 'fundamental absorption edge' or 'lattice absorption edge'. Absorption of light by different materials can induce various types of transitions such as band to band, between sub-bands, between impurity levels and bands, interactions with free carriers within a band and resonance due to vibration state of lattice and impurities. These absorptions lead to the appearance of absorption peaks in the absorption spectra. Hence the spectral positions of bands determine the types of transitions occurring during the process.

In the absence of any thermal energy, the only possible absorption that can take place is the one from valence band to conduction band when the incident radiation is of sufficient energy.

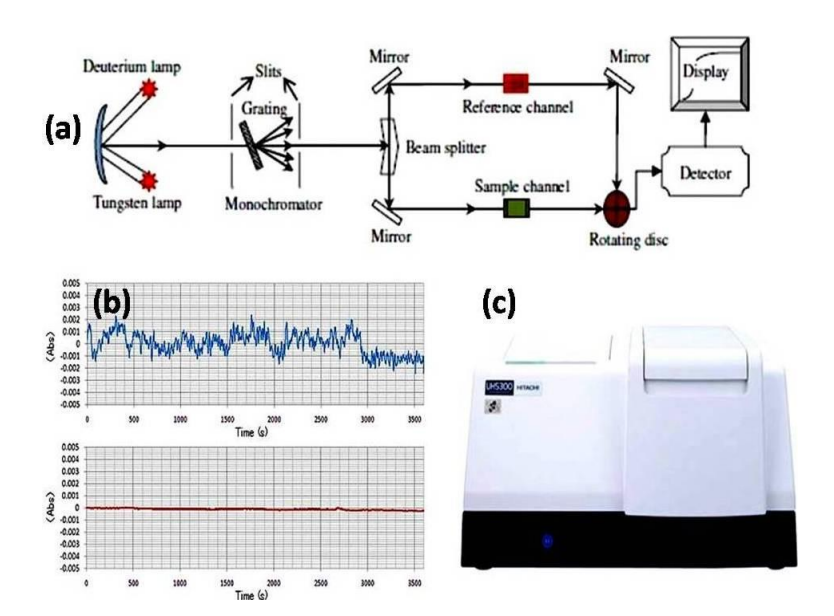


Fig. 3.17 (a) Schematic diagram (b) sample graph of absorption of light

## (c) Photograph of a double beam spectrophotometer

Electronic transition between valence and conduction bands can be direct or indirect. In both cases, it can be allowed as permitted by the transition probability (p) or forbidden where no such probability exists. Transition probability follows the relation, which relates the energy band gap of the films and the absorption coefficient, ( $\alpha$ ) as a function of photon energy, hv, [35,36].

$$(\alpha h v)^p = A (h v - E_g) \qquad ... (3.21)$$

where A is a constant and  $E_g$  is the optical energy band gap, h is Planck's constant and  $\nu$  is the frequency of electromagnetic radiation

Nature of transition can be determined by plotting  $(\alpha h v)^p$  against photon energy. For a suitable value of p, straight line behavior of the plot can be obtained and extrapolation of

which on to the energy axis gives the value of the energy band gap of the material. The value of p=2 and 3 represents the direct allowed and direct forbidden transitions respectively. Further, the value of p=1/2 and 1/3 represents the indirect allowed and indirect forbidden transitions respectively.

#### 3.7.7 Photoluminescence (PL) studies

Photoluminescence (PL) analysis is a powerful tool in the characterization of surfaces and interfaces (Fig. 3.18). Although a number of experimental techniques can provide detailed mechanical information about interfaces, the optoelectronics industry that drives most interface investigations is ultimately concerned with optical and electronic properties. Mechanical information is useful because it is closely correlated with these properties, but PL measurements explore electronic features directly. Other techniques can provide similar access, but they typically require more sophisticated excitation or detection schemes.

Photoluminescence Excitation (PLE) is simple, but it is also quite versatile. The excitation energy and optical intensity can be chosen to study different regions and recombination mechanisms near interfaces. Because absorption of the incident light depends on the excitation energy, this parameter determines the depth of the PL probe. Using PLE, absorption and emission energies are observed simultaneously to evaluate the distribution of electronic states. The excitation intensity is even more important, controlling the density of photo excited electrons. This density is critical in the interpretation of recombination dynamics. The PL signal itself is characterized by three essential features: energy, intensity and polarization. Because PL is the result of optical transitions between electronic states, the PL spectrum gives precise information on the energy levels available to electrons in the

material. The intensity of the PL signal depends on the rate of radiative and nonradiative events, which depends in turn on the density of nonradiative interface states. Although investigations of PL polarization are still relatively sparse and are not well understood, they can identify unique anisotropic features in the underlying crystal. Future work in this area should lead to a more complete picture of asymmetry at surfaces and interfaces. PL measurements are not sensitive to the pressure in the sample chamber and can be performed at virtually any temperature. These features make PL an excellent in situ probe of surface or interface modification. Even so, variation of the PL signal with external parameters such as temperature and applied bias can provide additional information on the nature of interfaces. Temperature-dependent thermal activation of electronic states can be used to estimate their depth below the intrinsic bands. An applied bias shifts the bands at the surface, permitting evaluation of the zero-bias band bending. Thus, the availability of PL under a wide variety of experimental conditions provides for advanced measurement opportunities [37].



Fig. 3.18 Photograph of varian cary eclipse photo luminescence spectrophotometer

Applications of PL analysis range from simple spatial scans of epitaxial wafers to exhaustive investigations of excitation-intensity-dependent PL in novel materials.

Furthermore, new PL techniques continue to emerge, expanding the arsenal of PL analysis. Because PLE is usually absorbed near the surface and interfaces tend to dominate electronic behavior in layered systems, PL is especially well suited to surface and interface investigations. Interfaces are increasingly important in new optoelectronic materials where layered structures are becoming thinner and more complex. Thus, although PL measurements have been useful for the characterization and refinement of such materials, they can be expected to play an even greater role in the future.

## **REFERENCES**

- [1] C. D. Lokhande, Mater. Chem. Phys. 27 (1991) 1.
- [2] G. B. Reddy, V. Dutta, D. K. Pandya and K. L. Chopra, Sol. Energy Mater; 15 (1987) 383.
- [3] P. K. Nair, M. T. S. Nair, A. Fernandez and M. Ocampo; J. Phys. D: Appl. Phys. 22 (1989) 829.
- [4] R. A. Boudreau and R. D. Rauh, J. Electrochem Soc. 130 (1983) 513.
- [5] M. E. Rincon, M. Sanchez, A. Olea, I. Ayala and P. K. Nair, Sol. Energy Mater. Sol. Cells, 52 (1998) 399.
- [6] M. A. Mickelsen and W. S. Chen, Appl. Phys. Lett, 36 (1980) 371.
- [7] T. R. Tuttle, M. A. Contrevas, J. S. Ward, A. L. Tennant, K. R. Ramanathan, J. Keone and R. Noufi in: C. M. Laport et.al (Ed), Proc. SPIE, Bellingham, 2531(1995) 194.
- [8] B. Basol and V. Kapur, IEEE Trans. Electron Dev. 37 (1990) 418.
- [9] Ashour, Turk J Phys. 27 (2003) 551- 558.
- [10] John B Mooney, Shirley B Radding, Ann. Rev. Mater. Sci. 12 (1982) 81.
- [11] M.S. Tomar and F.J. Garcia, Progress in Crystal Growth and Characterization of Materials 4(3) (1981) 221.
- [12] D.S. Albin and S.H. Risbud, Advanced Ceramic Materials 2(3A) (1987) 243.
- [13] B.R. Pamplin, Progress in Crystal Growth and Characterization of Materials 1(4) (1979) 395.
- [14] P.S. Patil, Mater. Chem. Phys., 59(3) (1999) 185.
- [15] P. Bohac, L.J. Gauckler, Oxygen Ion and Mixed Conductors and their Technological Applications, Kluwer Academic Publishers, Dordrecht (2000) 271.
- [16] A. A. Rizkalla, A. H. Lefebvre, J. Eng. Power 97(2) (1975) 173.
- [17] C.M. Lampkin, Progress in Crystal Growth and Characterization of Materials, 1(4) (1979) 405.
- [18] A.M. Ganan-Calvo, J. Davila, A. Barrero, J. Aerosol Sci., 28(2) (1997) 249.

- [19] W.M. Sears and M.A. Gee, Thin Solid Films, 165(1) (1988) 265.
- [20] W. Siefert, Thin Solid Films, 120(4) (1984) 267.
- [21] I.W. Lenggoro, T. Hata, F. Iskandar, M.M. Lunden, K. Okuyama, J. Mater. Res., 15(3) (2000) 733.
- [22] E.K. Oh and S.G. Kim, J. Aerosol Sci., 27(8) (1996) 1143.
- [23] J.C. Viguie and J. Spitz, J. Electrochem. Soc., 122(4) (1975) 585.
- [24] K.L. Choy and B. Su, Thin Solid Films, 388(1–2) (2001) 9.
- [25] C.H. Chen, E.M. Kelder and J. Schoonman, J. Eur. Ceram. Soc., 18 (1998) 1439.
- [26] V. Gowthami, P. Perumal, R. Sivakumar, C. Sanjeeviraja, Physica, B 452 (2014) 1.
- [27] L. I. Maissel, R. Glang, Handbook of thin film technology McGraw-Hill,India (1970)
- [28] D. K. Schroder, Semiconductor Materials and Device Characterisation, John Wiley and Sons New York (1998)
- [29] D. Milathianaki, J. Hawreliak, J. M. McNaney, B. S. El-Dasher, M. D.Saculla, D. C. Swift, H. E. Lorenzana, T. Ditmire, Rev. Sci. Instrum. 80(2009) 093904.
- [30] B. E. Warren, X-ray Diffraction, General Publishing Company Toronto (1969)
- [31] K. L. Chopra, I. Kaur, Thin film device applications Plenum Press New York (1983)
- [32] F. Wenner, Bur. Stand. (U.S.) Bull. 12 (1915) 469.
- [33] L. B. Valdes, Proc. Inst. Rad. Engrs. 42 (1954) 420.
- [34] P. E. J. Flewitt, R. K. Wild, Physical methods for materials characterization IOP Publishing Ltd London (2003).
- [35] O. S. Heavans, Optical properties of thin solid films Dover Publications New York (1991).
- [36] R. H. Bube, Photoelectronic properties of semiconductors Cambridge University press India (1992).
- [37] Timothy H. Gfroerer, photoluminescence in analysis of surfaces and interfaces, Encyclopedia of Analytical Chemistry, John Wiley & Sons, Ltd.(2006).

## CHAPTER - IV

# OPTIMIZATION OF SUBSTRATE TEMPERATURE IN CHEMICAL SPRAY PYROLYSIS TECHNIQUE TO GET P-TYPE LAYERS OF SnS THIN FILMS

Tin sulfide (SnS) thin films were prepared using chemical spray pyrolysis (CSP) technique at different substrate temperatures from 250 °C – 375 °C in steps of 25 °C for optimization, using the precursor solutions of stannous chloride and thiourea. Single-phase, p-type, stoichiometric, SnS film with direct band gap of 1.59 eV and having very high absorption coefficient (10<sup>5</sup>/cm) was deposited at an optimized substrate temperature of 325 °C. The role of substrate temperature (250 °C – 375 °C) in determining the optoelectronic and structural properties of SnS films was established. A comprehensive analysis of these films was done using x-ray diffraction, energy dispersive x-ray analysis, scanning electron microscopy, optical absorption and electrical measurements. Deposition temperatures required for growth of other binary sulfide phases of tin such as SnS<sub>2</sub>, Sn<sub>2</sub>S<sub>3</sub> were also determined.

## 4.1 INTRODUCTION

In terms of cost and efficiency, thin film solar cells hold an optimistic fervor as future resource for sustainable energy. Now the most developed thin film photovoltaic technologies are based on CdTe and CuInSe<sub>2</sub> absorber layers. Recently a maximum efficiency of 19.9% has been achieved at National Renewable Energy Radio frequency Laboratory, United States of America, using Cu(In,Ga)Se<sub>2</sub> based absorber layers [1]. But these materials, due to the difficulty in maintaining stoichiometry, especially in large area films, alleged environmental hazards and high cost of indium are not beneficial in the longer run [2]. Hence there is an urgent need for the development of materials that are easy to prepare, eco-friendly and having easily available constituents. Tin sulfide (SnS) is one such

material, which has high potential in device fabrication due to its non-toxicity and easy availability of the constituent materials. It is a IV–VI layered compound semiconductor with distorted NaCl type orthorhombic crystal structure [3]. Due to its interesting structural, optical and electrical properties, SnS has become an important material for optoelectronics and photovoltaics studies [4–7] with many promising technological applications [8, 9]. Further, properties like high absorption coefficient [10], direct band gap in the range 1.2–1.5 eV and indirect band gap in the range 1.0–1.2 eV [7,11] make SnS a more viable material for photovoltaic applications. Loferski theoretically proved that a maximum efficiency of 25% is achievable for this material [12]. Electronic structure and structural calculations of SnS were deduced from photoelectron spectra by Ettema et al. [13]. Opto-electronic properties suitable for the device fabrication were also reported by several groups [3–7].

SnS thin films could be prepared using different techniques such as vacuum evaporation [14], radio frequency sputtering [15], electro-chemical deposition [16,17], atmospheric pressure chemical vapor deposition [18], plasma enhanced chemical vapor deposition [19], brush plating [20], dip deposition [21], chemical bath deposition [22] and chemical spray pyrolysis (CSP) [23]. Among these, CSP is one of the simplest and cost effective means of thin film deposition, especially when large area deposition is required. Moreover, the ease of doping and flexibility of tailoring the stoichiometry make this technique more popular in the field and adopt well to our requirements of photovoltaic device fabrication. Hence this technique was selected for the deposition of SnS thin films, in the present work.

#### 4.2. EXPERIMENTAL DETAILS

Tin Sulfide (SnS) thin films were deposited at different substrate temperatures using the indigenously designed and fabricated using spray coating unit [24]. It consists of a base plate, in which a heater coil is embedded to facilitate heating, upon which the substrates for film deposition are to be placed. Substrate temperature ( $T_s$ ) was maintained with the help of a feedback circuit which controls the heater supply. Temperature of the substrate can be varied from room temperature to 450 °C using this coating unit. During the spray, temperature of the substrate was kept constant with an accuracy of  $\pm 2$  °C. Spray head and hot plate with substrates were kept inside a chamber provided with an exhaust fan for removing gaseous by-products and vapors of the solvent. Pressure of the carrier gas (air) used for spraying the precursor solution was adjusted manually from an air compressor unit. With the help of indigenously developed dispensing unit, the spray rate of the solution can also be precisely controlled. Spray rate is an important parameter in controlling different properties of the films which can be controlled with an automated spray pyrolysis unit so as to get good repeatability of film properties.

In the present work, precursor solution was a mixture of doubly hydrated stannous chloride  $(SnCl_2 \cdot 2H_2O)$  and thiourea  $(CS(NH_2)_2)$ . The usage of  $SnCl_2$  instead of  $SnCl_4$  reduces material cost as well as the temperature required for deposition substantially, which is very vital for device level applications [25].

Cleaned boro silicate glass slides, with dimensions of  $37\times24\times1.2~\text{mm}^3$  were used as the substrates. For the present study, we prepared sets of films at different substrate temperatures from 250 °C to 375 °C in steps of 25 °C. For all the sets, distance of spray head from the substrate was 30 cm and the total volume of the solution sprayed was 40 ml, which contained equal volumes (20 ml) of  $SnCl_2 \cdot 2 H_2O$  and  $(CS(NH_2)_2)$  respectively. The spray rate was fixed at 2 ml/min since low spray rate favored formation of films with superior surface morphology [24]. Further lowering of deposition rate would require longer coating durations, which is an undesirable condition. Films were prepared by varying  $T_s$  from 250 °C to 375 °C in steps of 25 °C with an accuracy of  $\pm 2$  °C while the molarity of

 $SnCl_2 \cdot 2H_2O$  ( $M_{Sn}$ ) and molarity of  $CS(NH_2)_2$  ( $M_s$ ) were kept constant at 0.1 M respectively. Higher value of  $T_S$  was chosen in considering the high vapor pressure of sulfur.

Thickness of the films was measured using Stylus method (Stylus thickness profiler). Structural analysis was performed by employing X-ray diffraction (XRD) using Rigaku (D.Max.C) x-ray diffractometer having  $CuK\alpha$  ( $\lambda=1.5405A^\circ$ ) radiation and Ni filter operated at 30 kV and 20 mA. All samples were scanned in the range  $10^\circ$  to  $80^\circ$  with a scan speed of  $5^\circ$ /min. Surface studies of the samples were done with the help of scanning electron microscopy (SEM) JOEL, JSM-840. Operating voltage for SEM measurements was 20 kV and the surface morphology of the samples was compared with 25,000 magnifications. Compositional variation of the samples was analyzed using energy dispersive x-ray (EDAX) analysis (operated at 20 kV), which is attached with the SEM (ZeissHR) instrument. Optical absorption studies were carried out using UV–Vis– NIR spectrophotometer (Jasco V-750 model) in the range of 300-1200 nm. Employing Keithley 236 source measure unit, electrical characterization was performed using Hall effect and four probe apparatus. Silver electrodes were painted on the surface of the film on a fixed area with uniform thickness, keeping a distance of 5 mm in between the electrodes for electrical characterizations.

## 4.3. RESULTS AND DISCUSSIONS

The thin films prepared with different substrate temperatures in the range 250 °C – 375 °C as said in the procedure given above, were uniform, free from pinholes and cracks with dark gray in color. Thicknesses of these six samples deposited with different substrate temperatures were determined using Stylus profiliometer. The variation of thickness as a function of substrate temperature is plotted as shown in Fig. 4.1. It reveals that the thickness had decreased linearly as a function of substrate temperature. A similar variation of thickness was observed for SnS films prepared at different substrate temperatures by

Sebastian et al [24]. This may be due to the re-evaporation of the compounds at elevated temperatures.

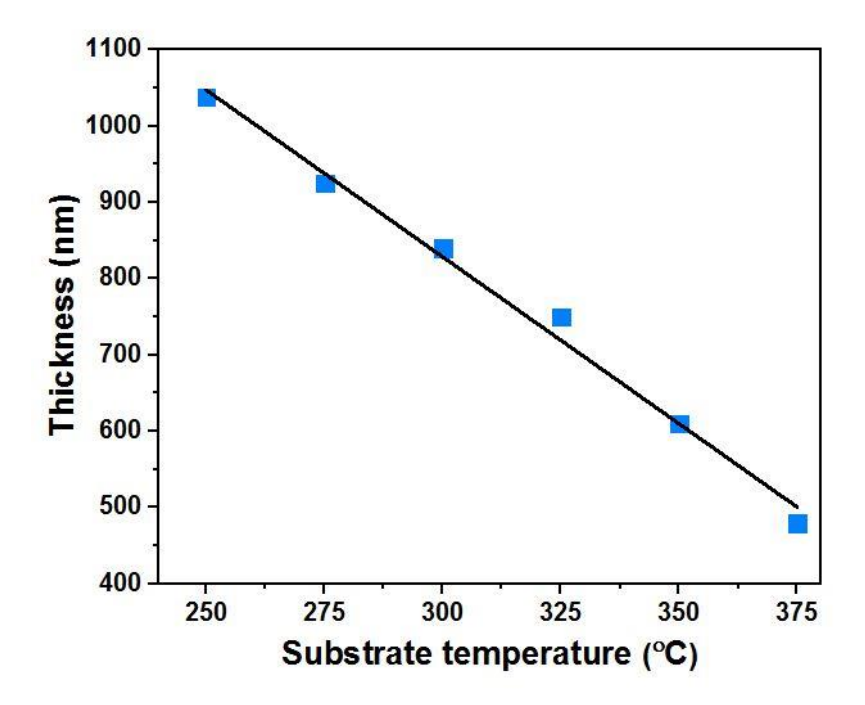


Fig. 4.1. Variation of film thickness of SnS thin films at different substrate temperatures

These films had predominant SnS phase, crystallized in Herzenbergate orthorhombic structure, as observed from the XRD patterns shown in Fig. 4.2. For  $T_s < 250~^{\circ}\text{C}$ , white spots were observed all over the film surface, which indicated the presence of unreacted precursors, as  $T_s$  was lower than the "pyrolytic temperature". For  $T_s > 375~^{\circ}\text{C}$  the films were white in color with prominent  $\text{SnO}_2$  phase. Fig. 4.2 shows XRD patterns of films deposited at different  $T_s$  (250  $^{\circ}\text{C}$ –375  $^{\circ}\text{C}$ ) with SnS peak orientation along (111) plane having Orthorhombic crystal structure with lattice parameters a=4.329~Å, b=11.19~Å, c=3.983~Å, at  $2\theta=31.4932^{\circ}\text{(JCPDS}$  data card 39-0354). The XRD pattern clearly indicated prominent peaks of  $\text{Sn}_2\text{S}_3$  phase at lower  $T_s$  (250  $^{\circ}\text{C}$ ) and  $\text{SnS}_2$  phase at higher  $T_s$  (>375  $^{\circ}\text{C}$ ). These impurity phases almost vanished for 325  $^{\circ}\text{C}$   $T_s$  the films were having better

crystallinity with a single-phase SnS. On increasing the substrate temperature above 350 °C, the peaks corresponding to SnS disappears and the compound was almost converted into SnO<sub>2</sub>. This is probably due to re-evaporation of sulphur from the film at such temperatures because of its high vapor pressure, leaving a tin riched surface which might have reacted with oxygen to form SnO<sub>2</sub> as the deposition was carried out at atmospheric pressure. Nair et al (25) has reported that the conversion of SnS into SnO<sub>2</sub> takes place when the films are annealed at such high temperatures. A similar behavior for the films having different phases deposited at different substrate temperature was reported by Koteeswara Reddy et al (27). Crystallite size of the films was calculated from the peak at  $2\theta = 31.4932^{\circ}$  using the Debye–Scherer formula,  $D = 0.9\lambda/(\beta cos\theta)$ , where D is the diameter of the crystallites forming the film,  $\lambda$  is the wavelength of CuK<sub> $\alpha$ </sub> line,  $\beta$  is the full width at half maximum in radians and  $\theta$  is the Bragg angle. Crystallite size increased slightly as the T<sub>S</sub> increased from 250 °C to 325 °C. (From 17nm to 39nm and slighty decreased after optimised temperature). Crystallite size of the film prepared at T<sub>S</sub> = 325 °C was 39 nm.

The crystallite size increased with the substrate temperature, which is evident from the decrease in the full width at a half maximum (FWHM) of the (111) peak. Fig 4.3 shows the crystallite size plotted against substrate temperature. The crystallite size increased from 17 to 39 nm when the substrate temperature increased from 250 °C to 325 °C and then decreased at 350 °C and 375 °C. Usually crystallite sizes in sprayed films are increasing with the deposition temperature. Reverse effect observed in sprayed tin sulfide films could be explained by the formation of secondary phases, which retard the growth of SnS crystallites. Sajeesh et al also observed a slight decrease in the SnS crystallite size using higher deposition temperatures.

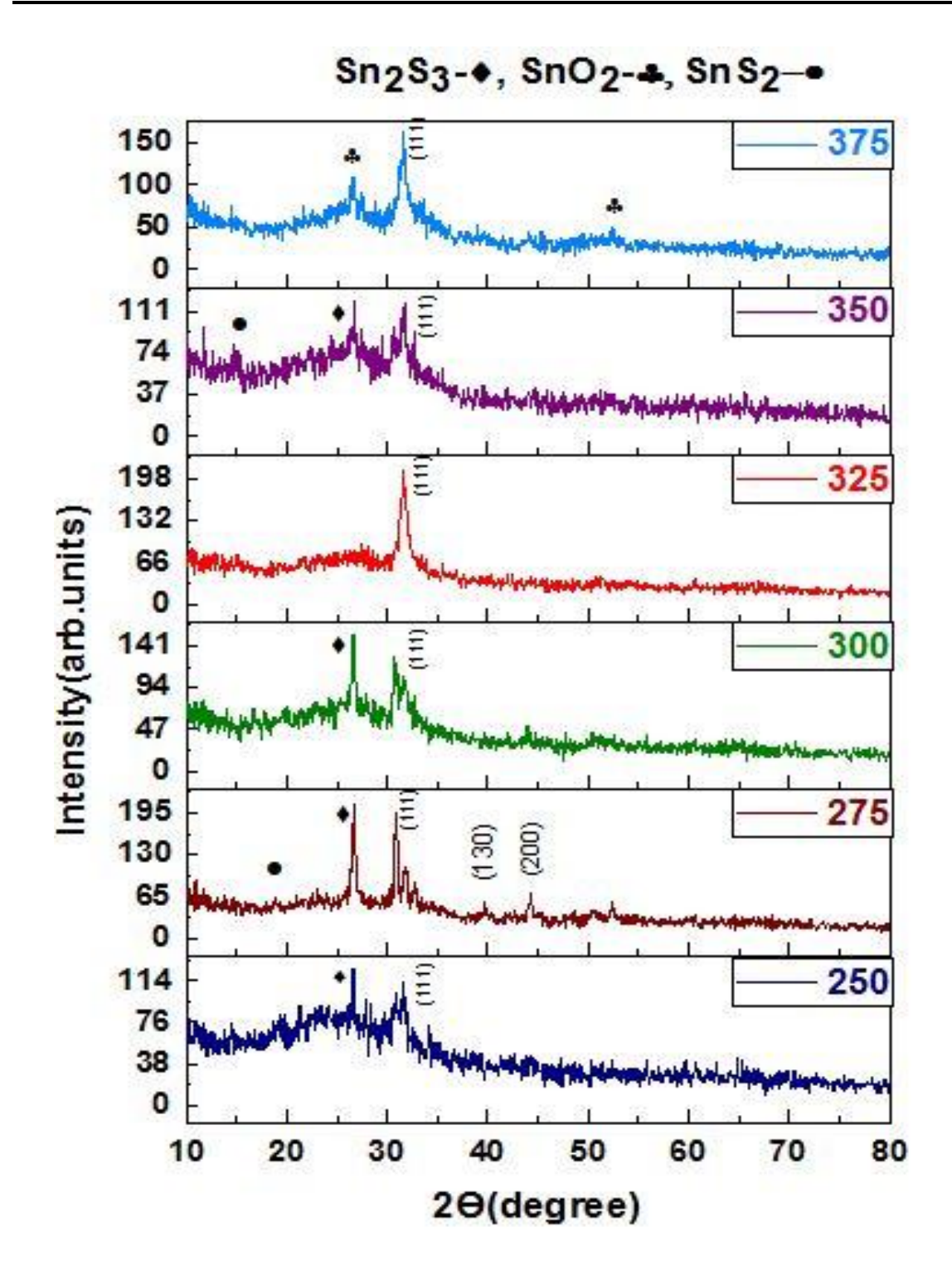


Fig.4.2. X-ray diffraction pattern of SnS thin films at different substrate temperatures (a)  $T_S$  =250°C (b)  $T_S$  =275°C (c)  $T_S$  = 300°C (d)  $T_S$  =350°C and (e)  $T_S$  = 375°C.

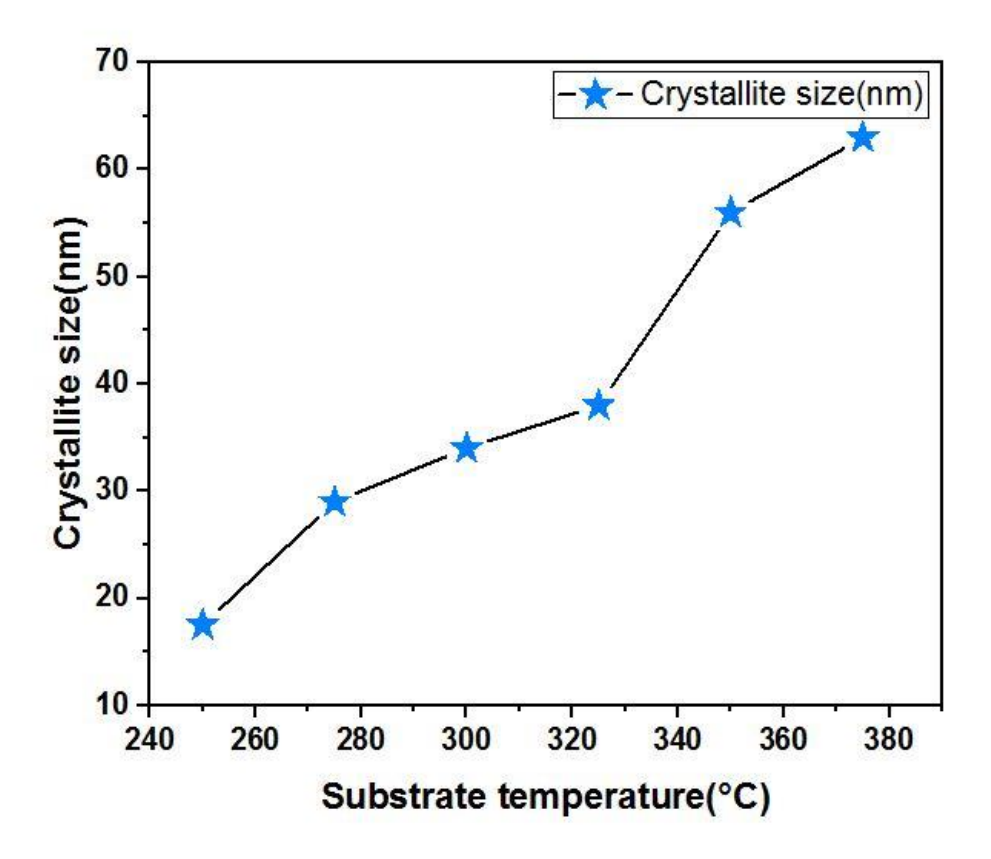


Fig.4.3. Variation of Crystallite size versus SnS thin films at different substrate temperatures

The lattice parameters for the orthorhombic phase were evaluated using the standard equation.

$$\frac{1}{d^2} = \frac{h^2}{a^2} + \frac{k^2}{b^2} + \frac{l^2}{c^2}$$
 ... (4.1)

Where h, k and l are the lattice planes and d is the interplanar distance and using the XRD data for the films deposited in the range of 250 °C-375 °C, we can observe that the unit-cell parameter for the powder of the SnS with a/c = 1.086. According with this, the lattice parameters exhibit a more pronounced change as the temperature of substrate increases. The closest value of the unit-cell parameters to the value of the powder is the SnS thin film with

the substrate temperature at 325 °C with a ratio of a/c=1.081 and the farther is for the SnS thin film grown at 375 °C substrate temperature with a ratio a/c=1.254.

The texture coefficient was determined in order to find the preferential orientation of the crystals in the polycrystalline SnS thin films. This factor can be compute from X-ray diffraction results using the following relation (2):

$$T_{(hkl)} = \frac{I_{m(hkl)}}{I_{0(hkl)}} \left( \frac{1}{N} \sum_{1}^{N} \left( \frac{I_{m(hkl)}}{I_{0(hkl)}} \right) \right)^{-1} \dots (4.2)$$

Where  $I_{m(hkl)}$  is the measured relative intensity of the reflection from the (hkl) plane,  $I_{0(hkl)}$  is that from the same plane in standard reference sample listed in the PDF#39-0354 database, N is the number or reflection peaks from the film. For a film to have a preferential orientation at any (hkl) plane, the texture coefficient must be at least one [25, 26]. From the results of the textured coefficient calculations for different planes, it was found that the preferential orientation of deposited films with different substrate temperatures was the (111) plane. Fig 4.4 shows the graph of the texture coefficient versus the planes of the XRD patterns of the thin films grown at different substrate temperatures.

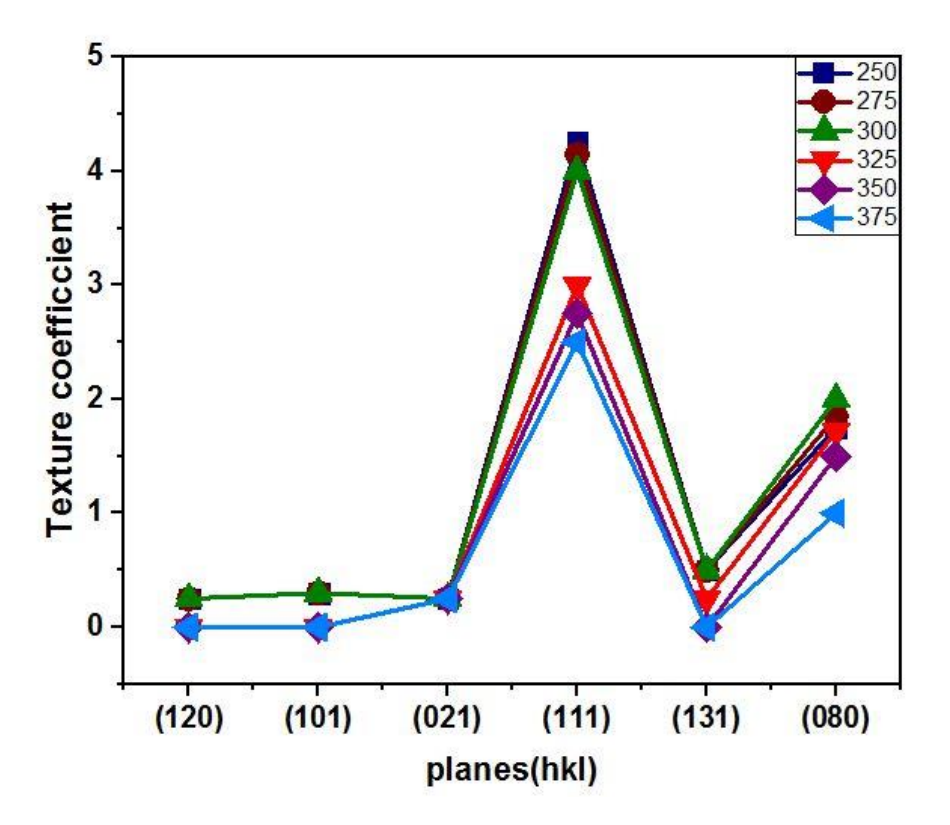


Fig. 4.4 Texture coefficient of the SnS thin films at different substrate temperatures

The strain was calculated using the FWHM's that can be expressed as a linear combination through the following equation:

$$\frac{\beta \cos \theta}{\lambda} = \frac{1}{\varepsilon} + \frac{\eta \sin \theta}{\lambda}$$
 ... (4.3)

Where  $\beta$  is the measured FWHM in radians,  $\theta$  is the Bragg angle of the diffraction peak,  $\lambda$  is the x-ray wavelength,  $\epsilon$  is the effective particle size and  $\eta$  is the effective strain. In the Fig 4.5 we observed a strain versus substrate temperature of the SnS thin films, the lower strain is for the thin films grown at a substrate temperature of the 250 °C and increase as the substrate temperature increase. The SnS thin film grown at 350 °C exhibit the highest value of the strain, this could be due to the high temperature of the substrate and consequently the low mobility of atoms to have a better arrangement in the poly crystal.

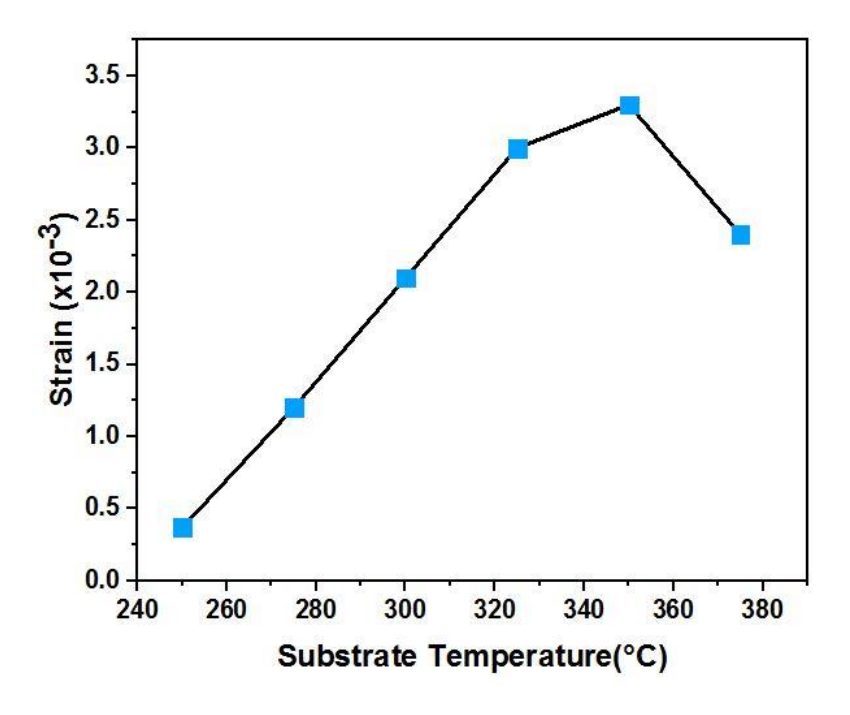


Fig. 4.5 Strain versus different substrate temperatures

# 4.3.1 Morphological Properties

Surface morphology of the sample showed noticeable changes when  $T_s$  increased from 300 °C to 375 °C. It is evident from the SEM image shown in Fig. 4.6d that the samples prepared at  $T_s = 325$  °C had needle like polycrystalline growth, while from Fig.4.6c, it is clear that for samples prepared at  $T_s = 300$  °C the surface is smooth with regular spherical grains. These images agreed well with the SEM images and confirm that film surface changed from regular spherical grain structure to needle like structures with increase in temperature from 250 °C to 325 °C

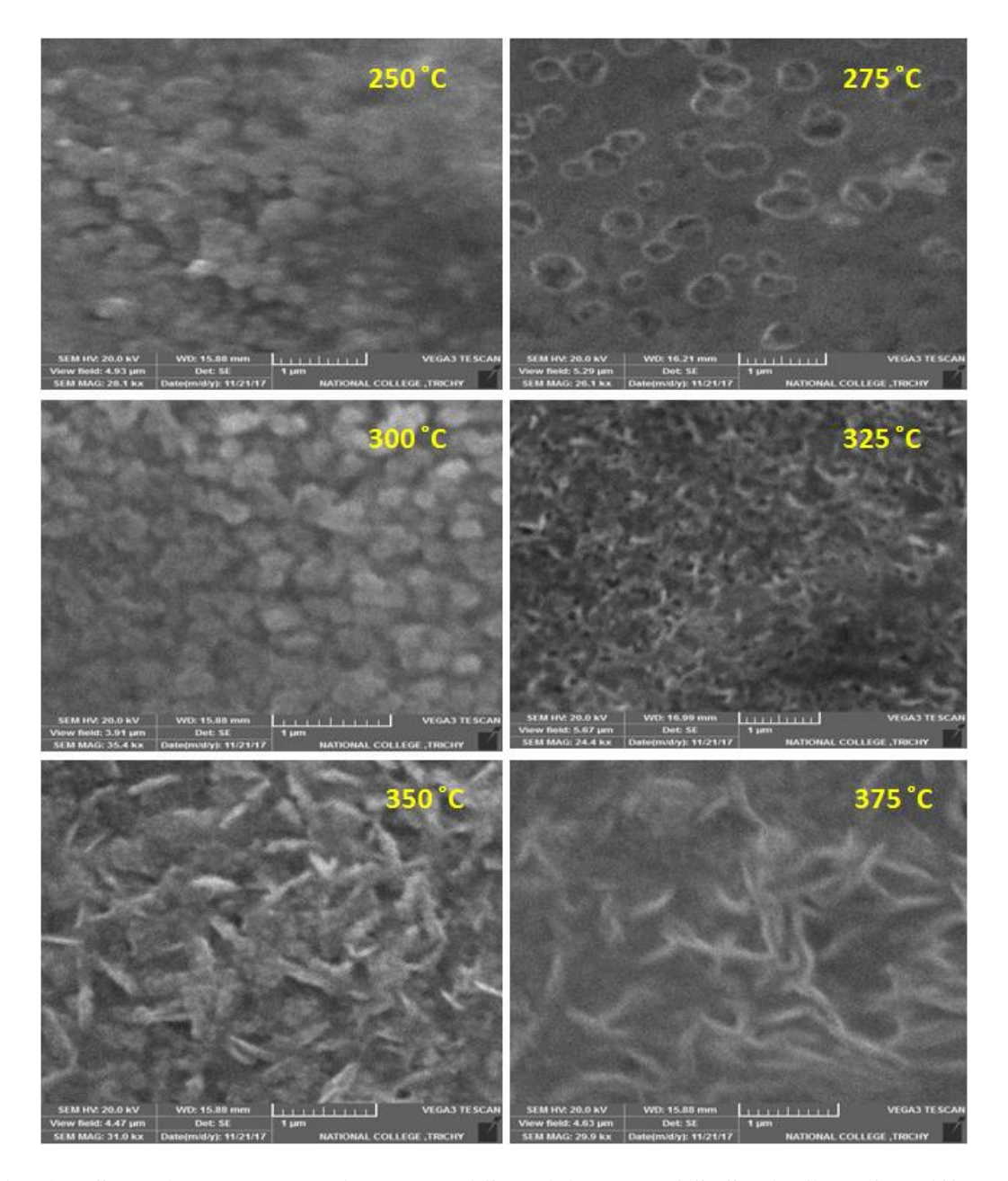


Fig. 4.6. Scanning electron microscope ( SEM ) images of SnS thin films for different substrate temperatures from 250  $^{\circ}C$  – 375  $^{\circ}C$ 

Thickness of the films decreased from 1.038  $\mu m$  to 0.45  $\mu m$  with the increase in  $T_s$  (Fig. 4.1). This might be due to the re-evaporation of the compounds at elevated temperatures. Such a decrease in thickness with increase in  $T_s$  for films fabricated using CSP has been reported earlier [24]

Atomic ratios of Sn and S in the films were examined using EDAX. Variation of Sn/S ratio in the films with respect to the  $T_s$  is depicted in Fig. 4.7. It was observed that, as  $T_s$  was increased, the sulfur incorporation in the film also increased and at  $T_s = 325$  °C we obtained nearly stoichiometric SnS films. But at still higher  $T_s$  (>375 °C) the sulfur content in the film started decreasing, probably due to re-evaporation of sulfur owing to its high vapor pressure.

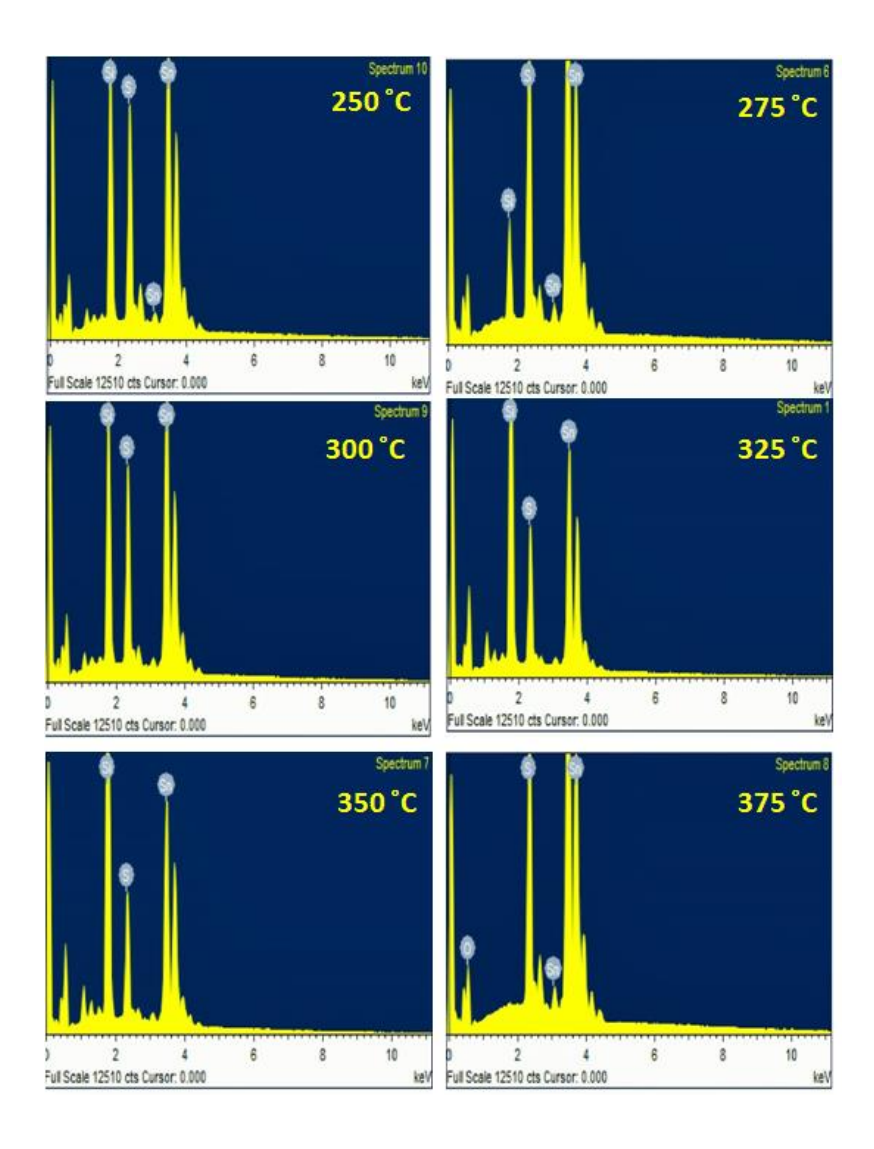


Fig.4.7 Energy dispersive X-ray (EDX) spectra of SnS thin films for different substrate temperatures from 250  $^{\circ}C$  – 375  $^{\circ}C$ 

# 4.3.2 Optical Properties

The dependence of absorption coefficient on photon energy is of importance in studying energy bandgap and transition of electrons. The relation between absorption coefficient ( $\alpha$ ) and the incident photon energy hv is given by

$$(\alpha h \nu)^2 = k(h \nu - E_g)$$

Where k is proportionality constant and  $E_g$  is the direct transition band gap. Thr transmittance spectrum recorded in the wavelength range 300-1200 nm using double beam spectrophotometer. From the Fig.9, the absorption edge primarily shifted from lower wavelength to higher wavelength region and then shifted towards lower wavelength with increase of substrate temperature. The existence of shifting near the fundamental absorption indicated the presence of different phases in the films.

Optical band gap of the films was determined from the  $(\alpha hv)^2$  versus hv plot (Fig. 4.10). All the samples had very high absorption coefficient  $(10^5 \text{ cm}^{-1})$ . Linearity of the graphs confirmed that all the  $Sn_xS_y$  thin films had direct band gap. Band gap of the SnS films prepared at  $T_s = 325$  °C was 1.59 eV which is almost same as that for single-phase SnS films. For SnS films deposited in the range 250 °C to 375 °C, band gap was found to vary. There was no significant variation in the grain size with  $T_s$ , in this temperature range which might affect the band gap. (Fig.4.12) depicts the variation of band gap for the entire range of  $T_s$ . Here we can observe close similarity with the graph giving the variation of Sn/S ratio (Fig.4.11). This indicates the dependence of band gap on composition. The high value of band gap at lower and higher temperature is probably due to the formation of  $Sn_2S_3$  and  $SnS_2$  phases respectively [27]. Nearly stoichiometric and single phase SnS films were observed at 325 °C, with an absorption coefficient of  $\alpha > 10^5 \text{ cm}^{-1}$  and the evaluated energy band gap was 1.59 eV which was good agreement with Akkari et al. on SnS deposited by

chemical bath deposition method. This similar type of variation in energy bandgap with substrate temperature was reported by Reddy et al., Lopez and Ortiz.

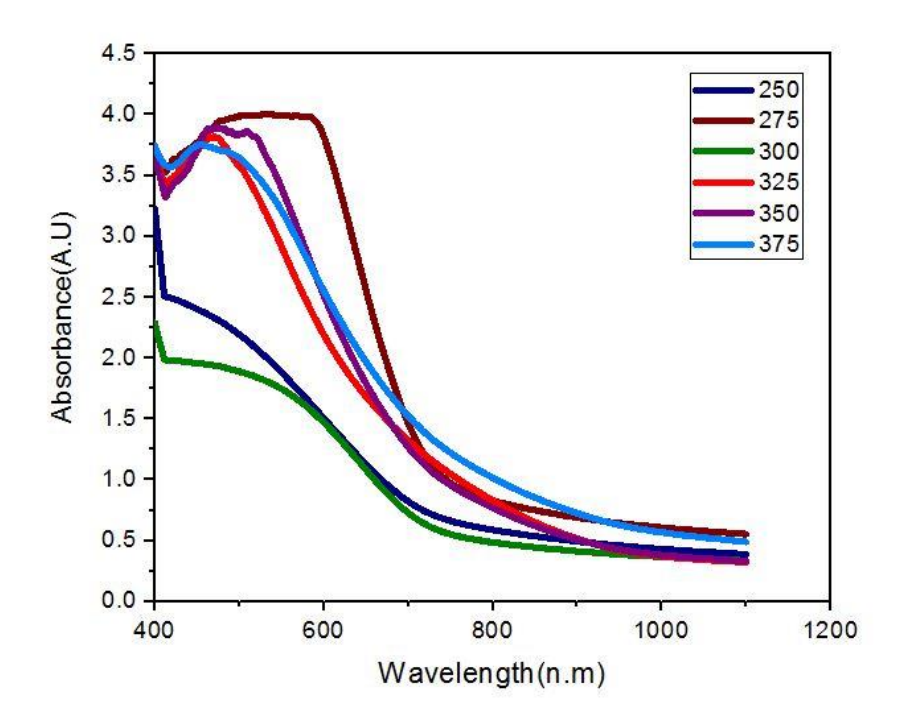


Fig.4.8. Absorbance spectra of SnS thin films at different substrate temperatures

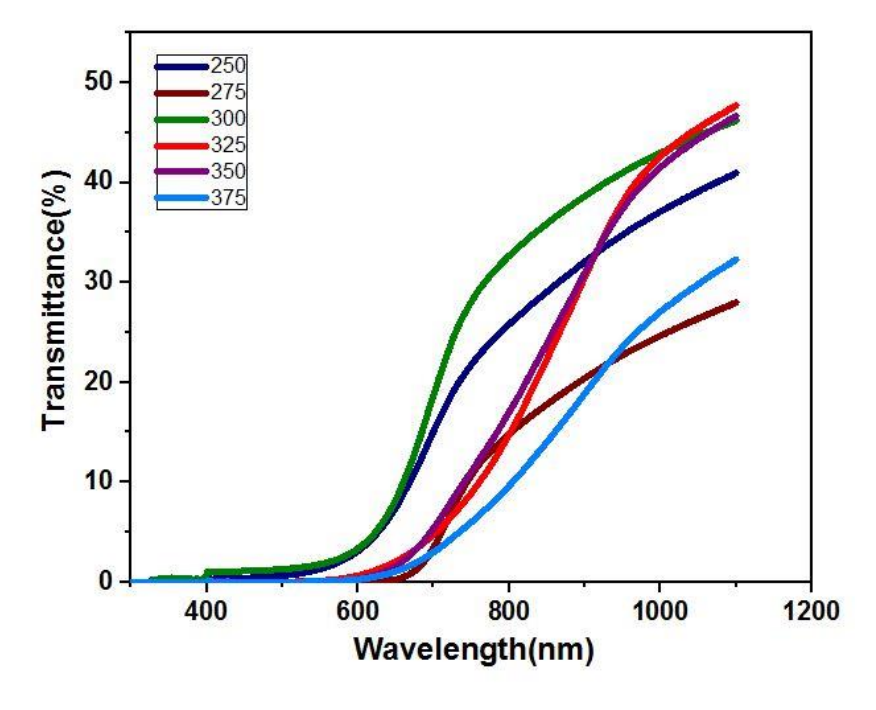


Fig.4.9. Transmittance spectra of SnS thin films at different substrate temperatures

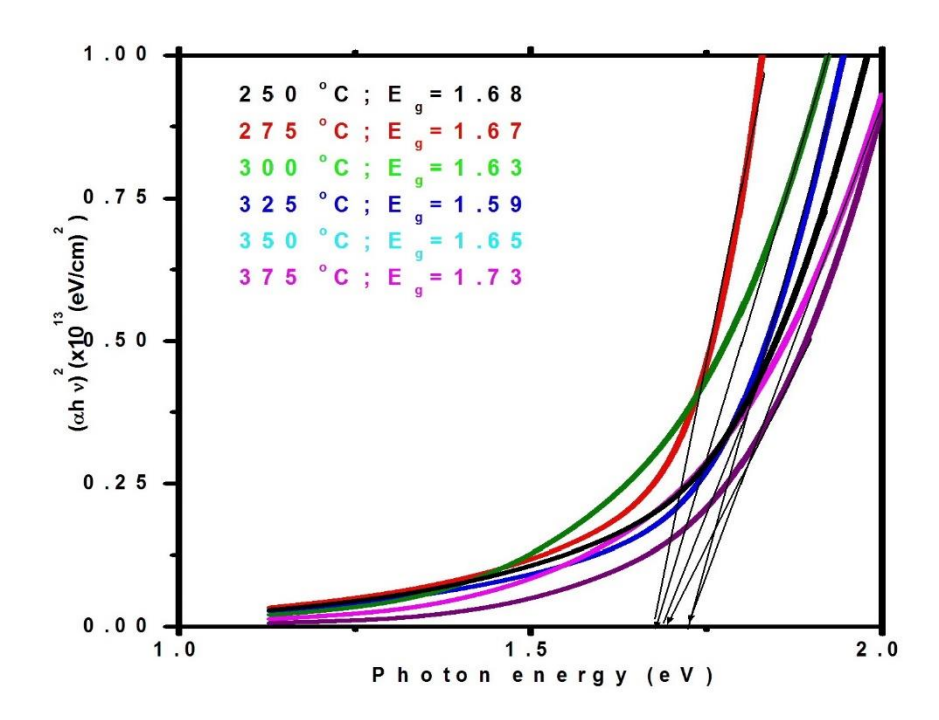


Fig.4.10. Energy band gap of SnS thin films at different substrate temperatures

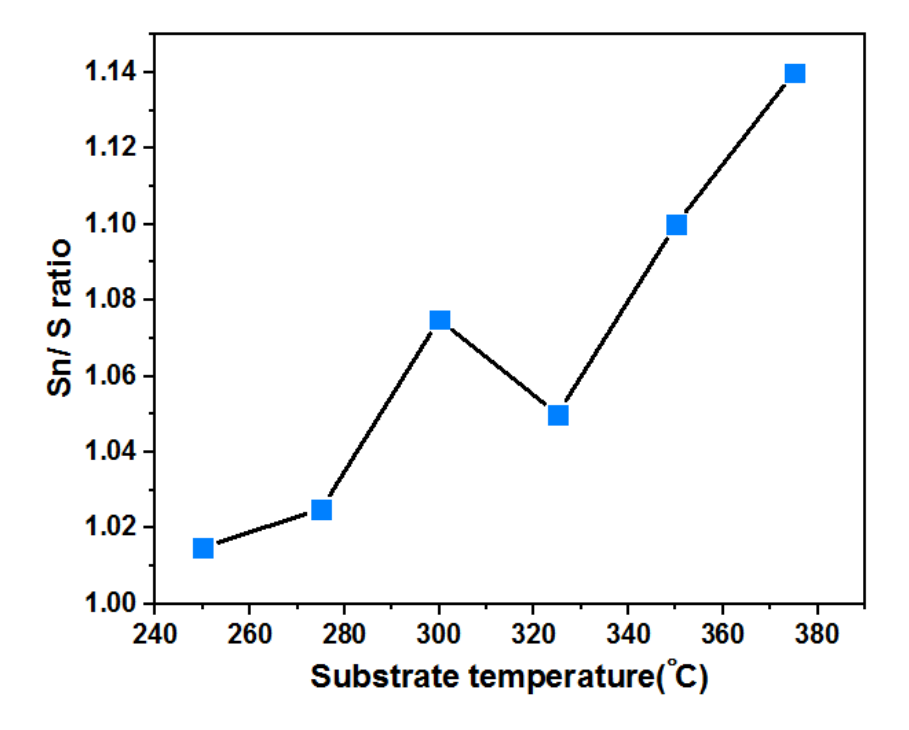


Fig.4.11. Variation of Sn/S ratio with different substrate temperatures

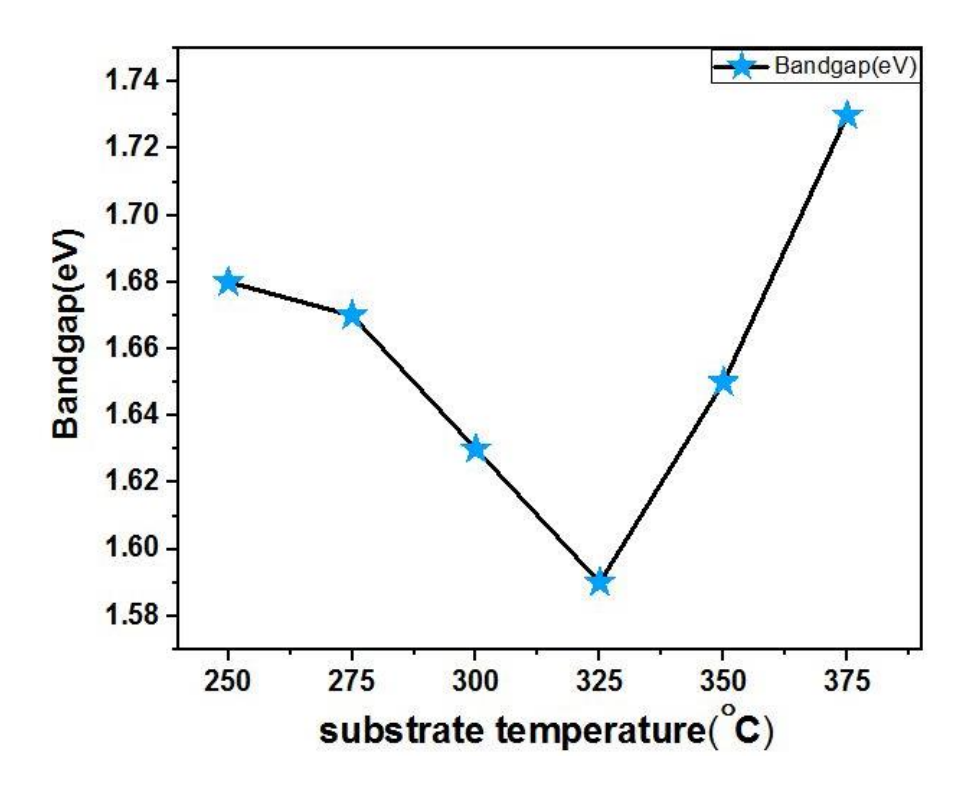


Fig.4.12. Variation of Band gap of the films with different substrate temperatures

# 4.3.3 Electrical Properties

Resistivity of the films decreased from  $5 \times 10^3~\Omega$  cm to  $5~\Omega$  cm with the increase in  $T_s$ . High value of resistivity of the films prepared below 300 °C was probably due to presence of mixed valent compound  $Sn_2S_3$ . Hot probe analysis was carried out on the sample to determine the conductivity type. This measurement indicated that the films prepared in the range  $T_s = 300~\text{°C}-375~\text{°C}$  were p-type and the films prepared at  $T_s = 300~\text{°C}$  showed fluctuating nature in hot probe analysis, which may be due to the very high resistivity of these films. Hence it can be concluded that films prepared at 325 °C have the optimal qualities of an absorber layer in terms of crystallinity, high absorption coefficient, band gap and stoichiometry. Therefore  $T_s = 325~\text{°C}$  was chosen for further deposition of SnS films.

The electrical resistivity, carrier concentration and mobility of the films deposited at different substrate temperature are given in table 1. The resistivity value increases rapidly with increasing substrate temperature the presence of mixed phases like  $SnS_2$  and  $Sn_2S_3$  with

SnS, that are highly[ resistive, might be responsible for the resistivity, exhibited by the films deposited at the lower temperature. The films formed at higher substrate temperature like 375 °C showed lower resistivity, which was due to presence of conductivity oxide phase of Sn-O-S along with SnS. However, single phase SnS film deposited at 325 °C had resistivity value of  $7.897 \times 10^3 \,\Omega$ -cm, a net carrier concentration of  $2.163 \times 10^{14}$  and mobility  $3.65 \times 10^{-1}$  cm<sup>2</sup>/Vs. The similar behaviour for SnS films has been reported by Koteeswara Reddy and Ramakrishna Reddy. 7.2.

Table 4.1 Electrical resistivity, Carrier concentration and Mobility for SnS thin films deposited at different substrate temperatures

Substrate temperature(° C)	Resistivity x10³ (Ω-cm)	Carrier concentration x10 <sup>14</sup> (cm <sup>-3</sup> )	Mobility (cm²/Vs) x10 <sup>-1</sup>
250	7.67	4.37	3.45
275	7.77	9.31	8.62
300	7.84	4.85	1.64
325	7.90	2.16	3.65
350	8.09	9.17	8.41
375	8.02	5.32	1.46

# **4.3.4.** Optimization of precursor at different temperature for p-type SnS absorber layer.

Ratio of anionic to cationic precursors in the spray solution plays a significant role in compound formation as well as in determining optoelectronic properties of the films, especially when the samples are prepared using CSP technique. Hence the films were prepared for optimizing concentration of precursors to obtain single-phase p-type SnS films so that it can be used as absorber layer in solar cells. Analyzing the films deposited by varying T<sub>s</sub>, we could optimize T<sub>s</sub> required for obtaining single-phase SnS at 325 °C of 0.1 M in the precursor solution resulted in the formation of films with SnS phase only. But for

 $T_s > 375$  °C,  $SnO_2$  was dominating and films showed presence of the 'mixed valency' compound  $Sn_2S_3$ , as observed from the XRD pattern (Fig. 2). From these results it appears that, for a given ratio of precursors, there will be an optimum pyrolytic temperature, which favors formation of a particular compound and when we select 0.1 M as the value of  $M_s$ , the substrate temperature of 325 °C is found to be optimum for depositing SnS films.

Hot probe analysis indicated that SnS films thus deposited were p-type and resistivity measurements using 'two probe method' gave a resistivity value of  $60~\Omega$  cm.

# 4.4. CONCLUSION

SnS thin films were prepared using Chemical spray pyrolysis technique at different deposition temperature using stannous chloride and thiourea as precursor solution and they were optimized for fabrication of stoichiometric SnS films that can be used as p-type, direct band gap absorber layer suitable for solar cells. Band gap engineering of single-phase SnS thin film was achieved in the temperature region 250 °C-375 °C, which finds application in fabrication of solar cells. For all the deposition temperatures, p-type SnS films were obtained and the films were highly absorbing with suitable direct energy bandgap for fabrication of SnS homojunction. Highly photosensitive SnS films which had photocurrent value thrice that of the dark current, can also find application as smart material.

#### **REFERENCES**

- [1] J.I. Repins, M.A. Contreras, B. Egaas, C. De, Prog. Photovoltaics Res. Appl. 16 (2008) 235.
- [2] T. Markvart, L. Castaner, Elsevier publication, New-York, 2003.
- [3] W. Albers, C. Hass, H.J. Vink, J.D. Wasscher, J. Appl. Phys. 32 (1961) 2220.
- [4] J.B. Johnson, H. Jones, B.S. Latham, J.D. Parker, R.D. Engelken, C. Barber, Semicond. Sci. Technol. 14 (1999) 501.
- [5] P. Pramanik, P.K. Basu, S. Biswas, Thin Solid Films 150 (1987) 269.
- [6] D. Avellaneda, G. Delgado, M.T.S. Nair, P.K. Nair, Thin Solid Films 515 (2007) 5771.
- [7] G. Valiukonis, D.A. Guseinova, G. Keivaitb, A. Sileika, Phys. Status Solidi B 135 (1986) 299.
- [8] T. Jiang, G.A. Ozin, A. Verma, R.L. Bedard, J. Mater. Chem. 8 (1998) 1649.
- [9] A.T. Kana, T.G. Hibbert, M.F. Mahon, K.C. Molloy, I.P. Parkin, L.S. Price, Polyhedron 20 (2001) 2989.
- [10] M. Parenteau, C. Carlone, Phys. Rev. B: Condens. Matter 41 (1990) 5227.
- [11] H. Noguchi, A. Setiyadi, H. Tanamura, T. Nagatomoto, O. Omoto, Sol. Energy Mater. Sol. Cells 35 (1994) 325.
- [12] J.J. Loferski, J. Appl. Phys. 27 (1956) 777.
- [13] A.R.H.F. Ettema, R.A. de Groot, C. Hass, T.S. Turner, Phys. Rev. B: Condens. Matter 46 (1992) 7363.
- [14] L. Price, I.P. Parkin, A.M.E. Hardy, R.J.H. Clark, Chem. Mater. 11 (1999) 1792.
- [15] W.G. Pu, Z.Z. Lin, Z.W. Ming, G.X. Hong, C.W. Quin, Proceedings of the first world conference on Photovoltaic Energy Conversion, Hawaii, Dec 5–9 1994, p. 365.
- [16] S. Cheng, Y. Chen, C. Huang, G. Chen, Thin Solid Films 500 (2006) 96.

- [17] Z. Zainal, M.H. Sussein, A. Kassim, A. Ghazali, Sol. Energy Mater. Sol. Cells 40 (1996) 347.
- [18] L.S. Price, I.P. Parkin, T.G. Hillbert, K.C. Molloy, Chem. Vapor. Depos. 4 (1998) 222.
- [19] A.S. Juarez, A. Ortiz, Semicond. Sci. Technol. 17 (2002) 931.
- [20] B. Subramanian, C. Sanjeeveiraja, M. Jayachandran, Sol. Energy Mater. Sol. Cells 79 (2003) 57.
- [21] C.R. Sehhar, K.K. Malay, D.D. Gupta, Thin Solid Films 350 (1999) 72.
- [22] P. Pramanik, P.K. Basu, S. Biswas, Thin Solid Films 150 (1987) 269.
- [23] H. Ben Haj Salah, H. Bouzouita, B. Rezig, Thin Solid Films 480–481 (2005) 439.
- [24] T. Sebastian, R. Jayakrishnan, C. Sudha Kartha, K.P. Vijayakumar, Open Surf. Sci. J. 1 (2009) 1.
- [25] G. Gordillo, L.C. Moreno, W. de. La Cruz, P. Teheran, Thin Solid Films 252 (1994) 61.
- [26] K.L. Chopra, S.R. Das, Plenum Press, New-York, 1983.
- [27] N. Koteeswara Reddy, K.T. Ramakrishna Reddy, Physica. B 368 [2005].

# CHAPTER - V

# EFFECT OF TIN PRECURSOR CONCENTRATION ON PHYSICAL PROPERTIES OF SPRAY DEPOSITED TIN SULFIDE THIN FILMS

# 5.1 INTRODUCTION

Semiconductor thin films have fascinating application in the field of photovoltaic energy conversion [1–3]. Tin sulfide is IV-VI class of compound forming a multiplicity of phases such as SnS, SnS<sub>2</sub>, Sn<sub>2</sub>S<sub>3</sub>, Sn<sub>3</sub>S<sub>4</sub>, etc. due to their varying coordinating characteristics of tin and sulfur. Amongst these semiconductors, tin sulfide (SnS) has NaCl type structure. Thin film of tin sulfide is composed of sheets of tin atoms and sheets of sulfur atoms [4] and has many properties like high optical absorption co-efficient (>10<sup>4</sup> cm<sup>-1</sup>) in the visible region [5], p-type electrical conductivity [6,7], wide optical band gap [8], etc. These properties support the use of this material as a window layer in thin film solar cells [9]. Ozin and co-workers reported that excellent gas sensors can be fabricated for sensing NH<sub>3</sub>, H<sub>2</sub>S or alcohols with nanoporous SnS. Thin films of SnS were fabricated by various techniques like close-spaced sublimation [11], sulphurization of metallic precursors [12], atmospheric pressure chemical vapor deposition [13], chemical vapor transport [14], chemical deposition [15], vacuum evaporation [16,17], dip coating [18,19], solvothermal process [20], chemical spray pyrolysis technique. The ratio of molarities of thiourea solution was kept constant at 0.2 M.

# 5.2 EXPERIMENTAL DETAILS

Tin sulfide thin films were deposited onto amorphous glass substrates with different precursor concentrations of tin species by spray pyrolysis technique. The molarity of thiourea solution was kept constant at 0.2 M and the concentration of the tin species varied from 0.05M to 0.25M in steps of 0.05M. A detailed description of the mechanism of spray

pyrolysis method has been given by Amalraj *et al.* [24]. The precursor solutions of tin II chloride di hydrate ( $M_{Sn}$ ) (SnCl.2H<sub>2</sub>O) and thiourea ( $M_{S}$ ) (CS (NH<sub>2</sub>)<sub>2</sub>) were prepared separately using a solvent containing de-ionized water and isopropyl alcohol in 1:1 ratio, respectively. Two drops of concentrated hydrochloric acid were added for complete dissolution. An equal volume of Tin II chloride di hydrate and thiourea solutions were mixed together and sprayed onto the hot glass substrates with an area of  $75 \times 24$  mm<sup>2</sup>. The deposition parameters like the substrate temperature, carrier gas pressure, volume of the solution and nozzle to substrate distance were fixed as  $325^{\circ}$  C, 0.8 Kg/cm<sup>2</sup>, 40 ml and 1 cm, respectively. After deposition of these films, it was allowed to cool to room temperature, cleaned with distilled water, dried and then stored in a desiccator.

#### 5.3 RESULTS AND DISCUSSION

The color of the thin film prepared with 0.05 M concentration was pale golden yellow with less adhesion to the substrate. Thin films prepared with 0.1 M, 0.15 M and 0.2 M concentrations had good adherence and were gray in color. The obtained film looked shiny with multiple colors due to internal multiple reflections and dark gray in color due to transmitted light. For 0.25 M concentration, the film appeared with brown color along the edges of the film and with a dark gray in the middle with good adhesion. This variation in the color may be due to light variation in the temperature of the substrate which may be evident and prominent at higher concentration. The thickness values were determined as 300, 350, 410, 555 and 520 nm for the samples prepared with the tin precursor concentrations of 0.05, 0.1, 0.15, 0.2 and 0.25 M, respectively.

# **5.3.1** Structural Studies

The XRD profiles of these five samples are shown in Figure 5.1. From the XRD profiles, all the SnS thin films showed a broad peak around 31.7° with a preferential orientation along (111) plane revealing the polycrystalline nature having the Orthorhombic structure. The peaks corresponding to other planes of SnS were not observed, indicating these SnS films were highly textured. This orientation (111) was well matched with the JCPDS file no-39-0354. The low intensity diffraction peak was observed around 31.7° at the precursor concentration of 0.05 M. The intensity of diffraction peak shows polycrystalline phase became more intense and sharp with the increase in precursor concentration up to 0.2 M, which shows an enhancement of the crystallinity of the layers. Above this precursor concentration, the peak intensity of the (111) is reduced and other peaks corresponding to Sn<sub>2</sub>S<sub>3</sub> and SnS<sub>2</sub> materials such as 21.33° (110) and 14.88° (001), respectively, started to appear. At higher precursor concentration of tin species, the presence of multi-phases (Sn<sub>2</sub>S<sub>3</sub> and SnS<sub>2</sub>) along with SnS phase might be due to less availability of sulfur atoms. These peaks are in good agreement with the standard JCPDS card No-72-0031 (Sn<sub>2</sub>S<sub>3</sub>) and 23-0677 (SnS<sub>2</sub>). At higher precursor concentration of 0.25 M, growth in the surface of the substrate and leads to the nonlinear growth in this precursor concentration leads to the homogeneous reaction which in turn leads to the peeling of the films, therefore the thickness with precursor concentration can attributed to the decrease in intensity of (111) peak.

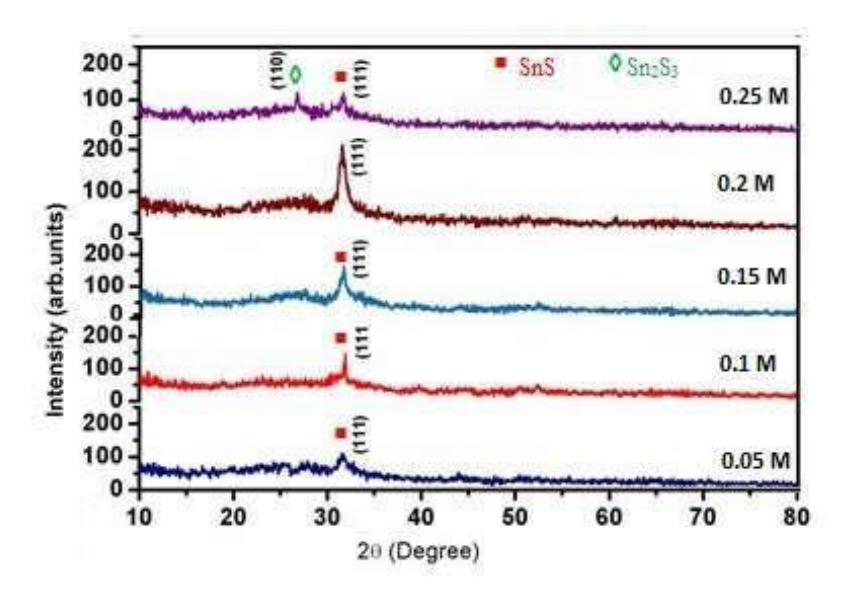


Fig. 5.1 XRD of SnS thin films with different precursor concentrations

From the XRD pattern of all the SnS films, the peak slowly increased with the increase in precursor concentration of 0.2 M, the peak fully disappeared and started to appear for further increase in precursor concentration. The hump of SnS film was formed due to X-rays reflected from the amorphous glass substrates. From the XRD profiles, it was concluded that single phase material of SnS could be prepared with cation precursor concentration in the range of 0.05 to 0.2 M, the latice parameter values of the peak were determined from the orthorhombic structure these values were comparable with JCPDS standard data (JCPDS card No.39-0354).

The peak position (2 $\theta$ ), FWHM values and stacking fault probability ( $\alpha$ \*) present in all the samples were calculated and listed in table. 5.1. The crystallite size, strain and dislocation density was determined [26] and was tabulated in table 5.1. The dislocation is an irregularity in the crystal structure. It can strongly affect many properties of the materials. Crystalline material contains periodic structure with the molecules or atoms placed in repeating fixed positions and this periodicity can be determined by the unit cell parameters. The dislocation or the crystallographic defects interrupt the regular periodic lattice structure.

The dislocation density ( $\delta$ ) can be evaluated using relation [27]. The stacking fault probability  $(\alpha^*)$  is a fraction of layers that undergo stacking sequence faults in a given crystal. The stacking fault probability affect the optoelectronic properties of the films due to the distorted lattice and was determined using the relation [28]. The sizes of the crystallites in all the cases are found to be in nano range (5 nm - 35 nm) and these nanocrystallites explain that the SnS thin films have larger nucleation rate than the growth rate due to more number of nucleation centers that exist on the substrate surface [29]. The size of the SnS crystallites found to increase from 5 nm to 35 nm with the increase in precursor concentration from 0.05 to 0.2M. The increase in crystallite size may be attributed to the improvement of the crystallinity and an increase in the cluster formation owing to increase of precursor concentration leading to agglomeration of small crystallites. These agglomerated crystallites combine together, resulting in the formation of larger crystallites with better crystallinity. The crystallite size decreased to 13 nm when the precursor concentration was increased up to 0.25 M, where the decrease may be due to the lesser thickness corresponding to 0.2 M film thickness and hence less agglomeration among them. Kherarchi et al. [30] had reported the similar crystallite size values (12.35 nm - 16.98 nm) on the influence of various tin molarities for SnS thin films prepared by an ultrasonic spray technique. The crystallite size of the SnS can be affected by so many factors such as impurities, defects and heating conditions. Figure 5.2 shows the variation in the crystallite size, strain and dislocation density of the films as a function of precursor concentrations. The lattice strain, dislocation density and stacking fault probability of the films decreases with an increase in precursor concentration up to 0.2 M and is increased for further increasing of molar concentration. From these observations, it is clear that when the precursor concentration of tin increases, the crystallite size increases and this leads to a decrease in grain boundaries, lattice strain, dislocation density and stacking fault probability.

The decrease in grain boundaries at higher precursor concentration (0.2 M) indicates the reduction of crystal lattice imperfections and formation of high-quality films.

Table 5.1 Variation of structural and elemental properties of SnS thin films with different precursor concentration

Precursor	Peak	FWHM	Crystallite size (nm)	Stacking fault (×10 <sup>-3</sup> J/m <sup>2</sup> )	Elemental composition		
(Msn)	position 20 (degree)				Sn (at.%)	S (at.%)	Sn/S ratio
0.05	31.7662	0.4920	11.9	20.82	50.5	49.5	1.02
0.1	31.7710	0.4920	17.5	9.5	52.2	47.8	1.12
0.15	31.7847	0.4920	19	5.5	56.3	46.7	1.14
0.2	31.7932	0.3936	29.2	4.1	53.9	46.1	1.17
0.25	31.6292	0.5904	14.6	8.6	54.4	45.6	1.19

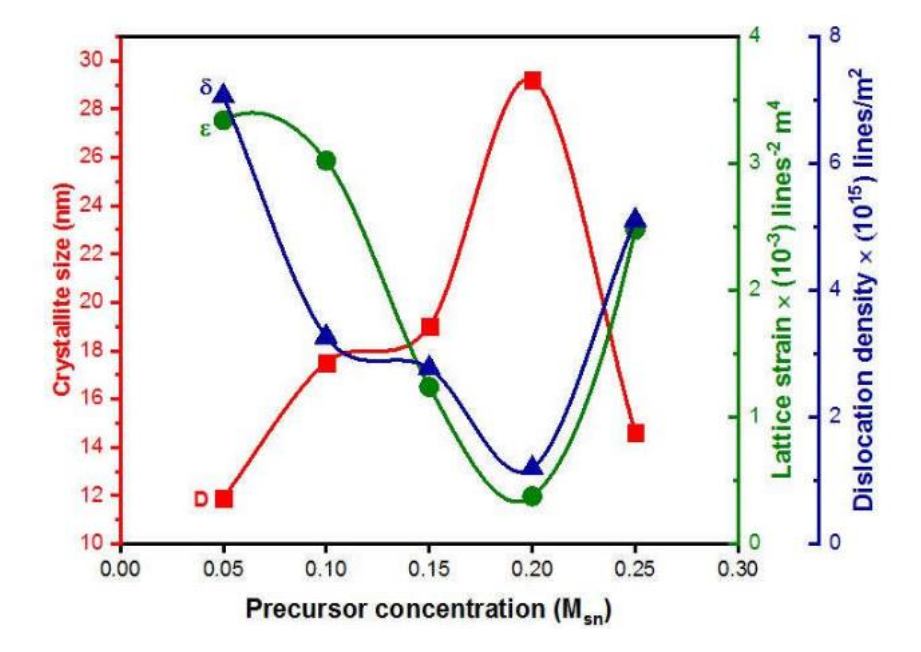


Fig. 5.2 The variation of structural parameters with different tin concentration of SnS thin films

# **5.3.2** Surface Morphology

The surface morphology of tin sulfide thin films was grown by spray pyrolysis technique with different tin precursor concentrations and was characterized and analyzed by photographing the scanning electron microscope images as shown in Figure 5.3. These SEM photographs were recorded with magnifications of about 20,000. The SEM images show that the surface morphology strongly depends upon molar concentrations of the tin species solutions. For the films formed with the molar concentrations of 0.05–0.2 M, the solution droplets containing tin chloride and thiourea reach the substrates where the evaporation of solvent occurs thereby forming a solid phase of SnS in the form of thread-like crystallites. The needle-shaped grains of SnS were spread homogeneously over the surface of the films. It has been observed that needle-shaped SnS grains are found to increase in size with an increase in precursor concentrations. The definite and well-grown plate like formation of grains was observed for the film prepared with the precursor concentration of 0.2 M. Similar needle-shaped grains for SnS films were observed in the earlier reports [13,31,32]. However, the surface morphology of the film prepared with the precursor concentration of 0.25 M is distinctly different from other SEM images. The high density of clusters or heaps was randomly distributed on the surface of the film at the higher precursor concentration of tin species due to faster nucleation and their grain boundary not being clearly visible. When increasing the precursor concentration from 0.2 to 0.25 M, there is a lower probability of rearrangement of the arriving material and the inhomogeneity increases inducing the formation of clusters [33]. Such morphology may be due to the presence of multiphase (SnS<sub>2</sub>) and Sn<sub>2</sub>S<sub>3</sub>) material along with SnS material which was evident from the XRD analysis discussed earlier.

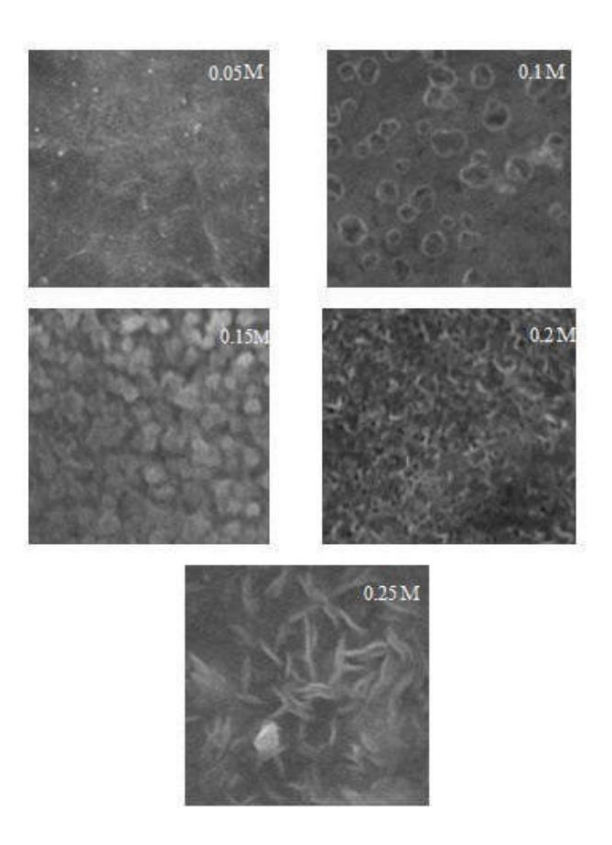


Fig. 5.3 SEM images of SnS thin films with different precursor concentrations

EDAX spectrum of tin sulfide thin film prepared with the precursor concentrations of 0.05-0.25 M was recorded in the binding energy region of 0.5–13.0 KeV as shown in Figure 5.5. The atomic percentage of tin and sulfur was observed as 50.5% and 49.5%, respectively, for the first sample (0.05 M). The atomic percentage of sulfur had decreased from 49.5% to 45.6% when increasing the precursor concentrations from 0.05 to 0.25 M, respectively. The nearly correct stoichiometric ratio of 49.5:50.5% was observed for tin and sulfur at the precursor concentration of 0.2 M. For 0.25 M precursor concentration, the atomic percentage of tin and sulfur was observed as 54.4 and 45.6%, respectively, which predicts the mixed phases of SnS<sub>2</sub>, Sn<sub>2</sub>S<sub>3</sub> and SnS present in this film prepared with a precursor concentration of 0.25 M. The changes observed in the stoichiometric ratio with precursor concentration were also supported by the structure analysis and surface

morphology. Variations of tin and sulfur percentage with different precursor concentrations were listed in Table 5.1.

Below 600 nm, multiple interference effect was not predominant in all the films, which may be due to the absorption of such photons and hence the absence of coherence [6]. The transmittance value of all the SnS films is in the visible region and it decreased with an increase in precursor concentration from 0.05 M to 0.2 M and with further increase in the precursor concentration to 0.25 M, the transmittance had increased. The decrease in transmittance may be attributed to the increase in film thickness which leads to an inversion in loss of intensity due to absorption and scattering. Thus the absorption coefficient "α" of the SnS thin film was calculated in the visible region using thickness "t" and the absorption spectrum. The variation of "α" with wavelength is plotted for these SnS thin films as shown in Figure 5.6. The calculated absorption coefficient value for SnS films exceeds 10<sup>4</sup> cm<sup>-1</sup>, which indicates that the layers were with high absorption value. Hence, the layers might be suitable for photo voltaic devices [35]. The absorption is more for high-energy photons in the recorded region for this SnS material. A similar absorption coefficient value had been reported by Wang *et al.* [31].

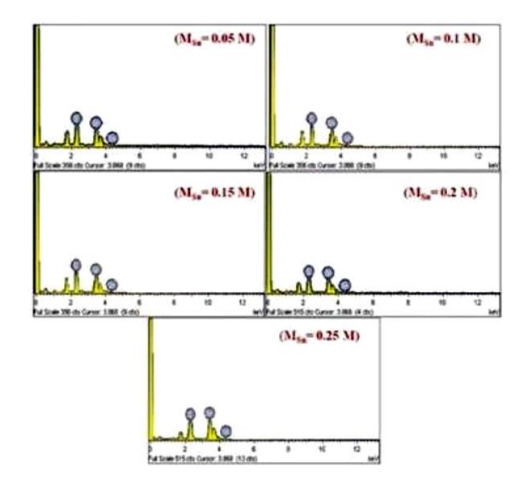


Fig. 5.4 EDAX images of SnS thin films with different precursor concentrations

# **5.3.3** Optical Properties

The optical transmittance spectra obtained from the recorded absorption spectra of the as grown SnS thin films prepared with different tin precursor concentrations are shown in Figure 5.5. The multiple interference effect was observed for all the five samples in the wavelength region of 400–1100 nm, which confirms the formation of uniform and smooth films.

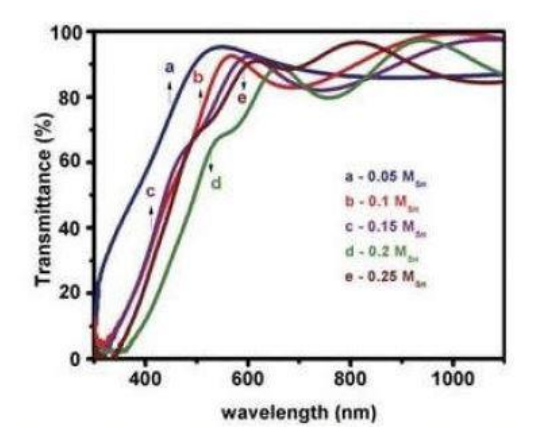


Fig. 5.5 A plot of transmittance spectra of SnS thin films with different precursor concentrations

Below 600 nm, multiple interference effect was not predominant in all the films, which may be due to the absorption of such photons and hence the absence of coherence [6].

The transmittance value of all the SnS films is in the visible region and it decreased with an increase in precursor concentration from 0.05 M to 0.2 M and with further increase in the precursor concentration to 0.25 M, the transmittance had increased. The decrease in transmittance may be attributed to the increase in film thickness which leads to an inversion in loss of intensity due to absorption and scattering.

Thus the absorption coefficient " $\alpha$ " of the SnS thin film was calculated in the visible region using thickness "t" and the absorption spectrum. The variation of " $\alpha$ " with

wavelength is plotted for these SnS thin films as shown in Figure 5.6. The calculated absorption coefficient value for SnS films exceeds  $10^4$  cm<sup>-1</sup>, which indicates that the layers were with high absorption value. Hence, the layers might be suitable for photo voltaic devices [35]. The absorption is more for high-energy photons in the recorded region for this SnS material. A similar absorption coefficient value had been reported by Wang *et al.* [31].

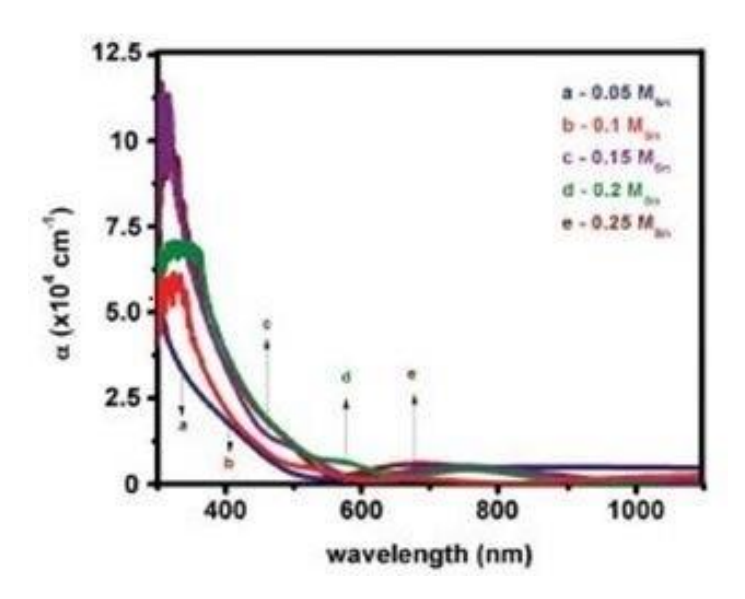


Fig. 5.6 A plot of absorption co-efficient with wavelength of SnS thin films with different precursor concentrations of tin species

The optical band gap (E<sub>g</sub>) can be determined from the absorption coefficient ( $\alpha$ ) and photon energy (hv) by the equation.  $(\alpha h v) = A(hv - E_g)^p$  where A is a constant, h is planck's constant, v is the frequency and p has 2, 3,  $\frac{1}{2}$  and  $\frac{3}{2}$  values for allowed indirect, forbidden indirect, allowed direct and forbidden direct transitions respectively. A graph was plotted against  $(\alpha h v)^2$  and photon energy (hv) as shown in Figure 5.8. The straight line portion was extrapolated to photon energy axis to give bandgap E<sub>g</sub>. The direct optical bandgap of SnS thin films were founded to be 1.78, 1.76, 1.75, 1.74 and 1.755 eV respectively coresponding to increase in precursor concentrations from 0.05 M to 0.25 M. Fadavieslam *et al* [36] had reported similar direct optical bandgap values from 1.63 to 1.81

eV for SnS thin films as a function of deposition conditions on the physical properties by spray pyrolysis method. Kherchachi [30] had studied the same energy bandgap value ranged from 1.23 to 1.8 eV for SnS thin films grown by ultrasonic spray pyrolysis method. The direct optical bandgap values decreased to a minimum of 1.23 eV at 0.2 M with an increase in precursor concentration from 0.05 M and with further increase in the precursor concentration to 0.25 M, the bandgap value had increased to 1.8 eV respectively. Generally the decrease in optical bandgap may be attributed to the increase in crystllite size [37], thickness and crystallinity[38], roughness and grain size. In the present study it is believed that increase in crystallite size and crystallinity is accountable for the decrease in the bandgap, which is evidenced by XRD results. The increase in bandgap at 0.25 M can be attributed to the decrease in thickness and crystallite size at that concentration comparing to 0.2 M, leading to its corresponding electronic structure. Since, the peak heights corresponding to SnS<sub>2</sub> and Sn<sub>2</sub>S<sub>3</sub> phases are very small compared to that of SnS, the presnce of those materials corresponding to the two phases other than SnS will be very small. The bandgap of values of Sn<sub>2</sub>S<sub>3</sub> and SnS<sub>2</sub> are of the order of 1.64 eV [39] and 2.75 eV [40], respectively. The 1.755 eV bandgap of 0.25 M film is more than that of 0.2 M (1.75 eV). This shows that the presence of other two phases does not have any influence on the band gap of SnS.

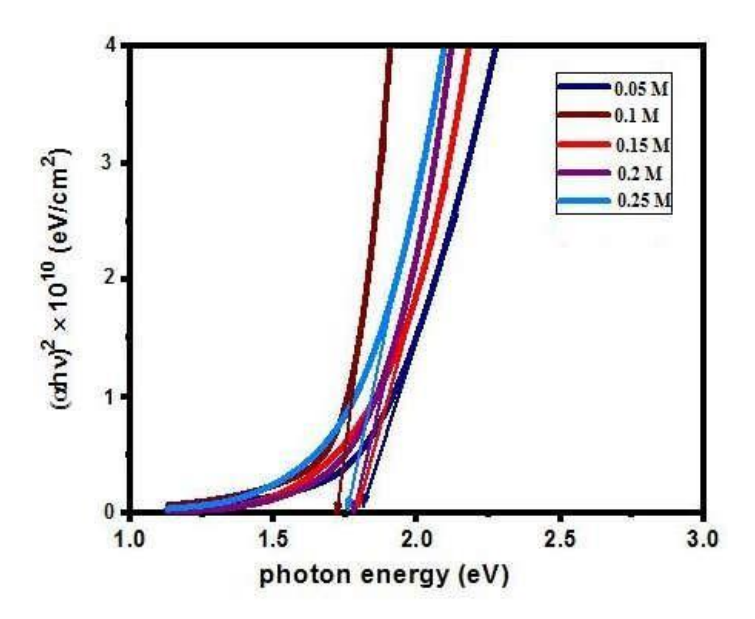


Fig. 5.7 The  $(\alpha hv)^2$  versus hv curves for the optical band gap determination of SnS thin films at different concentration of tin species

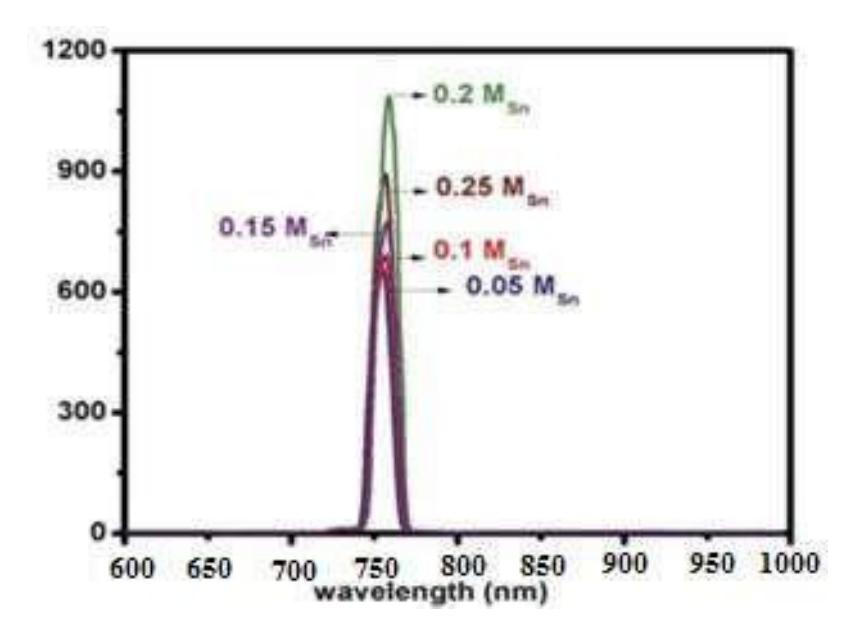


Fig. 5.8 PL spectra of SnS thin films with different precursor concentrations of tin species

In general, the luminesence property of the films has a close relation with the film crystallinity because the density of the defects in film reduces with an improvement of the crytallinity. The PL emission spectrum for all the samples was measured in the wavelength range of 650 to 750 nm at an excitation wavelength of 450 nm. PL spectra of SnS thin films

deposited at various Sn molarities are sholwn in Figure 5.9. All the SnS films exhibit a strong luminescence peak near band edge emissions (NBE) at 755 nm (1.75 eV) (blue) due to recombination of bound excitons. All the films show only the NBE peak in the visible region and IR and UV emission peaks were not observed in these films indicating a good optical quality of the films.

It is seen from the figure that the NBE emission peak very slightly shifted toward higher wavelength side when the precursor concentration is increased up to 0.2 M and with further increasing the precursor concentration it shifted toward lower wavelength side. This result is well matched with the optical band gap values. This result reveals that the peak is maximum for the sample prepared with the precursor concentration of 0.2 M. The single emission peak in the present study may indicate the compound SnS prepared by this nebulized spray pyrolysis technique is free from above defects like sulfur vacancies and interstitials tin atoms. It reveals the fact that no impurity levels or defect levels were present within the forbidden band gap. Wang et al. [41] had reported the PL emission peak at 420 nm for the SnS nanocrystallites. The gradual increase in peak intensity was observed with increasing the precursor concentration up to 0.2 M. The increase in peak intensity with an increase in precursor concentrations indicated the development in crystalline quality and hence an increase in density of free excitons [42]. The decrease in peak intensity was observed in PL spectra when the precursor concentration increased up to 0.25 M. As the thickness decreases, the number of molecules and hence the population will decrease which in turn decreases the peak height.

# **5.3.4** Electrical Properties

The electrical resistivity, carrier concentration and Hall coefficient of SnS thin films grown at different precursor concentrations were determined by Hall Effect measuring instrument at room temperature and the corresponding values are given in Table 2. The

resistivity of the SnS thin films decreases from  $585 \times 10^3~\Omega$  cm to  $2 \times 10^3~\Omega$  cm with the increase in precursor concentration from 0.05~M to 0.2~M. The decrease in resistivity may be attributed to the increase in crystallite size which leads to a decrement in the trapping states at grain boundary [43]. The grain boundary plays an important role between the crystallites and the carrier transport. It can act as a trap center in an incomplete atomic bonding, which depletes the free charge carriers and as a resultant, more number of free carriers become immobilized as trapping state increase. The resistivity again increases to  $9 \times 10^3~\Omega$  cm, while the precursor concentration had increased to 0.25~M. These thin films are found to exhibit n-type electrical conduction. The Hall mobility and bulk carrier concentration increases with increase in precursor concentration up to 0.2~M and decreases with the further increase in precursor concentration.

Table 5.2 The optical and electrical parameters of SnS thin films with different precursor concentrations of tin

Precursor Concentration (Msn)	Thickness (nm)	Band gap (eV)	Resistivity (×10 <sup>3</sup> Ω cm)	Carrier Concentration (×10 <sup>13</sup> cm <sup>-3</sup> )	Mobility (cm²/Vs)	Hall coefficient (×10 <sup>5</sup> cm³/c)
0.05	299	1.78	90.82	1.124	6.114	-5.55
0.1	338	1.76	18.24	1.974	17.33	-3.16
0.15	410	1.75	10.08	2.600	23.81	-2.41
0.2	555	1.74	2.192	7.683	37.15	-0.82
0.25	520	1.755	9.027	2.172	31.83	-2.87

#### 5.4 CONCLUSION

SnS thin films were prepared with different precursor concentrations of tin species from 0.05 M to 0.25 M (in steps of 0.05 M) by spray pyrolysis technique successfully. The ratio of Thiourea solution was kept constant at 0.1 M. The as-deposited SnS thin films were

smooth, shiny, adherent and dark brown in color. XRD studies showed polycrystalline nature of the films having orthorhombic structured crystallites with the preferential orientation of (111) plane for the above precursor concentrations. For the precursor concentration of 0.25 M, mixed phases of Hexagonal and Orthorhombic were present. Direct allowed optical band gap was found to be present in all these SnS thin films, which may be suitable for preparing better quality solar cells. The surface morphology of SnS thin films was defined with needle-like structure. The EDAX result revealed the exact stoichiometry for the SnS film prepared with the precursor concentration of 0.2 M. The electrical resistivity of SnS thin films had been decreased by increasing the precursor concentration from 0.05 to 0.2 M. A minimum electrical resistivity was observed as  $2.19 \times 10^3 \Omega$  cm for the precursor concentration of 0.2 M. These thin films were found to exhibit p-type electrical conduction. From the above results, it can be concluded that this tin sulfide thin film is a good candidate for the fabrication of solar cell and photo detector devices.

#### **REFERENCES**

- [1] Noguchi H, Setiyadi A, Tanamura H, *et al.* Characterization of vacuum-evaporated tin sulfide film for solar cell materials. Sol Energy Mater Sol Cells. 1994; 35: 325–331.
- [2] Ristov M, Sinadinovski G, Grozdanov I. Chemical deposition of tin sulphide thin films. Thin Solid Films. 1989; 173: 53–58.
- [3] Acharya S, Srivastava ON. Electronic behavior of SnS crystals. Phys Status Solidi. 1981; 65: 717–723.
- [4] Greenaway DL, Nitsche R. Preparation and optical properties of group IV-VI<sub>2</sub> chalcogenides having the CdI<sub>2</sub> structure. Phys Chem Solids. 1965; 26: 1445–1458.
- [5] Thangaraju B, Kaliannan P. Spray pyrolytic deposition and characterization of SnS and SnS<sub>2</sub> thin films. J Phys D Appl Phys. 2000; 33: 1054–1059.
- [6] Amalraj L, Sanjeeviraja C, Jayachandran M. Spray pyrolysized tin sulphide thin films and characterization. J Cryst Growth. 2000; 234: 683–689.
- [7] Deshpande NG, Sagade AA, Gudage YG, *et al*. Growth and characterization of tin sulfide (SnS) thin film deposited by successive ionic layer adsorption and reaction (SILAR) technique. J Alloys Compd. 2007; 436: 421–426.
- [8] Sankapal BR, Mane RS, Lokhande CD. Successive ionic layer adsorption and reaction (SILAR) method for the deposition of large area (~10 cm<sup>2</sup>) tin sulfide (SnS) thin films. Mater Res Bull. 2000; 35: 2027–2203.
- [9] Shi C, Chen Z, Shi G, *et al.* Influence of annealing on characteristics of tin sulfide thin films by vacuum thermal evaporation. Thin Solid Films. 2012; 520: 4898–4901.
- [10] Ozin GA, Jiang T, Verma A, *et al.* Absorption and sensing properties of micro porous layered tin sulfide materials. J Mater Chem. 1998; 8: 1649–1656.
- [11] Shi C, Yang P, Yao M, *et al.* Preparation of SnS<sub>2</sub> thin films by closed space sublimation at different source temperature. Thin Solid Films. 2013; 534: 28–31.
- [12] Malaquias J, Fernandes PA, Salomé PMP, *et al.* Assessment of the potential of tin sulphide thin films prepared by sulphurization of metallic precursors as cell absorbers. Thin Solid Films. 2011; 519: 7416–7420.
- [13] Price LS, Parkin IP, Hardy AME, *et al.* Atmospheric pressure chemical vapor deposition of tin sulfides (SnS, Sn<sub>2</sub>S<sub>3</sub> and SnS<sub>2</sub>) on glass. Chem Mater. 1999; 11: 1792–1799.

- [14] Matsumoto K, Takagi K. Chemical transport of SnS<sub>2</sub> using sulfur as a transporting agent. J Cryst Growth. 1983; 63: 202–204..
- [15] Lokhande CD. A chemical method for tin disulphide thin film deposition. J Phys D Appl Phys. 1990; 23: 1703–1705.
- [16] Kawano K, Nakata R, Sumita M. Effects of substrate temperature on absorption edge and photocurrent in evaporated amorphous SnS<sub>2</sub> films. J Phys D Appl Phys. 1989; 22: 136–141.
- [17] George J, Joseph KS. Absorption edge measurements in tin disulphide thin films. J Phys D Appl Phys. 1982; 15: 1109–1116.
- [18] Panda SK, Antonakos A, Liarokapis E, *et al*. Optical properties of nanocrystalline SnS<sub>2</sub> thin films. Mater Res Bull. 2007; 42: 576–583.
- [19] Sekar Ray C, Karanjai MK, Das Gupta D. Structure and photoconductive properties of dip-deposited SnS and SnS<sub>2</sub> thin films and their conversion to tin dioxide by annealing in air. Thin Solid Films. 1999; 350: 72–78.
- [20] Hai B, Tang K, Wang C. Synthesis of SnS<sub>2</sub> nanocrystals via a solvothermal process. J Cryst Growth. 2001; 25: 92–95.
- [21] Khélia C, Boubaker K, Nasrallah TB. Morphological and thermal properties of β-SnS<sub>2</sub> sprayed thin films using Boubaker polynomials expansion. J Alloys Compd. 2009; 477: 461–467.
- [22] Vijayakumar K, Sanjeeviraja C, Amalraj L. Characterization of tin disulphide thin films prepared at different substrate temperature using spray pyrolysis technique. J Mater Sci Mater Electron. 2011; 22: 929–935.
- [23] Reddy NK, Reddy KTR. Preparation and characterization of sprayed tin sulfide films grown at different precursor concentrations. Mater Chem Phys. 2007; 102: 13–18.
- [24] Raj Mohamed J, Amalraj L. Effect of precursor concentration on physical properties of nebulized spray deposited In<sub>2</sub>S<sub>3</sub> thin films. J Asian Ceram Soc. 2016; 4: 357–366.
- [25] Anitha N, Anitha M, Amalraj L. Influence of precursor solution volume on the properties of tin disulphide (SnS<sub>2</sub>) thin films prepared by nebulized spray pyrolysis technique. Optik. 2017; 148: 28–38.
- [26] Anitha M, Anitha N, Amalraj L. Influence of precursor concentration on physical properties of CdO thin films prepared by spray pyrolysis technique using nebulier. Appl Phys A. 2017; 123: 764–779.

- [27] Raj Mohamed J, Sanjeeviraja C, Amalraj L. Influence of substrate temperature on physical properties of (111) oriented CdIn<sub>2</sub>S<sub>4</sub> thin films by nebulized spray pyrolysis technique. J Asian Ceram Soc. 2016; 4: 191–200.
- [28] Anitha M, Anitha N, Amalraj L, *et al.* Investigations on the structural, electrical and optical properties of thin films of CdO<sub>(111)</sub>. J Mater Sci Mater Electron. 2017; 28: 17297–17307.
- [29] Rajathi S, Kirubavathi K, Selvaraju K. Structural, morphological, optical and photoluminescence properties of nanocrystalline PbS thin films grown by chemical bath deposition. J Arab J Chem. 2014; 11: 057–065.
- [30] Kherchachi IB, Saidi H, Attaf A, *et al.* Influence of solution flow rate on the properties of SnS<sub>2</sub> films prepared by ultrasonic spray. Optik. 2016; 127: 2266–2270.
- [31] Wang S, Wang S, Chen J, *et al.* Influence of the deposition parameters on the properties of SnS<sub>2</sub> films prepared by PECVD method combined with solid sources. J Nanopart Res. 2014; 16: 2610–2622.
- [32] Voznyi A, Kosyak V, Opanasyuk A, *et al.* Structural and electrical properties of SnS<sub>2</sub> thin films. Mater Chem Phys. 2016; 173: 52–61.
- [33] Panda NR, Acharya BS, Nayak P, *et al.* Studies on growth morphology, UV absorbance and luminescence properties of sulphur doped ZnO nanopowders synthesized by the application of ultrasound with varying input power. J Ultrason Sonochem. 2014; 21: 582–589.
- [34] Bhushan B, Fuchs H, Tomitori M. Applied scanning probe methods VIII Scanning probe microscopy techniques. Berlin: Springer; 2008.
- [35] Ramakrishna Reddy KT, Chalapathy RBV. Structural properties of CuGa<sub>x</sub>In<sub>1-x</sub>Se<sub>2</sub> thin films deposited by spray pyrolysis. Cryst Res Technol. 1999; 34: 127–132.
- [36] Fadavieslam MR, Shahtahmasebi N, Rezaee-Roknqgqei M, *et al.* Effect of deposition conditions on the physical properties of SnxSy thin films prepared by spray pyrolysis technique. J Semicond. 2011; 32: 113002–113008.
- [37] Jundale DM, Joshi PB, Sen S, *et al.* Nanocrystalline CuO thin films: synthesis, microstructural and opto-electronic properties. J Mater Sci Mater Electron. 2012; 23: 1492–1499.
- [38] Liu F, Lai Y, Liu J, *et al.* Characterization of chemical bath deposited CdS thin films at different deposition temperatures. J Alloys Compd. 2010; 493: 305–308.

- [39] Srinivasa Reddy T, Santhosh Kumar MC. Effect of substrate temperature on the physical properties of co-evaporated Sn<sub>2</sub>S<sub>3</sub> thin films. Ceram Int. 2016; 42: 12262–12270.
- [40] Srinivasa Reddy T, Santhosh Kumar MC. Co-evaporated SnS this films for visible light photodetector applications, RSC Adv. 2016; 6: 95680-95692.
- [41] Wang C, Tang K, Yang Q, *et al.* Raman scattering, far infrared spectrum and photoluminescence of SnS<sub>2</sub> nanocrystallites. Chem Phys Lett. 2002; 357: 371–375.
- [42] Gowri Manohari A, Santhosh Kumar K, Mahlingam T, *et al.* Buffer layer of antimony doped tin disulfide thin films for heterojunction solar cells. Mater Lett. 2015; 155: 121–124.

# CHAPTER - VI

# INFLUENCE OF SUBSTRATE TEMPERATURE ON PHYSICAL PROPERTIES OF NEBULIZED SPRAY DEPOSITED SnSe THIN FILMS

#### 6.1 INTRODUCTION

In recent past, more importance has been committed in the field of IV-VI class of semiconducting compounds on account of their optoelectronic properties and applications [1-5]. Tin Selenide (SnSe) is a narrow band gap, binary IV–VI semiconductor, suitable for various optoelectronic applications like memory switching devices, photovoltaic, light emitting devices (LED) and holographic recording systems [6-8]. Because of their anisotropic character, the tin chalcogenides are attractive layered compounds and can be used as cathode materials in lithium intercalation batteries [9] and decreasing the photo corrosion reaction [10]. Considerable attention has been devoted by various authors to the preparation of SnSe thin films by different methods like vacuum evaporation [11-21], flash evaporation [22], hot wall epitaxy [23,24], reactive evaporation [25], electrodeposition [26– 29], laser ablation [30,31], brush plating [32], chemical bath deposition (CBD) [33], electrochemical atomic layer epitaxy (ECALE) [34] and spray pyrolysis [35,36] to study various physical properties. Among these methods, although high quality and uniform films are prepared by physical technique, they are comparably costly and highly energy consuming. Nebulized spray pyrolysis is a simple, versatile, inexpensive, time saving and efficient way of growing thin films at room atmosphere. This technique can be scalable to larger area deposition. The nebulized spray pyrolysis technique (NSP) has been widely used to deposit binary and ternary oxide thin films such as MgO [37], tin doped zinc oxide [38], Cd-doped SnO<sub>2</sub> [39], Gd<sub>x</sub>Zn<sub>1-x</sub>O [40] and Na-doped ZnO [41]. Xiaorong et al [37] reported

that this technique has advantages like the simplicity of the apparatus and low price of raw materials. E.E.Ebsenso et al [42] had reported deposition of a quaternary oxide, Ln<sub>1-x</sub>Sr<sub>x</sub>CoO<sub>3</sub> (Ln=La, Nd and Gd) and ternary oxide, SrRuO<sub>3</sub> thin films by nebulized spray pyrolysis technique. It was observed that the film prepared by this technique exhibits low resistivity than other techniques which can be exploited for use as electrodes in several situations. SnSe Thin films were not deposited previously by NSP technique.

In this work, an attempt was made to deposit SnSe thin films by simple nebulized spray pyrolysis technique. The observations of this study reveal that SnSe thin films have good semiconducting nature and seem to be a promising candidate for solar cell applications. The structural, morphological, compositional, optical and electrical properties of the films were investigated and analyzed.

# **6.2 EXPERIMENTAL TECHNIQUE**

The problems associated with solution-based methods can be addressed to some extent by using fabrication technique based on nebulized spray pyrolysis technique of thin films. In the following section, we will discuss in detail of material and methods used for preparing SnSe thin films and the characterizing techniques for analyzing the SnSe thin films.

#### **6.2.1** Materials and methods

SnSe thin films were deposited on glass substrate by spraying an aqueous solution containing  $0.1 \, \text{M}$  of SnCl<sub>2</sub> (Sigma-Aldridch) and Se powder (Himedia) with nebulized spray technique. Substrate cleaning plays an important role in the deposition of thin films. The contamination of the substrate surface may cause nucleation sites facilitating the growth, which results in non-uniform film growth. Hence, the micro glass substrates of dimensions  $7.5 \times 2.5 \times 0.25 \, \text{cm}^3$  were first washed well with detergent. The washed glass slides were

put in hot chromic acid for 1h to remove grease or oil. Then, they were rinsed with acetone and double distilled water before the deposition of the films. In this study, different substrate temperatures  $(T_s)$  were used for thin film deposition. The air as carrier gas, flow rate was kept at  $1 \text{ kg/cm}^2$  corresponding to an average pressure solution rate of 5ml per 15 minutes. The volume of solution was taken as 10 ml per substrate. Films are very shiny and color in blackish gray. All the films were kept on the hot plate until the substrate temperature is reached to room temperature and then preserved them in sealable pockets.

# **6.2.2** Characterization technique

The chemical and structural phases of the SnSe films were determined by X-Pert Pro X-ray diffractometer ( $CuK_{\alpha}$ ,  $\lambda$ =1.5418 Å) over a 20 range of 10 - 70°. The optical properties using optical absorption spectrum were measured using UV-Vis-NIR double beam spectrophotometer (HITACHI U3410 model) over the wavelength range 300 – 1100 nm. Scanning electron microscope (SEM) was used to detect the dispersion of particles, rough morphology and the particle size on the surface of the film. The surface morphology of the as-deposited SnSe films was examined by scanning electron microscope (SEM, GENESIS model). The chemical composition of Sn and Se was determined by energy dispersive analysis by x-rays (EDAX) on K and L lines. The electrical conductivity of the as-deposited films was determined by Hall Effect measurement system by ECOPIA-HMS 5000 model. The thickness of the SnSe layers was found with a stylus profile meter (MITUTOYO, SJ-301). The variation of electrical conductivity with temperature was studied from 313 to 388K the four-probe technique with Keithley 2000 electrometer.

# 6.3 RESULTS AND DISCUSSION

To study the impact of substrate temperature on the physical properties while adopting the NSP technique, the following procedure was followed. The deposited SnSe thin films visually found to be blackish gray in color with good adhesion to the substrate at

high temperature. The color of the thin film deposited at the substrate temperature of 250 °C was the gray color with less adhesion to the substrate. The adherence of the films increased with the increase of substrate temperature. Thin films at 275, 300 and 325 °C were good adherence and blackish gray in color. The thickness values were determined as 264, 382, 456 and 634 nm for the samples prepared with the different substrate temperature of 250, 275, 300 and 325 °C respectively (Table 6.2).

# **6.3.1** Structural properties on SnSe thin films

Fig. 6.1 shows the X-ray diffraction pattern of nebulized spray deposited SnSe thin films at different substrate temperatures. As seen, the obtained diffraction patterns show a predominant peak at  $2\theta = 30.47^{\circ}$  which can be assigned to the (111) plane of orthorhombic SnSe of 250 °C. With the increase of substrate temperature up to 300 °C there is an increase in intensity and sharpening of this peak, which is caused by improving crystallinity of the films. From the Fig. 6.1 SnSe films exhibit also two diffraction peaks at 37.77, 49.72° they are assigned to the (311), (511) reflections planes in the SnSe orthorhombic structure of substrate temperature 250-325 °C. Electron diffraction patterns with the standard JCPDS card No 48 – 1224 value shows a close agreement with the reported results in the literature. As seen in Fig. 6.1, the XRD pattern of prepared SnSe film at T<sub>s</sub>= 225 °C indicated that it is amorphous in nature. The existing amorphous nature is due to the insufficient energy at low temperature to convert the amorphous tin layers into polycrystalline films. This intimates that the as-deposited SnSe films are formed with small crystallites embedded in an amorphous tissue. At the substrate temperature of 250 and 275 °C, the diffraction peaks at13.01° and 52.30° corresponding to SnSe<sub>2</sub> was observed along with the peaks of SnSe. It is also noticed from Fig. 6.1 that intensity of SnSe films along (111) plane is increased with increase in substrate temperature up to 300 °C; after reaching a maximum at T<sub>s</sub>=325 °C it starts to decrease and there is small peaks at 14.42 and 41.51° that indicated the formation

of SnO<sub>2</sub>. The film prepared at 300 °C has a better crystalline quality of SnSe in mono-phase as indicated from XRD pattern. Singh et al [43] and Kumar et al [44] had obtained orthorhombic structured crystallites for their SnSe thin films prepared using hot wall epitaxy and thermal evaporation methods respectively.

Crystalline size is estimated by using Scherrer's formula given by equation [45]

$$D = \frac{k \lambda}{\beta \cos \theta} \qquad \dots (6.1)$$

where k varies from 0.89 to 1.39. But in most of the cases, it is closer to 1,  $\lambda$  is the wavelength of X-ray,  $\beta$  is the full width at half of the peak maximum in radians and  $\theta$  is Bragg's angle. The crystalline size was calculated for all the planes of reflection. The FWHM values are found to decrease with the substrate temperature up to 300 °C and further found to increase with increase in substrate temperature. It is observed that crystalline size increases initially with the increase in substrate temperature attains the maximum of 55.82 nm at 300 °C and thenceforth it goes on decreasing with the increase in substrate temperature. Increase in crystallinity and crystalline size with substrate temperature is owing to the optimum rate of supply of thermal energy for recrystallization with substrate temperature [46]. From particle size analysis it is clear that the films are nanocrystalline in nature.

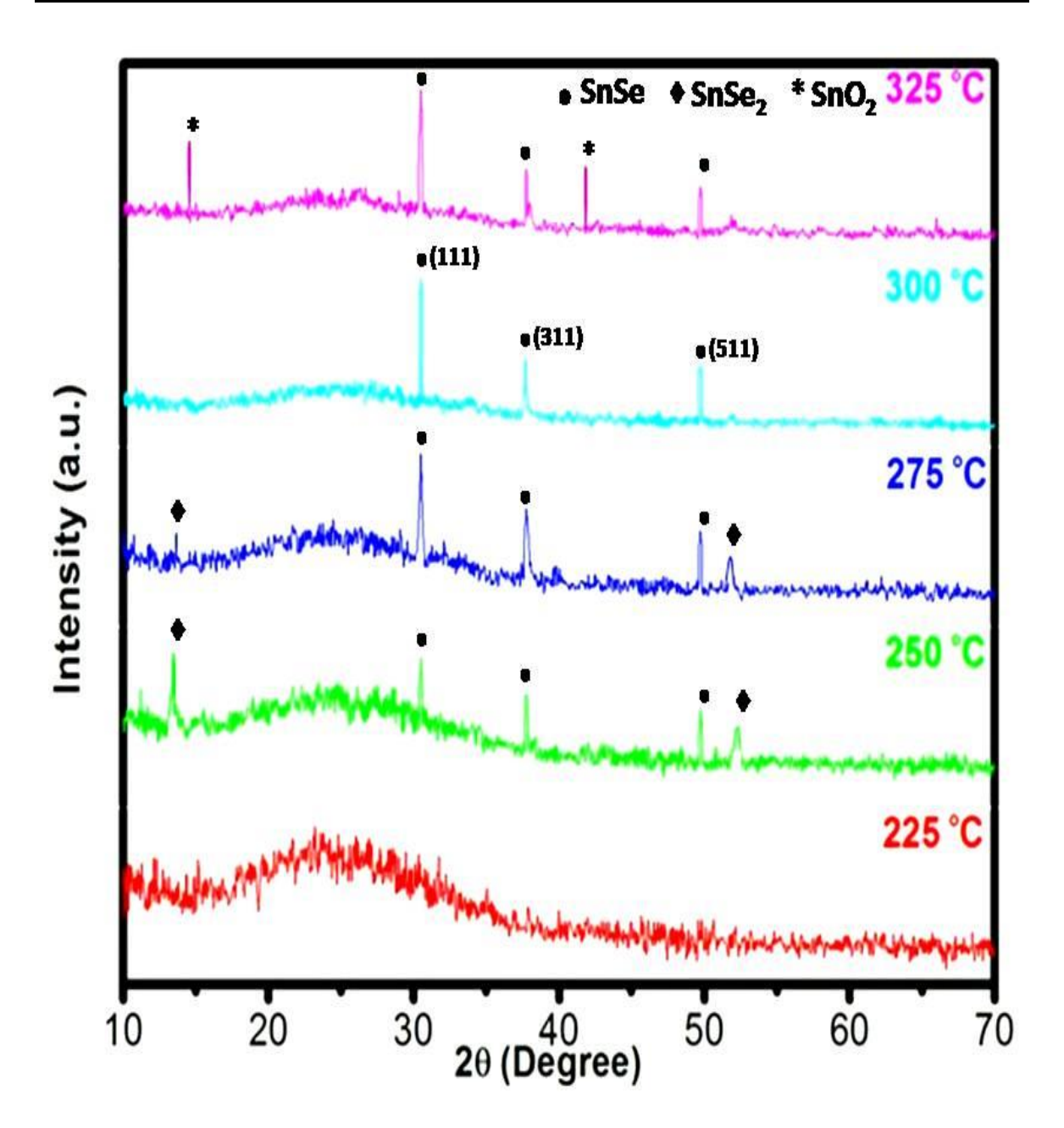


Fig. 6.1 X-ray diffraction pattern of SnSe thin films deposited for different substrate temperature

The lattice strain  $(\varepsilon_s)$  of all the films was determined using the formula

$$\varepsilon_{s} = \frac{\beta \cos \theta}{4} \qquad \dots (6.2)$$

The dislocation density ( $\delta$ ) defined as length of fracture lines per unit volume of the crystal using crystallite size values (D) has been determined using the Williamson and Smallman's

formula [47] as in the  $N = t/D^2$  and the number of crystallites per unit area can be calculated by the equation.

Table 6.1 Structural parameters of SnSe thin films at different substrate temperature

T <sub>s</sub>	hkl	FWHMβ	Crystallite size	Strain
(°C)		(degrees)	(nm)	X10 <sup>-3</sup>
250	(111)	0.197	41.87	8.28
	(311)	0.310	25.66	13.51
	(511)	0.525	15.72	22.04
275	(111)	0.195	42.21	8.21
	(311)	0.285	27.91	12.42
	(511)	0.410	20.14	17.22
300	(111)	0.148	55.82	6.21
	(311)	0.149	53.75	6.45
	(511)	0.190	43.45	7.98
325	(111)	0.236	34.88	9.94
	(311)	0.245	32.46	10.68
	(511)	0.275	30.02	11.55

Table 6.1 exhibits the full width at half maximum (FWHM) value, crystallite size and micro strain of the different (hk)l planes of SnSe thin films at different substrate temperatures from 250 to 325 °C. At lower substrate temperature, the crystallite size is low since the deposited atoms in lieu of incorporating to the neighbouring crystallites and increasing their size are condensed and stay stuck to the region to form small nuclei and clusters. At higher substrate temperature  $T_s = 300$  °C, a large crystallite size is ascertained due to the increasing mobility of the surface of atoms and increasing cluster formation. It is observed that the crystallite size increases and attains a maximum 55.82 nm at 300 °C. Mariappan et al [48] obtained orthorhombic structured crystallite size of 39 to 66 nm for their SnSe thin films prepared using spray pyrolysis technique. Fig. 6.2 shows the variation of average crystallite size value with different substrate temperature was calculated for all the samples found to be increased from 27.75 to 51.01 nm. The decrease in lattice strain was observed by increasing the substrate temperature.

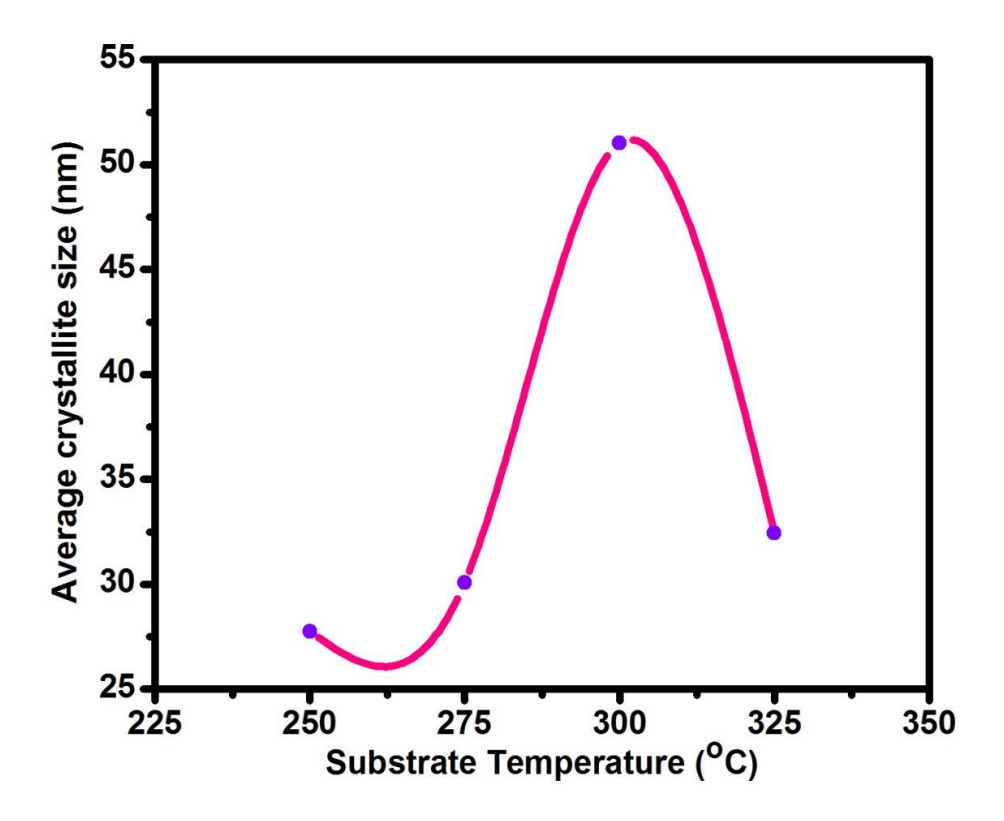


Fig. 6.2 Variation of average crystallite size as a function of temperatures

Indeed, the strain in the films is tensile at the initial stage of SnSe films formation and tends to the compression and lattice strain of the films prepared at the terminal stage. The minimum value of dislocation density is obtained for the film grown at the substrate temperature 300 °C. The dislocation density of as prepared SnSe films decreased as the substrate temperature increased. The change in crystallite size with substrate temperature explained this behaviour. Indeed, the larger crystallites have a smaller surface to volume ratio, thus giving up a rise to the dislocation network.

Table 6.2 expresses the change in texture coefficient, dislocation density and number of crystallites of SnSe thin films at different temperatures from 250 °C to 325 °C. From Table 6.2, it is observed that dislocation density and number of crystallites exhibit higher value at 250 °C and the further increase of temperature decrease the values. This ensures the increase in the volume fraction of its crystallized phase.

Table 6.2 Value of texture coefficient, dislocation density and number of crystallites for different temperatures from 250  $^{\circ}C$  to 325  $^{\circ}C$ 

T <sub>s</sub> (°C)	Texture coefficient	Dislocation Density X10 <sup>15</sup> (Lines/m²)	No. of Crystallites x10 <sup>16</sup> (m²)	Thickness (nm)
225	4	-	122	213
250	1.2528	0.8218	1.4936	264
275	1.0459	0.5705	0.7621	382
300	1.0365	0.5613	0.5079	456
325	1.3572	0.3209	0.3597	634

#### 6.3.2 Analysis of surface morphology of SnSe thin films

The surface morphology of the SnSe thin films deposited at different substrate temperatures was analysed by photographing the scanning electron microscope images of the above samples respectively as shown in Fig. 6.3. These SEM pictures were recorded with the same magnification of 100000x for comparison. It is observed that the surfaces of the films are found to be uniform and homogeneous. As it can be seen, the surface of the asdeposited SnSe thin film grown at T<sub>s</sub>=250 °C was found to be little circular grains gradually spread along horizontal of the substrate. The average grain size of these films is approximately 60-170 nm. With the increase in the substrate temperature up to 300 °C, the SnSe film grows mature to form uniform over-grained morphology composed of nano circular shaped grains. These circular grains change into the small circular grains when the substrate temperature was increased further to 325 °C which is evidenced by the coincidence

of nano-circular grains shown in Fig. 6.3. Similar spherical-shaped grains for SnS films were observed by Zainal et al in the chemical bath deposition method [33].

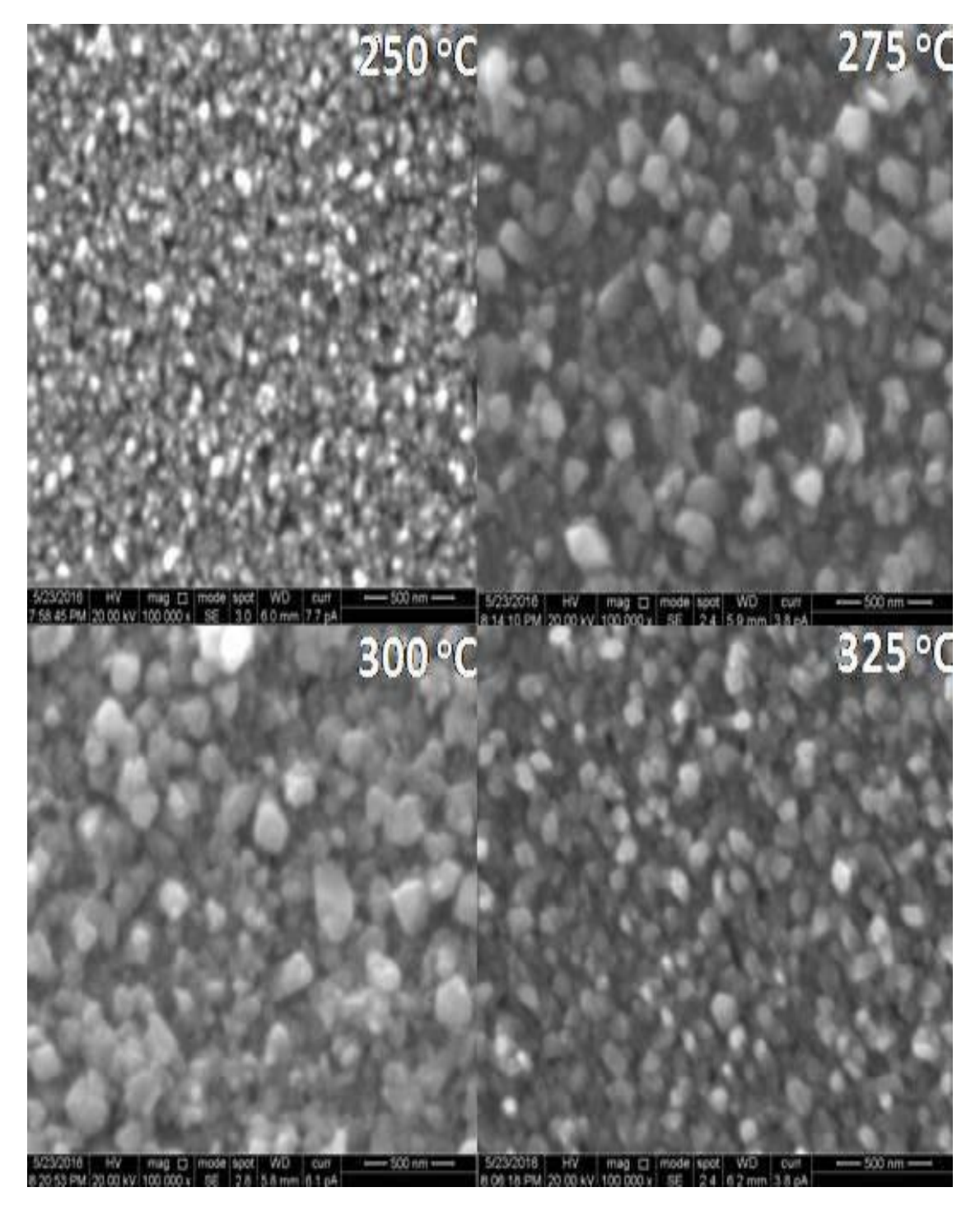


Fig. 6.3 SEM photographs of the SnSe films deposited at different substrate temperature  $% \left( 1\right) =\left( 1\right) \left( 1\right)$ 

#### 6.3.3 Compositional analysis of SnSe thin films

The purity and the specific composition of the as-deposited SnSe thin films were determined by EDX study, which exposed the presence of Sn and Se as elementary components. The typical EDX spectra of SnSe thin films are shown in Fig. 6.4. The numerical atomic percentage of the compositional elements such as Sn and Se present in SnSe thin films are given as inset of Fig. 6.4. Two different peaks related to Sn and Se are found in the SnSe spectrum, which supports the SnSe thin film. The EDX analysis affirms their nominal percentage and chemical purity of system. Initially, the as-deposited SnSe thin film is selenium rich but increase in substrate temperature to SnSe thin film show increase in the percentage of tin in order to reach the stoichiometric ratio of 1:1. The quantitative weight percentage of the compositional elements such as Sn and Se from  $T_s = 250$  to 325 °C are listed in Table 6.3. The atomic percentage of tin is increased from 47.43 to 52.52 by increasing the substrate temperature from 250 to 300 °C and then it decreased to 47.24 at the substrate temperature 325 °C. EDX spectrum exhibits that the weight percentage is closely equal to their nominal stoichiometry within the experimental error. Higher temperatures increased the Sn to Se ratio. Engelken et al [49] and Fernandez et al [50] had also reported similar findings with ZnSe and Sb<sub>2</sub>Se<sub>3</sub> films.

Table 6.3 Variation of elemental analysis of SnSe thin films at different substrate temperature

Т <sub>s</sub> (°С)	Atomic percent	Sn/Se ratio	
( 6)	Sn	Se	ratio
225	46.16	53.84	0.86
250	47.43	52.27	0.91
275	48.12	51.88	0.93
300	52.52	47.48	1.11
325	47.24	52.76	0.90

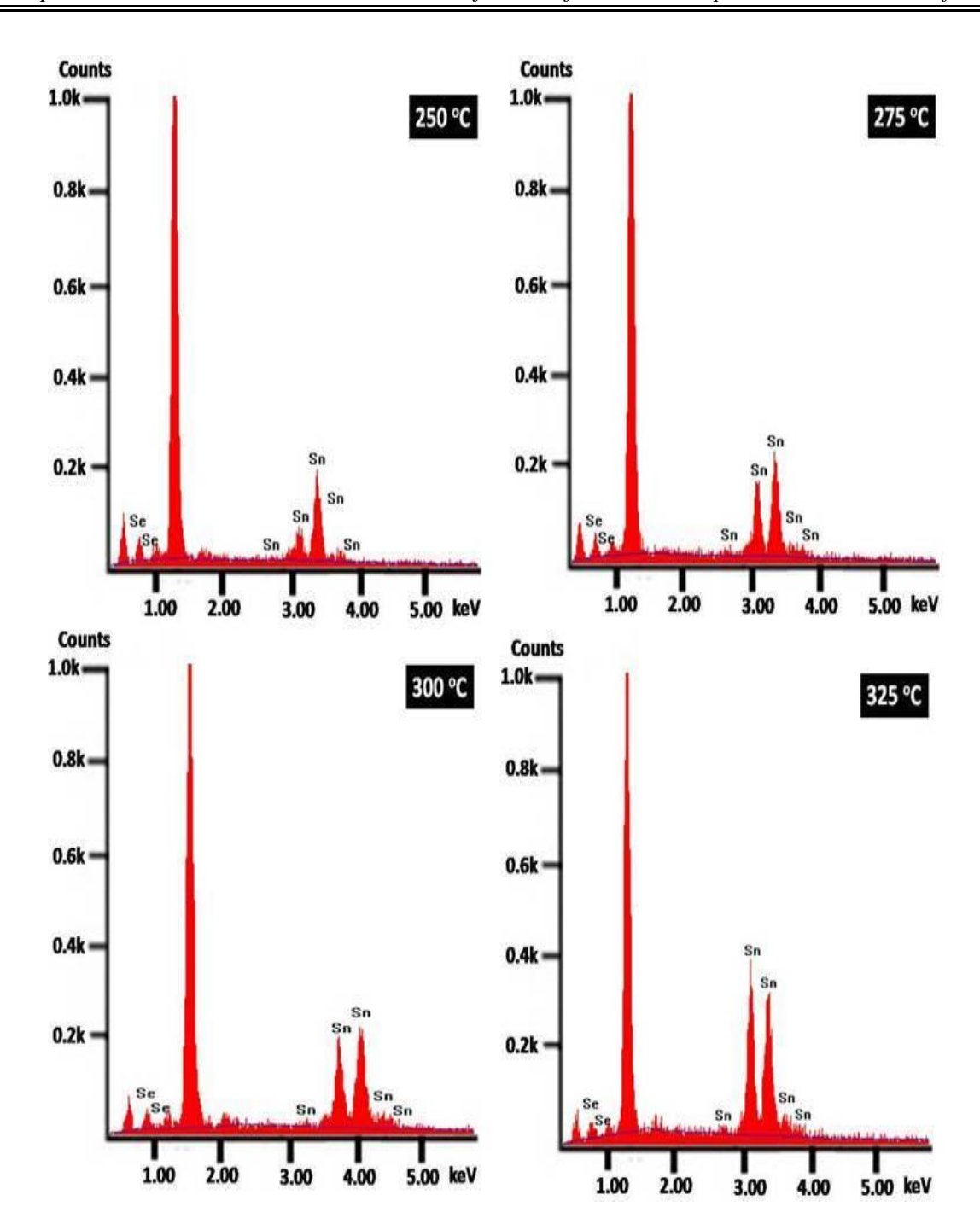


Fig. 6.4 EDAX spectra of SnSe films prepared at different substrate temperature

#### 6.3.4 A report on optical absorption analysis of SnSe thin films

The optical transmittance spectra of SnSe thin films prepared at different substrate temperatures by nebulized spray pyrolysis technique, in the wavelength range of 300 - 1100 nm are presented in Fig. 6.5. It is observed that the transmittance with increases wavelength,

which points better crystallinity of the films. A close observation designates that the transmittance gets down at lower wavelengths and increases at higher wavelengths when increasing the substrate temperatures up to 300 °C and decreasing at 325 °C as seen from Fig. 6.5 where the film deposited at 250 °C has high transmittance. The detected changes in the transmission are owing to the thickness variation and the cardinal differences in the film absorption. The nature of this transmittance variation may be proposed as being eligible as a window material fabrication for solar cells. The optical absorption spectra of nebulized spray deposited SnSe thin films have been used to calculate the coefficient of absorption, optical band gap and the nature of transition concerned. The photon energy dependence of the absorption coefficient of SnSe films is shown in Fig. 6.6. It is established that high optical absorption coefficient ( $\alpha = 10^4$  cm<sup>-1</sup>) was ascertained for all the compositional parameters. The absorption through the film is comparatively high at higher wavelength region designating high concentration of defects and free carriers. The absorption reduces suddenly in the lower wavelength.

The optical band gap of as-deposited SnSe thin films is calculated by employing the Tauc's model [51]. For semiconductors, n=1/2, 2, 3/2, 3 values related to the allowed direct, allowed indirect, forbidden direct and forbidden indirect transition only. Since n=1/2 and the absorption coefficient is of the order of  $10^4$  cm<sup>-1</sup> sustains the direct band gap nature of SnSe semiconductor for allowed direct transition. The band gap of SnSe thin films was found for each film by plotting  $(\alpha hv)^2$  versus photon energy. The Tauc's plot is used to find the band gap of SnSe thin films as in Fig. 6.7.

The direct optical band gaps of SnSe thin films was found to be decreased from 1.24, 1.19, 1.14 eV with the increase of substrate temperature from 250 to 300 °C and then increased to 1.22 eV with the further increase in the substrate temperature to 325 °C.

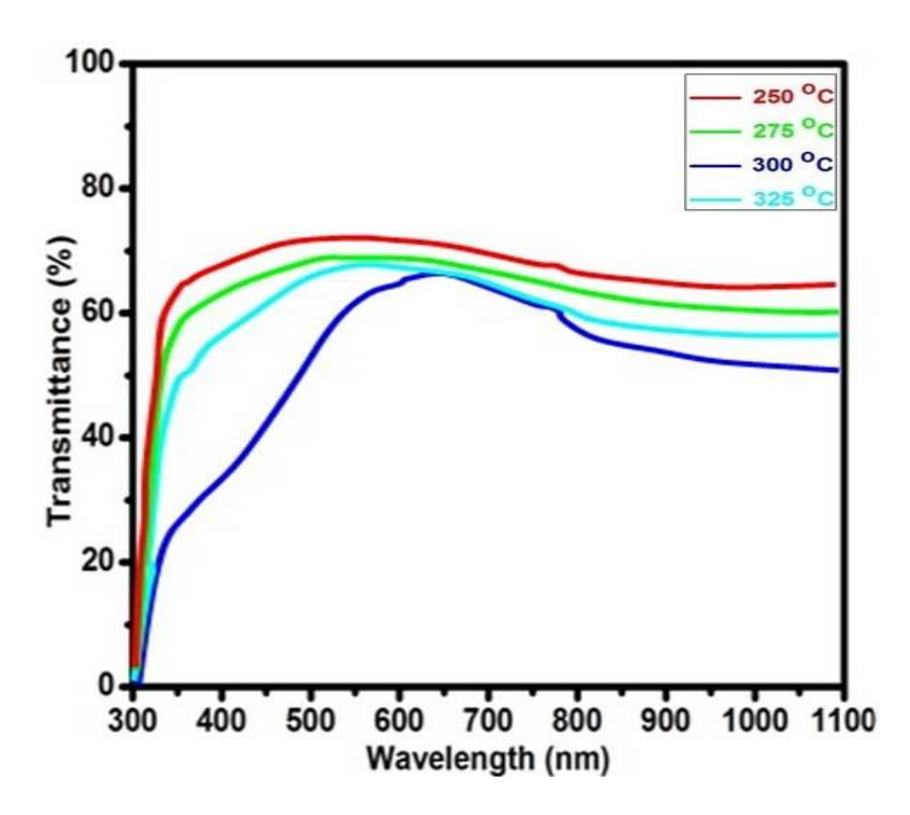


Fig. 6.5 Transmittance spectra of nebulized spray deposited SnSe thin films at different substrate temperature

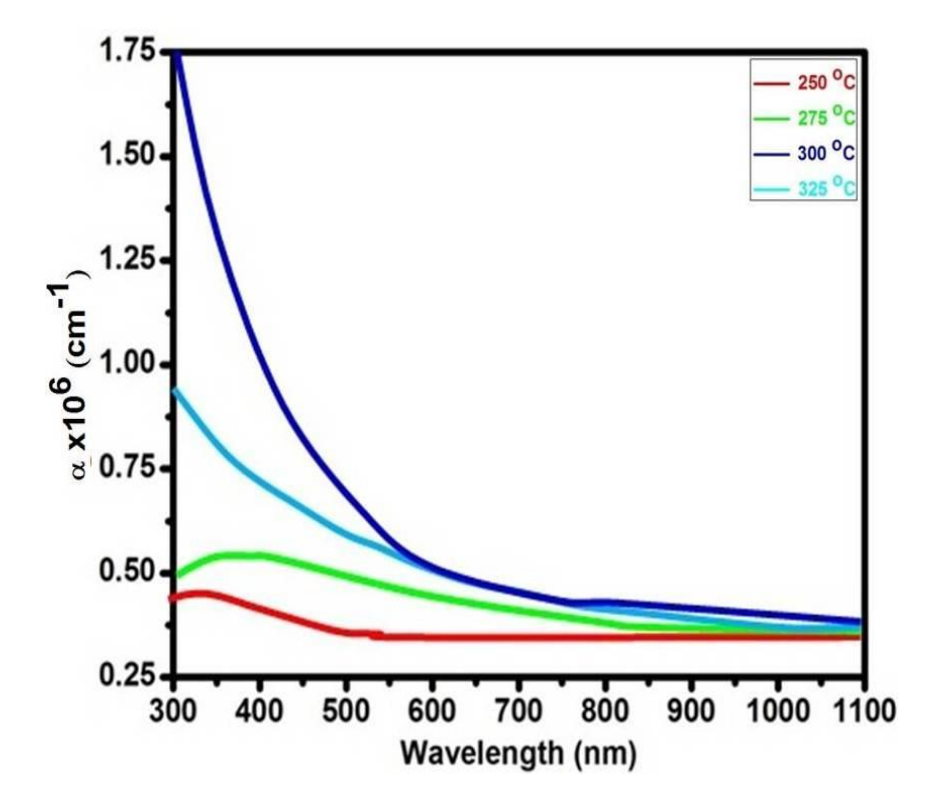


Fig. 6.6 Absorption coefficient spectra of nebulized spray deposited SnSe thin films at different substrate temperature

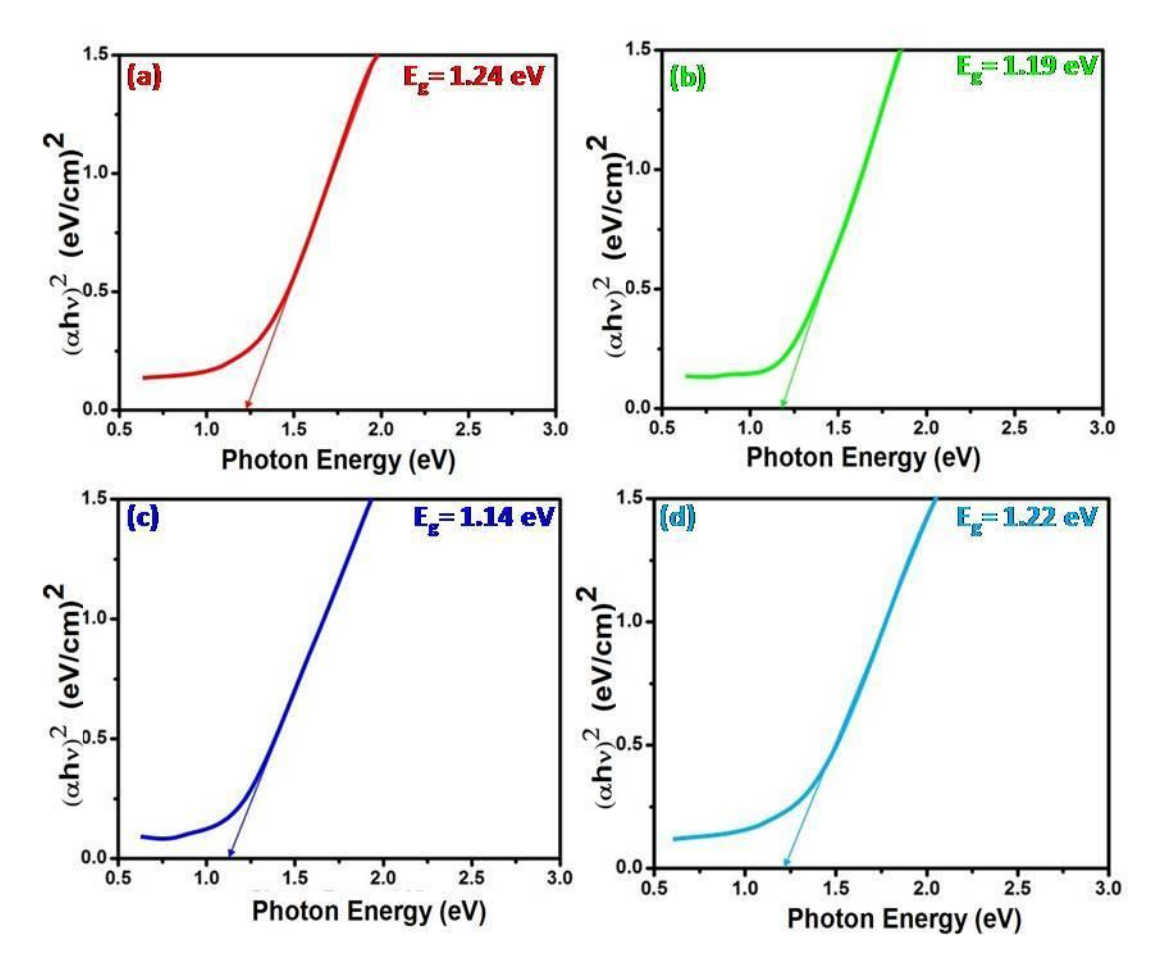


Fig. 6.7 Plot of (αhv)<sup>2</sup> versus photon energy for nebulized spray deposited SnSe thin films at substrate temperatures a) 250 °C b) 275 °C c) 300 °C, d) 325 °C

The direct band gap values of SnSe thin films reported in the literature extend from 0.9 eV up to 1.3 eV [52,53]. The sharp augmentation of energy band gap at higher substrate temperature could be due to the constitution of localized states in the band gap region and that the crystallinity of the polycrystalline SnSe films improves with increasing substrate temperature [54].

#### 6.3.5 Photoluminescence studies on SnSe thin films

The correlation between structure and property is investigated by PL spectra which originate from the recombination of the surface states [55]. The PL is one of the significant studies which can give us more important information on the crystal quality and purity of

the material. The presence of defects such as electron—hole recombination centres, oxygen vacancies and defects are responsible for optical absorption and the emission spectra. The room temperature photoluminescence spectra of the SnS thin films in the wavelength region from 400 nm to 550 nm are shown in Fig.6.8. The low intensity luminescence peaks observed in the films might be attributed to inter-impurity transitions and larger stoichiometric deviations in the films. The peaks at 420, 485 and 498 nm may be ascribed to defect centers attributed to excitonic transitions which are size dependent and excitation wavelength-independent in certain wavelength range [56]. The emission peak at 529 nm may be due to the presence of electron hole recombination via trap states or imperfection sites [57]. These impurities or defects that were not traced in the XRD analysis might be developed or formed at the time of growth of SnSe films.

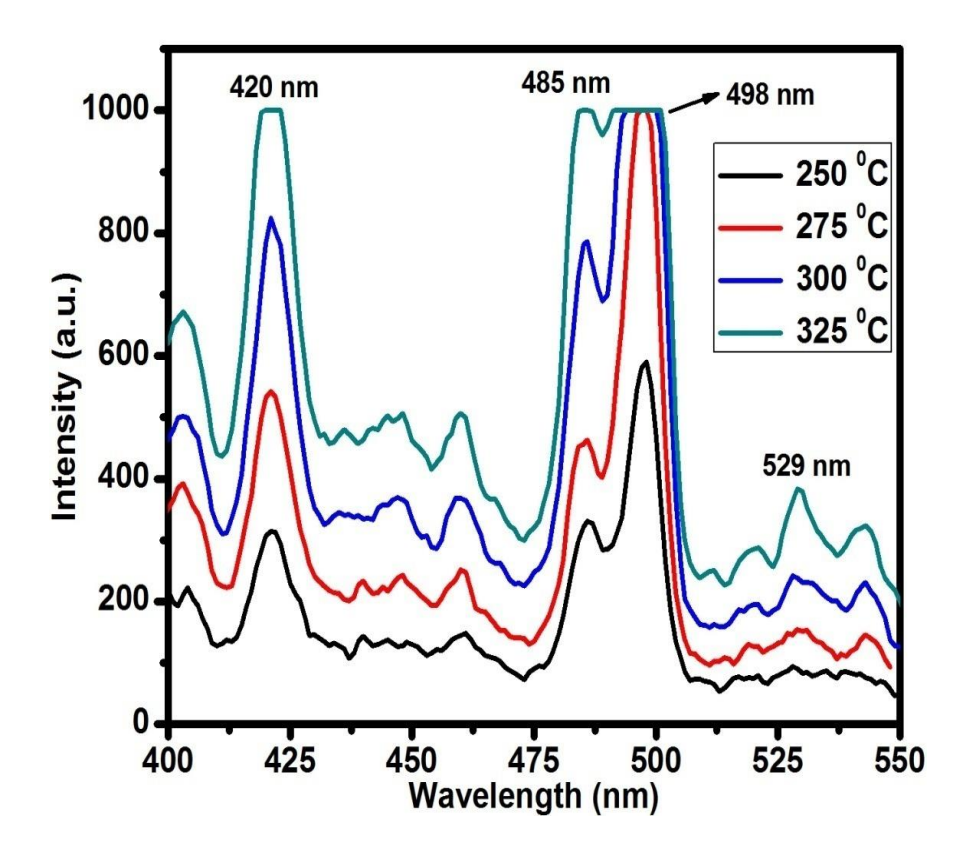


Fig. 6.8 Photoluminescence (PL) spectra of SnSe thin films deposited under different substrate temperatures

#### 6.3.6 Electrical conductivity studies on SnSe thin films

The electrical conductivity, Hall coefficient and mobility of nebulized spray deposited SnSe thin films deposited at the different substrate temperatures from 250 to 325 °C were determined by Hall effect measuring instrument and the corresponding values were listed in Table 6.4.

The Hall positive coefficient values confirm that the as-deposited SnSe films had an p-type nature. Fig. 6.9 shows the variation in the resistivity, carrier concentration and Hall mobility of the films as a function of substrate temperature. The resistivity of the SnSe films decreases with the increase of substrate temperature from 250 to 300 °C and then it increases with the further increase in the substrate temperature to 325 °C. The lowest resistivity value was 4.84 Ωcm at the substrate temperature of 300 °C. The decrease of the electrical resistivity of the film layers after increasing the substrate temperature from 250 to 300 °C can be explained using the Petritz barrier model [58]. Since the crystallites do not grow sufficiently large at low temperatures, the intercrystalline regions offered high resistance for the movement of the charge carriers. At high substrate temperatures, the formation of fewer nucleation centres results in large crystallite sizes, which may ultimately decrease the intercrystalline barriers, hence decreasing the electrical resistivity and then is decreased by a further rise in substrate temperature of 325 °C. Lots of reports have been reported in the resistivity of SnSe thin films whereas Hema Chandra et al. [59] had reported the closer resistivity value from 8.1 to 30  $\Omega$ cm after performing with the substrate temperature range 303-513 K for the SnSe thin films deposited by the flash evaporated technique. The bulk carrier concentration and mobility of the SnSe thin films increase with increasing substrate temperature from 250 to 300 °C up to 5.676 x 10<sup>17</sup> cm<sup>-3</sup> and 7.8 cm<sup>2</sup>/Vs and then they decrease to 2.542 x 10<sup>17</sup> cm<sup>-3</sup> and 5.2 cm<sup>2</sup>/Vs respectively by a further rise in substrate temperature.

The mobility increases as a result of reconstituting and the crystallinity prosperity of the material. The increased bulk carrier concentration caused by increasing substrate temperature shrunken the grain boundary potential barrier. Because of that, the carrier mobility of the SnSe films also increases. The results showed in this work have presented the feasibility of using SnSe thin films suitable for fabrication of solar cells.

The activation energy of SnSe thin film can be calculated using the Eq. (4.6). The temperature dependence of resistivity was studied from room temperature to 313 K. The decrease of resistivity ( $\rho$ ) is usually expressed by the Eq. (4.6). An Arrhenius plot of log ( $\rho$ ) versus 1000/T for four typical SnSe thin films at different substrate temperature has been shown in Fig. 6.10.

The curves clearly show two conduction regions. The slope is high in the low temperature region but decrease with further increase of temperature. From the slopes of an Arrhenius plot, the activation energies are calculated and presented in Table 6.4. The value of pre-exponential factor  $\rho_0$ , which is the resistivity of the film as the temperature reaches to infinity, is determined to be 20.44, 12.63, 2.74 and 15.34  $\Omega$ cm for the SnSe films prepared at different substrate temperatures from 250 to 325 °C. It is seen from the activation energies that the films do not possess the intrinsic resistivity strictly in this entire range of applied temperature. The shallow trapping states preferably due to those interstitial tin or selenium vacancies are expected to dominate the extrinsic resistivity near the room temperature whereas those deep trap states influence at high temperature range. Kumar et al [60] have reported the activation energy for the SnSe thin film deposited in the range of 300-450 K using thermal evaporation method is 0.14-0.28 eV.

Table 6.4 Variation of optical and electrical properties of SnSe thin films at different substrate temperature

T, (°C)	Band gap (eV)	Conductivity (Ω-cm) <sup>-1</sup>	Mobility (cm²/Vs)	Hall coefficient (cm <sup>-3</sup> /C)	Activation energy (eV)
250	1.24	0.04	2.6	61.70	0.10
275	1.19	0.05	4.4	17.30	0.15
300	1.14	0.21	7.8	11.01	0.16
325	1.22	0.07	5.2	24.59	0.27

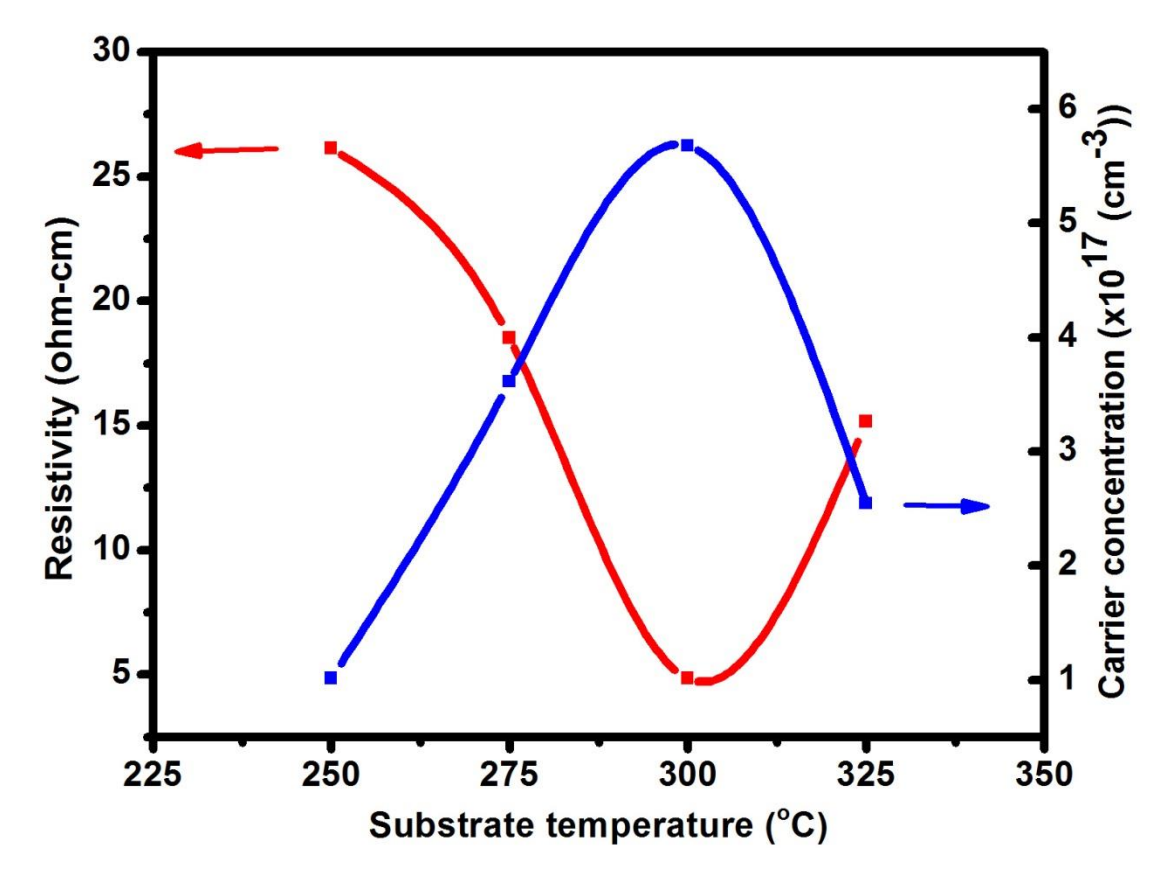


Fig. 6.9 Variation of resistivity, carrier concentration and mobility of SnSe thin films of different substrate temperature

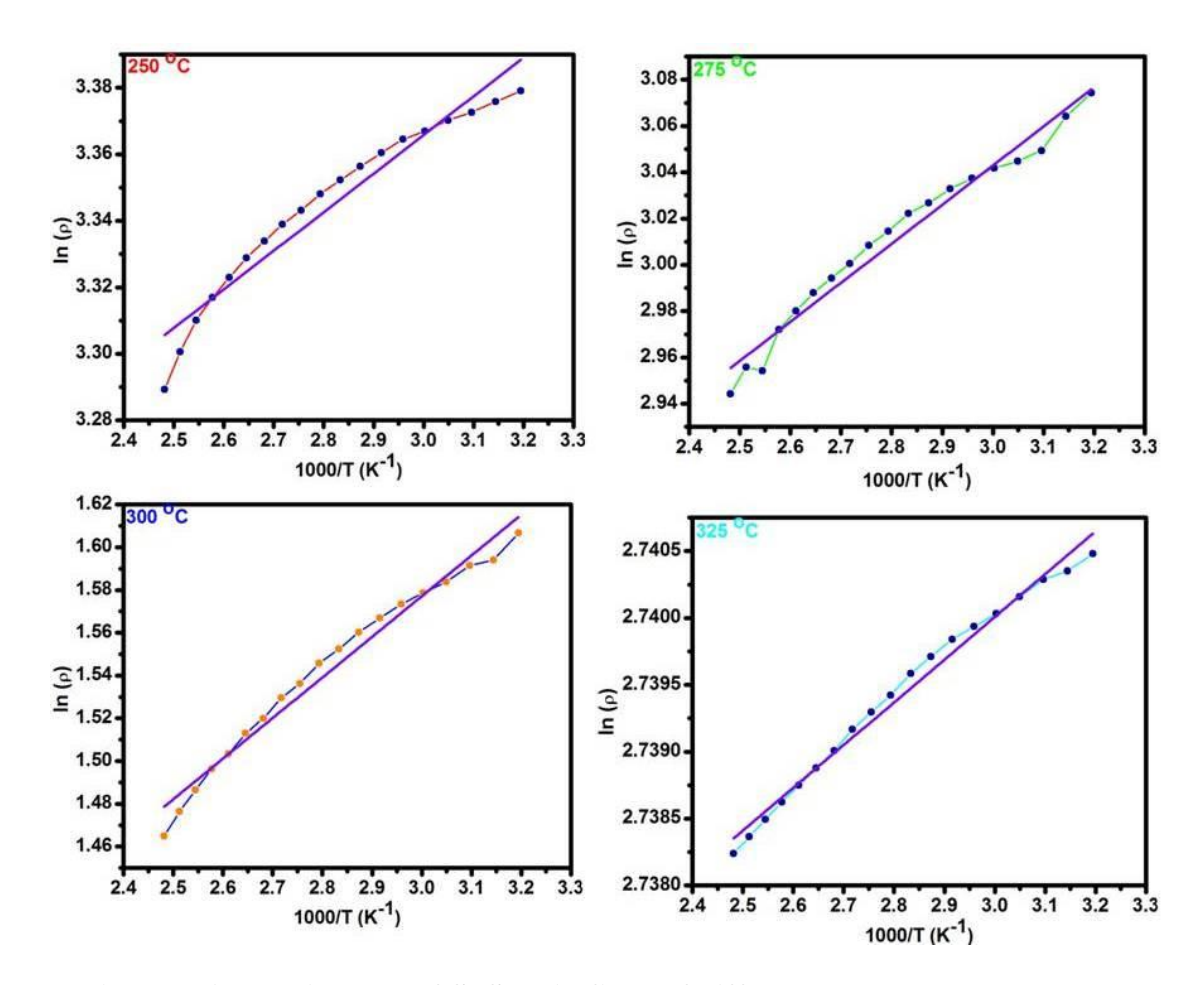


Fig. 6.10 Arrhenius plot of SnSe thin films of different substrate temperature

# 6.4 CONCLUSION

The p-type semiconducting SnSe thin films have been successfully deposited by simple and inexpensive nebulized spray pyrolysis technique. Polycrystalline nature of asdeposited SnSe thin films was confirmed from X-ray diffraction studies. X-ray diffraction studies depicted orthorhombic crystal structure irrespective of substrate temperature. Scanning electron microscopy studies revealed uniform deposition with the grain size in the nano metre range. Stoichiometric films of SnSe were observed from energy dispersive analysis by X-ray studies. The optical band gap was found to be in the range of 1.14 – 1.24 eV with the direct allowed transition depending on substrate temperature. The lower absorption and high transmittance in the visible region observed at lower substrate temperature represented the good optical quality of the crystals with the low absorption or

scattering losses which lead to the applications particularly as a window layer in solar cells. Electrical studies showed that the films are semiconducting which may be used in optoelectronic devices. The structural, optical, morphological and electrical conductivity studies of tin selenide thin films confirmed that the optimum substrate temperatures for depositing SnSe thin films by this NSP technique is 300 °C. The corresponding results obtained by preparing SnSe thin films may be suitable for conventional absorber layer in solar cells.

#### **REFERENCES**

- [1] I. R. Chávez Urbiola, J. A. Bernal Martínez, V. P. Makhniy, R. Ramírez Bon, Y. V. Vorobiev, Inorganic Materials 50(6) (2014) 546.
- [2] R.J. Ellingson, M.C.Beard, J.C. Johnson, P. Yu, O.I. Micic, A.J. Nozik, A. Shabaev, A.L. Efros, Nano Lett., 5 (2005) 865.
- [3] R. Dalven, Infrared Phys. Technol., 9 (1969) 141.
- [4] S.K.J. Al-Ani, H.H. Mohammed, E.M.N. Al-Fwade, Renew. Energy 25 (2002) 585.
- [5] Sushil Kumar, Zishan H. Khan, M.A. Majeed Khan, M. Husain, Curr. Appl. Phys., 5 (2005) 561.
- [6] C. R. Baxter, W. D. Mclennan, J. Vac. Sci. Technol., 12 (1975) 110.
- [7] N. R. Mathews, Solar Energy 86 (2012) 1010.
- [8] K. M. Chung, D. Wamwangi, M. Woda, M. Wuttig and W. Bensch, J. Appl. Phys. 103 (2008) 083523.
- [9] J. Yamaki, A. Yamaji, Physica B 150 (1981) 466.
- [10] K. Zweibel, Solar Energy Mater. Solar Cells 63 (2000) 375.
- [11] A. Bennouna, P.Y. Tessier, M. Priol, Q. Dang Tran, S. Robin, Phys. Status Solidi B 117 (1983) 51.
- [12] D.T. Quan, Phys. Status Solidi A 86 (1984) 421.
- [13] T. Subba Rao, B.K. Samantha Ray, A.K. Chaudhuri, J. Mater. Sci. Lett. 4 (1985) 743.
- [14] T. Subba Rao, A.K. Chaudhuri, J. Phys. D: Appl. Phys. 18 (1985) L35.
- [15] T. Subba Rao, A.K. Chaudhuri, J. Phys. D: Appl. Phys. 19 (1986) 861.
- [16] D.T. Quan, Thin Solid Films 149 (2) (1987) 197.
- [17] T. Subba Rao, B.K. Samanata Ray, A.K. Chaudhuri, Thin Solid Films 165 (1988) 257.
- [18] H.S. Soliman, D.A. Abdel Hady, K.F. Abdel Rahman, S.B. Yossef, A.A. EL-Shazly, Physica A 216 (1995) 77.

- [19] P. Suguna, D. Mangalaraj, S.A.K. Narayandass, P. Meena, Phys. Status Solidi A 155 (1996) 405.
- [20] D.P. Padiyan, A. Marikani, K.R. Murali, Crystal Res. Technol. 35(8) (2000) 949.
- [21] J. Sharma, G. Singh, A. Thakur, G.S.S. Saini, N. Goyal, S.K. Tripathi, J. Optoelectron. Adv. Mater. 7 (4) (2005) 2085.
- [22] J.P. Singh, R.K. Bedi, Thin Solid Films 199 (1991) 9.
- [23] J.P. Singh, R.K. Bedi, J. Appl. Phys. 68 (6) (1990) 2776.
- [24] J.P. Singh, J. Mater. Sci: Mater. Electron. 2 (2) (1991) 105.
- [25] K.J. John, B. Pradeep, E. Mathai, J. Mater. Sci. 29 (6) (1994) 1581.
- [26] B. Subramanian, T. Mahalingam, C. Sanjeeviraja, M. Jayachandran, M.J. Chockalingam, Thin Solid Films 357 (2) (1999) 119.
- [27] Z. Zainal, A. Jimale Ali, A. Kassim, M.Z. Hussein, Sol. EnergyMater. Sol. Cells 79 (2) (2003) 125.
- [28] Z. Zainal, S. Nagalingam, A. Kassim, M.Z. Hussein, W.M.M. Yunus, Sol. Energy Mater. Sol. Cells 81 (2) (2004) 261.
- [29] A. Lukinskas, V. Jasulaitiene, P. Lukinskas, I. Savickaja, P. Kalinauskas, Electrochim. Acta 51 (7) (2006) 6171.
- [30] R. Teghil, A. Giardini-Guidoni, A. Mele, S. Piccirillo, G. Pizzella, V. Marotta, Thin Solid Films 241 (1994) 126.
- [31] R. Teghil, A. Santagata, V. Marotta, S. Orlando, G. Pizzella, A. Giardini-Guidoni, A. Mele, Appl. Surf. Sci. 90 (4) (1995) 505.
- [32] B. Subramanian, C. Sanjeeviraja, M. Jayachandran, J. Crystal Growth 234 (2) (2002) 421.
- [33] Z. Zainal, N. Saravanan, K. Anuar, M.Z. Hussein, W.M.M. Yunus, Mater. Sci. Eng. B 107 (2) (2004) 181.
- [34] Z. Qiao, W. Shang, C. Wang, J. Electroanal. Chem. 576 (2005) 171.
- [35] J.S.N. Rios, M. Ramachandran, D.M. Escobar, A.S. Juarez, J. Semicond. 34 (2013) 013001.
- [36] Sharmistha Anwar, S. Gowthamaraju, B.K. Mishra, S.K. Singh, Shahid Anwar Materials Chemistry and Physics 153 (2015) 236.

- [37] X. Fu, G. Wu, S. Song, Z. Song, X. Duo, C. Lin, Appl. Surf. Sci. 148 (1999) 223.
- [38] R.Mariappan, V.Ponnuswamy, P.Suresh, Superlattice. Microst. 52 (2012) 500.
- [39] R.Mariappan, V.Ponnuswamy, P.Suresh, R.Suresh, M.Ragavendar, C.Sankar, Mater. Sci. Semicond. Proc. 16 (2013) 825.
- [40] R.Mariappan, V.Ponnuswamy, P.Suresh, R.Suresh, M.Ragavendar, Superlattic.Micros. 59 (2013) 47.
- [41] R.Mariappan, V.Ponnuswamy, R.Suresh, P.Suresh, A.Chandra Bose, M.Ragavendar, J. Alloys. Compd. 582 (2014) 387.
- [42] E.E.Ebsenso, K.Sardar, M.Chandrasekhar, A.R.Raju, C.N.R.Raju, Solid State Sci. 2 (2000) 833.
- [43] J. P. Singh, R. K. Bedi, Journal of Applied Physics 68 (1990) 2776.
- [44] N. Kumar, V. Sharma, U. Parihar, R. Sachdeva, N. Padha, C. J. Panchal, J. Nano Electron Phys. 3(1) (2011) 117.
- [45] P. Scherrer, Gothinger Nachri-Chten 2 (1918) 98.
- [46] V.M. Nikale, N.S. Gaikwad, K.Y. Rajpure, C.H. Bhosale, Mater. Chem. Phys. 78 (2003) 363.
- [47] G.B. Williamson, R.C. Smallman, Philos.Mag., 1 (1956) 34.
- [48] R. Mariappan, M. Ragavendar, G. Gowrisankar, Chalcogenide Letters 7 (3) (2010) 211.
- [49] R.D. Engelken, A.K. Berry, T.P. Van Doren, J.L. Boone, A. Shahnazary, J. Electrochem. Soc. 133 (1986) 581.
- [50] A.M. Fernandez, M.G. Merino, Thin Solid Films 366 (2000) 202.
- [51] J.I.Pankove, Optical Processes in Semiconductors, Prentice and Hall, Inc., New Jersey, (1971) pp 36.
- [52] P. Ramasamy, P. Manivasakan, J. Kim, Cryst Eng Comm 17 (2015) 807.
- [53] Ling L, Zhang Q, Zhu L, Wang C-F, Chen S, RSC Adv 5 (2014) 2155.
- [54] N. Kumar, V. Sharma, N. Padha, N. M. Shah, M. S. Desai, C. J. Panchal, I. Yu. Protsenko, Cryst. Res. Technol. 45(1) (2010) 53.
- [55] N. Chestony, T.D. Harris, R. Hull, L.E. Brus, J. Phys. Chem. 90 (1986) 3393.

- [56] J. Srivind, V.S. Nagarethinam, A.R. Balu, Materials Science-Poland 34(2) (2016) 393.
- [57] S.Chaura, N. B. Chaura, R.K. Pandey, Physica E 28 (2005) 439.
- [58] R.L. Petritz, Phys. Rev. 104 (1956) 1508.
- [59] G. Hema Chandra, J. Naveen Kumar, N. Madhusudhana Rao, S. Uthanna, Journal of Crystal Growth 306 (2007) 68.
- [60] N. Kumar, U. Parihar, R. Kumar, K. J. Patel, C. J. Panchal, N. Padha, American Journal of Materials Science 2(1) (2012) 41.

## CHAPTER - VII

# EFFECT OF PRECURSOR CONCENTRATION ON PHYSICAL PROPERTIES OF NEBULIZED SPRAY DEPOSITED SnSe THIN FILMS

The effect of precursor concentration on various properties of nebulized spray pyrolysised SnSe thin films were studied using the precursor solutions of Tin (II) chloride and Selenourea. X-ray diffraction (XRD) pattern confirmed SnSe thin film with orthorhombic structure. The variation in grain size and energy gap by increasing precursor concentration made the samples as a promising candidate for the applications of optoelectronic device such as photodiodes and solar cells. The high transmittance and lower absorption in the visible region observed at lower concentrations illustrated the good optical quality of the crystals with the low absorption or scattering losses which leads to the applications especially as an absorber layer in solar cells. The optical parameters such as direct band gap energy decreased from 1.24 to 1.12 eV by increasing the concentrations. The change in morphology of SnSe thin films for different precursor concentration was studied by scanning electron microscope. Energy dispersive X-ray pattern confirmed the presence of Sn and Se with the chemical stoichiometric. The selenium percentage decreased from 48.37 to 44.59 by increasing precursor concentration from 0.025 to 0.150 M. The electrical resistivity of as-deposited SnSe thin films decreased by increasing the precursor concentration to 0.125 M and increased slightly at 0.150 M. The maximum carrier mobility of 8.1 cm<sup>2</sup>/Vs was obtained at 0.125 M. The investigation results of the SnSe thin films deposited by nebulized spray pyrolysis technique ensure the stability of the film and their employability in solar cell application.

#### 7.1. INTRODUCITON

Tin selenide (SnSe) is a binary compound semiconductor with an orthorhombic crystal structure. This material possess the following qualities that make it a potential candidates in photo electrochemical solar cells. Their band gap lies between 1.0 and 2.0 eV hence it absorbs light energy from the high energy end of the solar spectrum [1]. They are also both chemically and electrochemically stable in either acid or alkaline condition and their constituent elements are abundantly available on earth. Tin selenide (SnSe) which has been used in memory switching devices, holographic recording systems, infrared electronic devices and solar cell applications [2]. SnSe has been studied in the form of both single crystal and thin films. The use of tin selenide for these purposes suppresses photo corrosion and enhances the fill factor in electrical switches and p-n junction devices [3]. For large scale production of solar cells, a thin film deposition technique that can be easily handled at low cost is important. Thin films of SnSe can be prepared using different techniques such as vacuum thermal evaporation [4], laser ablation [5], brush plating [6], chemical bath deposition(CBD) [2], spray pyrolysis [7-9], chemical vapor deposition [10] and electro deposition [11,12]. The physical deposition techniques are comparably very expensive and high energy consuming even though it provided quality and uniform films. Nebulized spray pyrolysis (NSP) technique is a simple and cost effective by which an efficient way of growing thin films is possible. Binary and ternary semiconductor oxide thin films such as MgO [13], tin doped zinc oxide [14] and Cd-doped SnO<sub>2</sub> [15] have been deposited by NSP technique. A ternary chalcogenide CdSnSe thin film had also been deposited by this technique [16]. Although NSP synthesis has been widely used to prepare a variety of thin films, studies on the nebulized spray pyrolysis preparation of SnSe thin films did not exist. Herein, we report on a nebulized spray pyrolysis technique to fabricate SnSe thin films on

glass substrate of different precursor concentration. The structural, optical, morphological, elemental and electrical conductivity properties of SnSe thin films have been investigated.

In this paper, the optimizing temperature was found as 325 °C for the as-deposited SnSe thin films. Furthermore, the optimization condition should also be evaluated by optimizing other preparative parameter such as precursor concentration. This will be useful for obtaining clear idea about the structural, optical and other properties of the samples. In the present investigation, the binary SnSe thin films have been deposited on the micro glass substrate by NSP technique for different precursor concentration (m<sub>c</sub>) from 0.050 M to 0.150 M in steps of 0.025 M. Structural, optical, morphological, elemental and electrical conductivity properties of nebulized spray deposited SnSe thin films have been reported.

#### 7.2 EXPERIMENTAL TECHNIQUE

In the following section, we will discuss in detail about the material and deposition method used for the preparation of SnSe thin films of different precursor concentration and the characterizing techniques for analysing the films have been furnished for ready reference.

#### 7.2.1 Materials and methods

For the preparation of SnSe thin films, high purity chemicals (> 99% purity) such as Tin chloride (SnCl<sub>2</sub>) (Sigma-Aldridge) and selenium powder (Himedia) were used as precursor without further purification. The precursor SnCl<sub>2</sub> and selenium powder were used as source materials of Sn and Se ions respectively. Micro glass slides have been used as substrates to deposit SnSe thin films. Substrate cleaning leads to a major role in the thin film deposition. The contamination on the surface of the substrate may create nucleation sites alleviating the growth, which results in non-uniform film growth. Hence, the micro glass

substrate of dimension 7.5 x 2.5 x 0.25 cm³ was first water washed well with soap detergent. The washed glass slides were kept in hot chromic acid for an hour to remove grease or oil presented during the manufacturing process of glass plates. After that, they were rinsed with acetone and double distilled water before the deposition of the films. In this work, the SnSe thin films were deposited with different precursor concentration from 0.050 M to 0.150 M. The substrate temperature was constrained by an iron-constantan type thermocouple and kept constant as its optimized value of 325 °C. The air as carrier gas flow rate was maintained at 1 kg/cm² corresponding to an average pressure solution rate of 10ml per 10 minutes. The precursor solution was held in the nebulizer unit, which is connected to an air compressor. The compressed air is transported by tubing and stimulates the precursor solution through an "L" glass tube. The mist like tiny droplets of particles was carried from the glass tube to deposit onto the glass substrate kept in the uniform hot zone of the furnace. After deposition, the films were allowed to cool at room temperature and then preserved them in desiccators.

#### 7.3. RESULTS AND DISCUSSION

The recent tremendous advancement of materials science in general is due to the discovery of development of modern characterization equipments. In this section, various characterizing techniques are described for the as-deposited SnSe thin films for different precursor concentration and the results for the corresponding films have been discussed. The color of the thin film prepared with 0.050 M concentration was pale gray with less adhesion to the substrate. Thin films prepared with 0.075 M, 0.100 M, 125 M and 0.150 M concentrations had good adherence and were blackish gray in color. These films looked shiny with multiple color due to internal multiple reflections and blackish gray in color due

to transmitted light. Further, the films prepared at precursor concentration up to 0.150 M depicted the crystallinity increased with the increase in precursor concentration.

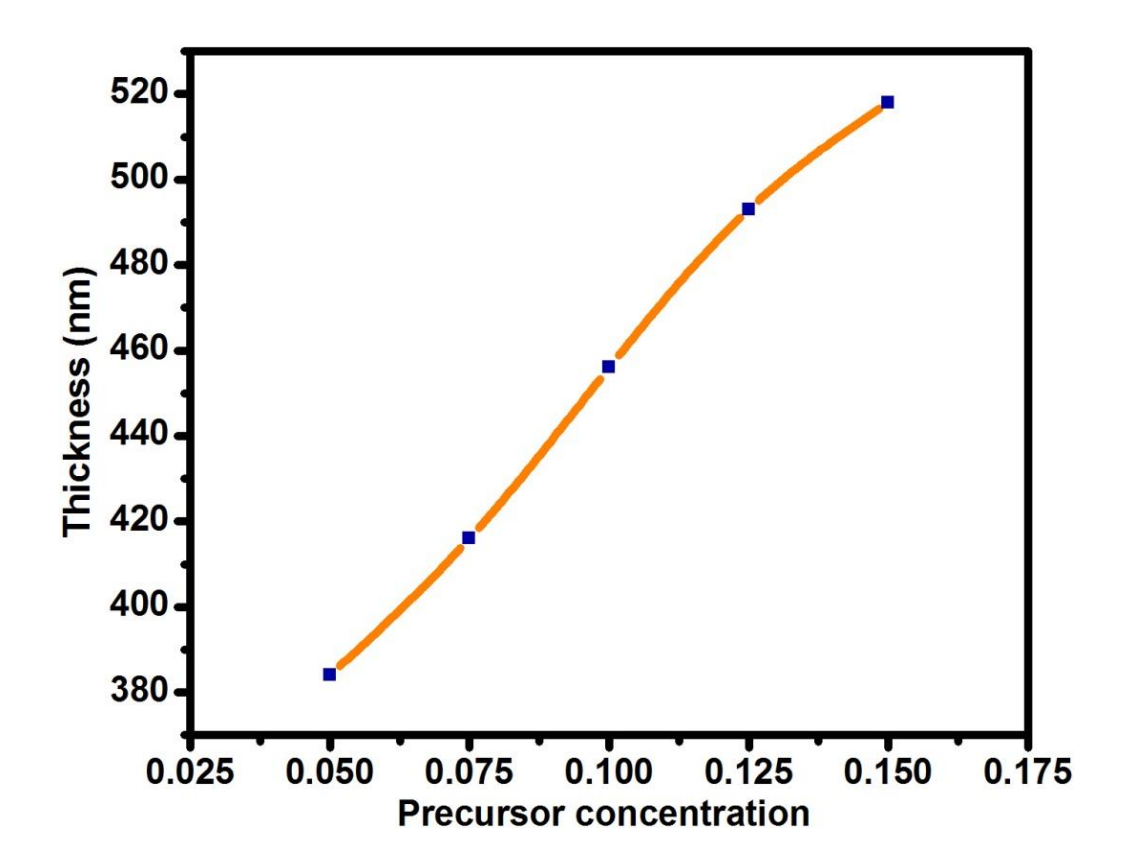


Fig. 7.1 Variation of thickness of SnSe thin films at different precursor concentrations

Fig.7.1 shows the variation of thickness as a function of precursor concentrations from 0.050 M to 0.150 M. When precursor concentration is increased from 0.050 M to 0.150 M the film thickness increases from 384 to 518 nm. The preparative parameters as substrate temperature, deposition time, molar ratio, pressure etc. decide the growth and quality of the film.

# 7.3.1 X-ray diffraction studies of SnSe thin films for different Precursor concentration

Fig. 7.2 depicts the X-ray diffraction patterns for SnSe thin films deposited at different precursor concentration of optimized substrate temperature of 300 °C with the SnSe thin films show three major diffraction peaks related to the diffraction angles 30.47° (111), 37.72° (311) and 49.72° (511) with a preferred orientation along (111) plane of orthorhombic structure. The standard diffraction peaks exhibited by SnSe thin film are matched with the JCPDS card No. 48-1224 corresponding to orthorhombic phase. The degree of texture along the (111) preferred orientation depends on the SnSe phase only. The intensity of the diffraction peaks with orthorhombic phase turned more intense and sharp with the increase of precursor concentration up to 0.150 M, which notices an improvement of the crystallinity of the grain layers. At lower concentration  $m_c = 0.050$  M, the presence of SnO<sub>2</sub> with diffraction angle of 33.61 ° along with SnSe phase might be due to less availability of sulphur, selenium might react with atmospheric oxygen to obtain stabilised structure and forms phases belongs Sn-O-S complex. At higher concentration m<sub>c</sub> =0.150 M, the presence of SnO<sub>2</sub> with diffraction angles of 14.41 and 33.71 ° along with SnSe phase might be due to the lack of thermal energy of top clusters. Kumar et al. [17] reported orthorhombic structured SnSe thin films with (111) preferential orientations grown by thermal evaporation method.

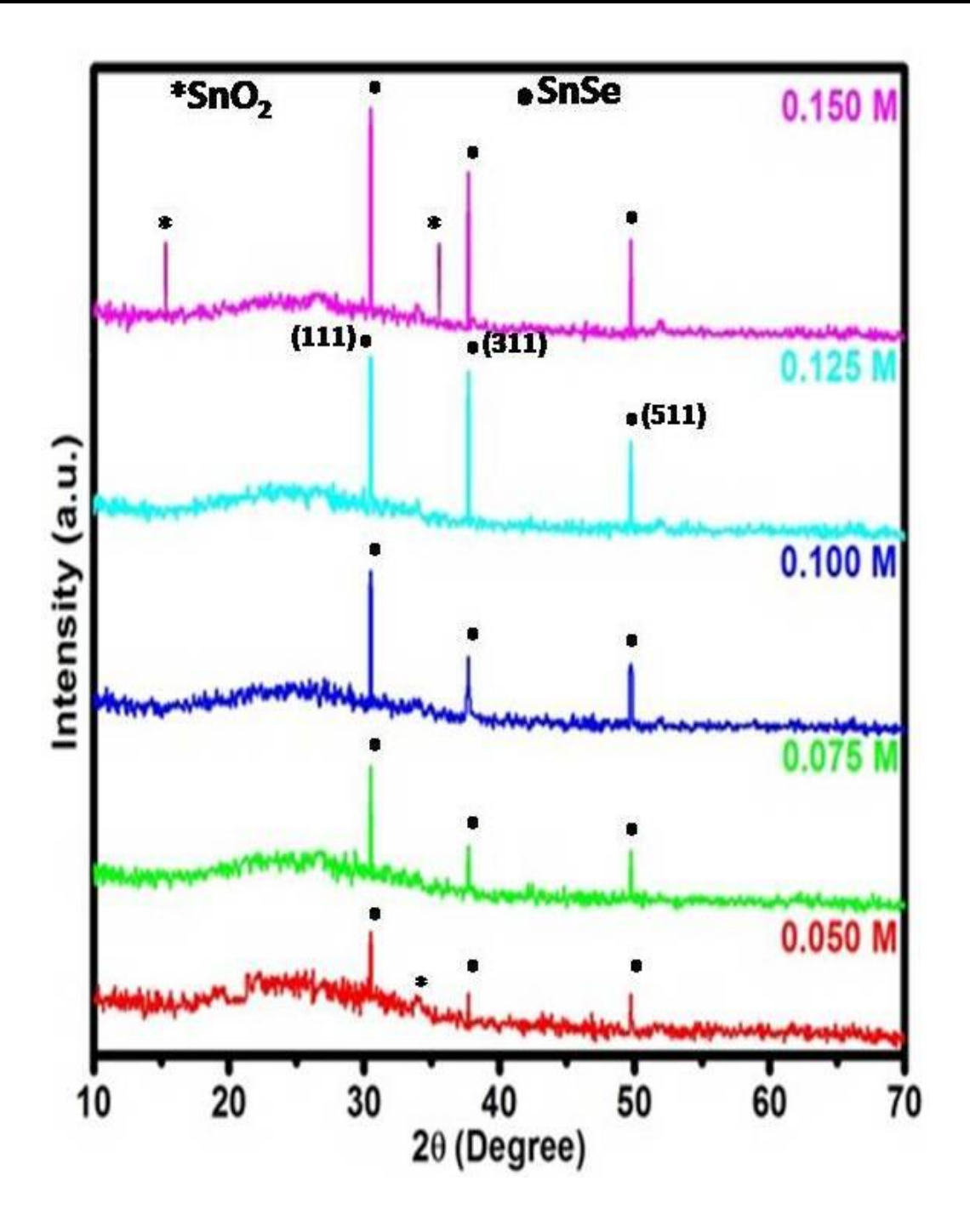


Fig 7.2 X-ray diffraction pattern of SnSe thin films prepared at different precursor concentration

According to Bauer [18], there are two attainable mechanism of the orientation owing to nucleation and final growth, both of which effect from the nucleation at the film substrate with the inclination of nuclei to work out a minimum free energy configuration.

The final growth orientation results from the endurance of nuclei having an energetically unstable plane parallel to the substrate surface amidst randomly oriented nuclei due to their different growth rates. This means that the growth orientation is formulated into one crystallographic direction of the lowest surface energy.

Then, the grains became larger as the film grows with lower surface energy density. As thickness reckons on the band gap of thin film deposition at higher molar concentrations are thicker as compared to films deposited at lower molar concentration. Since in thin films, the average crystallite size is proportional to thickness of films, the decrease in band gap with the increase in film thickness in this study indicates that there is no charge accumulation at grain boundaries in SnSe thin films.

Table 7.1 Structural parameters of SnSe thin films deposited at different precursor concentration  $(m_c)$ 

m <sub>c</sub> (M)	hkl	FWHM (degrees)	Crystallite size (nm)	Strain X10 <sup>-3</sup>
0.050	(111)	0.187	44.01	7.88
).VJV	(311)	0.293	27.14	12.77
	(511)	0.501	16.48	21.04
	(111)	0.175	46.98	7.38
).075	(311)	0.267	29.78	11.64
	(511)	0.314	26.29	13.18
	(111)	0.148	55.82	6.21
0.100	(311)	0.149	53.75	6.45
	(511)	0.190	43.45	7.98
105	(111)	0.135	60.99	5.68
).125	(311)	0.140	56.79	6.10
	(511)	0.163	50.65	6.84
	(111)	0.137	60.01	5.78
).150	(311)	0.167	47.61	7.28
	(511)	0.191	43.22	8.02

The texture coefficient  $T_{c(hkl)}$  of the films [19] has been calculated from the XRD data using Eq. (7.1). The preferred orientation of the films can be confirmed by the higher value of texture coefficient. The increased number of grains along the plane associates the increase in preferred orientations [20].

The dislocation density ( $\delta$ ) defined as length of dislocation lines per unit volume of the crystal using crystallite size values (D) has been determined using the Williamson and Smallman's formula [21] Eq. (3.2).

The optoelectronic properties of the films are affected by stacking fault probability due to the distorted lattice and was appraised using the relation [22]

$$a^* \left( \frac{2\pi}{45(3\tan\theta)^{\frac{1}{2}}} \right) \beta \qquad \dots (7.2)$$

Table 7.1 shows the FWHM, crystallite size (D) and lattice strain ( $\epsilon_s$ ) of SnSe thin films with different precursor concentration. The crystallite size is low at lower precursor concentration since the deposited atoms in lieu of incorporating to the neighbouring grains and increasing their size are condensed and stay stuck to the region to constitute small nuclei and clusters. At higher precursor concentration, a large crystallite size is noticed due to the increasing mobility of the surface of atoms and increasing cluster formation.

It is observed that the crystallite size increases and obtains a maximum value of 60.99 nm at  $m_c = 0.125 \text{ M}$  whereas the decrease in lattice strain was observed by increasing the precursor concentration. Surely, the lattice strain is decreased owing to the prevailing re-crystallization process in the SnSe polycrystalline thin films. The observed decrease of full width at half maximum (FWHM) of diffraction peaks with increase of precursor concentration can be attributed to the increase in crystallite size up to 0.125 M. The increase in crystallite size may be attributed to the improvement of the crystallinity and an increase in the cluster formation owing to increase of precursor concentration leading to agglomeration of small crystallites. These agglomerated crystallites combine together, resulting in the formation of larger crystallites with better crystallinity. At  $m_c = 0.150 \text{ M}$ , a

small decrease in value of crystallite size as 60.01 nm, where the decrease may be due to the less agglomeration among them. The crystallite size of the SnSe can be affected by so many factors such as impurities, defects and heating conditions.

Table 7.2 Value of texture coefficient, dislocation density, number of crystallites and stacking fault for different precursor concentration (m<sub>c</sub>)

m <sub>c</sub> (M)	Texture coefficient	Dislocation Density X10 <sup>15</sup> (Lines/m <sup>2</sup> )	No. of Crystallites x10 <sup>16</sup> (m <sup>2</sup> )	Stacking fault (x10 <sup>-3</sup> ) (1/m²)	Thickness (nm)
0.050	1.0856	0.5162	0.4504	43.46	384
0.075	1.0421	0.4532	0.4013	40.72	416
0.100	1.0365	0.3209	0.2621	34.26	456
0.125	1.0144	0.2689	0.2173	31.36	493
0.150	1.0181	0.2767	0.2397	41.61	518

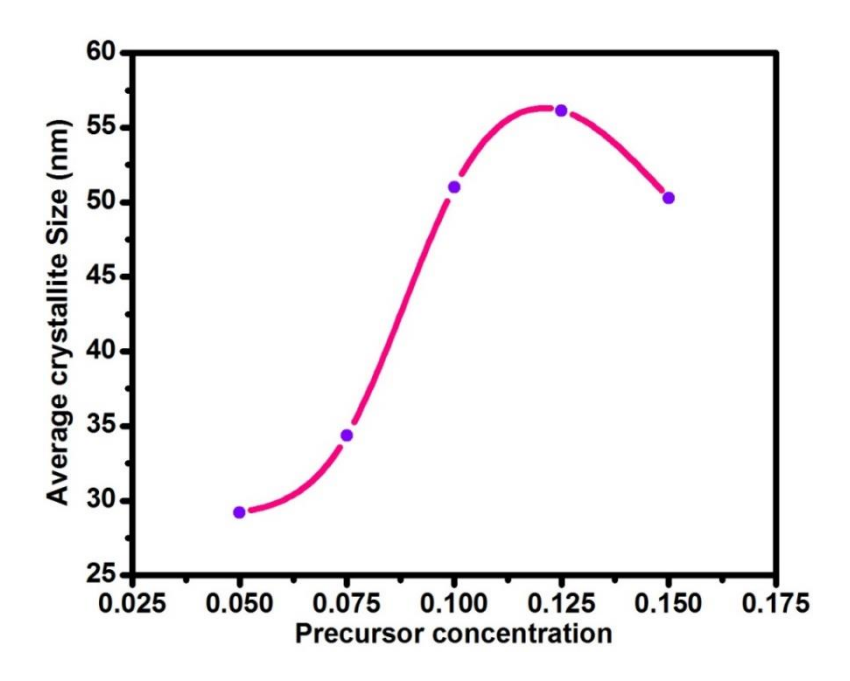


Fig. 7.3 The variation average crystallite size with different precursor concentration of SnSe thin films

The average crystallite size calculated for all the samples prepared at precursor concentration from 0.050 to 0.150 M was found to be increased from 27.75 to 51.01 nm

(Fig. 7.3). In table 7.2 shows the texture coefficient, dislocation density and stacking fault probability of the films decreases with an increase in precursor concentration up to 0.125 M and is increased for further increasing of molar concentration of 0.150 M. The change in grain size with precursor concentration explained this behaviour. Indeed, the larger crystallites have a smaller surface to volume ratio, thus giving up a rise to the dislocation network. The number of crystallites per unit area (N) depends on the parameters like equidimensional crystallites and the degree of the agglomeration of the thin films. It is ascertained that the number of crystallites decreases as the precursor concentration parameter increases up to 0.125 M. From these observations, it is clear that when the precursor concentration of tin increases, the crystallite size increases and this leads to a decrease in grain boundaries, lattice strain, dislocation density and stacking fault probability. The decrease in grain boundaries at higher precursor concentration of 0.150 M indicates the reduction of crystal lattice imperfections and formation of high-quality films.

# 7.3.2 Surface morphological studies of SnSe thin films for different precursor concentration using SEM

SEM is an auspicious technique for the surface morphological study of the films and it furnishes the worthy information about the shape and size of the grains or particles. The surface morphology of SnSe thin film deposited at different precursor concentration is shown in Fig. 7.4. These SEM photographs were recorded with magnifications of about 100000. The SEM micrograph of thin film contains particles with almost spherical shape aggregated severely. These results are in good agreement with some other reports [23]. The SEM micrograph of film shows a distribution of particles which covers the surface of the substrate completely. No pin holes or cracks could be observed. One can see the uniform distribution of grain size over total coverage of the substrate with a compact and fine grained morphology. This type of morphology has also been observed by others for nanocrystalline SnSe [6,17,24,25]. However, as the precursor concentration was increased from 0.050 to

0.125 M also the grain size increased. It is also clear that the grain size increases with the increase of precursor concentration. Samples prepared at higher concentration of 0.125 M have larger grain size; clearly the average grain size of thin films is in nanometer range of 47-170 nm.

## 7.3.3 Compositional analysis of SnSe thin films by EDAX

The distinct composition and the purity of as-deposited SnSe thin films deposited at different precursor concentration were determined by EDX study, which brought out the presence of Sn and Se as elementary components. The characteristic EDX spectra of SnSe thin films grown at substrate temperature 300 °C of precursor concentration from 0.050 to 0.150 M are shown in Fig. 7.5. The quantitative weight percentage of the compositional elements such as Sn and Se in SnSe thin films for different precursor concentration is presented in Table 7.3. Two different peaks related to Sn and Se are found in the spectrum (Fig. 7.5) for the films deposited at precursor concentration from 0.050 to 0.150 M, which confirms the SnSe thin films. The atomic percentage of tin and selenium was observed as 51.63% and 48.37% respectively, for the concentration 0.050 M. The atomic percentage of selenium had decreased from 48.37% to 44.59% when increasing the precursor concentrations from 0.050 to 0.150 M, respectively. EDX spectrum exhibits that the weight percentage is closely equal to their nominal stoichiometry of 0.050 M within the experimental error. The atomic percentage of tin is increased from 51.63 to 55.41 by increasing the precursor concentration. For 0.150 M precursor concentration, the atomic percentage of tin and selenium was observed as 55.41 and 44.59%, respectively, which predicts the mixed phases of SnO<sub>2</sub> and SnSe present in this film prepared with a precursor concentration of 0.150 M.

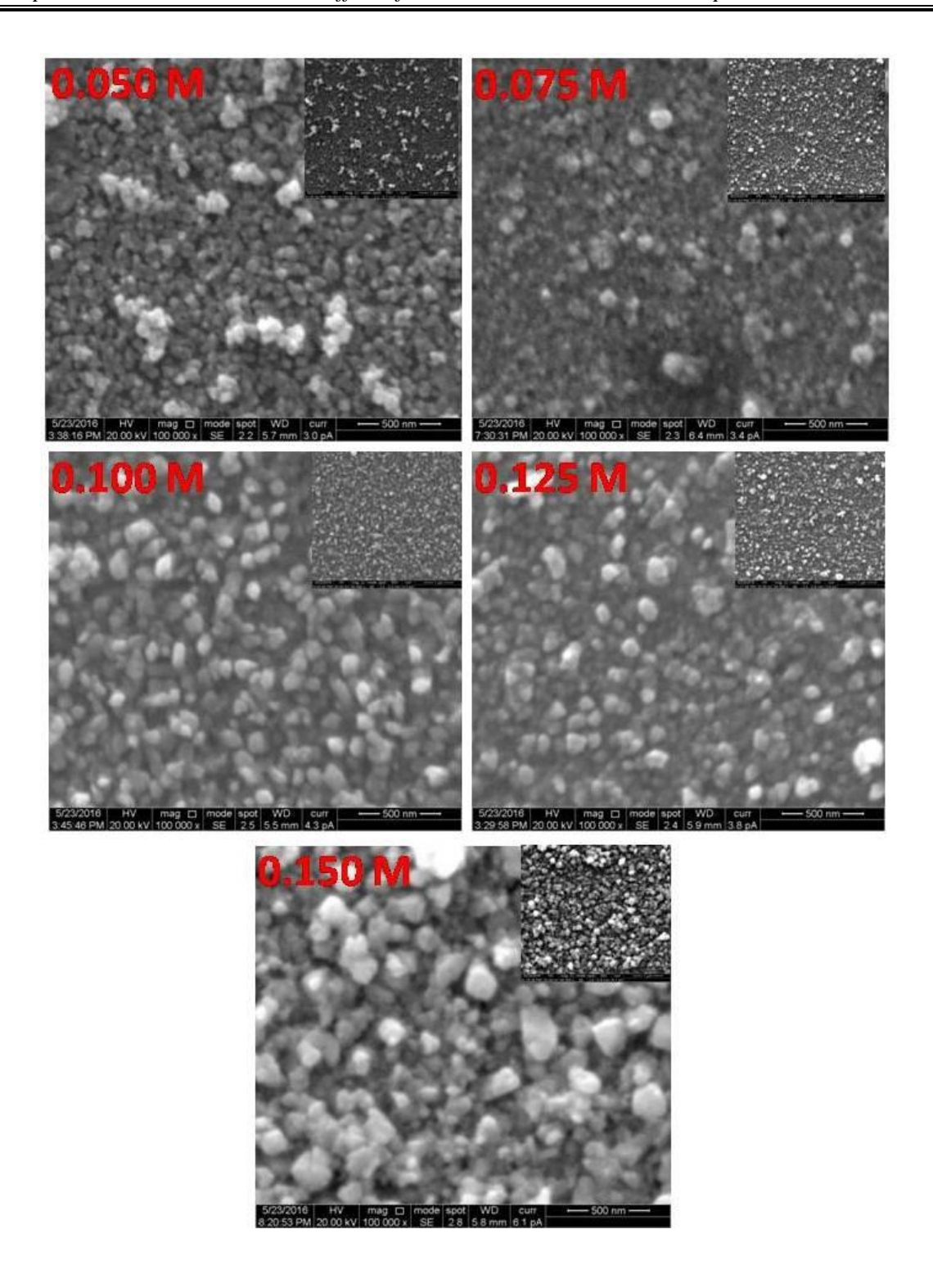


Fig. 7.4 Scanning electron microscope (SEM) images of SnSe thin films for different precursor concentration

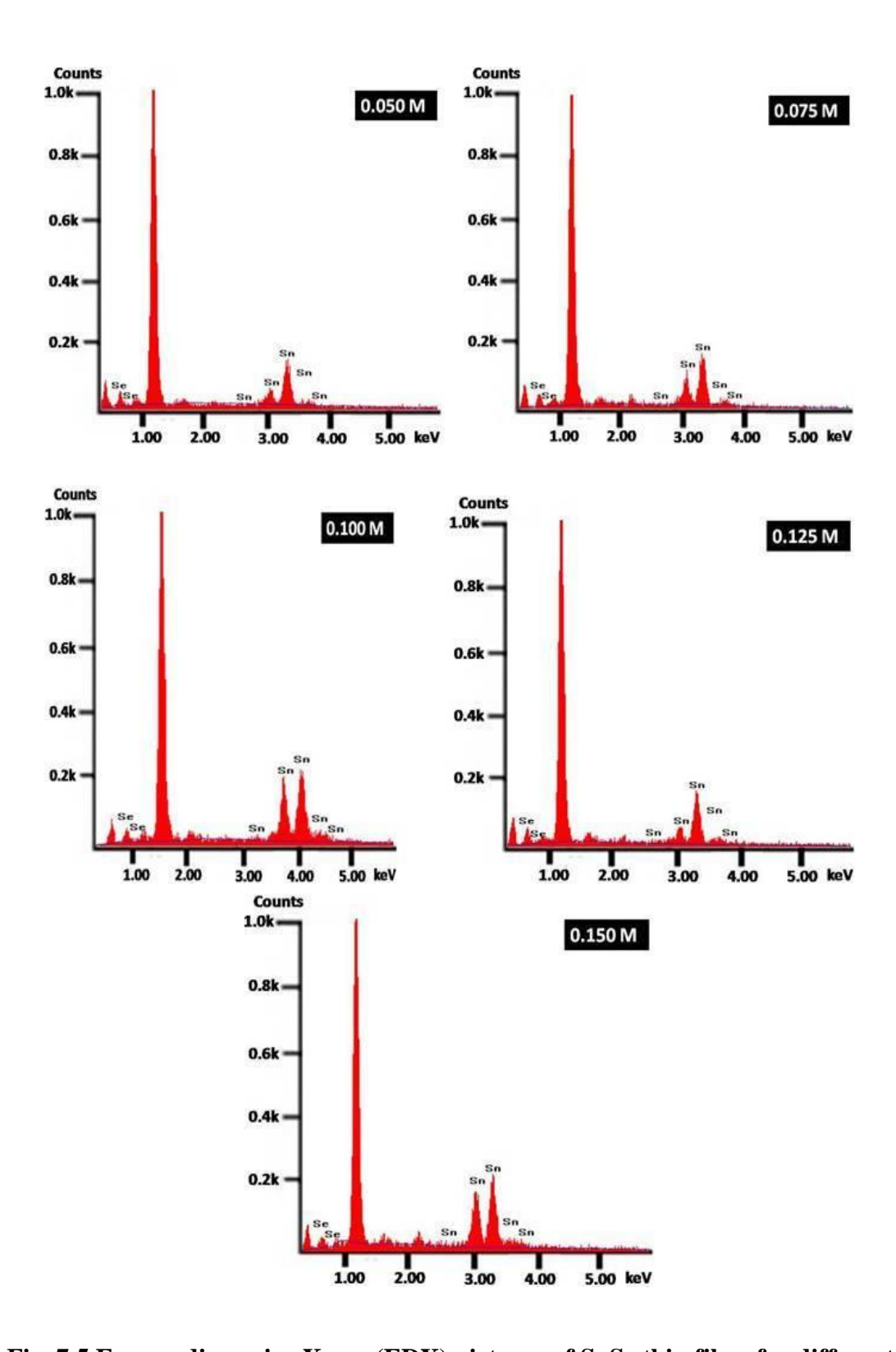


Fig. 7.5 Energy dispersive X-ray (EDX) pictures of SnSe thin films for different precursor concentration

Table 7.3: The quantitative analysis of the weight percentage of the compositional elements presents in the SnSe thin films at different precursor concentration

т <sub>с</sub> (М)	Atomic percent	Sn/Se ratio	
- X ( )	Sn	Se	33334
0.050	51.63	48.37	1.07
0.075	52.01	47.99	1.08
0.100	52.52	47.48	1.11
0.125	52.99	47.01	1.13
0.150	55.41	44.59	1.24

## 7.3.4 Optical absorption analysis of SnSe thin films

The precursor concentration influenced change in transmittance and optical absorption coefficient spectra of SnSe films recorded in the wavelength range of 300-1100 nm are presented in Fig.7.6 and Fig.7.7 respectively. Fig. 7.6 shows that the average transmittance of the film varies between 50 and 70%. It is noticed that large percentage of transmittance for the films grown at precursor concentration of 0.050 M is due to the low thickness of the films. This is because as the film thickness increases, the strain value decreases because of the influence of the glass-SnSe lattice mismatch implied generation of defects in the SnSe layer close to the glass substrate. These defects gradually decrease as the film thickness increases.

It was observed that, SnSe thin films of 0.150 M concentration had the highest absorption coefficient while thin films with a concentration of 0.050 M had the least absorption coefficient as shown in Fig. 7.7. This is because of reduction in stacking faults and lattice defects as film thickness increased; thus an improvement in film crystallinity [26].

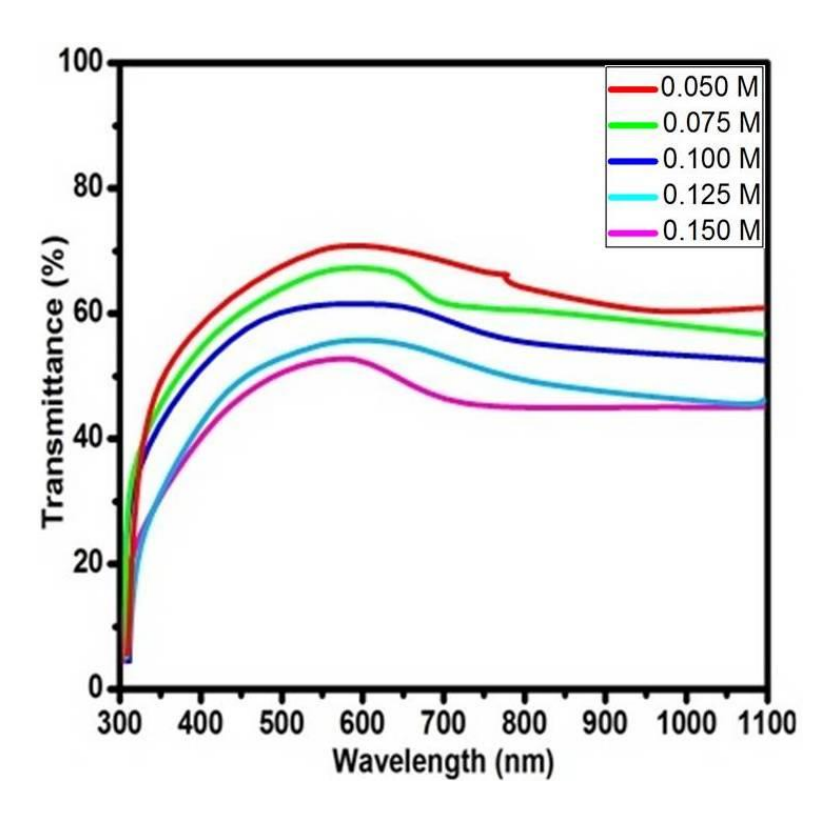


Fig. 7.6 Transmittance spectra of SnSe thin films at different precursor concentration

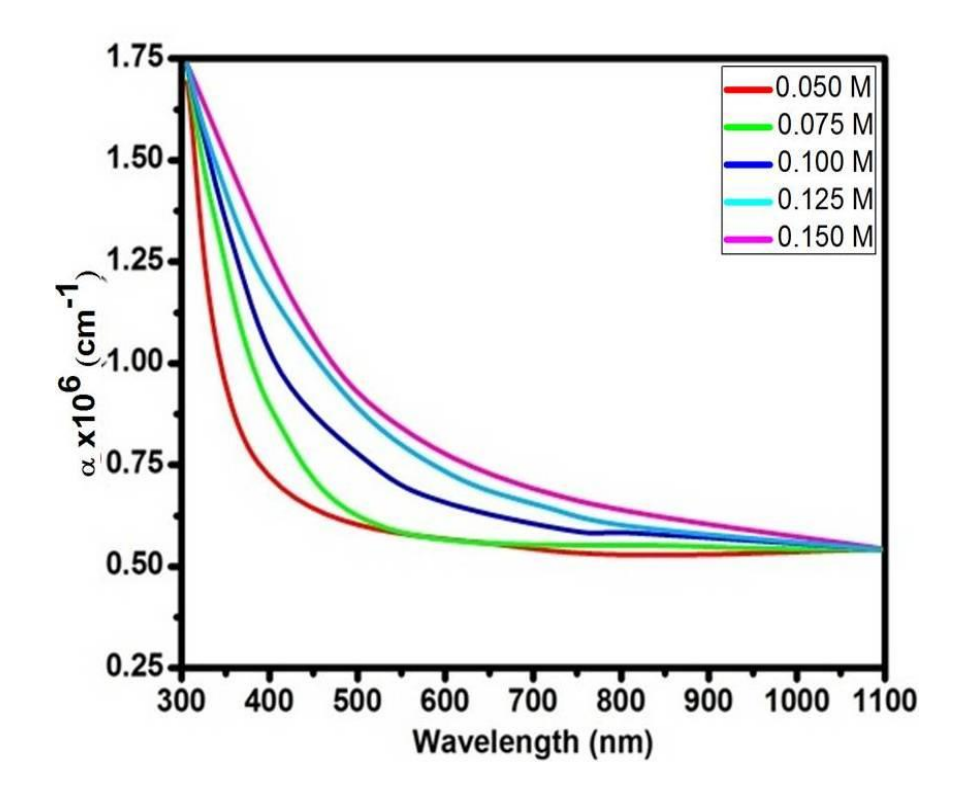


Fig. 7.7 Absorption coefficient ( $\alpha$ ) spectra for SnSe thin films prepared for different precursor concentration

High absorption coefficient is achieved when the photon energy is higher than the energy gaps of a semiconductor material. The minimum absorption in the visible and infrared region for all the films is observed and it shows a similar evaluation in the transmittance spectra with different precursor concentration. The optical band gap of as deposited SnSe thin films is determined by applying the Tauc model [27]. For semiconductors, n=1/2, 2, 3/2, 3 and values corresponding to the allowed direct, allowed indirect, forbidden direct and forbidden indirect transition, respectively. Since, n=1/2 and the absorption coefficient is of the order of 10<sup>4</sup> cm<sup>-1</sup> supports the direct band gap nature of SnSe semiconductor for allowed direct transition. Fig. 7.8 shows the plot for the variation of  $(\alpha h v)^2$  versus hv. The direct optical band gap values decreased to a minimum of 1.09 eV at 0.125 M with an increase in precursor concentration from 0.050 M and with the further increase in the precursor concentration to 0.150 M, the band gap value had increased to 1.12 eV. Enue Barrios-Salgado et al. [28] had reported band gap values of 0.95-1.14 eV for the film prepared by chemical deposition method on glass substrates. Generally, the decrease in optical band gap may be attributed to the increase in crystallite size, thickness and crystallinity, roughness and grain size. In the present study, it is believed that the increase in crystallite size and crystallinity is accountable for the decrease in the band gap, which is evidenced by XRD results. The increase in band gap at 0.150 M can be attributed to the decrease in thickness as well as the crystallite size at that concentration comparing to 0.125 M, leading to its corresponding electronic structure. The 1.12 eV band gap of 0.150 M film is more than that of 0.125 M film (1.09 eV). This shows that the presence of SnO<sub>2</sub> phase with SnSe influence on the band gap of SnSe.

## 7.3.5. Photoluminescence studies on SnSe thin films

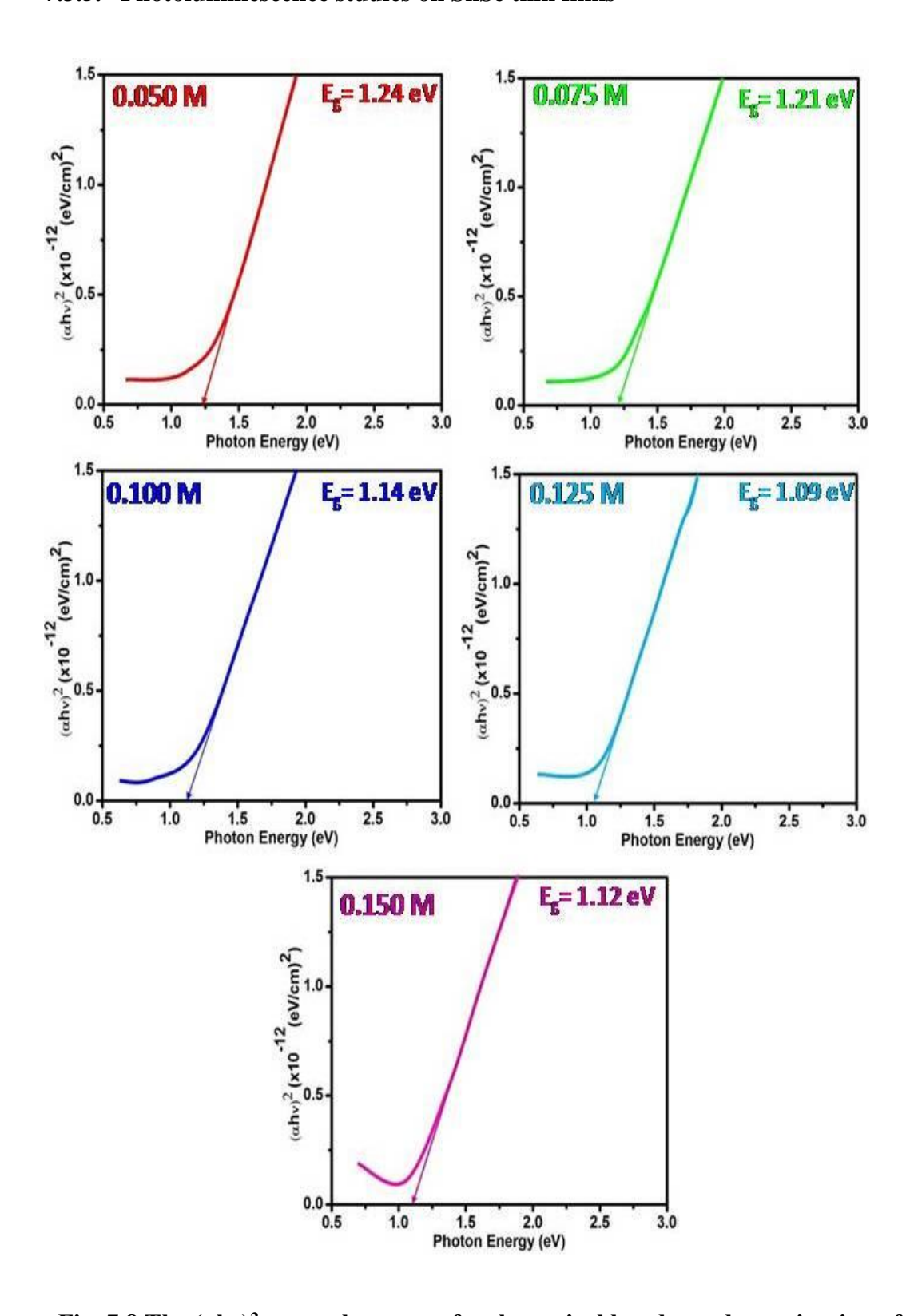


Fig. 7.8 The  $(\alpha h v)^2$  versus hv curves for the optical band gap determination of SnSe thin films of different precursor concentration

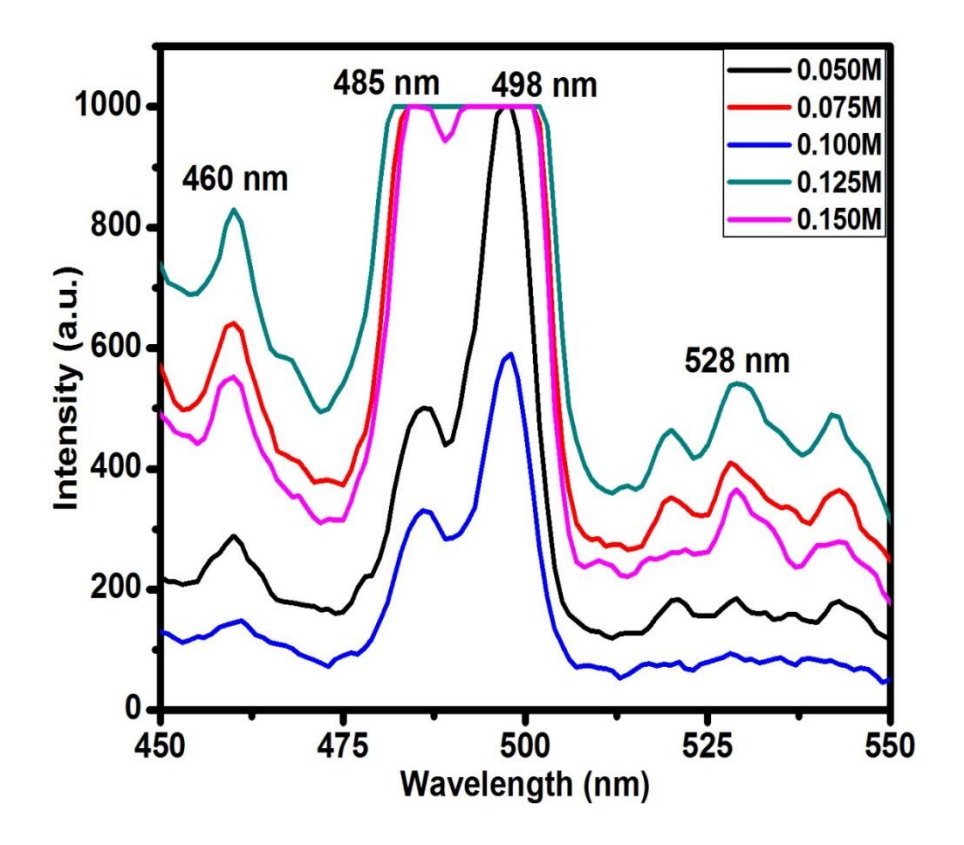


Fig. 7.9 Photoluminescence (PL) spectra of SnSe thin films under different precursor concentration

The correlation between structure and property is investigated by PL spectra which originate from the recombination of the surface states [29]. The PL is one of the significant studies which can give us more important information on the crystal quality and purity of the material. The presence of defects such as electron—hole recombination centres, oxygen vacancies and defects are responsible for optical absorption and the emission spectra. The room temperature photoluminescence spectra of the SnSe thin films in the wavelength region from 450 nm to 550 nm are shown in Fig.7.9. The peaks at 460, 485, 498 and 528 nm may be ascribed to defect centers attributed to excitonic transitions which are size dependent and excitation wavelength-independent in certain wavelength range [30]. In these

values are quite so different from optical band gap value but photo luminescence have some limitation to determine the range. From this spectrum, it can be found that the SnSe thin films have high luminescence properties in the visible region. The low intensity luminescence peaks observed in the films might be attributed to inter-impurity transitions and larger stoichiometric deviations in the films.

## 7.3.6. Electrical conductivity studies on SnSe thin films

The electrical conductivity, Hall coefficient and bulk carrier concentration of SnSe thin films deposited at different precursor concentration were determined by Hall effect measuring instrument and the corresponding values were listed in Table 7.3. The Hall coefficient values confirm that all the films had an p-type characteristic. Fig. 10 depicts the resistivity and Hall mobility of the films as a function of precursor concentration. The resistivity of the as-deposited films decreases with increase of precursor concentration from 0.050 to 0.125 M. The lowest resistivity value was 3.04  $\Omega$ -cm at the concentration of 0.125 M. The decrease in resistivity may be attributed to the increase in crystallite size which leads to a decrement in the trapping states at grain boundary [31]. The grain boundary plays an important role between the crystallites and the carrier transport. It can act as a trap center in an incomplete atomic bonding, which depletes the free charge carriers and as a resultant, more number of free carriers become immobilized as trapping state increase. The resistivity again increases to 4.83  $\Omega$ -cm, while the precursor concentration had increased to 0.150 M.

The bulk carrier concentration and mobility of the SnSe thin films increase with increasing precursor concentration up to 0.125 M of 5.757 x 10<sup>17</sup> cm<sup>-3</sup> and 8.1 cm<sup>2</sup>/Vs, respectively and decreases with the further increase in precursor concentration of 0.150 M. The increased bulk carrier concentration caused by increasing concentration reduced the grain boundary potential barrier. Due to that, the carrier mobility of the films also increases.

As a result, the resistivity diminishes with increasing precursor concentration attained a minimum.

The activation energy of SnSe thin films can be calculated by using Eq. 7.3.

$$\rho = \rho_0 \exp^{\left(\frac{E}{KT}\right)} \qquad \dots (7.3)$$

The Arrhenius plot is drawn with the experimental data as shown in Fig. 7.11, which it can be predicted that the variation of resistivity of this SnSe film is being assisted by a single activation process with activation energy is tabulated in Table 7.3, which are determined by the best fit of the experimental data to Eq. (7.4). The Arrhenius plot is drawn as shown in Fig. 7.11 for various precursor concentrations. Activation energy for SnSe thin films were calculated as 0.201 eV, 0.198 eV, 0.194 eV, 0.189 eV and 0.191 eV corresponding to 0.050 M, 0.075 M, 0.100 M, 0.125 M and 0.150 M precursor concentrations respectively. Kumar et al. [32] had reported the activation energy of SnSe thin film using thermal evaporation method is in the range of 0.14 eV-0.28 eV.

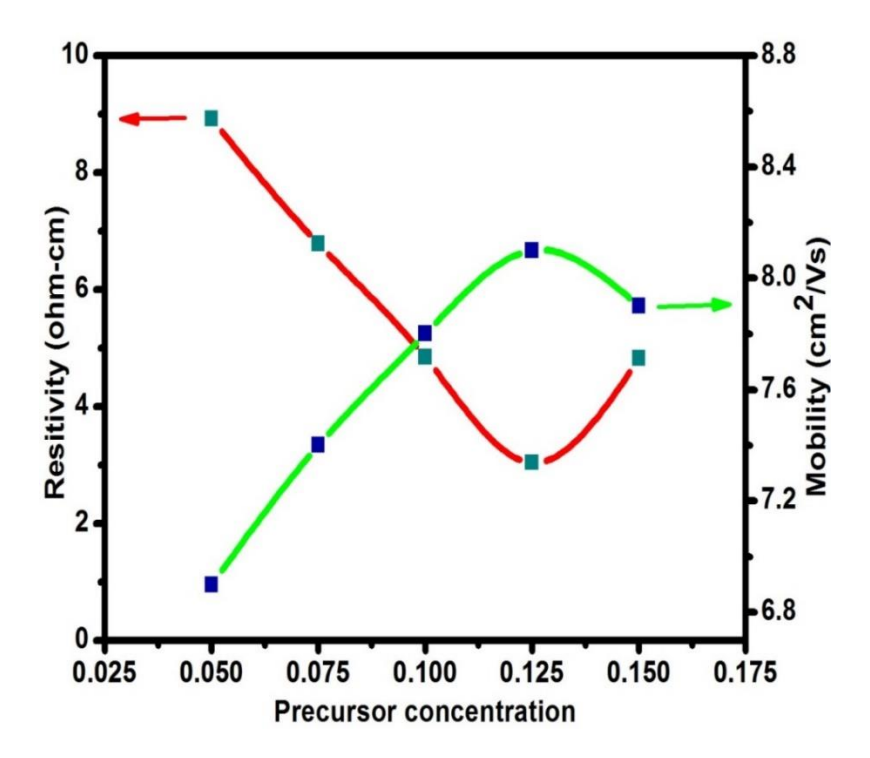


Fig. 7.10 Variation of resistivity and mobility of SnSe thin films at different precursor concentration

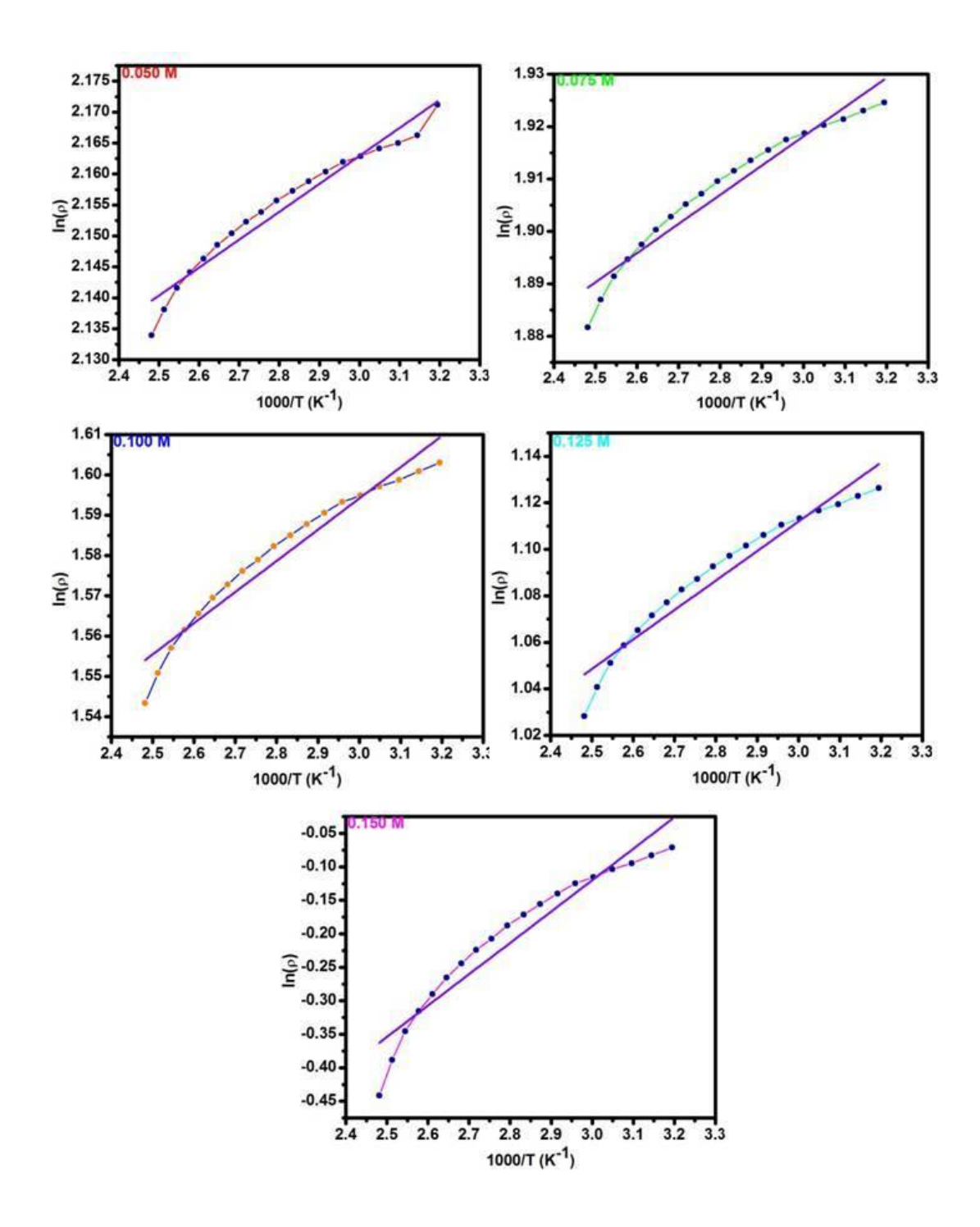


Fig. 7.11 Arrhenius plot for SnSe thin films at different precursor concentration

Table 7.4 Variation of optical and electrical properties of SnSe thin films at different precursor concentration

m <sub>c</sub> (M)	Band gap (eV)	Conductivity (Ωcm) <sup>-1</sup>	Carrier concentration (cm <sup>-3</sup> )	Hall coefficient (cm <sup>-3</sup> /C)	Activation energy (eV)
0.050	1.24	0.112	4.872x10 <sup>17</sup>	12.83	0.201
0.075	1.21	0.147	5.023x10 <sup>17</sup>	12.44	0.198
0.100	1.14	0.207	5.676x10 <sup>17</sup>	11.01	0.194
0.125	1.09	0.329	5.757x10 <sup>17</sup>	10.86	0.189
0.150	1.12	0.207	5.689x10 <sup>17</sup>	11.05	0.191

Such differences activation energies may be due to varying preparation parameters and the presence of different defect states during the growth of SnSe thin films. It was found that the activation energy values decreases with increase in precursor concentration up to 0.125 M and then increases for the further increase in precursor concentrations. The decrease in activation energy with the increase in precursor concentration may be attributed to the change in the electronic structure corresponding to the increase in thickness values [33]. The corresponding pre-exponential factor ( $\rho_0$ ) for the SnSe thin films prepared at substrate temperatures of 300 °C of different precursor concentration from 0.050 to 0.150 M is determined to be 7.60, 5.76, 3.11, 2.08 and 0.22  $\Omega$ -cm for the films by the fit to the y-intercept of the Fig. 7.11. The minimum value of pre-exponential factor value was obtained for the film prepared at the precursor concentration of 0.150 M.

## 7.4 CONCLUSION

The effect of precursor concentration on various properties of nebulized spray pyrolysised SnSe thin films were studied in detail. X-ray diffraction (XRD) pattern confirmed SnSe thin film with orthorhombic structure. The variation in grain size and

energy gap by increasing precursor concentration made the samples as a promising candidate for the applications of optoelectronic device such as photodiodes and solar cells. The high transmittance and lower absorption in the visible region observed at lower concentrations illustrated the good optical quality of the crystals with the low absorption or scattering losses which leads to the applications especially as an absorber layer in solar cells. The optical parameters such as direct band gap energy have been discussed in detail. The change in morphology of SnSe thin films for different precursor concentration was studied by scanning electron microscope. Energy dispersive X-ray pattern confirmed the presence of Sn and Se with the chemical stoichiometric. The percentage of selenium decreased from 48.37 to 44.59 by increasing precursor concentration from 0.025 to 0.150 M. The electrical resistivity of as-deposited SnSe thin films decreased by increasing the precursor concentration to 0.125 M and increased slightly at 0.150 M. The maximum carrier mobility of 8.1 cm²/Vs was obtained at 0.125 M. The investigation results of the SnSe thin films deposited by nebulized spray pyrolysis technique ensure the stability of the film and their employability in solar cell application.

## **REFERENCES**

- [1] Z. Zainal, N. Saravanan, K. Anuar, Z. Mohd, W. Hussein, M. Mahmood, Solar Energy Materials and Solar Cells. 81 (2004) 261.
- [2] K. Bindu, P. Nair, J. Semiconductor Sci. Technol.19 (2004) 1348.
- [3] G. Hema, J. Naveen, S. Uthanna, Journal of Crystal Growth 306 (2007) 68.
- [4] J. Sharma, G. Singh, A. Thakur, G.S.S. Saini, N. Goyal, S.K. Tripathi, J. Optoelectron. Adv. Mater. 7 (2005) 2085.
- [5] M. Popescu, F. Sava, A. Lőrinczi, G. Socol, I.N. Mihailescu, A. Tomescu, J. Non-Cryst. Solids 353 (2007) 1865.
- [6] B. Subramanian, C. Sanjeeviraja, M. Jayachandran, J. Cryst. Growth 234 (2002) 421.
- [7] L. Amalraj, M. Jayachandran, C. Sanjeeviraja, Mater. Res. Bull. 39 (2004) 2193.
- [8] R. Mariappan, M. Ragavendar, G. Gowrisankar, Chalcogenide Lett. 7 (2010) 211.
- [9] J.S. Narro Rios, M. Ramachandran, D. Martínez Escobar, A. Sánchez Juárez, J. Semicond. 34 (2013) 1.
- [10] N.D. Boscher, C.J. Carmalt, R.G. Palgrave, I.P. Parkin, Thin Solid Films 516 (2008) 4750.
- [11] M. Biçer, İ. Şişman, Appl. Surf. Sci. 275 (2011) 2944.
- [12] N.R. Mathews, Sol. Energy 86 (2011) 1010.
- [13] X. Fu, G. Wu, S. Song, Z. Song, X. Duo, C. Lin, Appl. Surf. Sci. 148 (1999) 223.
- [14] R. Mariappan, V. Ponnuswamy, P. Suresh, Superlattices Microstruct. 52 (2012) 500.
- [15] R. Mariappan, V. Ponnuswamy, P. Suresh, R. Suresh, M. Ragavendar, C. Sankar, Mater. Sci. Semicond. Proc. 16 (2013) 825.
- [16] R. Mariappan, V. Ponnuswami, M. Ragavendar, Mater. Sci. Semicond. Proc. 15 (2012) 199.
- [17] N. Kumar, V. Sharma, U. Parihar, R. Sachdeva, N. Padha, C. J. Panchal, J. Nano Electron Phys. 3(1) (2011) 117.
- [18] E. Bauer, M.H. Francombe, H. Sato, Single Crystal Films, first ed., Pergamon, London, 1964.

- [19] R. Mariappan, V. Ponnuswamy, P. Suresh, R. Suresh, M. Ragavendar, Superlattic.Micros., 59 (2013) 47.
- [20] R. Suresh, V. Ponnuswamy, R. Mariappan, N. Senthilkumar, Ceram. Int. 40 (2014) 437.
- [21] G.B. Williamson, R.C. Smallman, Philos. Mag. 1 (1956) 34.
- [22] J.I. Pankove, Optical Processes in Semiconductors, Prentice and Hall, Inc., New Jersey (1971) 37.
- [23] Dong-Hau Kuo, Wei-Di Haung, Ying-Sheng Huang, Jiun-De Wu, Yan-Jih Lin, Thin Solid Films 518(24) (2010) 7218.
- [24] Z. Zainal, N. Saravanan, K. Anuar, M. Z. Hussein, W. M. M. Yunus, Mater. Sci. Eng. B 107 (2004) 181.
- [25] B. Subramanian, T. Mahalingam, C. Sanjeeviraja, M. Jayachandran, M. J. Chockalingam, Thin Solid Films 357 (1999) 119.
- [26] S. Venkatachalam, D. Mangalaraj, S. Narayandass, S. Velumani, P. Schabes Rechkiman, J. Ascencio, Material Chemistry and Physics 103 (2007) 305.
- [27] J.I. Pankove, Optical Processes in Semiconductors, Prentice and Hall, Inc., New Jersey, 1971, pp 37.
- [28] Enue Barrios-Salgado, M. T. S. Nair, P. K. Nair, ECS Journal of Solid State Science and Technology 3 (8) (2014) Q169.
- [29] N. Chestony, T.D. Harris, R. Hull, L.E. Brus, J. Phys. Chem. 90 (1986) 3393.
- [30] J. Srivind, V.S. Nagarethinam, A.R. Balu, Materials Science-Poland 34(2) (2016) 393.
- [31] P. Prathap, Y.P.V Subbaiah, K.T. Ramakrishna Reddy, J Phys D Appl Phys. 40 (2007) 5275.
- [32] N. Kumar, V. Sharma, N. Padha, N. M. Shah, M. S. Desai, C. J. Panchal, I. Yu. Protsenko, Cryst. Res. Technol. 45 (1) (2010) 53.
- [33] M. Devika, N. Koteeswara Reddy, K Ramesh, Semicond Sci Technol. 21 (2006) 1125.

## CHAPTER - VIII

# STRUCTURAL, OPTICAL AND PHOTOSENSING PROPERTIES OF SPRAY PYROLYZED SnSSe THIN FILMS

## 8.1 INTRODUCTION

Stannous Sulphide (SnS) and Stannous Selenide (SnSe) are becoming an emerging prominent materials in recent years because of their potential technological importance. The synthesis of binary metal chalcogenide of II-VI semiconductors in thick film, thin film a nd nanocrystalline form has been rapidly growing area in the material research due to their important non-linear optical, photo luminescent and other physical and chemical properties [1]. It is found that the band gap of Stannous Selenide material is 1.1 eV where as of Stannous Sulphide is 1.8 eV, both these are suitable for solar spectrum. This feature makes these materials useful for solar energy conversion in photovoltaic form [2]. These materials can be synthesized in thin film form from several methods like Thermal evaporation [3, 4], Sputtering, ion, Chemical bath deposition[5], Flux Techniques [6], Molecular beam epitaxy [7], Spray Pyrolysis[8]. etc., Out of these, Spray Pyrolysis is the most promising for producing inexpensive thin films of good quality with various dopants over a large area.

Here the efforts were taken to synthesize the ternary material of Stannous sulpho selenide by altering the concentration of sulphur and selenium componeent for the study of effect of the concentration for the change in energy gap and its effect on photosensing and photoluminescent performance of the material. SnSSe is ternary compound has recently attracted much interest in solar energy conversion because of the bandgap in tailoring effected by incorporation of S in SnSe. The two compounds SnS and SnSe form a continuous series of mixed crystals with a minimum melting point of 1128 K. The crystals are all p-type with hole concentration of about 10<sup>18</sup> cm<sup>-3</sup>. The band edge absorption is found

to be allowed indirect transitions. The band gap of SnS and SnSe at 573 K was found to be 1.08 and 0.9 eV respectively. The bandgap of mixed crystals SnSSe varies linnearly with the x composition.

Structural properties of the material play a vital role in the performance of the devices and a knowledge of the influence of the deposition parameters on the structural properties [11-12]. The mixed crystals of commposition SnSSe have the same crystal structure as SnS and SnSe. The unit cell contains eight atoms, placed in position about the scaled coordinates. The atoms are arranged in two adjacent double layers orthogonal to the largest dimensions [13,14].

The aim of this work is to produce SnSSe thin films of equal sulphur and selenium concentration by spray pyrolysis and to study the Crystal structure, Structural, Optical, Electrical, Photo sensing and Photo luminescent properties.

## 8.2 EXPERIMENTAL MATERIALS AND METHODS

The SnSSe films were prepared by spraying equimolar mixture of aqueous solutions of Thiourea as source of Sulphur, Selenourea as source of Selenium and Stannous chloride Sn(Cl2) each of 0.05M as starting solution in deionized water. The proportions of the precursors are maintained such that Stannous precursor is 50% of the composition and remaining 50% composition is of equal parts of sulphur and selenium precursors. The substrates used were insulated microscopic plane glass slides of area 7.5 cm x 2.5 cm, were heated at the optimized temperature of 325 °C + 5 °C. The following reaction was taken place at the surface of heated substrate for synthesis of SnSSe thin film by spray Pyrolysis.

$$SnCl_2 + (NH_2)_2 CSe + (NH_2)_2 CS + 2H_2O \rightarrow SnSSe + 2NH_4C1 \uparrow + CO_2 \uparrow ...(8.1)$$

The as deposited thin films were annealed at 500  $^{\circ}$ C in nitrogen atmosphere for 30 minutes.

The major preparatory parameters in the spray pyrolytic process are substrate temperature, the concentration and molar ratios of starting solutions. The spray rate was 1 ml/min and the distance between the spray nozzle and substrate was 29 cm. After deposition, the films were first cooled to room temperature. The texture of the films was observed under Epignost microscope. The films were observed to be quiet uniform and free from pinholes throughout the sample.

## 8.3 RESULTS AND DISCUSSION

#### **8.3.1** Structural properties

The ternary compound has recently attracted much interest in the field of solar energy conversion because of the bandgap tailoring effected by the incorporation of SnSSe. Preparation and properties of mixed crystals of SnS(1-x)Se have been already reported [15].

Structural properties of the material play a dominant role in the performance of the devices and a knowledge of the influence of various deposition parameters of thin films is essential before the application of these materials in the devices. The mixed crystals of composition of Tin Sulpho Selenide have the same crystal structure of SnS and SnSe. The unit cell contains eight atoms placed in posion by the scaled coordinates (111) or - and (v,1/4,v) and + or - (1/2,v,1/4,1/2,v) The atoms are arranged in two adjacent double layers orthogonal to the largest cell dimensions as shown in figure [16,17]. Within either double layer, each atom has three nearest atoms lies in the other double layer and provides the bond between the double neighbours and the two next neighbours. The resulting highly layered structure, typical of all orthogonal chalcogenide crystals, causes a strong anisotropy of the physical properties of these compounds [16].

X-ray diffraction method is one of the best methods for the estimation of the crystallographic parameters. Figure 8.2 represents the XRD pattern of SnSSe thin film [18].It was observed that the diffraction peak corresponding to (111) orientation was the predominant. The unit cell dimensions of the orthorhombic SnSe lattice was calculated as a=4.444 Å, b=11.496 Å and c=4.151 Å. These dimensions compared to the low temperature phase orthorhombic structure of SnSe. The peak intensities are high and the narrow width indicated larger grain sizes. This observation was supported by the larger grain sizes are seen in SEM micrographs [17].

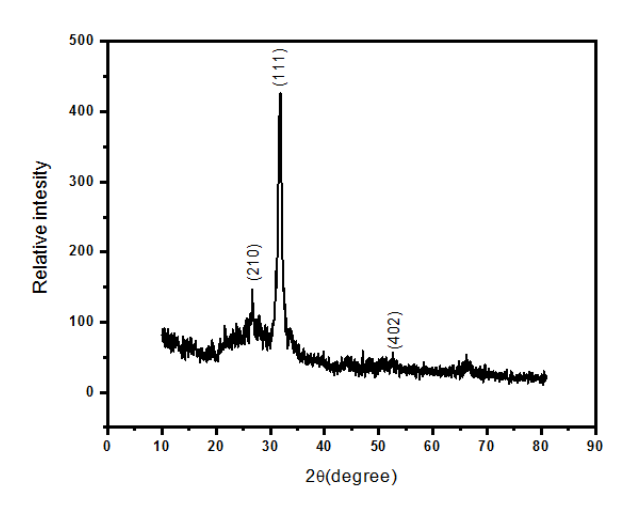


Fig 8.1 XRD pattern of SnSSe thin film deposited at 325  $^{\circ}$  C

As there are only few reports available on SnSSe in the literature to our knowledge. Patel *et al* [24] prepared SnSSe thin films by flash evaporation on NaCl crystal as well as on glass substrates. Thin films deposited at 300 K were poor crystalline and fine grained in nature, which is attributed in electron beam heating, whereby electron charge or thermal gradient is set up in the poorly conducting beam where subjected to electron beam. Therefore all the beams are examined under low beam current. The d-spacing values (interplanar distance) calculated from the electron diffraction pattern were fairly agreement with the XRD obtained from bulk SnSSe. The electron diffraction patterns revealed that

orthorhombic plane (111) is highly preferred orientation. It was also observed that SnSSe films grown are single phase polycrystalline in nature.

## 8.3.2 Optical Properties of SnSSe films

The optical absorption of spray pyrolysed SnSSe thin films were obtained in the wavelength range 300 nm to 1200 nm at 325 °C. The spectrum of the Tin sulpho selenide had been shifted towards shorter wavelength exhibited direct bandgap of 0.9 eV, it was found to be in the same order as Bhatt *et al*, have calculated absorption coefficient upto 2 × 10<sup>4</sup>cm <sup>-1</sup>. This was attributed to the surface nature of the films. The variation of optical bandgap with thickness of the film was found to be decreased with the increasing thickness. The variation was explained due to the quantum effect. The transmission effect of single crystals of SnSSe was measured at 325 °C. The square root of the absorption coefficient in this region was found to be linear function of photon energy which indicated absorption was due to the direct and indirect transitions of electrons from valence band to conduction band [19]. Optical absorption of flash evaporated SnSSe thin films were obtained in the wavelength of 200 nm to 1500 nm at room temperature [20]. It was noted that the bandgap increased with increasing substrate temperature, which led to an improvement in crystallinity of the films.

For the optical band gap study the square of αhv was plotted against hv for each sample as shown in Fig 8.3. The extrapolation of the each curve to zero yields an direct character of band gap. The value of band gap (Eg) obtained for SnSSe was found to be 0.9 eV which is in agreement with Albers *et al.* [28] indirect band gap of SnSe is 0.90 and Bhatt *et al.* [30] reported it as 0.936. Also according to Yu *et al.* [33] it is 0.923 whereas it is 0.948 as reported by Elkorashy [31]. The observed indirect character of band gap is a common property of orthorhombic IV–VI compounds [26,27] and has been confirmed by band structure calculations for SnSe single crystals [28,29].

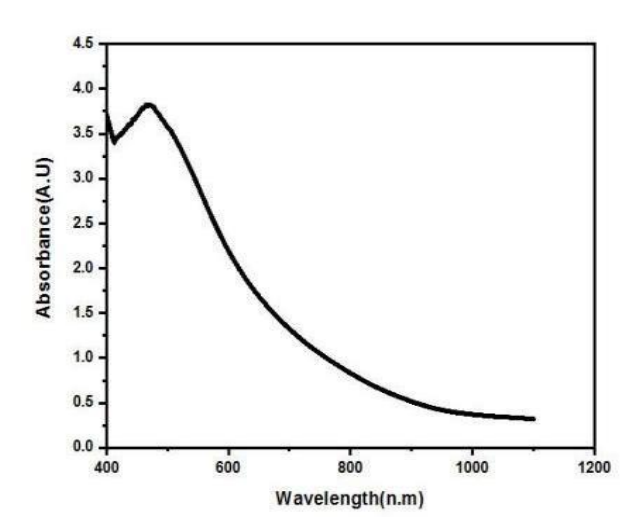


Fig 8.2. Absorbance spectra of SnSSe thin films deposited at 325  $^{\circ}$ C

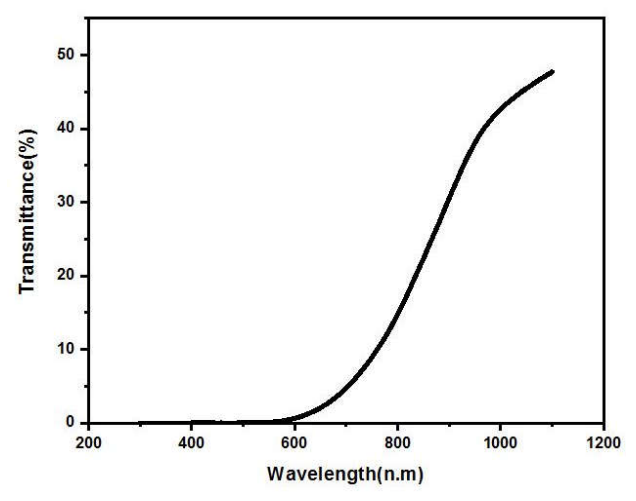


Fig 8.3. Transmittance spectra on SnSSe thin films deposited at 325  $^{\circ}\text{C}$ 

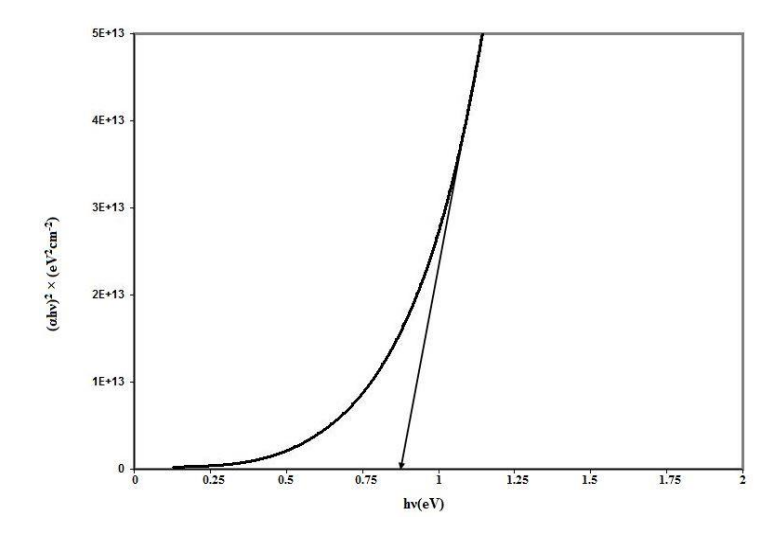


Fig 8.4 Band gap of SnSSe thin films deposited at 325  $^{\circ}$ C

## **8.3.3** Electrical Properties

The electrical properties of SnSe films deposited by flash evaporation on glass, mica and KCL substrates are reported [21]. The films deposited at KCL substrates showed a lower resistivity than those deposited on glass and mica substrates. The films were found to be ptype in nature. Single crystals of SnSSe were used for hall voltage and resistivity measurements according to vander pauws method [22]. Good electrical contacts were obtained using silver paint or by welding 100 micro gold wires to the samples. The SnSSe thin films prepared by spray pyrolysis were p-type with a free hole concentration at 325 °C will be 80  $\Omega$ cm, 59 cm<sup>2</sup>V<sup>-1</sup>s<sup>-1</sup> and 9.5 ×10 <sup>16</sup> c m<sup>-3</sup>. Hot probe measurements indicated that the films are p-type with a free hole concentration between 10<sup>17</sup> and 5 ×10 <sup>18</sup> cm<sup>-3</sup>. The temperature dependence of the hole mobility measured on the cleavage plates of SnSSe showed that at high impurity concentrations, the mobility was observed to decrease drastically at low temperatures.

## **8.3.4** Photo Sensing Performance

When light radiations incident on the semiconducting sample, excess electron hole pairs are created in semiconducting materials, thereby results in increase in conductivity. This gives important applicability to the material as sensors of radiations. During present investigation, the samples were illuminated by 100W tungsten filament lamp as source of light. Incident from 12 cm distance from as deposited SnSe thin films and the photosensitivity was measured by the equation as shown below:

Photosensitivity 
$$(P_s) = \frac{I_{illu \min ated}}{I_{dark}}$$
 ...(8.2)

Intensity of the light radiation was varied by dimmerstat. The observations were taken for the intensity of light radiations at 60 V a. c. to 230 V a. c. mains by the step of 10

V a. c. customized the photo sensing performance of the thin films by arranging the unimolecular layers of nanostructured materials.

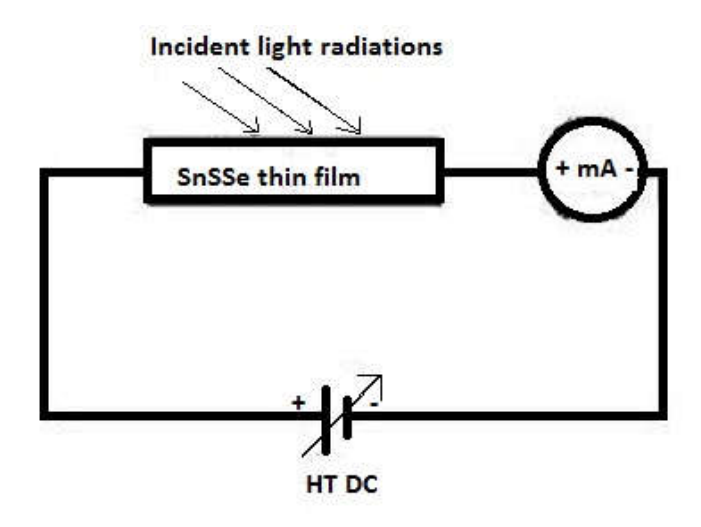


Fig 8.5 Experimental setup of measurement of photosensitivity.

The photosensitivity performance of the SnSSe thin film was observed to be maximum, at the 150 Vdc across the film. There are imperfections created in the SnSSe thin film structure. These imperfections associated with the incorporation of atoms of elements other than the host elements can be termed as impurity imperfections or simply impurities. The imperfections associated with structural deviations from atomic arrangement in the compositions create defects in the semiconducting materials sample. This defect category of the imperfections includes vacancies, interstitial atoms, dislocations, etc. there is increasing experimental evidence that similar electronic defects can be caused by both impurities and defects [9,10].

Optical excitation and PL emission spectra under 389 nm excitation of thin film recorded at room temperature and indicated in figure 8.7. Figure shows that there intense band in green region at 521 nm and less intense in blue region at 485 nm. This is in close agreement of the work of J. P. Singh *et. al.* [34] Figure showing the large stokes shift between optical absorption spectrum and Pl emission band may be attributed to presence of

one deep trapping site and electron hole recombination via trap state or imperfection site (12) Such lattice phenomena is observed in nanomaterials, This predicts the spray deposited SnSSe thin film in present investigation is nanocrystalline thin film. It is also reported that in nanocrystalline thin films, the deep states are mainly associated with stiochiometric defects or presence of external atoms like oxygen [35]

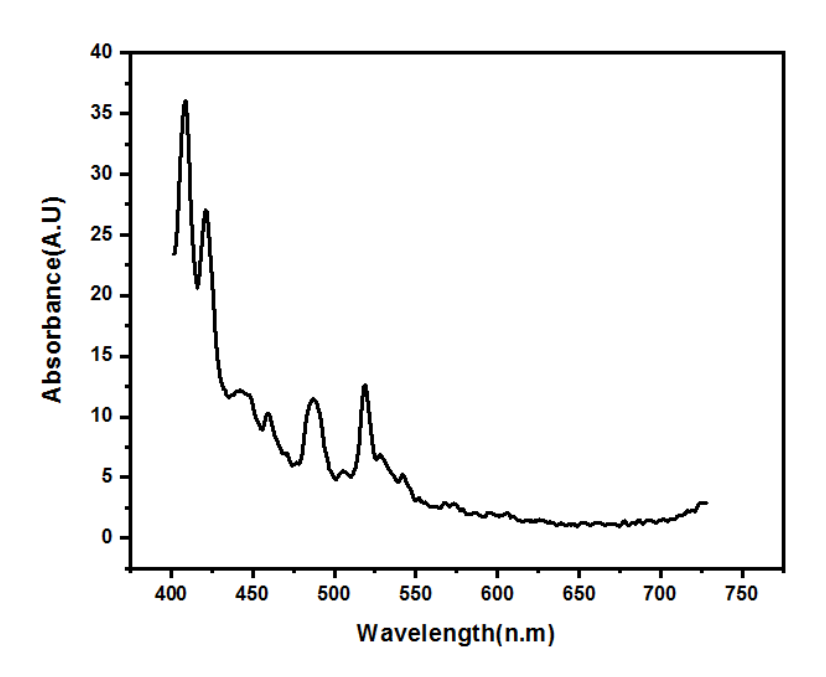


Fig 8.6 Photoluminescence of SnSSe thin films deposited at 325 °C

SnSSe thin film indicate that photoresponse of the sample which increases gradually with a. c. voltage, (intensity of light radiation) may be attributed to knocking of charge carriers from the base materials, releasing them from the bulk of the materials and makes available the charge carriers to carry the current independently, which causes to enhance the conductivity of the films. Initially, the sensitivity was observed to increase by negligibly small amount and then slowly and thereafter the sensitivity increases suddenly with intensity of light radiations. This may be attributed to the creation of EHPs by light agitation. This increases the carrier concentration in the material, which helps in carrying the current, which constitutes the rise of sensitivity.

Photo sensing performance of the SnSe thin films shows enhanced photo sensing properties and we can tailor any value of photo sensing property from this material for desired intensity of light. Photo luminescent spectra show the major peak at 485.44 and 511.16, which are in close agreement of the reported peaks of 485nm and 521nm. [14] This indicates that the material has good photo luminescent properties and thus the as formed material is good for phosphor applications.

## 8.4 CONCLUSION

Tin sulpho selenide (SnSSe) thin films were prepared by chemical spray pyrolysis technique using precursor Stannous chloride, Thiourea and Selenourea for deposition kept at optimized temperature 325 °C. X-ray diffraction studies show that the films are polycrystalline in nature with orthorhombic crystal structure. Crystallite size of the film was found to be 292 nm.SEM micrographs revealed larger spherical grains with stochiometric value. Optical absorption study reveals a band gap of 0.9 eV. Photo sensing properties of the SnSSe thin films indicates the response of the synthesized material to the incident radiations for equal concentration of sulphur and selenium. A Photoluminescence spectrum shows the peaks in the close agreement of the reported values of SnSSe material. Thus SnSSe would very useful for the fabrication of solar cells and phosphor material.

## **REFERENCES**

- [1] H Tributsch, Proceeding, Indian Acad Science, Chem sci, 105, (1993), 305 Jaspart Singh, Semiconductor Optoelectronic Devices; Physics and Technology, (1995)
- [2] E S Sabisky, Solar energy materials Solar cells, (1995).
- [3] H J Hovel, Semiconductors and semi metals, New York (1975).
- [4] P A Lee, G Said, R Davis and T H Lim, J Phys Chem Solids, 30(1969) 2719.
- [5] D I Bletskan, I F Kopinets, P P Pogorsh, E N Salkova and D V Chepor Kristallographia, 20 (1978) 1008.
- [6] V P Bhatt, K Ganesan and F M Desai, Crys Res Technol, 24 (1989) 187.
- [7] M F Ladd and R A Palmer, Structure determination of X-ray Crystallography. Plenum Press, New york (1964) 71.
- [8] H E Bennet and J M Bennet in G Hass and E Thund (Eds), Physics of Thin Films Vol 4, Academic press, New York (1967).
- [9] D Bhattacharya, S Chaudhari, A K Patel and S K Bhattacharya, Vacuum, 42, (1991) 1113.
- [10] W Albers, C Haas, H Ober, G R Schodder and J D Wascher, J Phys Chem Solids, 23 (1962), 215.
- [11] R W G Wycoff, Crystal Structure, Wiley New York, (1963). B Subramanian, C Sanjeeviraja and M Jayachandran, J Crystal Growth, 234, (2002)421-426,.
- [12] B Subramanian, C Sanjeeviraja, T Mahalingam and Mary Juliana Chokalingam, Thin Solid Films, 357, (1969), 119.
- [13] F Huiller, Structural chemistry of layer type phases in (eds), F Ley, D ReichelDordrecht Holland (1976).
- [14] B Foutachi, A Katty and O Gorochov, *Journal of Electrochem society*, 132, (1985) 2181.
- [15] R D Engelkan and McCloud, Bulletin of American Chemical Society 29, (1984), 2806.
- [16] O H Hausser, H Von Kanel and F Levy, *Journal of Electro Chem Society*, 183, (1985), 810.

- [17] B Foutachi, A Katty and O Gorochov, *Journal of Electro Chem Soc*, 131 (1984) 2806.
- [18] B Foutachi, A Katty and O Parsons, Journal of Electro Chem Soc, 183 (1985),303.
- [19] S Adachi and T Taguchi Physics Rev B 43, (1991) 9569.
- [20] B Subramanian, C Sanjeeviraja, M Jayachandran, S Mohan and Mary Juliana Chokalingam, Proc SPIE International Symposium on Photonics and Applications(ISPA) vol 3896, (1999) 398.
- [21] S G Patel, S K Arora, R G Patel, Ajay Agarwal, Thin Film chracterization and Applications, Proceedings of National conference, S A K Narayanadas. (1996).
- [22] R D Engelkan, H E McClaud, C Lee, M S layton and A Goreishi, Journal of Electroc Chem Soc, 134, (1987), 2696. J P Singh and R K Bedi Thin Solid Films (1991)
- [23] P Ambros, D Geralaes, N A Economon, Phy Chem Solids, (1974) 537.
- [24] M Nikolic, S S Vijitovic, O H Hughes, C J Stran and J M Chamberlain, Proceedings of the International conference in Physics and Semiconductors (1974).
- [25] W. Albers, C. Hass, H. Ober, G.R. Schrodder, Journal of Phys Chem Solids 23 (1962), 215
- [26] V.P. Bhatt, K. Ganesan, G.R. Pandya, Journal of Crystal growth 96, (1989), 649.
- [27] A M. Elkorashy, *Journal of Phys Chem Solids*, 47, (1986), 497.
- [28] A W Park, G P Srivatsava, Phys Status Soilidi B 101, (1980).
- [29] J C Yu , A S Yue, O M Staffsud, Journal of Crys Growth 54, (1981), 248.
- [30] J P singh and R K Bedi, Journal of Applied physics 29(1990) 869.
- [31] J Reichmann and M A Russake, Photo effects of Semiconductor interface, 146, (1981)359.

## CHAPTER – IX

## **SUMMARY AND CONCLUSIONS**

The significance of energy crisis, solar energy conversion, need of low-cost photovoltaic technology, the special features and different of types of photovoltaic cells such as silicon solar cells, thin film chalcogenide solar cells particularly CIGS solar cells and nano photovoltaic solar cells were discussed and presented. With suitable data and relevant references, it has been recognized that the main focus of the departments of research and development of photovoltaic industries is the realization of cost reduction for the utilization of photovoltaic energy. The fabrication of low cost PV materials with thin film geometry is the requirement for economic solar cells. The characteristics of metal chalcogenide thin films as an absorbing material or buffer layer - one of the key element of solar cells had been discussed in detail. In particular, a review of SnS and SnSe thin films has been presented. Then, scope and social relevance of the present work have been given in brief.

A simplified nebulized spray pyrolysis system attached with nebulizer which is particularly used for providing treatment of asthma patients, replacing spray gun assembly in the spray pyrolysis technique has been indigenously designed and fabricated with the help of which, SnS and SnSe thin films have been deposited after optimizing the parameters such as substrate temperature, precursor concentration, volume of solution, nozzle to substrate distance, spray rate etc. The structural, electrical, optical, surface morphological and elemental properties have been studied using various characterization techniques and the obtained results are discussed with the help of appropriate references.

Thin films of SnS with crystallites of nano dimensions had been deposited on to glass substrates by nebulized spray pyrolysis technique at different substrate temperatures. Polycrystalline nature of the film with orthorhombic structure grown with high preferential orientation along (111) Miller plane with low strain is identified. All the SnS thin films were deposited in the thickness range of 375-1038 nm and are found to exhibit p-type electrical conduction. A thermal activation process with an activation energy is determined with respect to the substrate temperature. The optical transparency was increased up to 55% with the rise in substrate temperatures. The structural, optical, morphological and electrical studies of tin sulfide thin films confirmed that the optimum substrate temperature for preparing SnS thin film by this technique is 325 °C. They were deposited with different precursor concentration at the optimized substrate temperature. The variation in grain size and energy gap by increasing precursor concentration made the samples as a favourable candidate for the applications of solar cells. The high transmittance in the visible region observed at lower precursor concentrations, represented the good optical quality of thin film with the low absorption or scattering losses which may lead to the applications particularly as an absorber layer in solar cells. The optimized value of precursor concentration was found using different characterizing techniques as 0.2 M. Such SnS thin films prepared with these optimized conditions could be a potential candidate for opto-electronic devices, particularly for solar cell device as an absorbing material.

SnSe thin films were deposited at different substrate temperatures using the NSP technique with other constant preparative parameters. Polycrystalline nature of as-deposited SnSe thin films was confirmed with standard orthorhombic structure from X-ray diffraction studies. The optical studies indicated that films posses direct band gaps. The high transmittance in the visible region observed at different substrate temperature symbolished the good optical quality of the crystals with the low absorption or scattering losses which

results to the applications particularly as an absorber layer in solar cells. Electrical studies showed that the films are p-type semiconducting material which may be used in optoelectronic devices. The optimized substrate temperature was confirmed at 300 °C by using all characterization results.

The influence of precursor concentration on various properties of nebulized spray pyrolysised SnSe thin films were studied in detail. X-ray diffraction (XRD) pattern confirmed SnSe thin film with orthorhombic structure. The optical parameters such as direct band gap energy had been discussed in detail. Electrical conductivity studies showed the semiconductor nature of the film with p-type conductivity. This nebulized spray pyrolysised SnSe thin film is found to have a direct allowed transition with a band gap of  $E_g = 1.05 \text{ eV}$  at 0.150 M. The mentioned optimum band gap and resistivity studies suggest that the polycrystalline SnSe thin films prepared in the present work under the optimized conditions could be used as a promising semiconductor materials in the development of low cost and efficient thin film solar cell devices. The investigation results of SnSe thin films deposited by nebulized spray pyrolysis technique ensure the stability of the film and their employability in solar cell application.

## **Future scope**

Natural progression of present research would be its application in solar cell fabrication. Fabricating a solar cell using tin sulfide, indium sulphide and tin selenide thin films as an absorbing material or buffer layer of solar cells can be the direction of future research. IV–VI semiconductors are already used in solar photovoltaic converters, providing a high absorption coefficient in the visible and near infra red spectral range and, because of that, a smaller quantity of material is needed for complete absorption of solar radiation, thus leading to a smaller cost. The involvement in this material is stimulated owing to its applications in optoelectronic devices as a buffer layer in photovoltaic structures and as an

absorber layer in nanostructured solar cells. In solar cell technology indium sulphide has been identified as a desirable alternative to cadmium sulphide (CdS) buffer layer in thin film solar cells. The wide band gap photosensitive material developed can be optimized for its potential application in Se through PV modules. The simplicity of the process is quite admirable and this can be utilized in producing absorbing material in fabricating a solar cell. This has opened up a new avenue of cell fabrication that has to be further optimized for optimal performance. Fine adjustments in the thickness of layers, adding dopants and substrate temperatures may result in better efficiency of the cell. In addition to the cost benefits, the proposed metal chalcogenide thin films using nebulized spray pyrolysis technique such as SnS and SnSe thin films may improve the efficiency of the PV cells over 20 percent.

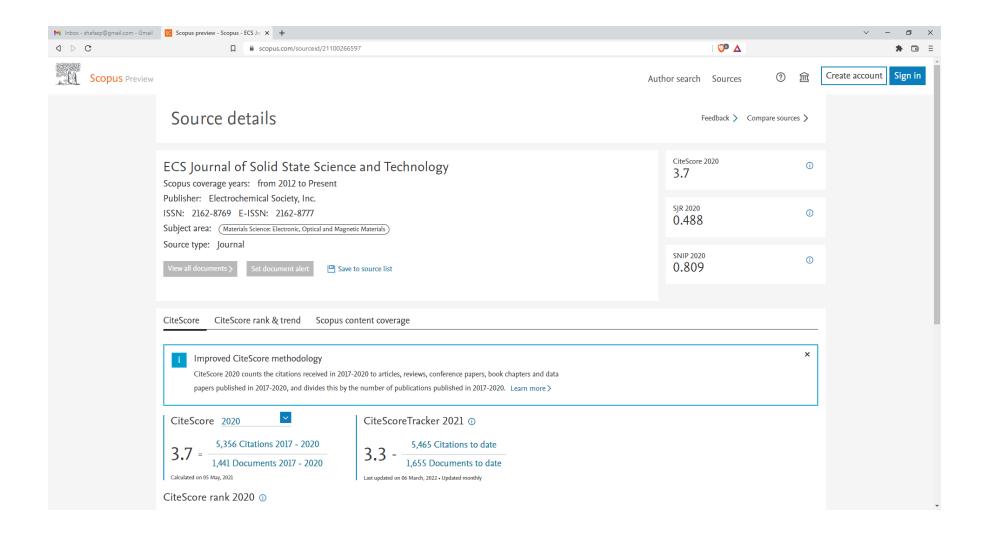
## LIST OF PAPERS PRESENTED IN CONFERENCES

NATIONAL CONFERENCES : 03

INTERNATIONAL CONFERENCES : 03

## PARTICIPATION IN WORKSHOP / CONFERENCES

- Presented a Paper on SnS Thin Films Prepared By Chemical Spray Pyrolysis At
  Different Substrate Temperatures for Photovoltaic Application in International
  conference ICRAM15 conducted by Anna university of Technology, Trichy.
- 2. Presented a paper and published in an International Conference Proceeding entitled "Preparation and Characterisation of SnS thin films by Chemical spray pyrolysis technique, ICRAM 17, August 31, Urumu Dhanalakshmi College, Trichy.
- 3. Poster Presentation entitled Tin sulphide (SnS) Thin Films with Different [S]/[Sn] Ratios Prepared by Chemical Spray Pyrolysis Technique, ICRAM 18,KSR college of Arts and science, Tiruchengode.
- 4. Presented a paper entitled Effect of Substrate temperatures of spray deposited Tin Selenide thin films by Spray Pyrolysis technique, National conference in National college, Trichy on Feb 2019.
- Presented a paper entitled "Effect of Precursor Concentration on Physical Properties
  of Nebulized Spray Deposited Tin Selenide Thin Films, AVVM Sri Poondi
  pushpam college, National conference in Sep 2019.
- 6. Presented a paper on" Effect of precursor solution volume of Sprayed SnSe thin films for photovoltaic applications" in National conference at Urumu Dhanalakshmi college, Trichy on February 2020.







# Influence of Substrate Temperature on Physical Properties of Nebulized Spray Deposited SnSe Thin Films

A. Anitha Ezhil Mangaiyar Karasi, 1,2,2 S. Seshadri, L. Amalraj, and R. Sambasivam

<sup>1</sup>Department of Physics, Shrimati Indira Gandhi College, Trichy, India

<sup>2</sup>PG & Research Department of Physics, Urumu Dhanalakshmi College, Trichy, India

<sup>3</sup>Research Department of Physics, VHNSN College, Virudhunagar, India

Tin-based binary chalcogenide semiconductors SnSe and SnS have created increased interest in the production of earth-abundant and eco-friendly thin film solar cells. Thin films of SnSe were prepared on glass substrates at different temperatures via a nebulized spray pyrolysis technique using Stannous chlroride dihydrate and Se powder. Deposited films were characterized by structural, morphological, compositional, optical, and electrical properties. X-ray diffraction studies confirm the films are of polycrystalline orthorhombic crystal structure irrespective of substrate temperature. Scanning electron microscopy studies revealed uniform deposition with nanometer range grain size. Stoichiometric films of SnSe were observed from energy dispersive analysis by X-ray studies. UV–vis spectroscopy confirmed the formation of good adherence thin films with an average transmittance of  $\sim$ 70% in the visible region. Optical band gap was in the range of 1.14–1.24. The lower absorption and high transmittance in the visible region observed at lower substrate temperature represented the good optical quality of the crystals with low absorption or scattering losses. The lower electrical resistivity value of 4.84  $\Omega$ cm showed that the films are semiconducting. The structural, optical, morphological, and electrical conductivity studies of tin selenide thin films confirmed that the optimum substrate temperatures for depositing SnSe thin films by this NSP technique is 300°.

© 2021 The Electrochemical Society ("ECS"). Published on behalf of ECS by IOP Publishing Limited. [DOI: 10.1149/2162-8777/ac1e6b]

Manuscript submitted July 4, 2021; revised manuscript received August 7, 2021. Published August 30, 2021.

In this scenario, tin-based binary semiconductors such as SnS and SnSe are expected to a play a crucial role in replacing toxicating cadmium compounds and scarced elements based CIGS absorbers in photo-voltaic devices. They are relatively earth abundant, non-toxic nature and easy controllability of stoichiometric. Moreover, the annual production of tin, sulphur, and selenium is large (low-price) as compared to other absorber elements. These materials exhibit favourable properties such as high chemical stability, suitable band gap (1.0 eV to 1.5 eV) and high absorption co-efficient ( $\sim\!10^5~{\rm cm}^{-1}$ ) with P-type conductivity. On the other hand, the solar cells fabricated from SnSe thin films exhibited lower efficiencies ( $\leq\!1\%$  by non-vacuum methods and  $>\!5\%$  by vacuum methods) than CIGS and CZTS solar cells.

In recent past, more importance has been committed in the field of IV-VI class of semiconducting compounds on account of their optoelectronic properties and applications. 1-5 Tin Selenide (SnSe) is a narrow band gap, binary IV-VI semiconductor, suitable for various optoelectronic applications like memory switching devices, photovoltaic, light emitting devices (LED), and holographic recording systems. 6-8 Because of their anisotropic character, the tin chalcogenides are attractive layered compounds, and can be used as cathode materials in lithium intercalation batteries<sup>9</sup> and decreasing the photo corrosion reaction. 10 Considerable attention has been devoted by various authors to the preparation of SnSe thin films bely different methods like vacuum evaporation, <sup>11–21</sup> flash evaporation, <sup>22</sup> hot wall epitaxy, <sup>23,24</sup> reactive evaporation, <sup>25</sup> electrodeposition, <sup>26–29</sup> laser ablation, <sup>30,31</sup> brush plating, <sup>32</sup> chemical bath deposition (CBD),<sup>33</sup> electrochemical atomic layer epitaxy (ECALE)<sup>34</sup> and spray pyrolysis<sup>35,36</sup> to study various physical properties. Among these methods, although high quality and uniform films are prepared by physical technique, they are comparably costly and highly energy consuming. Nebulized spray pyrolysis is a simple, versatile, inexpensive, time saving and efficient way of growing thin films at room atmosphere. This technique can be scalable to larger area deposition. The nebulized spray pyrolysis technique (NSP) has been widely used to deposit binary and ternary oxide thin films such as MgO,<sup>37</sup> tin doped zinc oxide,<sup>38</sup> Cd-doped SnO<sub>2</sub>,<sup>39</sup> Gd<sub>x</sub>Zn<sub>1-x</sub>O,<sup>40</sup> and Na-doped ZnO.41 Xiaorong et al.37 reported that this technique has advantages like the simplicity of the apparatus and low price of raw materials. E. E. Ebsenso et al. 42 had reported deposition of a quaternary oxide,  $Ln_{1-x}Sr_xCoO_3$  (Ln=La, Nd, and Gd) and ternary oxide,  $SrRuO_3$  thin films by nebulized spray pyrolysis technique. It was observed that the film prepared by this technique exhibits low resistivity than other techniques which can be exploited for use as electrodes in several situations. SnSe Thin films were not deposited previously by NSP technique.

In this work, an attempt was made to deposit SnSe thin films by simple nebulized spray pyrolysis technique. The observations of this study reveal that SnSe thin films have good semiconducting nature and seem to be a promising candidate for solar cell applications. The structural, morphological, compositional, optical and electrical properties of the films were investigated and analyzed.

#### **Experimental Technique**

The problems associated with solution-based methods can be addressed to some extent by using fabrication technique based on nebulized spray pyrolysis technique of thin films. In the following section, we will discuss in detail of material and methods used for preparing SnSe thin films and the characterizing techniques for analyzing the SnSe thin films.

Materials and methods.—SnSe thin films were deposited on glass substrate by spraying an aqueous solution containing 0.1 M of SnCl<sub>2</sub> (Sigma-Aldridge) and Se powder (Himedia) with nebulized spray technique. Substrate cleaning plays an important role in the deposition of thin films. The contamination of the substrate surface may cause nucleation sites facilitating the growth, which results in non-uniform film growth. Hence, the micro glass substrates of dimensions  $7.5 \times 2.5 \times 0.25$  cm<sup>3</sup> were first washed well with detergent. The washed glass slides were put in hot chromic acid for 1 h to remove grease or oil. Then, they were rinsed with acetone and double distilled water before the deposition of the films. In this study, different substrate temperatures (T<sub>s</sub>) were used for thin film deposition. The air as carrier gas, flow rate was kept at1 kg cmcorresponding to an average pressure solution rate of 5 ml per 15 min. The volume of solution was taken as 10 ml per substrate. Films are very shiny and color in blackish gray. All the films were kept on the hot plate until the substrate temperature is reached to room temperature and then preserved them in sealable pockets.

Characterization technique.—The chemical and structural phases of the SnSe films were determined by X-Pert Pro X-ray

diffractometer (CuK<sub> $\alpha$ </sub>,  $\lambda = 1.5418 \,\text{Å}$ ) over a  $2\theta$  range of  $10^{\circ}$ – $70^{\circ}$ . The optical properties using optical absorption spectrum were measured using UV-vis-NIR double beam spectrophotometer (HITACHI U3410 model) over the wavelength range 300-1100 nm. Scanning electron microscope (SEM) was used to detect the dispersion of particles, rough morphology and the particle size on the surface of the film. The surface morphology of the as-deposited SnSe films was examined by scanning electron microscope (SEM, GENESIS model). The chemical composition of Sn and Se was determined by energy dispersive analysis by X-rays (EDAX) on K and L lines. The electrical conductivity of the as-deposited films was determined by Hall Effect measurement system by ECOPIA-HMS 5000 model. The thickness of the SnSe layers was found with a stylus profile meter (MITUTOYO, SJ-301). The variation of electrical conductivity with temperature was studied from 313 to 388 K the four-probe technique with Keithley 2000 electrometer.

Results and Discussion .- To study the impact of substrate temperature on the physical properties while adopting the NSP technique, the following procedure was followed. The well established scratch test using a hemispherical diamonded stylus, loaded tangentially to the plane of the surface which offers a high degree of reproducibility at the expense of information about the adherent quality of the film. The deposited SnSe thin films visually found to be blackish gray in color with good adhesion to the substrate at high temperature. The color of the thin film deposited at the substrate temperature of 250 °C was the gray color with less adhesion to the substrate. The adherence of the films increased with the increase of substrate temperature. Thin films at 275, 300 and 325 °C were good adherence and blackish gray in color. Thickness of the tin selenide thin films were determined using stylus profiliometer by measuring the step height between the film and the substrate and the thickness values were determined as 264, 382, 456 and 634 nm for the samples prepared with the different substrate temperature of 250, 275, 300 and 325 °C respectively (Table II).

Structural properties on SnSe thin films.—Figure 1 shows the X-ray diffraction pattern of nebulized spray deposited SnSe thin films at different substrate temperatures. As seen, the obtained diffraction patterns show a predominant peak at  $2\theta = 30.47^{\circ}$  which can be assigned to the (111) plane of orthorhombic SnSe of 250 °C. With the increase of substrate temperature up to 300 °C there is an increase in intensity and sharpening of this peak, which is caused by improving crystallinity of the films. From the Fig. 1 SnSe films exhibit also two diffraction peaks at 37.77, 49.72° they are assigned to the (311), (511) reflections planes in the SnSe orthorhombic structure of substrate temperature 250 °C-325 °C. Electron diffraction patterns with the standard JCPDS card No 48-1224 value shows a close agreement with the reported results in the literature. As seen in Fig. 1, the XRD pattern of prepared SnSe film at  $T_s = 225$  °C indicated that it is amorphous in nature. The existing amorphous nature is due to the insufficient energy at low temperature to convert the amorphous tin layers into polycrystalline films. This intimates that the as-deposited SnSe films are formed with small crystallites embedded in an amorphous tissue. At the substrate temperature of 250 and 275 °C, the diffraction peaks at 13.01° and 52.30° corresponding to SnSe2 was observed along with the peaks of SnSe. It is also noticed from Fig. 1 that intensity of SnSe films along (111) plane is increased with increase in substrate temperature up to 300 °C, after reaching a maximum at  $T_s = 325$  °C it starts to decrease and there is small peaks at 14.42 and 41.51° that indicated the formation of SnO<sub>2</sub>. The film prepared at 300 °C has a better crystalline quality of SnSe in mono-phase as indicated from XRD pattern. Singh et al.<sup>23</sup> and Kumar et al.<sup>43</sup> had obtained orthorhombic structured crystallites for their SnSe thin films prepared using hot wall epitaxy and thermal evaporation methods respectively.

Crystalline size is estimated by using Scherrer's formula given by equation  $^{44}$ 

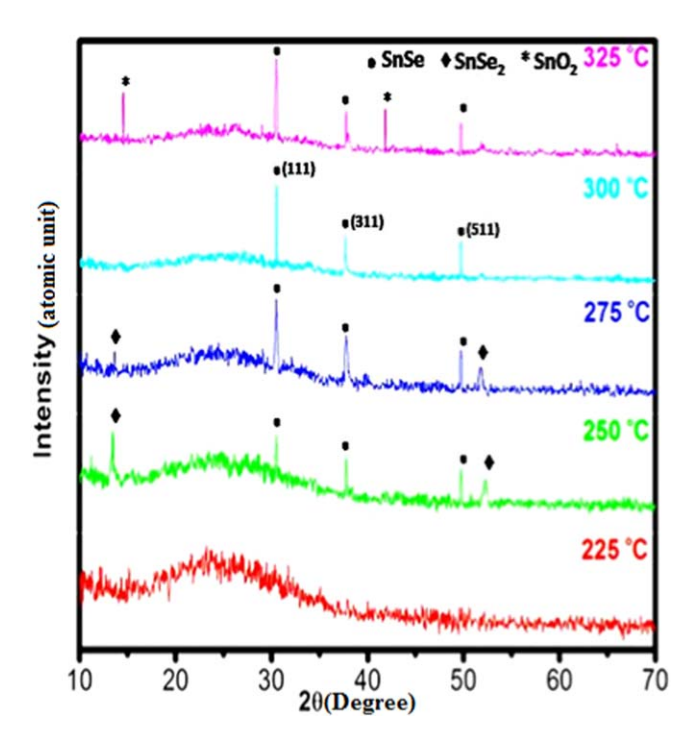


Figure 1. X-ray diffraction pattern of SnSe thin films deposited for different substrate temperature.

$$D = \frac{k\lambda}{\beta\cos\theta}.$$
 [1]

Where D is the mean crystalline size, k is the shape factor value 0.94,  $\lambda$  is the wavelength of an X-ray used (CuK $_{\alpha}$  radiation),  $\beta$  is the Full Width Half Maximum in radians and  $\theta$  is the Bragg's angle.

It is observed that crystalline size increases initially with the increase in substrate temperature attains the maximum of 55 nm at 300 °C and henceforth it goes on decreasing with the increase in substrate temperature. Increase in crystallinity and crystalline size with substrate temperature is owing to the optimum rate of supply of thermal energy for recrystallization with substrate temperature. From particle size analysis it is clear that the films are nanocrystalline in nature.

The lattice strain  $(\varepsilon_{\rm s})$  of all the films was determined using the formula

$$\varepsilon_s = \frac{\beta \cos \theta}{4}.$$
 [2]

The dislocation density  $(\delta)$  is defined as length of fracture lines per unit volume of the crystal using crystallite size values (D) has been determined using the Williamson and Smallman's formula<sup>46</sup>

$$\beta_{hkl}\cos\theta = \frac{k\lambda}{D} + 4\varepsilon\sin\theta.$$
 [3]

and the number of crystallites per unit area can be calculated by the equation

$$N = \frac{t}{D^3}.$$
 [4]

Table I exhibits the full width at half maximum (FWHM) value, crystallite size and micro strain of the different (hk)l planes of SnSe thin films at different substrate temperatures from 250 to 325 °C. At lower substrate temperature, the crystallite size is low since the deposited atoms in lieu of incorporating to the neighbouring crystallites and increasing their size are condensed and stay stuck

Table I. Structural parameters of SnSe thin films at different substrate temperatures.

$T_S$ (°C)	hkl	FWHM $\beta$ (degree)	Crystalline size (nm)	Strain ×10 <sup>-3</sup>
250	(111)	0.197	41	8.28
230	(311)	0.310	25	13.51
	(511)	0.525	15	
275	(111)	00.195	42	8.21
	(311)	0.285	27	12.42
	(511)	0.410	20	17.22
300	(111)	0.148	55	6.21
	(311)	0.149	53	6.45
	(511)	0.190	43	7.98
325	(111)	0.236	34	9.94
	(311)	0.245	32	10.68
	(511)	0.275	30	11.55

to the region to form small nuclei and clusters. At higher substrate temperature  $T_s = 300$  °C, a large crystallite size is ascertained due to the increasing mobility of the surface of atoms and increasing cluster formation. It is observed that the crystallite size increases and attains a maximum 55 nm at 300 °C. Mariappan et al. obtained orthorhombic structured crystallite size of 39 to 66 nm for their SnSe thin films prepared using spray pyrolysis technique. Figure 2 shows the variation of average crystallite size value with different substrate temperature was calculated for all the samples found to be increased from 27 to 51 nm. The decrease in lattice strain was observed by increasing the substrate temperature. Indeed, the strain in the films is tensile at the initial stage of SnSe films formation and tends to the compression and lattice strain of the films prepared at the terminal stage. The minimum value of dislocation density is obtained for the film grown at the substrate temperature 300 °C. The dislocation density of as prepared SnSe films decreased as the substrate temperature increased. The change in crystallite size with substrate temperature explained this behaviour. Indeed, the larger crystallites have a smaller surface to volume ratio, thus giving up a rise to the dislocation network.

Table II expresses the change in texture coefficient, dislocation density and number of crystallites of SnSe thin films at different temperatures from 250 °C to 325 °C. From Table II, it is observed that dislocation density and number of crystallites exhibit higher value at 250 °C and the further increase of temperature decrease the values. This ensures the increase in the volume fraction of its crystallized phase.

Analysis of surface morphology of SnSe thin films.—The surface morphology of the SnSe thin films deposited at different substrate temperatures was respectively as shown in Fig. 3. These SEM pictures were recorded with the same magnification of  $100000 \times \text{for}$ comparison. It is observed that the surfaces of the films are found to be uniform and homogeneous. As it can be seen, the surface of the as-deposited SnSe thin film grown at  $T_s = 250$  °C was found to be little circular grains gradually spread along horizontal of the substrate. The average grain size of these films is approximately 60-170 nm. With the increase in the substrate temperature up to 300 °C, the SnSe film grows mature to form uniform over-grained morphology composed of nano circular shaped grains. These circular grains change into the small circular grains when the substrate temperature was increased further to 325 °C which is evidenced by the coincidence of nano-circular grains shown in Fig. 3. Similar spherical-shaped grains for SnS films were observed by Zainal et al. in the chemical bath deposition method.<sup>33</sup>

Compositional analysis of SnSe thin films.—The purity and the specific composition of the as-deposited SnSe thin films were determined by EDX study, which exposed the presence of Sn and

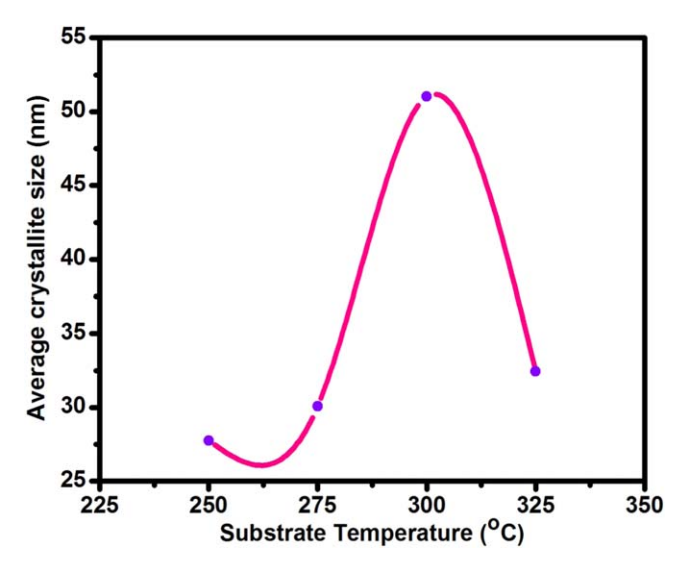


**Figure 2.** Variation of average crystallite size as a function of temperatures.

Se as elementary components. The typical EDX spectra of SnSe thin films are shown in Fig. 4. The numerical atomic percentage of the compositional elements such as Sn and Se present in SnSe thin films are given as inset of Fig. 4. Two different peaks related to Sn and Se are found in the SnSe spectrum, which supports the SnSe thin film. The EDX analysis affirms their nominal percentage and chemical purity of system. Initially, the as-deposited SnSe thin film is selenium rich but increase in substrate temperature to SnSe thin film show increase in the percentage of tin in order to reach the stoichiometric ratio of 1:1. The quantitative weight percentage of the compositional elements such as Sn and Se from  $T_s = 250$  to 325 °C are listed in Table III. The atomic percentage of tin is increased from 47.43 to 52.52 by increasing the substrate temperature from 250 to 300 °C and then it decreased to 47.24 at the substrate temperature 325 °C. EDX spectrum exhibits that the weight percentage is closely equal to their nominal stoichiometry within the experimental error. Engelken et al.<sup>47</sup> and Fernandez et al.<sup>48</sup> had also reported similar findings with ZnSe and Sb<sub>2</sub>Se<sub>3</sub> films. On increasing Ts at 325 °C, the peaks corresponding to selenium content in the film started decreasing (deficiency of selenium). This is probably due to re-evaporation of selenium owing to its high vapour pressure, leaving a tin riched surface reacts with oxygen to form SnO<sub>2</sub>.

A report on optical absorption analysis of SnSe thin films.—The optical transmittance spectra of SnSe thin films prepared at different substrate temperatures by nebulized spray pyrolysis technique, in the wavelength range of 300 nm-1100 nm are presented in Fig. 5. It is observed that the transmittance increases with gradual increase in wavelength (300-600 nm), which points better crystallinity of the films. A close observation designates that the transmittance gets down at lower wavelengths and slightly increases at higher wavelengths when increasing the substrate temperatures from 250 to 300 °C and decreasing at 325 °C as seen from Fig. 5. The film deposited at 250 °C has high transmittance. The detected changes in the transmission are owing to the thickness variation and the cardinal differences in the film absorption. The nature of this transmittance variation may be proposed as being eligible as a window material fabrication for solar cells. The optical absorption spectra of nebulized spray deposited SnSe thin films have been used to calculate the coefficient of absorption, optical band gap and the nature of transition concerned. The photon energy dependence of the absorption coefficient of SnSe films is shown in Fig. 6. It is established that high optical absorption coefficient ( $\alpha = 10^4 \text{ cm}^{-1}$ ) was ascertained for all the compositional parameters. The absorption through the film is comparatively high at higher wavelength region designating high concentration of defects and free carriers. The

Table II. Value of texture coefficient, dislocation density and number of crystallites for different temperatures from 250 °C to 325 °C.

T <sub>S</sub> (°C)	Texture coefficient	Dislocation Density $\times 10^{15}$ (Lines m <sup>-2</sup> )	No. of Crystallites $\times 10^{16} (m^2)$	Thickness (nm)
225	_	_	_	213
250	1.2528	0.8218	1.4936	264
275	1.0459	0.5705	0.7621	382
300	1.0365	0.5613	0.5079	456
325	1.3542	0.3209	0.3597	634

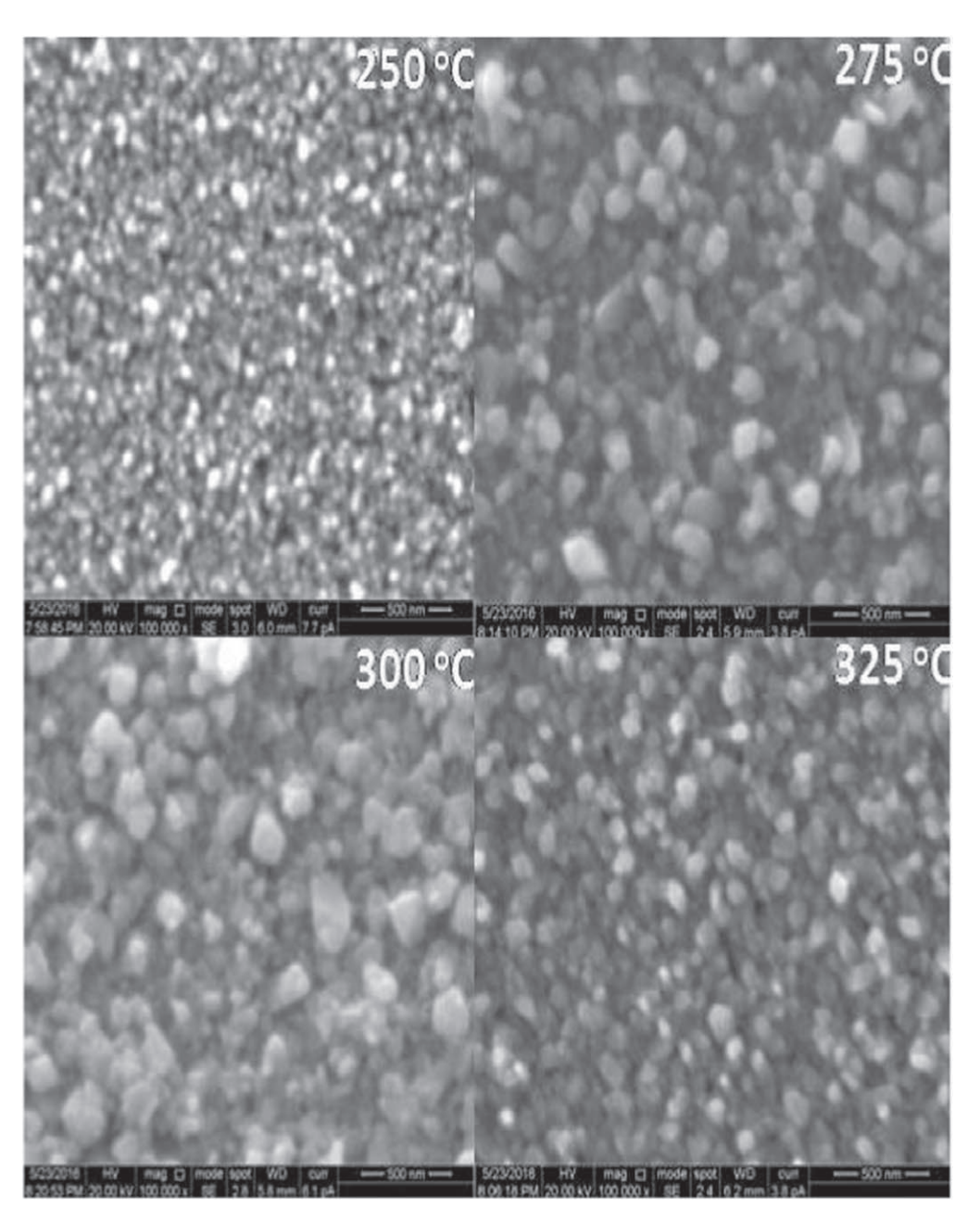


Figure 3. SEM photographs of the SnSe films deposited at different substrate temperature.

absorption reduces suddenly in the lower energy region at 325  $^{\circ}\mathrm{C}$  due to the formation of tin oxide.

The optical band gap of as-deposited SnSe thin films is calculated by employing the Tauc's model. For semiconductors,  $n=1/2,\,2,\,3/2,\,3$  values related to the allowed direct, allowed indirect, forbidden direct, and forbidden indirect transition only. Since n=1/2 and the

absorption coefficient is of the order of  $10^4\,\mathrm{cm}^{-1}$  sustains the direct band gap nature of SnSe semiconductor for allowed direct transition. The band gap of SnSe thin films was found for each film by plotting  $(\alpha h \nu)^2$  vs  $h \nu$  photon energy and then extrapolating to the linear portion to the energy basis at  $\alpha=0$ . The Tauc's plot is used to find the band gap of SnSe thin films as in Fig. 7.

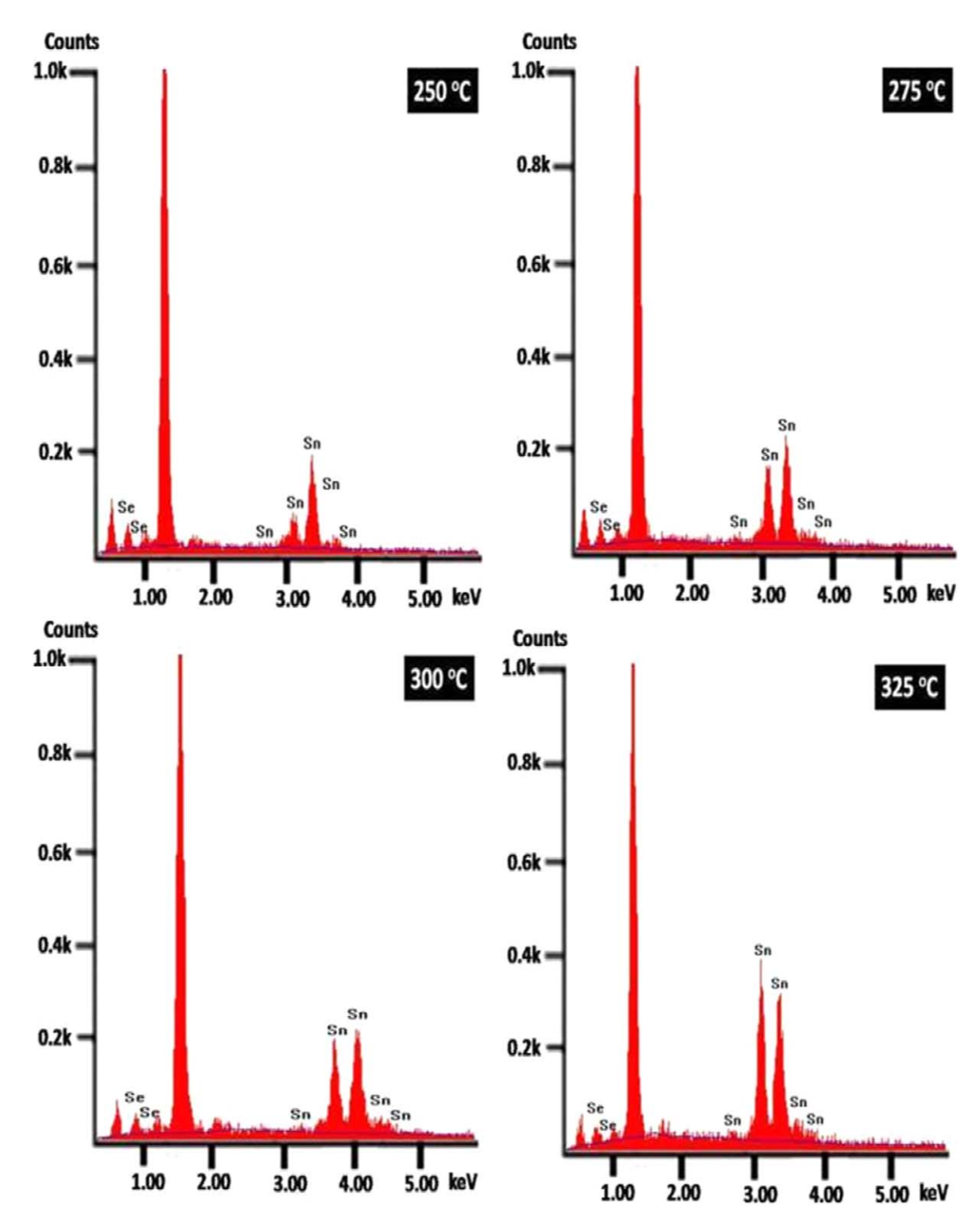


Figure 4. EDAX spectra of SnSe films prepared at different substrate temperature.

The direct optical band gaps of SnSe thin films was found to be decreased from 1.24, 1.19, 1.14 eV with the increase of substrate temperature from 250 to 300 °C and then increased to 1.22 eV with the further increase in the substrate temperature to 325 °C. The direct band gap values of SnSe thin films reported in the literature extend from 0.9 eV up to 1.3 eV. <sup>50</sup> The sharp augmentation (reduction) of energy band gap at higher substrate temperature could be due to the constitution of localized states in the band gap region and these states must be elicited in the band gap on account of the structural

disorder owing to the selenium deficiency. Thus the crystallinity of the polycrystalline SnSe films improves with increasing substrate temperature upto 300  $^{\circ}\text{C}.^{51}$ 

Photoluminescence studies on SnSe thin films.—The correlation between structure and property is investigated by PL spectra which originate from the recombination of the surface states.<sup>52</sup> The PL is one of the significant studies which can give us more important information on the crystal quality and purity of the material. The

Table III. Variation of elemental analysis of SnSe thin films at different substrate temperature.

Atomic percentage of the elements (%)

$T_S$ (°C)	Sn	Se	Sn/Se ratio
225	46.16	53.84	0.86
250	47.43	52.27	0.91
275	48.12	51.88	0.93
300	52.52	47.48	1.11
325	47.24	52.76	0.90

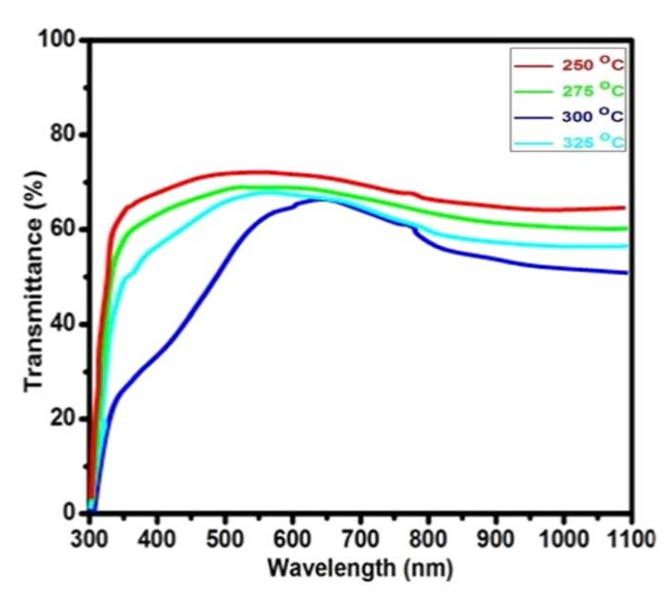
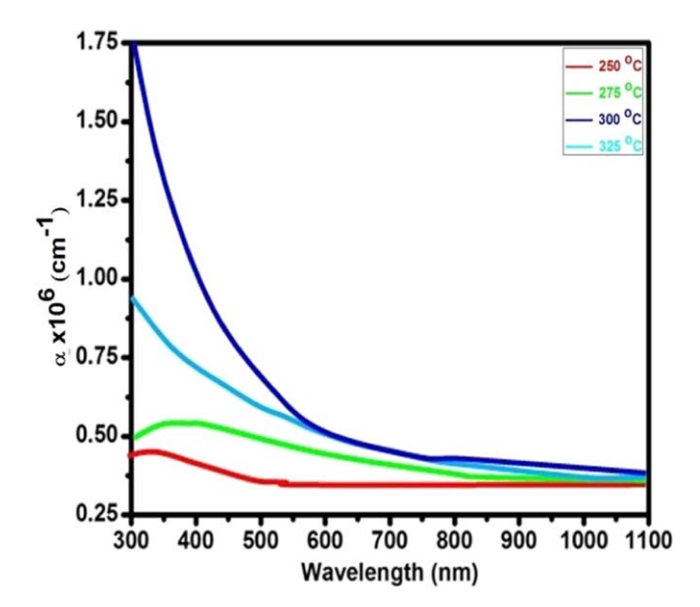


Figure 5. Transmittance spectra of nebulized spray deposited SnSe thin films at different substrate temperature.



**Figure 6.** Absorption coefficient spectra of nebulized spray deposited SnSe thin films at different substrate temperature.

presence of defects such as electron-hole recombination centres, oxygen vacancies and defects are responsible for optical absorption and the emission spectra. The room temperature photoluminescence spectra of the SnSe thin films in the wavelength region from 400 nm

to 550 nm are shown in Fig. 8. The low intensity luminescence peaks observed in the films might be attributed to inter-impurity transitions and larger stoichiometric deviations in the films. The peaks at 420, 485 and 498 nm may be ascribed to defect centers attributed to excitonic transitions which are size dependent and excitation wavelength-independent in certain wavelength range.<sup>53</sup> The emission peak at 529 nm may be due to the presence of electron hole recombination via trap states or imperfection sites.<sup>54</sup> These impurities or defects that were not traced in the XRD analysis might be developed or formed at the time of growth of SnSe films.

Electrical conductivity studies on SnSe thin films.—The electrical conductivity, Hall coefficient and mobility of nebulized spray deposited SnSe thin films deposited at the different substrate temperatures from 250 to 325 °C were determined by Hall effect measuring instrument and the corresponding values were listed in Table IV.

The Hall positive coefficient values confirm that the as-deposited SnSe films had an p-type nature. Figure 9 shows the variation in the resistivity, carrier concentration and Hall mobility of the films as a function of substrate temperature. The resistivity of the SnSe films decreases with the increase of substrate temperature from 250 °C to 300 °C and then it increases with the further increase in the substrate temperature to 325 °C. The lowest resistivity value was 4.84 Ωcm at the substrate temperature of 300 °C. The decrease of the electrical resistivity of the film layers after increasing the substrate temperature from 250 °C to 300 °C can be explained using the Petritz barrier model.<sup>55</sup> Since the crystallites do not grow sufficiently large at low temperatures, the intercrystalline regions offered high resistance for the movement of the charge carriers. At high substrate temperatures, the formation of fewer nucleation centres results in large crystallite sizes, which may ultimately decrease the intercrystalline barriers, hence decreasing the electrical resistivity and then is decreased by a further rise in substrate temperature of 325°C. Lots of reports have been reported in the resistivity of SnSe thin films whereas Hema Chandra et al.<sup>56</sup> had reported the closer resistivity value from 8.1 to 30  $\Omega$ cm after performing with the substrate temperature range 303-513 K for the SnSe thin films deposited by the flash evaporated technique. The bulk carrier concentration and mobility of the SnSe thin films increase with increasing substrate temperature from 250 to 300 °C up to  $5.676 \times 10^{17} \, \mathrm{cm^{-3}}$  and  $7.8 \, \mathrm{cm^2 \, V^{-1} \, s^{-1}}$ , and then they decrease to  $2.542 \times 10^{17} \, \mathrm{cm^{-3}}$  and  $5.2 \, \mathrm{cm^2 \, V^{-1} \, s^{-1}}$  respectively by a further rise in substrate temperature.

The mobility increases as a result of reconstituting and the crystallinity prosperity of the material. The increased bulk carrier concentration caused by increasing substrate temperature shrunken the grain boundary potential barrier. Because of that, the carrier mobility of the SnSe films also increases. The results showed in this work have presented the feasibility of using SnSe thin films suitable for fabrication of solar cells.

The activation energy of SnSe thin film can be calculated using the equation

$$\rho = \rho_0 \exp\left(\frac{E}{KT}\right). \tag{5}$$

The temperature dependence of resistivity was studied from room temperature to 313 K. An Arrhenius plot of log  $(\rho)$  vs 1000/T for four typical SnSe thin films at different substrate temperature has been shown in Fig. 10.

The curves clearly show two conduction regions. The slope is high in the low temperature region but decrease with further increase of temperature. From the slopes of an Arrhenius plot, the activation energies are calculated and presented in Table IV. The value of pre-exponential factor  $\rho_0$ , which is the resistivity of the film as the temperature reaches to infinity, is determined to be 20.44, 12.63, 2.74 and 15.34  $\Omega$ cm for the SnSe films prepared at different substrate temperatures from 250 to 325 °C. It is seen from the activation energies that the films do not possess the intrinsic

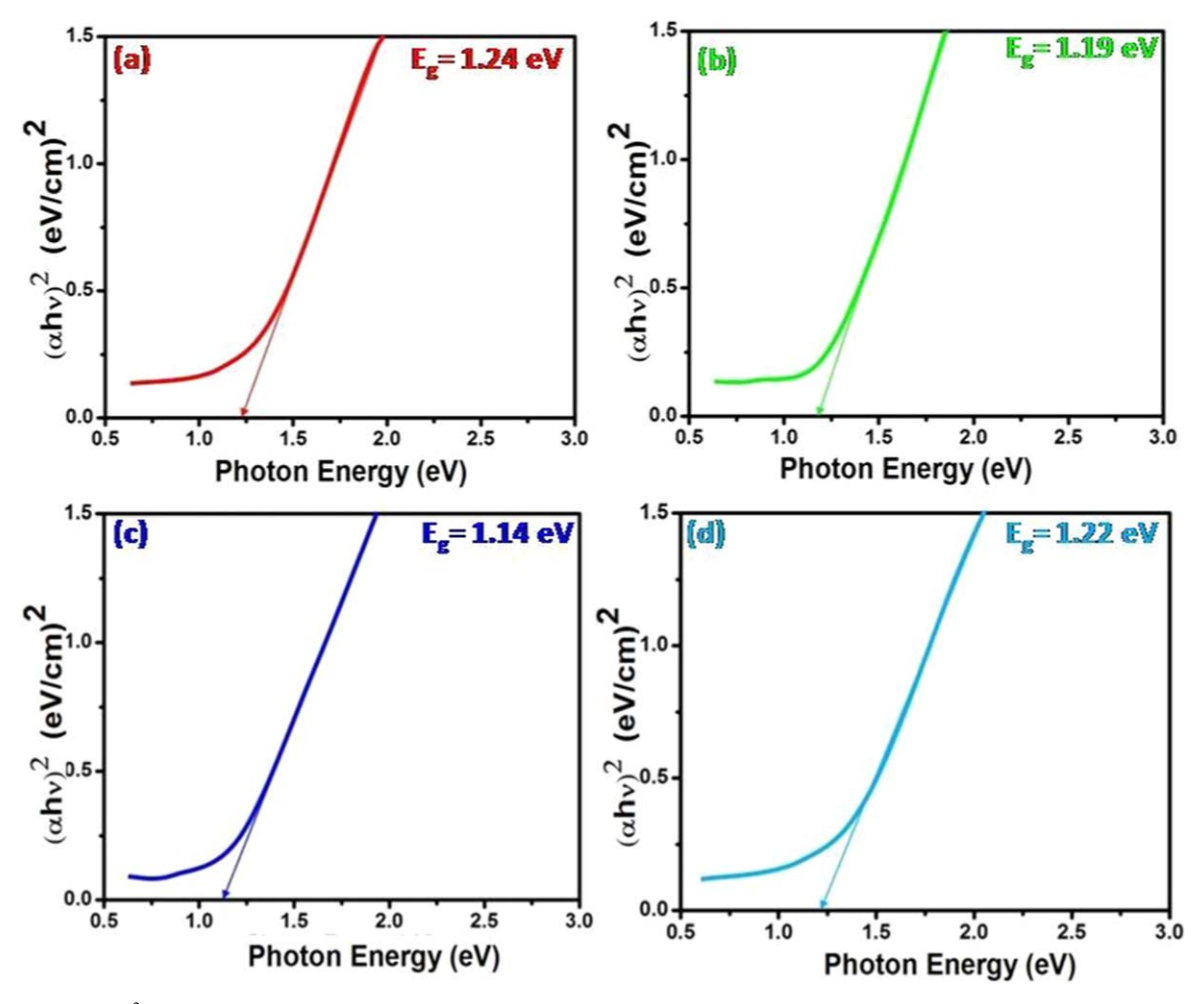


**Figure 7.** Plot of  $(\alpha h \nu)^2$  vs photon energy for nebulized spray deposited SnSe thin films at substrate temperature (a) 250 °C, (b) 275 °C, (c) 300 °C, (d) 325 °C.

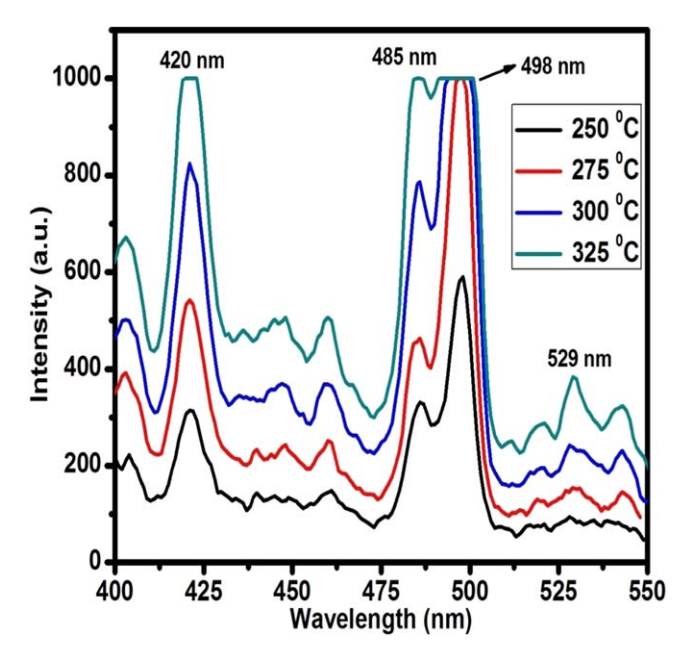


**Figure 8.** Photoluminescence (PL) spectra of SnSe thin films deposited under different substrate temperature.

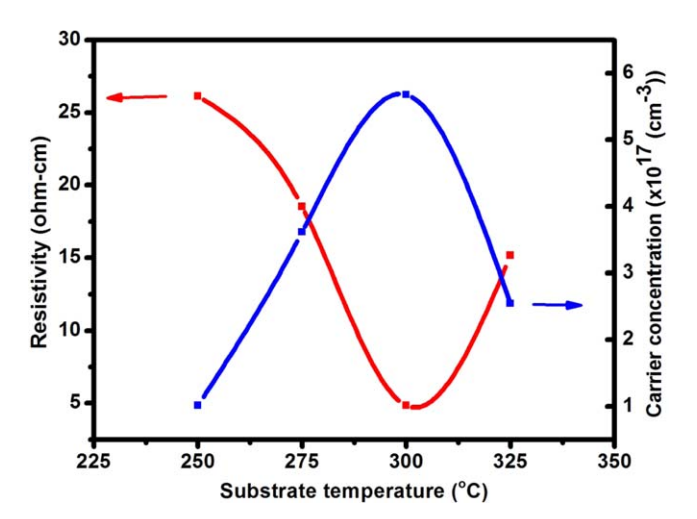


**Figure 9.** Variation of resistivity, carrier concentration and mobility of SnSe thin films of different substrate temperature.

resistivity strictly in this entire range of applied temperature. The shallow trapping states preferably due to those interstitial tin or selenium vacancies are expected to dominate the extrinsic resistivity

Table IV. Variation of optical and electrical properties of SnSe thin films at different substrate temperature.

T <sub>S</sub> (°C)	Band gap (eV)	Conductivity $(\Omega\text{-cm})^{-1}$	Mobility (cm $^2$ V $^{-1}$ s $^{-1}$ )	Hall coefficient (cm <sup>-3</sup> C <sup>-1</sup> )	Activation energy (eV)
250	1.24	0.04	2.6	61.70	0.10
275	1.19	0.05	4.4	17.30	0.15
300	1.14	0.21	7.8	11.01	0.16
325	1.22	0.07	5.2	24.59	0.27

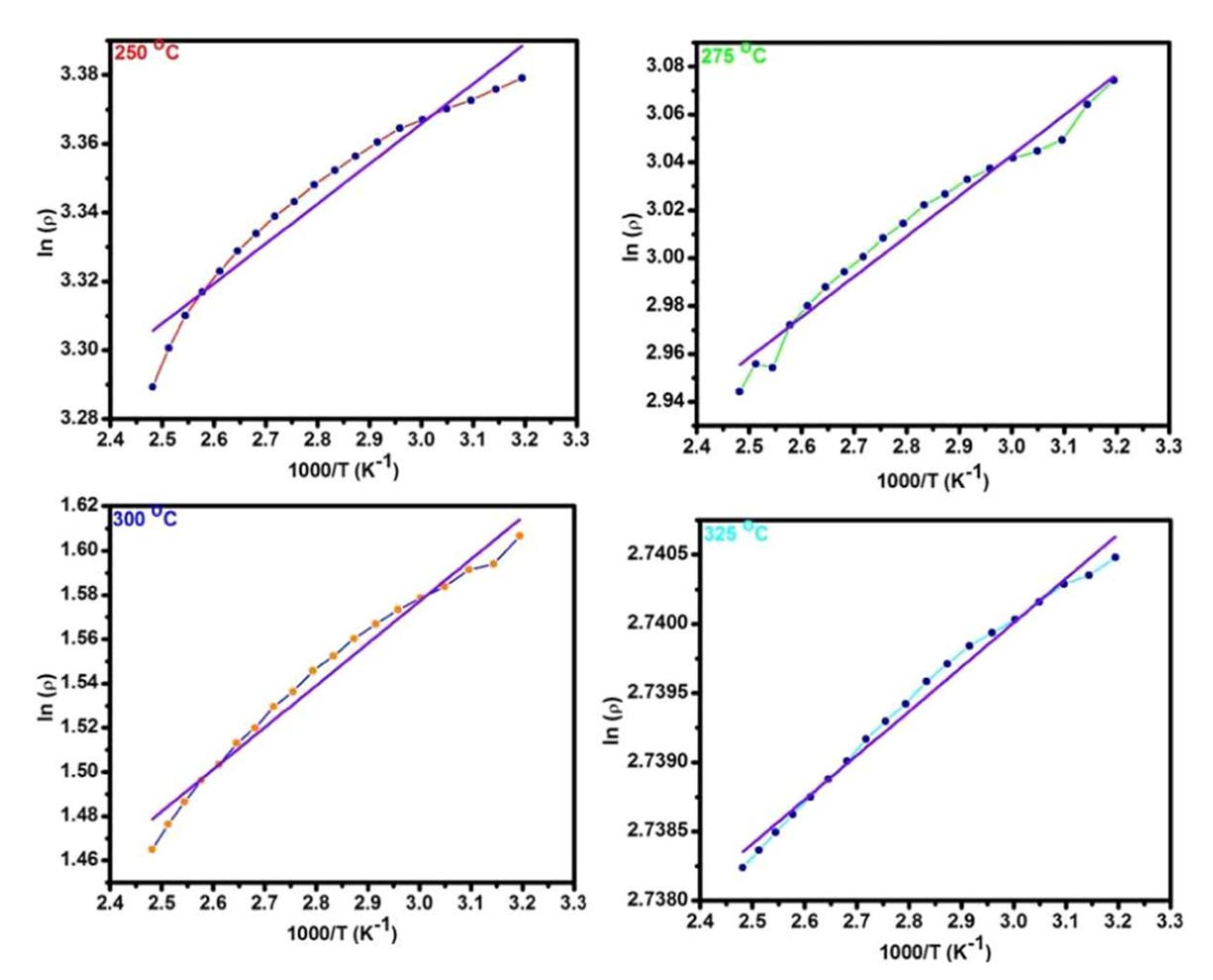


Figure 10. Arrhenius plot of SnSe thin films of different substrate temperature.

near the room temperature whereas those deep trap states influence at high temperature range. Kumar et al.  $^{57}$  have reported the activation energy for the SnSe thin film deposited in the range of 300–450 K using thermal evaporation method is 0.14–0.28 eV.

#### Conclusions

The p-type semiconducting SnSe thin films have been successfully deposited by simple and inexpensive nebulized spray pyrolysis technique. Polycrystalline nature of as-deposited SnSe thin films was confirmed from X-ray diffraction studies. X-ray diffraction studies depicted orthorhombic crystal structure irrespective of substrate temperature. Scanning electron microscopy studies revealed uniform deposition with the grain size in the nano metre range. Stoichiometric films of SnSe were observed from energy dispersive analysis by X-ray studies. The optical band gap was found to be in the range of 1.14–1.24 eV with the direct allowed transition depending on substrate temperature. The lower absorption and high transmittance in the visible region observed at lower substrate

temperature represented the good optical quality of the crystals with the low absorption or scattering losses which lead to the applications particularly as a window layer in solar cells. Electrical studies showed that the films are semiconducting which may be used in optoelectronic devices. The structural, optical, morphological and electrical conductivity studies of tin selenide thin films confirmed that the optimum substrate temperatures for depositing SnSe thin films by this NSP technique is 300 °C. The corresponding results obtained by preparing SnSe thin films may be suitable for conventional absorber layer in solar cells.

#### Data availability statement

N.A

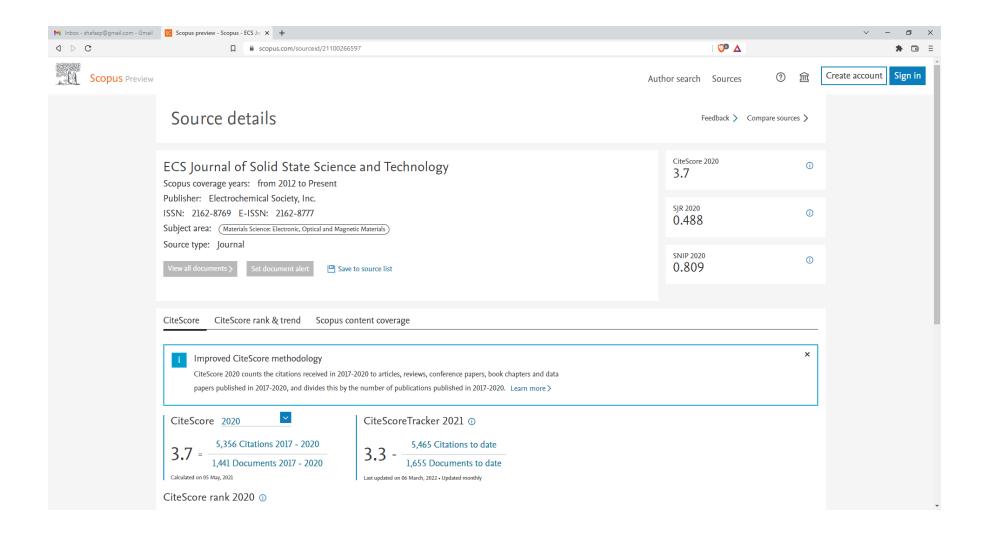
#### ORCID

A. Anitha Ezhil Mangaiyar Karasi https://orcid.org/0000-0002-4816-0826

#### References

- 1. I. R. Chávez Urbiola, J. A. Bernal Martínez, V. P. Makhniy, R. Ramírez Bon, and Y. V. Vorobiev, *Inorg. Mater.*, 50, 546 (2014).
- 2. J. Ellingson, M. C. Beard, J. C. Johnson, P. Yu, O. I. Micic, A. J. Nozik, A. Shabaev, and A. L. Efros, Nano Lett., 5, 865 (2005).
- 3. R. Dalven, Infrared Phys. Technol., 9, 141 (1969).
- 4. S. K. J. Al-Ani, H. H. Mohammed, and E. M. N. Al-Fwade, Renew. Energy, 25, 585 (2002).
- 5. S. Kumar, Z. H. Khan, M. A. Majeed Khan, and M. Husain, Curr. Appl Phys., 5, 561 (2005)
- 6. C. R. Baxter and W. D. Mclennan, J. Vac. Sci. Technol., 12, 110 (1975).
- 7. N. R. Mathews, Sol. Energy, 86, 1010 (2012).
- 8. K. M. Chung, D. Wamwangi, M. Woda, M. Wuttig, and W. Bensch, J. Appl. Phys., 103, 083523 (2008).
- 9. J. Yamaki and A. Yamaji, *Physica B*, **150**, 466 (1981).
- 10. K. Zweibel, Solar Energy Mater. Solar Cells, 63, 375 (2000).
- 11. A. Bennouna, P. Y. Tessier, M. Priol, Q. Dang Tran, and S. Robin, Phys. Status Solidi b, 117, 51 (1983).
- 12. D. T. Quan, Phys. Status Solidi a, 86, 421 (1984).
- 13. T. Subba Rao, B. K. Samantha Ray, and A. K. Chaudhuri, J. Mater. Sci. Lett., 4,
- 14. T. Subba Rao and A. K. Chaudhuri, J. Phys. D: Appl. Phys., 18, L35 (1985).
- 15. T. Subba Rao and A. K. Chaudhuri, *J. Phys. D: Appl. Phys.*, **19**, 861 (1986).
- 16. D. T. Quan, Thin Solid Films, 149, 197 (1987).
- 17. T. Subba Rao, B. K. Samanata Ray, and A. K. Chaudhuri, Thin Solid Films, 165, 257 (1988)
- 18. H. S. Soliman, D. A. Abdel Hady, K. F. Abdel Rahman, S. B. Yossef, and A. A. EL-Shazly, *Physica. A*, 216, 77 (1995).
- 19. P. Suguna, D. Mangalaraj, S. A. K. Narayandass, and P. Meena, *Phys. Status Solidi* a, 155, 405 (1996).
- 20. D. P. Padiyan, A. Marikani, and K. R. Murali, Crystal Res. Technol., 35, 949 (2000).
- 21. J. Sharma, G. Singh, A. Thakur, G. S. S. Saini, N. Goyal, and S. K. Tripathi, J. Optoelectron. Adv. Mater., 7, 2085 (2005).
- 22. J. P. Singh and R. K. Bedi, *Thin Solid Films*, 199, 9 (1991).
- 23. J. P. Singh and R. K. Bedi, J. Appl. Phys., 68, 2776 (1990).
- 24. J. P. Singh, J. Mater. Sci., Mater. Electron., 2, 105.s (1991).
- K. J. John, B. Pradeep, and E. Mathai, *J. Mater. Sci.*, 29, 1581 (1994).
   B. Subramanian, T. Mahalingam, C. Sanjeeviraja, M. Jayachandran, and M. J. Chockalingam, *Thin Solid Films*, 357, 119 (1999).
- 27. Z. Zainal, A. Jimale Ali, A. Kassim, and M. Z. Hussein, Sol. EnergyMater. Sol. Cells, 79, 125 (2003).
- 28. Z. Zainal, S. Nagalingam, A. Kassim, M. Z. Hussein, and W. M. M. Yunus, Sol. Energy Mater. Sol. Cells, 81, 261 (2004).
- 29. A. Lukinskas, V. Jasulaitiene, P. Lukinskas, I. Savickaja, and P. Kalinauskas, Electrochim. Acta, 51, 6171 (2006).
- 30. R. Teghil, A. Giardini-Guidoni, A. Mele, S. Piccirillo, G. Pizzella, and V. Marotta, Thin Solid Films, 241, 126 (1994).

- 31. R. Teghil, A. Santagata, V. Marotta, S. Orlando, G. Pizzella, A. Giardini-Guidoni, and A. Mele, Appl. Surf. Sci., 90, 505 (1995).
- 32. B. Subramanian, C. Sanjeeviraja, and M. Jayachandran, J. Crystal Growth, 234, 421 (2002)
- 33. Z. Zainal, N. Sarayanan, K. Anuar, M. Z. Hussein, and W. M. M. Yunus, Mater. Sci. Eng. B, 107, 181 (2004).
- 34. Z. Qiao, W. Shang, and C. Wang, J. Electroanal. Chem., 576, 171 (2005).
- 35. J. S. N. Rios, M. Ramachandran, D. M. Escobar, and A. S. Juarez, J. Semicond., 34, 013001 (2013).
- 36. S. Anwar, S. Gowthamaraju, B. K. Mishra, S. K. Singh, and S. Anwar, Mater. Chem. Phys., 153, 236 (2015).
- 37. X. Fu, G. Wu, S. Song, Z. Song, X. Duo, and C. Lin, Appl. Surf. Sci., 148, 223 (1999).
- 38. R. Mariappan, V. Ponnuswamy, and P. Suresh, Superlattice. Microst., 52, 500
- 39. R. Mariappan, V. Ponnuswamy, P. Suresh, R. Suresh, M. Ragavendar, and C. Sankar, Mater. Sci. Semicond. Proc., 16, 825 (2013).
- 40. R. Mariappan, V. Ponnuswamy, P. Suresh, R. Suresh, and M. Ragavendar, Superlattic, Micros., 59, 47 (2013). 41. R. Mariappan, V. Ponnuswamy, R. Suresh, P. Suresh, A. Chandra Bose, and
- M. Ragavendar, J. Alloys Compd., 582, 387 (2014).
- 42. E. E. Ebsenso, K. Sardar, M. Chandrasekhar, A. R. Raju, and C. N. R. Raju, Solid State Sci., 2, 833 (2000).
- 43. N. Kumar, V. Sharma, U. Parihar, R. Sachdeva, N. Padha, and C. J. Panchal, J. Nano Electron Phys., 3, 117 (2011).
- 44. P. Scherrer, Gothinger Nachri-Chten, 2, 98 (1918).
- 45. V. M. Nikale, N. S. Gaikwad, K. Y. Rajpure, and C. H. Bhosale, Mater. Chem. Phys., 78, 363 (2003)
- 46. G. B. Williamson and R. C. Smallman, *Philos. Mag.*, 1, 34 (1956).
- 47. R. Mariappan, M. Ragavendar, and G. Gowrisankar, Chalcogenide Letters, 7, 211 (2010).
- 48. R. D. Engelken, A. K. Berry, T. P. Van Doren, J. L. Boone, and A. Shahnazary, J. Electrochem. Soc., 133, 581 (1986).
- 49. A. M. Fernandez and M. G. Merino, Thin Solid Films, 366, 202 (2000).
- 50. J. I. Pankove, Optical Processes in Semiconductors (Prentice and Hall, Inc., New Jersey) p. 36 (1971).
- 51. P. Ramasamy, P. Manivasakan, and J. Kim, Cryst. Eng. Comm., 17, 807 (2015).
- 52. L. Ling, Q. Zhang, L. Zhu, C.-F. Wang, and S. Chen, RSC Adv., 5, 2155 (2014).
- 53. N. Kumar, V. Sharma, N. Padha, N. M. Shah, M. S. Desai, C. J. Panchal, and I. Y. Protsenko, Cryst. Res. Technol., 45, 53 (2010). N. Chestony, T. D. Harris, R. Hull, and L. E. Brus, J. Phys. Chem., 90, 3393 (1986).
- 55. J. Srivind, V. S. Nagarethinam, and A. R. Balu, Materials Science-Poland, 34, 393
- (2016).
- 56. S. Chaura, N. B. Chaura, and R. K. Pandey, *Physica E*, 28, 439 (2005).
- 57. R. L. Petritz, Phys. Rev., 104, 1508 (1956).
- 58. G. Hema Chandra, J. Naveen Kumar, N. Madhusudhana Rao, and S. Uthanna, . Cryst. Growth, 306, 68 (2007).
- 59. N. Kumar, U. Parihar, R. Kumar, K. J. Patel, C. J. Panchal, and N. Padha, American Journal of Materials Science, 2, 41 (2012).







## Effect of Substrate Temperature on Structural, Electrical and Optical Properties of Sprayed Tin Selenide Thin Films Applicable for Photovoltaic Measurements

Anitha Ezhil Mangaiyar Karasi, 1,2,z R. Sambasivam, S. Seshadri, and Amalraj Anitha Ezhil Mangaiyar Karasi, 1,2,z R. Sambasivam, S. Seshadri, and Amalraj

Thin films of Tin selenide (SnSe) have been prepared on glass substrates at different temperatures in the range of 250 °C–375 °C in steps of 25 °C for optimization were discussed. The deposited tin selenide thin films were characterized using X-ray diffraction analysis (XRD), Elemental dispersive X-ray analysis (EDAX), Scanning electron microscopy (SEM), Optical absorption, Photoluminescence (PL), Raman spectroscopy and electrical measurements. From XRD analysis a single-phase tin selenide thin film having orthorhombic crystalline structure with crystallite size of 17 nm to 62 nm were investigated. The surface morphology revealed the presence of uniformly distributed spherical grains of SnSe thin films without pores and voids. Optical absorption spectrum revealed a direct band gap of 1.15 eV and having very high absorption coefficient ( $^{\circ}$ 10 $^{4}$ /cm) was calculated. The Raman scattering analysis confirmed the presence of B $_{3g}$  and Ag vibrational modes of SnSe thin films. PL studies revealed a strong luminescence peak near-band-edge (NBE) emission at 785 nm due to recombination of bound excitons. Photoconductivity characteristics of SnSe thin films were due to the existence of continuous distribution of localized states in the band gap data. Thus tin selenide thin films were used as an absorber layer in the photovoltaic application.

© 2022 The Electrochemical Society ("ECS"). Published on behalf of ECS by IOP Publishing Limited. [DOI: 10.1149/2162-8777/ac4ffd]

Manuscript submitted August 28, 2021; revised manuscript received January 12, 2022. Published February 9, 2022.

In this scenario, tin-based binary semiconductors such as SnS and SnSe are expected to a play a crucial role in replacing toxicating cadmium compounds and scarced elements based CIGS absorbers in photo-voltaic devices. They are relatively earth abundant, non-toxic nature and easy controllability of stoichiometric. Moreover, the annual production of tin, sulphur, and selenium is large (low-price) as compared to other absorber elements. These materials exhibit favourable properties such as high chemical stability, suitable band gap (1.0 eV to 1.5 eV) and high absorption co-efficient ( $\sim 10^5 \, {\rm cm}^{-1}$ ) with P-type conductivity. On the other hand, the solar cells fabricated from SnSe thin films exhibited lower efficiencies ( $\leq 1\%$  by non-vacuum methods and > 5% by vacuum methods) than CIGS and CZTS solar cells.

In recent years, semiconducting compounds play a vital role for the researcher due to their potential application in the solar energy conversion, sensors, laser materials, thin films polarizer and thermoelectric cooling materials. 1-5 Tin selenide (SnSe) is a IV-VI binary semiconductor that crystallizes in orthorhombic crystallographic structure whose atomic arrangement within the crystal resembles like distorted NaCl structure. The existence of the tightly bound double layers of tin and selenium atoms stacked along the crystallographic c-axis and anisotropic character, thus tin based chalcogenide semicoductors are attractive layered compounds which can be used as cathode materials in lithium ion batteries<sup>7</sup> and decreasing the photo corrosion.<sup>8</sup> It is a narrow band semiconductor with high chemical stability, p-type conductivity and their band gap lies between 1.0 eV and 2.0 eV and absorbs light energy from the high energy end of the solar spectrum. SnSe has numerous applications in memory switching devices, in holographic recording systems or as an anode material to improve light diffusivity. 9-13 Owing to this, SnSe has been studied in the form of both single crystal and thin films. 14-16 Researchers investigated a number of methods to prepare SnSe thin films viz. epitaxial laser ablation method, <sup>17</sup> atomic layer deposition, <sup>18</sup> closed space vapor transport, <sup>19</sup> chemical bath deposition, <sup>20–22</sup>chemical vapor deposition, <sup>23</sup> vacuum deposition, <sup>24</sup> spray pyrolysis, <sup>25,26</sup> etc. Among these techniques spray pyrolysis is a simple and low cost technique for the preparation of semiconductor thin films. It has capability to produce large area, high quality adherent films of uniform thickness, low temperature growth, enable

morphological and film thickness controlled by electrical parameters.

In the present work, SnSe thin films were grown on glass substrates, held at different substrate temperatures ( $T_s$ ), by the spray pyrolysis technique. We study the effect on the structural, morphological, optical and electrical properties of SnSe thin films sprayed at different substrate temperature ranging from 250 °C to 375 °C.

#### **Experimental**

Tin selenide (SnSe) thin films were deposited onto glass substrates at different substrate temperatures using the spray pyrolysis unit.<sup>26</sup> It consists of a spray nozzle, a furnace for heating the substrate, and a mechanical system for rotor, thermocouple included temperature controller and air compressor. A hot plate (base plate) made up of iron disc is used to measure the temperature in which a maximum temperature of 450 °C can be achieved with the help of chromel—alumel thermocouple. Substrate temperature (T<sub>s</sub>) was maintained with the help of a feedback circuit which controls the heater supply. Temperature of the substrate can be varied from room temperature to 450 °C using this coating unit. During the spray, temperature of the substrate was kept constant with an accuracy of ±2 °C. The nozzle is made up of borocil glass and consists of solution tube which is surrounded by a glass bulb. Due to air pressure of the carrier gas, a vacuum is created at the tip of the nozzle to suck the solution from the tube after which the spray starts. Spray head and hot plate with substrates were kept inside a chamber provided with an exhaust fan for removing gaseous byproducts and vapours of the solvent. Pressure of the carrier gas (air) used for spraying the precursor solution was adjusted manually from an air compressor unit. With the help of indigenously developed dispensing unit, the spray rate of the solution can also be precisely controlled. Spray rate is an important parameter in controlling different properties of the films which can be controlled with an automated spray pyrolysis unit. In the spray mechanism, the nature of the substrate surface is very important in order to get uniform film at the entire surface. The basic principle involved in chemical spray pyrolysis was that when a droplet of the spray solution reaches the substrate owing to the pyrolytic decomposition of the solution, well adherent films are deposited. Substrate cleaning plays a dominant role since the contaminated surface provides nucleation sites facilitating in non uniformity grow of thin films.

<sup>z</sup>E-mail: anivishaal123@gmail.com

<sup>&</sup>lt;sup>1</sup>PG & Research Department of Physics, Urumu Dhanalakshmi College, Trichy (Affiliated to Bharathidasan University), India

<sup>&</sup>lt;sup>2</sup>Department of Physics, Shrimati Indira Gandhi College, Trichy (Affiliated to Bharathidasan University), India <sup>3</sup>Research Department of Physics, VHNSN College, Virudhunagar, India

Cleaned boro silicate glass slides, with dimensions of 37  $\times$  24  $\times$ 1.2 mm<sup>3</sup> were used as the substrates. First of all the glass slides were boiled in chromic acid for 30 min, then washed with liquid detergent and rinsed in acetone. Finally the slides were ultrasonically cleaned with double distilled water for 20 min before deposition. In this study, Tin Mono Selenide thin films were prepared onto glass substrates from an aqueous solution containing doubly hydrated Stannous chloride (SnCl<sub>2</sub>·2H<sub>2</sub>O) and Selenourea (SeC(NH<sub>2</sub>)<sub>2</sub>) of 0.1 molarity each dissolved in deionised water in separate beakers. Aqueous solutions of stannous chloride and selenourea were used as the sources of tin and selenium respectively. Both the solutions were mixed for 1 h with a magnetic stirrer to get a clear solution. The film was prepared by varying substrate temperatures from 250 °C to 375 °C in steps of 25 °C. The colourless precursor solution turned gray in colour and then to gray-black in colour. The other deposition parameters like solution flow rate, carrier gas pressure, nozzle to substrate distance were kept as 2 ml min<sup>-1</sup>,0.8 kg cm<sup>-2</sup>, 30 cm and the total volume of the solution sprayed was 40 ml, which contained equal volumes (20 ml) of SnCl<sub>2</sub>·2H<sub>2</sub>O and (SeC(NH<sub>2</sub>)<sub>2</sub>) respectively. The spray rate was fixed at 2 ml min<sup>-1</sup> since low spray rate favoured formation of films with superior surface morphology.<sup>26</sup> Further lowering of deposition rate would require longer coating durations, which is an undesirable condition for preparing SnSe thin films.

The tin selenide thin films of blackish dark gray coloured films were obtained. Thickness of the films was measured using Stylus method (Stylus thickness profiler). The structural analysis was performed by employing X-ray diffraction (XRD) using Rigaku (D. Max.C) X-ray diffractometer having CuK $\alpha$  ( $\lambda = 1.5405$ Å) radiation and Ni filter operated at 30 kV and 20 mA. All samples were scanned in the range  $10^{\circ}$  to  $80^{\circ}$  with a scan speed of  $5^{\circ}$  min<sup>-1</sup> Surface studies of the samples were done with the help of Scanning electron microscopy (SEM) JOEL, JSM-840 operating voltage for SEM measurements was 20 kV and the surface morphology of the samples was compared with 25k magnification. Compositional variation of the samples was analyzed using energy dispersive X-ray (EDAX) analysis (operated at 20 kV), which is attached with the SEM (ZeissHR) instrument. Optical absorption studies were carried out using UV-Vis-NIR Spectrophotometer (JascoV-750 model) in the range of 400-1100 nm. Employing Keithley 236 source measure unit, electrical characterization was performed using Hall effect and four probe apparatus. Silver electrodes were painted on the surface of the film on a fixed area with uniform thickness, keeping a distance of 5 mm in between the electrodes for electrical characterizations. Photoluminescence effect was measured by fluorescence spectrophotometer (PL, Schimadzu

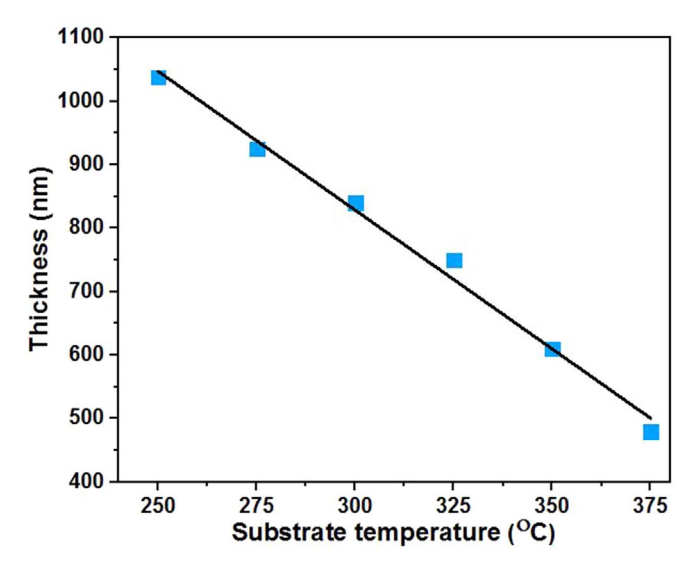


Figure 1. Variation of film thickness with T<sub>S</sub>.

RF-5301) by studying the spectra of thin films wavelengths between 400 nm to 800 nm.

#### **Results and Discussions**

The thin films prepared with different substrate temperatures in the range 250 °C–375 °C as said in the procedure given above, were uniform, free from pinholes and cracks with dark gray in colour. Thicknesses of these six samples deposited with different substrate temperatures were determined using Stylus profiliometer. The variation of thickness as a function of substrate temperature is plotted as shown in Fig. 1. It reveals that the thickness had decreased linearly with respect to increase in substrate temperature. A similar variation of thickness was observed for SnSe films prepared at different substrate temperatures by Kumar et al. <sup>27</sup>This may be due to the re-evaporation of the compounds at higher temperatures.

Structural studies.—The X-ray diffraction pattern of SnSe thin films deposited at different substrate temperatures are shown in Fig. 2. The XRD patterns of films deposited at different  $T_s$  (250 °C–375 °C) with SnSe peak orientation along (111) plane having orthorhombic crystal structure with lattice parameters  $a=4.151\,\text{Å},$   $b=11.46\,\text{Å},$   $c=4.444\,\text{Å},$  at  $2\theta=30.5\,$  °(JCPDS data card 32-1382). <sup>28–30</sup> For  $T_s=250\,$  °C, the spectra showed presence of different phases like Sn<sub>2</sub>Se<sub>3</sub> white spots were observed all over the film surface, which indicated the presence of unreacted precursors of

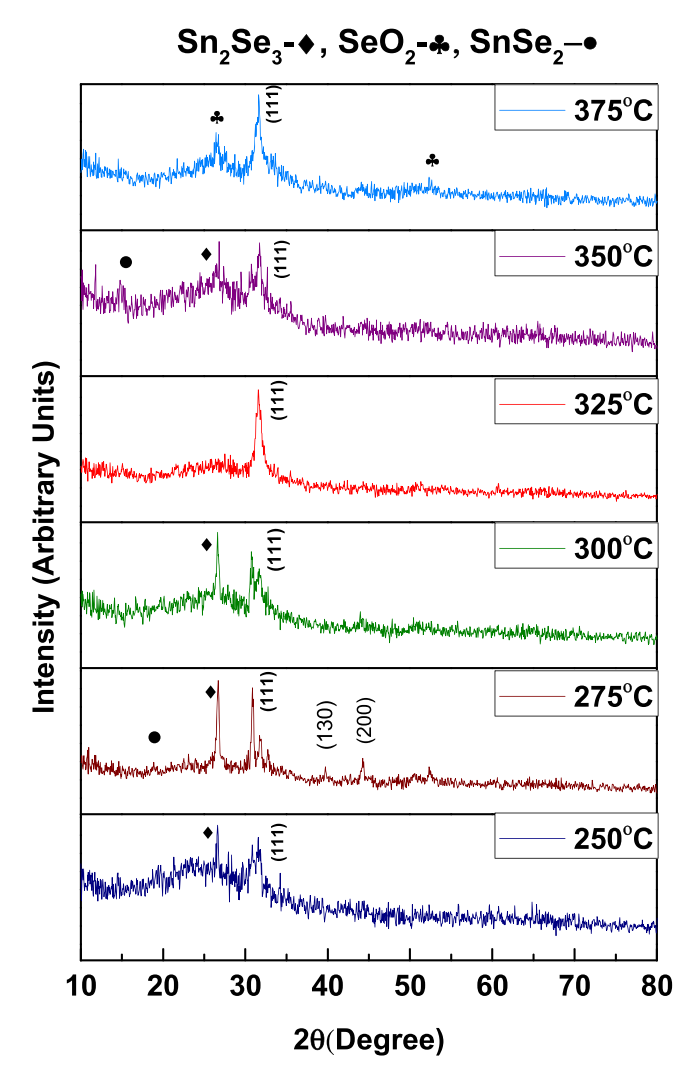


**Figure 2.** XRD patterns of SnSe films prepared at (a)  $T_S = 250$  °C (b)  $T_S = 275$  °C (c)  $T_S = 300$  °C (d)  $T_S = 325$  °C (e)  $T_S = 350$  °C and (f)  $T_S = 375$  °C.

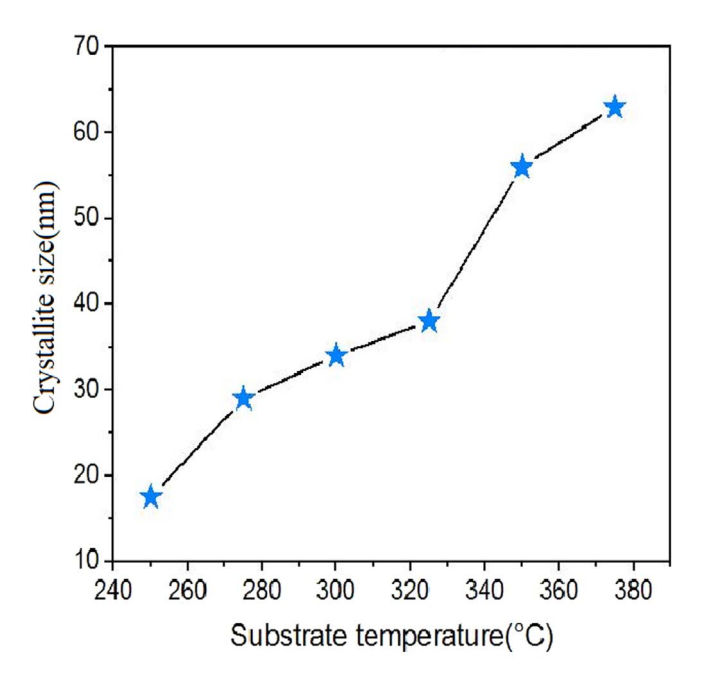


Figure 3. Crystallite size vs Substrate temperature.

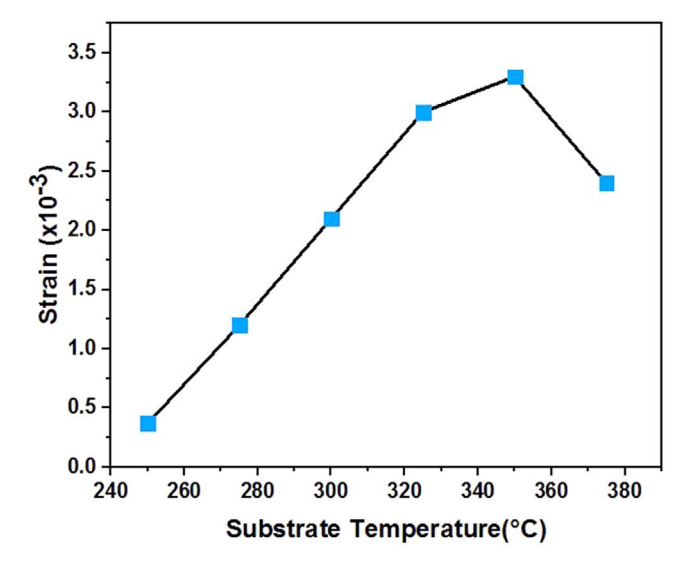


Figure 4. Strain vs Substrate temperature of SnSe thin films.

Stannous chloride and Selenourea, as  $T_s$  was lower than the 'pyrolytic temperature. For  $T_s=275\,^{\circ}\text{C}$ , mixed phases of  $\text{SnSe}_2$  and  $\text{Sn}_2\text{Se}_3$  were present. For 300 °C, peak intensity of  $\text{Sn}_2\text{Se}_3$  decreases and at 325 °C only single phase SnSe films was observed and at 350 °C there will be the deficiency of selenium contents and for 375 °C the films were white in color with the conversion of selenium contents into oxide phase as prominent  $\text{SeO}_2$ . Since when the  $T_s$  is

very low the deposits were amorphous due to the spatial influence experienced by impinging atoms due to the lack of regularity of the substrate atoms at the contact region. The pre-nucleation adsorption sites will have no orientation influence on the deposit. When the substrate temperature increases, two phenomena takes place (1) increase in the crystallite size and (2) enlargement of the nucleation centres which might result in increased density of crystallites and intensity of the diffraction peaks.

The XRD pattern clearly indicated prominent peaks of Sn<sub>2</sub>Se<sub>3</sub> phase at lower T<sub>s</sub> (250 °C) and SnSe converts as oxide phase at higher T<sub>s</sub> (> 375 °C). These impurity phases almost vanished for 325 °C T<sub>s</sub> the films were having better crystallinity with a singlephase SnSe. On increasing the substrate temperature above 350 °C, the peaks corresponding to SnSe decreases and the compound was almost converted into SeO<sub>2</sub>. This is probably due to re-evaporation of selenium from the film at such temperatures because of its high vapor pressure, leaving a tin riched surface which might have reacted with oxygen to form SeO<sub>2</sub> as the deposition was carried out at atmospheric pressure. Mariappan et al. has reported that the conversion of SnSe into SeO<sub>2</sub> takes place when the films are annealed at such high temperatures. A similar behavior for the films having different phases deposited at different substrate temperature was reported by Kumar et al. Bhatt et al.<sup>31</sup> and by Dang Tran Quan, <sup>32</sup> H. Chandra et al. had observed (400) diffraction plane for films grown by flash evaporation technique and Teghil et al. had reported the orientation of grains with (011) and (200) crystallographic plane by laser ablation method. The various preferred orientation of the grains by various deposition techniques indicate that the mode of deposition plays a dominant role for the growth of structure of films. The analysis of diffraction patterns also reveals that SnSe thin films deposited at 325 °C had single phase highly preferred orientation along (111) direction. No other peaks were observed which confirms the optimized temperature.

Crystallite size of the films were calculated using the Scherrer formula,

$$D = k\lambda/(\beta cos\theta)$$
 [1]

Where D is the diameter of the crystallites forming the film,  $\lambda$  is the wavelength of  $\text{CuK}_{\alpha}$  line, k is the shape factor value is 0.94,  $\beta$  is the full width at half maximum in radians and  $\theta$  is the Bragg angle of the diffraction peak. As the substrate temperature increases from 250 °C to 375 °C, the crystallite size also increases from 17 nm to 62 nm and slightly decreased after optimised temperature. The crystallite size of the film prepared at  $T_s = 325$  °C was 37 nm.

The crystallite size increased with the increase in substrate temperature, which is evident from the decrease in the full width at half maximum (FWHM) of the (111) peak. Figure 3 shows the crystallite size plotted against substrate temperature. The crystallite size of a vapour-deposited polycrystalline film increased with substrate temperature may be due to the increased surface mobility of ad atoms and clusters during deposition. The variation of crystallite size with substrate temperature can be recognized by melting point for the vapour source, adatoms interact strongly with each other to become chemisorbed with little surface migration, thereby resulting in a fine grained deposit and higher the surface mobility more marked the film thickness. Usually crystallite sizes in

Table I. Value of Crystallite size, Strain, Dislocation density and Thickness of SnSe thin films at different substrate temperature.

Temp (°C)	Peak intensity	d-spacing	FWHM	Crystallite size(nm)	Strain $\times 10^{-3}$	Dislocation density $\times$ 10 <sup>16</sup>	Thickness (nm)
250	30.59	2.9395	0.7872	17	0.37	0.836	1038
275	30.57	2.9392	0.4920	29	1.2	3.269	925
300	30.56	2.9170	0.5904	32	2.1	4.710	840
325	30.5	2.9048	0.1962	37	3	2.036	750
350	30.49	2.9029	0.4428	50	3.3	2.648	610
375	30.42	2.9031	0.1968	62	2.4	5.234	480

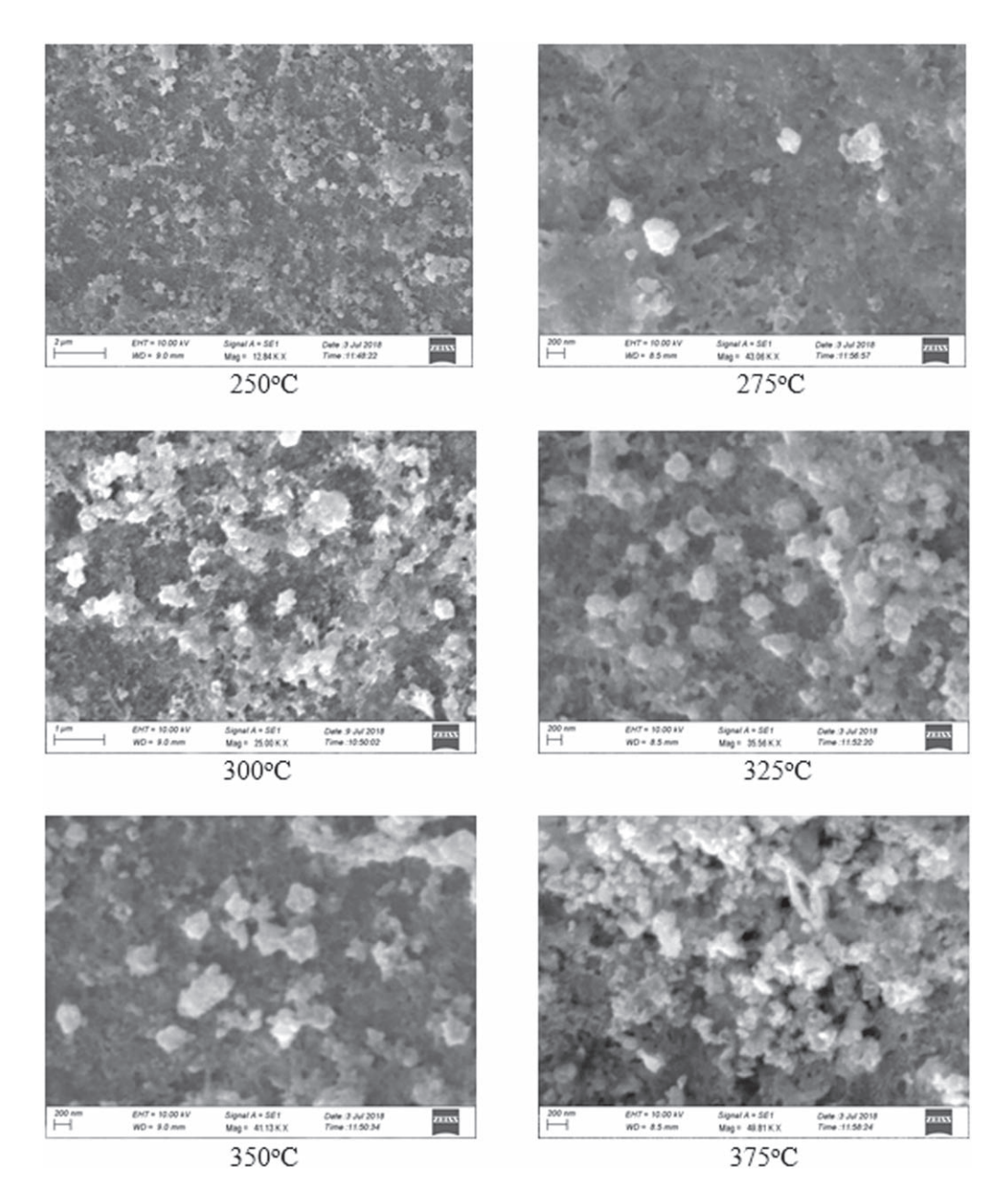


Figure 5. SEM images of SnSe films at 250 °C-375 °C.

sprayed films are decreasing with the deposition temperature. Reverse effect observed in sprayed tin selenide films could be explained by the formation of secondary phases, which retard the growth of SnSe crystallites at different substrate temperatures, which is in agreement with S. Anwar et al.

The micro strain was calculated by the equation

$$\varepsilon_s = \frac{\beta \cos \theta}{4} \tag{2}$$

From the Fig. 4 we observed a strain vs substrate temperature of the SnSe thin film, the lower strain is for the thin films grown at a substrate temperature of the 250 °C and increased as the substrate temperature increases. The SnSe thin film grown at 350 °C exhibit the highest value of the strain, this could be due to the high temperature of the substrate and consequently the low mobility of atoms to have a better arrangement in the polycrystal. The value of crystallite size, dislocation density and thickness of SnSe thin films will be given in Table I.

#### **Morphological Properties**

Scanning electron microscope (SEM) studies provide microscopic information of the surface topography. Thus SEM studies were carried out to assess the quality of the SnSe thin films spray deposited at different temperatures from 250 °C to 375 °C. These SEM photographs were recorded with the magnifications of about 25,000. SEM images show that the surface morphology of the sample strongly depends upon the concentrations of tin species solutions at different T<sub>s</sub> It is evident from the SEM image that the grains are distributed to cover the surface of the substrate completely. No pin holes or cracks could be observed for the samples. From Fig. 5d that the samples prepared at  $T_s = 325$  °C had cluster of spherical grains such that the grains are distributed uniformly to cover the surface of the substrate completely with increase in grain size and the density of the grain decreases. While from Fig. 5a, it is clear that for samples prepared at  $T_s = 250$  °C the surface is smooth with a close packed adherent films. At  $T_s = 275$  °C the images reveals the presence of dense structures and above this temperature

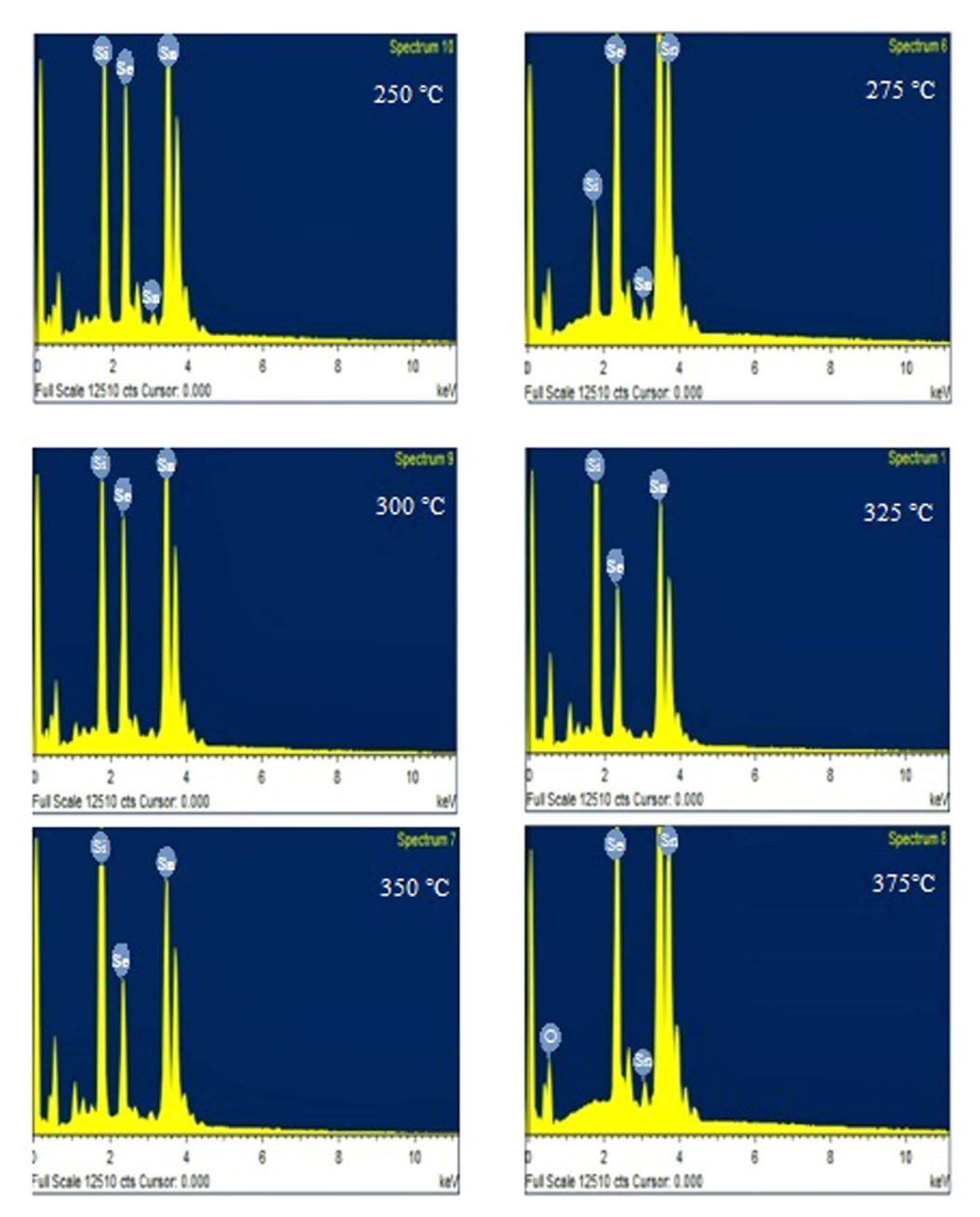


Figure 6. EDAX images of SnSe films at 250 °C-375 °C.

spherical grains are formed without pores, voids or cracks. These images confirm that film surface changed from regular spherical grain structure to cluster like crystallite structures with increase in temperature from 250 °C to 375 °C, with the conversion of SnSe into SeO<sub>2</sub> due to deficiency of selenium compounds. Thus the SEM images showed increase in substrate temperature has the significant effects on the grains and modify the structure of crystallites. The results obtained from SEM coincidence with the XRD results.

**EDAX analysis.**—The chemical composition and purity of the deposited SnSe thin films (Atomic ratios of Sn and Se) in the films were examined using EDAX spectrum in the binding energy region of 1 eV to 10 eV. Variation of Sn/Se ratio in the films with respect to the  $T_s$  is depicted in Fig. 6. The quantitative weight percentage of the compositional elements such as Tin and Selenium was presented in Table III. It was observed that, as  $T_s$  was increased, the composition of selenium compounds in the film also increased, and at  $T_s = 325\,^{\circ}\text{C}$  we obtained nearly stoichiometric SnSe thin films which is in

good agreement with the reports of Tomkiewicz et al. and Skyllas Kazcos and Miller et al.  $^{33}$  But at still higher  $T_s$  (>325 °C) the selenium content in the film started decreasing, probably due to reevaporation of selenium owing to its high vapour pressure and conversion of selenium into oxides.

Optical properties.—Band gap energy is the most significant semiconducting property which plays a vital role in the determination of application fields of materials. Temperature is one of the factor affects the band gap of the materials which changes the structure of compounds. Two reasons were significant for temperature band gap dependence (1) influence of electron-phonon interaction and phonon dispersion due to band gap shrinkage (2) semiconducting devices worked at high temperature range.

The most important factor for a semiconducting material is the transmittance which provides information about band gap energy by revealing absorption rate of a material. The transmittance value suddenly drops off near the absorption edge due to band to band

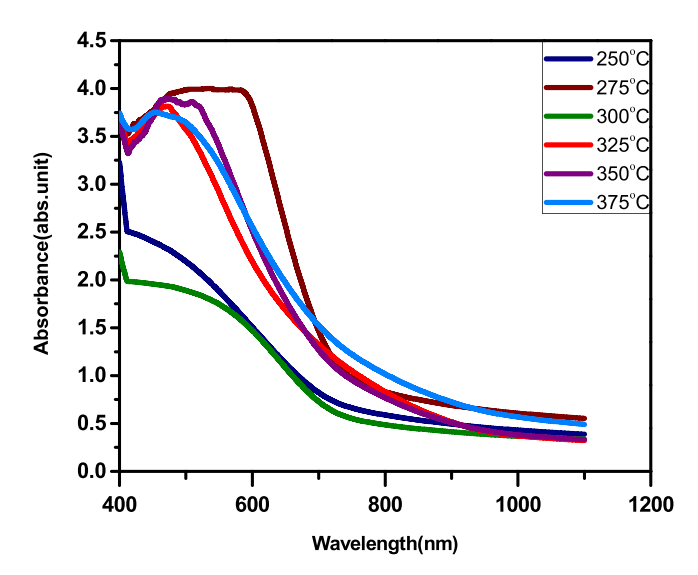


Figure 7. Absorbance vs wavelength for the different temperature.

transitions in the figure 8. From the analyses of transmission spectrum we can found band gap energy of a semiconducting material and transition of electrons. The relation between absorption coefficient  $(\alpha)$  and the incident photon energy  $h\nu$  is given by

$$(\alpha h \nu)^2 = k(h\nu - E_g)$$
 [3]

Where k is proportionality constant and  $E_{\rm g}$  is the direct transition band gap. The transmittance spectrum recorded in the wavelength range 300 nm–1200 nm using double beam spectrophotometer. From the figure7, the absorption edge primarily shifted from lower wavelength to higher wavelength region and then shifted towards lower wavelength with increase of substrate temperature. The existence of shifting near the fundamental absorption edge indicated the presence of different phases in the films. This behaviour indicates that band gap of the thin films decreased with increase of temperature.

Optical band gap of the films was determined from the  $(\alpha h \nu)^2$  vs  $h\nu$  plot (Fig. 9). All the samples had very high absorption coefficient  $(10^5 \text{ cm}^{-1})$ . Linearity of the graphs confirmed that all the SnSe thin films had direct band gap. Band gap of the SnSe films prepared at  $T_s = 325$  °C was 1.15 eV which is almost same as that for single-phase SnSe films. For SnSe films deposited in the range 250 °C to 375 °C, band gap was found to vary as 1.35 eV to 1.25 eV. (Fig. 11)

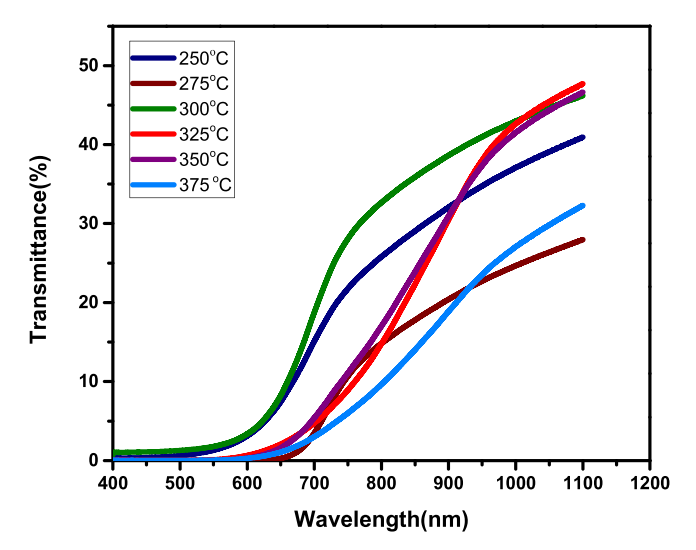


Figure 8. Transmittance vs wavelength at different temperature.

depicts the variation of band gap for the entire range of  $T_s$ . Here we can observe close similarity with the graph giving the variation of Sn/Se ratio (Fig 10). This indicates the dependence of band gap on composition. The high value of band gap at lower and higher temperature is probably due to the formation of  $\rm Sn_2Se_3$  and  $\rm SnSe_2$  phases respectively.  $^{34-38}$  Nearly stoichiometric and single phase SnSe films were observed at 325 °C, with an absorption coefficient of  $\alpha > 10^5$  cm $^{-1}$  and the evaluated energy band gap was 1.15 eV which was good agreement with Mariappan et al. and Kumar et al. on SnSe deposited by spray pyrolysis and thermal evaporation method.

Photoluminescence studies.—The Photoluminescence (PL) study is an important parameter to analyze the defects and their effects on optical studies. In general the photoluminescence properties of the films were associated with the crystallinity of the films because the density of defects reduces improvement in crystallinity. The PL spectra recorded with an excitation wavelength of 585 nm for SnSe thin films deposited at different substrate temperatures are shown in Fig. 12. The PL spectra revealed the presence of strong intense peak corresponding to the wavelength between 400nm--800nm centred at 785 nm (maximum emission) may be due to donor acceptor pair transition between a selenium vacancy and tin compounds. 39,40 All the SnSe thin films exhibit a strong luminescence peak near band edge emissions (NBE) at 785 nm (1.15 eV) (blue) due to recombination of bound excitons. All the films show only NBE peak in the visible region and IR and UV peaks were not observed in these films indicating a good optical quality of thin films. It is seen in the figure that the NBE emission peak is slightly shifted towards lower wavelength from higher wavelength. This result is well matched with the results of the optical band gap. The gradual increase in peak intensity was observed with an increase in substrate temperature indicated the development in crystalline quality and hence increase in density of free excitons. As the thickness decreases the number of molecules and hence decreases the peak height.

**Raman studies.**—Raman spectroscopy is a powerful tool for analyzing the phase, spatial location and structure of SnSe thin films. Raman spectra were analyzed to confirm the presence of tin selenide phase and other phases such as SnSe<sub>2</sub> and Sn<sub>2</sub>Se<sub>3</sub>. Raman spectra of SnSe thin films deposited at different substrate temperatures were shown in Fig. 13. It is clear that peaks located at 150 cm<sup>-1</sup> is the most peak in Raman spectra of given samples. This peak refers to Ag1 mode. Broad peaks located at 255 cm<sup>-1</sup> refers to SeO<sub>2</sub>.

Resistivity measurement.—The electrical resistivity, carrier concentration and Hall coefficient of SnSe thin films deposited at different substrate temperatures were determined by Hall Effect measuring instrument at room temperature and the corresponding values are given in Table II. For all electrical measurements performed in this study, non rectifying ohmic contact with the investigated tin selenide thin films were achieved using silver paste electrodes. The type of electrical conduction was verified using hot probe method while the resistivity measurements were carried out using standard Hall-effect set up. Resistivity of the films decreased from  $7 \times 10^3 \Omega$  cm to  $7 \Omega$  cm with the increase in  $T_s$ . The decrease in resistivity may be attributed to the increase in crystallite size which leads to the decrement in trapping states at the grain boundary. Grain boundary plays an important role between crystallites and the carrier transport. It can act as a trap center in a complete atomic bonding, which depletes the free charge carriers and as a result immobilized as trapping state increase. The electrical resistivity of a polycrystalline thin film is a complex phenomenon, involving charge carriers through the bulk part and inter-crystalline boundaries of a semiconductor. Thus the electrical resistance of semiconducting thin films decreases with increase in T<sub>s</sub> which was due to the increase in drift-mobility of the charge carriers and freecarrier density due to lattice vibrations. High value of resistivity of

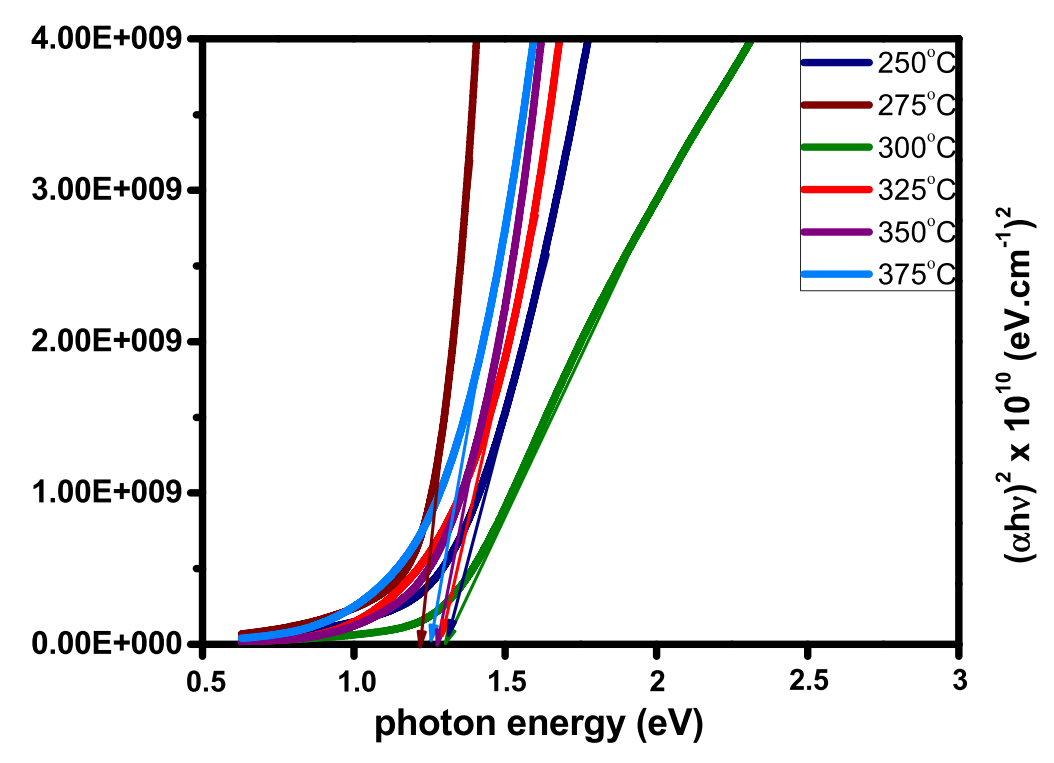


Figure 9. Energy band gap of SnSe at different temperature.

Table II. Variation of electrical properties of SnSe thin films at different substrate temperature.					
Substrate temperature (°C)	Resistivity $\times 10^3  (\Omega\text{-cm})$	Carrier concentration $\times 10^{14} \text{ (cm}^{-3})$	Mobility (cm $^{2} V^{-1} s^{-1}$ ) × 10 $^{-1}$		
250	7.67	4.37	3.45		
275	7.77	9.31	8.62		
300	7.84	4.85	1.64		
325	7.90	2.16	3.65		
350	8.09	9.17	8.41		
375	8.02	5.32	1.46		

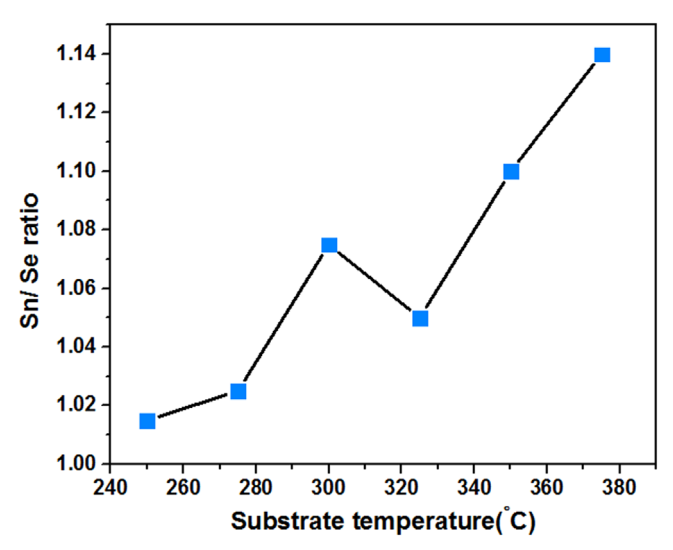


Figure 10. Variation of Sn/Se ratio with T<sub>s</sub>.

the films prepared below 300 °C was probably due to presence of mixed compound  $\rm Sn_2Se_3.$  Hot probe analysis was carried out on the sample to determine the conductivity type. This measurement indicated that the films prepared in the range  $T_s=250$  °C–375 °C were p-type and the films prepared at  $T_s=300$  °C showed fluctuating nature in hot probe analysis, which may be due to the very high resistivity of these films. Hence it can be concluded that films prepared at 325 °C have the optimal qualities of an absorber layer in terms of crystallinity, high absorption coefficient, band gap and stoichiometric. Therefore  $T_s=325$  °C was chosen for further deposition of SnSe films.

The electrical resistivity, carrier concentration and mobility of the films deposited at different substrate temperature are given in Table II. The resistivity value decreases rapidly with increasing substrate temperature showed the presence of increase in crystalline size and due to the presence of mixed phases like  $SnSe_2$  and  $Sn_2Se_3$  with SnSe, that are highly resistive might be responsible for the resistivity, exhibited by the films deposited at the lower temperature. The films formed at higher substrate temperature like 375 °C showed lower resistivity, which was due to presence of conductivity oxide phase of Sn-O-Se along with SnSe. However, single phase SnSe film deposited at 325 °C had resistivity value of 7.897 x  $10^3\ \Omega$ -cm, a

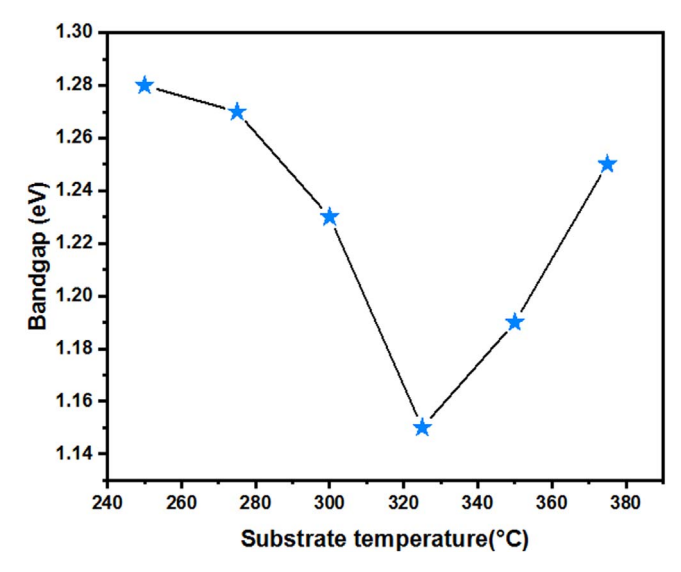


Figure 11. Variation of Bandgap of the films with T<sub>s</sub>.

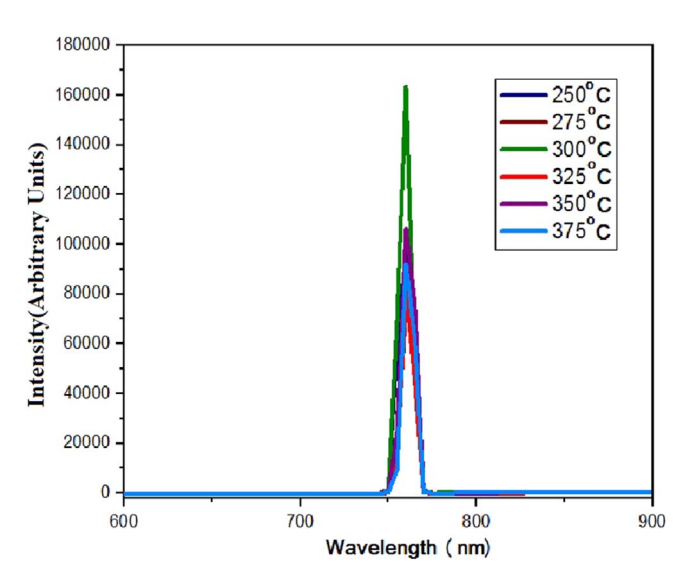


Figure 12. PL spectra of SnSe thin films deposited at different substrate temperature.

net carrier concentration of  $2.163 \times 10^{14}$  and mobility  $3.65 \times 10^{-1}$  cm $^2$  Vs $^{-1}$ . The similar behaviour for SnSe films has been reported by H. Chandra et al. and Mariappan et al. $^{41,42}$ 

**Photoconductivity.**—The photoconductivity and photosensitivity (s) of the films were calculated by the relation

$$S = \frac{\sigma_{light} - \sigma_{dark}}{\sigma_{dark}}$$
 [4]

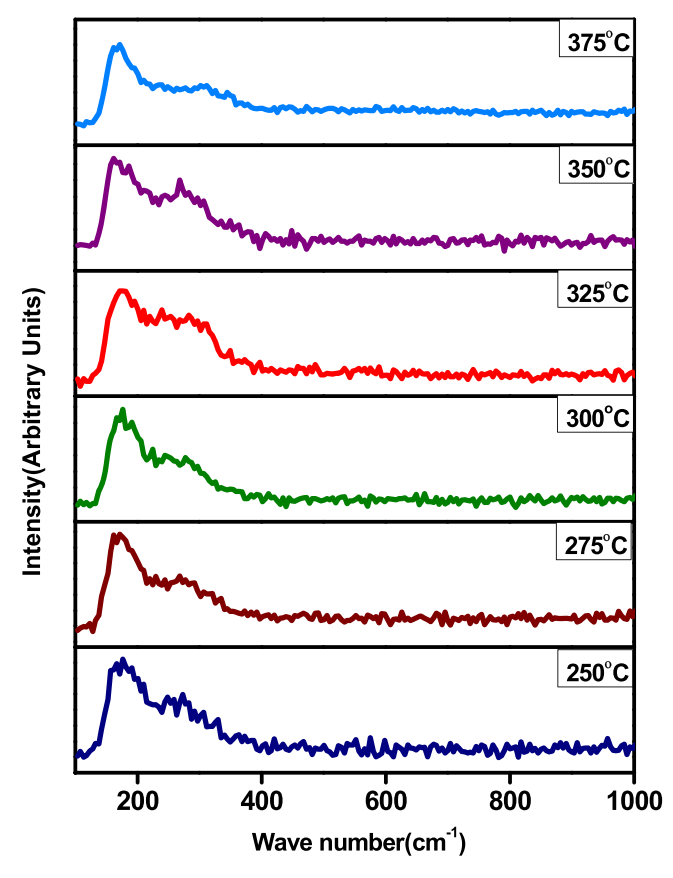


Figure 13. Raman spectra of SnSe thin films deposited at different substrate temperature.

Where I is the measured current, d is the film thickness, V is the applied voltage, A is the device area and SnSe thin films coated with silver ohmic contacts. The samples are connected to the experimental set up and the current values are recorded in the sequence of 20 s in dark condition and 20 s under illumination. The photoconductivity of SnSe thin films deposited at different substrate temperatures. It was found that at low temperature the photoconductivity increases and at higher temperature it decreases due to the oxidation of material leading to the formation of selenium oxide SeO<sub>2</sub>. The persistent photoconductivity (PPC) effect was observed for the SnSe thin films deposited at 325 °C under the dark condition. The transient decay current under the dark, which followed the illumination period indicate the presence of charge carrier traps in the films.

#### **Conclusions**

SnSe thin films were prepared using Chemical spray pyrolysis technique at different deposition temperature using stannous chloride and selenourea as precursor solution and they were optimized. Single-phase SnSe thin film with the orthorhombic polycrystalline was achieved in the temperature region 325 °C, optimized with needle like

Table III. Variation of elemental analysis of SnSe thin films at different substrate temperature.

	Atomic percentage	0.40	
Substrate Temperature (° C)	Sn	Se	Sn/Se ratio
250	50.1	49.9	1.01
275	50.7	49.3	1.03
300	51.8	48.2	1.07
325	51	49	1.04
350	52.5	47.5	1.10
375	53.3	46.7	1.14

structures along the stoichiometric elemental composition. For all the deposition temperatures, p-type SnSe films were obtained and the films were highly absorbing with suitable direct energy band gap for fabrication of SnSe homojunction. The resistivity value decreases rapidly with increasing substrate temperature showed the presence of mixed phases like SnSe<sub>2</sub> and Sn<sub>2</sub>Se<sub>3</sub> with SnSe, that are highly resistive might be responsible for the resistivity, exhibited by the films deposited at the lower temperature. The films formed at higher substrate temperature like 375 °C showed lower resistivity, which was due to presence of conductivity oxide phase of Sn–O–Se along with SnSe. However, single phase SnSe film deposited at 325 °C had resistivity value of 7.897 x  $10^3$   $\Omega$ -cm, a net carrier concentration of  $2.163 \times 10^{14}$  cm<sup>-3</sup> and mobility  $3.65 \times 10^{-1}$  cm<sup>2</sup> Vs<sup>-1</sup>.

#### **ORCID**

Anitha Ezhil Mangaiyar Karasi https://orcid.org/0000-0002-4816-0826

#### References

- 1. K. Zweibel, Sol. Energy Mater. Sol. Cells, 63, 375 (2000).
- X. Zhou, Q. Zhang, L. Gan, H. Li, J. Xiong, and T. Zhai, "Booming development of group IV–VI semiconductors: fresh blood of 2D family." Adv. Sci., 3, 1600177-1 (2016).
- N. K. Reddy, M. Devika, and E. S. R. Gopal, "Review on tin (II) sulfide (SnS) material: synthesis, properties, and applications." *Crit. Rev. Solid State Mater. Sci.*, 40, 359 (2015).
- V. R. M. Reddy, S. Gedi, B. Pejjai, and C. Park, "Perspectives on SnSe-based thin film solar cells:a comprehensive review." J. Mater. Sci., Mater. Electron., 27, 5491 (2016).
- L. D. Zhao, S. H. Lo, Y. Zhang, H. Sun, G. Tan, C. Uher, C. Wolverton, V. P. Dravid, and M. G. Kanatzidis, "Ultralow thermal conductivity and high thermoelectric figure of merit in SnSe crystals." *Nature*, 508, 373 (2014).
- K. S. Urmila, T. A. Namitha, J. Rajani, R. R. Philip, and B. Pradeep, "Optoelectronic properties and Seebeck coefficient in SnSe thin films." J of Semiconductors, 37, 1 (2016).
- M. X. Wang, G. H. Yue, Y. D. Lin, X. Wen, D. L. Peng, and Z. R. Geng, "Synthesis, optical properties and photovoltaic application of the SnS quasi-onedimensional nanostructures." *Nano-Micro Lett.*, 5, 1 (2013).
- N. R. Mathew, "Electrodeposited tin selenide thin films for photovoltaic applications." Sol. Energy, 86, 1010 (2012).
- M. A. Franzman, C. W. Schlenker, M. E. Thompson, and R. L. Brutchey, "Solutionphase Synthesis of SnSe nanocrystals for use in solar cells." *J. Am. Chem. Soc.*, 132, 4060 (2010).
- D. V. Shinde, S. K. Min, M. M. Sung, N. K. Shrestha, R. S. Mane, and S. H. Han, "Photovoltaic properties of nanocrystalline SnSe-CdS." *Mater. Lett.*, 115, 244 (2014).
- P. G. Naik, C. Desai, R. C. Shah, and S. S. Siddiqui, "Preparation and characterization of SnSe/In junction, in semiconductor devices." SPIE Int. Soc. Opt. Eng., 2733, 547 (1996).
- W. Shi, M. Gao, J. Wei, J. Gao, C. Fan, E. Ashalley, H. Li, and Z. Wang, "Tin Selenide (SnSe): growth, properties, and applications." *Adv. Sci.*, 5, 1700602 (2018).
- V. E. Drozd, L. O. Nikiforova, V. B. Bogevolnov, A. M. Yafyasov, E. O. Filatova, and D. Papazoglou, "ALD synthesis of SnSe thin layers and nanostructures." J. Phys. D, 42, 125306 (2009).
- G. H. Chandra, J. N. Kumar, N. M. Rao, and S. J. Uthanna, "Preparation and Characterization of flash evaporated tin selenide thin films." *J. Cryst. Growth*, 306, 68 (2007).
- J. Sharma, G. Singh, A. Thakur, G. S. S. Salini, N. Goyal, and S. K. Tripathi, "Preparation and Characterization of SnSe nanocrystalline thin films." *J. Optoelectron. Adv. Mater.*, 7, 2085 (2005).

- J. P. Singh and R. K. Bedi, "Tin selenide films grown by hot wall epitaxy." J. Appl. Phys., 68, 2776 (1990).
- R. Teghil, A. Santagata, V. Marotta, S. Orlando, G. Pizzella, A. Giardini-Guidoni, and A. Mele, "Characterization of the plasma plume and of thin film epitaxially produced during laser ablation of SnSe." *Appl. Surf. Sci.*, 90, 505 (1995).
- Z. Qiao, W. Shang, and C. Wang, "Fabrication of SnSe compounds on a gold electrode by electrochemical atomic layer epitaxy." *J Electro Chem*, 576, 171 (2005).
- H. Yanuar, U. Lazuardi, and J. Copriady, "Preparation and Characterization of thin film SnSe used by closed spaced vapor transport technique." *Chalcogenide Letters*, 14, 181 (2017).
- O. D. Nnanyere, "Optical properties of tin selenide thin films prepared by chemical bath deposition technique." J. Nat. Sci. Res, 5, 124 (2015).
- Z. Zainal, N. Saravanan, K. Anuar, and M. Z. Hussein, "Chemical bath deposition of tin selenide thin films." *Mater. Sci. Eng. B*, 107, 181 (2004).
- N. A. Okereke and A. J. Ekpunobi, "Structure and optical properties of chemically deposited tin selenide thin films." *Chalcogenide Letters*, 7, 531 (2010).
- P. Kevin, S. N. Malik, M. A. Malika, and P. O' Brien, The Aerosol Assisted Chemical Vapor Deposition, 50/92, 14328 (2014).
- D. P. Pandiyan, A. Marikani, and K. R. Murali, "Electrical and photoelectrical properties of vacuum deposited tin selenide thin films." *Crys. Res. Technol.*, 35, 949 (2000).
- J. S. N. Rios, M. Ramachandran, and D. M. Escobar, *J. Semicond.*, 34, 013001 (2013).
- S. Anwar, S. Gowthamaraju, B. K. Mishra, and S. K. Singh, *Mater. Chem. Phys.*, 153, 236 (2015).
- N. Kumar, U. Prihar, R. Kumar, S. Patel, C. J. Panchal, and N. Padha, "Effect of film thickness and on optical properties of deposited tin selenide thin films prepared by thermal evaporation for photovoltaic applications." *American J of materials*, 2, 41 (2012).
- Hanawait and Gates Rector, Powder Diffraction File, Joint Committee on Powder Diffraction Standards (ASTM, 20,63-73) (1998), (Card no. 32-1382).
- B. D. Cullity, Elements of X-ray Diffraction (Addison-Wesley Publishing Co., Inc., Reading, Massachusetts) (1956).
- G. K. Williamson and R. E. Smallman, "III Dislocation densities in some annealed and cold-worked metals from measurements on the X-ray Debye–Scherrer spectrum." *Philos. Mag.*, 1, 34 (1956).
- 31. V. P. Bhatt, K. Gireesan, and C. F. Desai, Cryst. Res. Technol., 24, 187 (1989).
- 32. D. T. Quan, Phys. Status Solidi A, 86, 421 (1984).
- 33. M. Skyllas Kazcos and B. Miller, Journal of Electro chem. Soc., 127, 2016 (1980).
- 34. A. J. Moulson, Electroceramics (Wiley, USA) p. 26 (1990).
- K. Chung, D. Wamwangi, M. Woda, M. Wuttig, and W. Bensch, "Investigation of SnSe, SnSe<sub>2</sub>, and Sn2Se3 al-loys for phase change memory applications." *J. Appl. Phys.*, 103, 083523 (2008).
- C. R. Baxter and W. D. Mclennan, "Ovonic type switching in tin selenide thin films." J. Vac. Sci. Technol., 12, 110 (1975).
- I. Lefebvre, M. A. Szymanski, J. Olivier-Fourcade, and J. C. Jumas, "Electronic structure of tin mono chalcogenides from SnO to SnTe." *Phys. Rev. B*, 58, 1896 (1998).
- H. S. Soliman, D. A. Abdel Hady, and K. F. Abdel Chaudhuri, *Thin Solid Films*, 165, 257 (1988).
- N. Kumar, V. Sharma, U. Parihar, R. Sachdeva, N. Padha, and C. J. Panchal, "Structure, optical and electrical characterization of Tin selenide thin films deposited at room temperature using thermal evaporation method." *J. Nano-Electron. Phys.* 3, 117 (2011).
- Z. Zainal, N. Saravanan, K. Anuar, M. Z. Hussein, and W. M. M. Yunus, "Tin Selenide thin films prepared through combination of chemical precipitation and vacuum evaporation technique." *Mater. Sci.*, 21, 225 (2003).
- J. Tauc, Amorphous and Liquid Semiconductors (1974), chapter 4, ed. J. Tauc (Plenum, New York, London).
- R. Mariappan, M. Ragavendar, and C. Gowrisankar, "Growth and characterization of SnSe thin films prepared by spray pyrolysis technique." *Chalcogenide Letters*, 7, 211 (2010)